THE UNIVERSITY OF SHEFFIELD

DEPARTMENT OF CIVIL AND STRUCTURAL ENGINEERING

PROJECTILE PENETRATION INTO ROCK/ELASTOMER COMPOSITES

by

MARTYN ROBERT JOHNSON, B.Sc. (Leeds)

A thesis presented to the University of Sheffield for the degree of Doctor of Philosophy

May 1981

TEXT BOUND INTO

THE SPINE

SUMMARY

Composite materials cast from polyurethane resin, rock aggregates and sand have been examined to determine their resistance to penetration by 7.62mm ball and armour piercing high velocity projectiles. The effects of using different polymer and rock types were investigated, and the resultant composite mixes were optimised in terms of cost effectiveness to obtain a protective material which may be used to clad buildings.

Optimisation was carried out using response surface theory, initially using a linear response surface, but subsequently a quadratic one. Variables considered in the mix optimisation were % polymer by weight, % rock aggregate by weight, rock aggregate particle size, and polymer hardness. Penetration tests were carried out on the optimised composites to determine the thickness required for a given confidence level of bullet containment, and to assess the effect of composite temperature on impact behaviour.

The static uniaxial compressive, bending and creep characteristics of the best composite were determined to identify any limitations in its use as cladding units.

ACKNOWLEDGEMENTS

This research was carried out in the Department of Civil and Structural Engineering of the University of Sheffield, for which the author expresses his gratitude to Professors D. Bond and T. H. Hanna, for the use of the facilities.

The author would like to thank the Procurement Executive, Ministry of Defence for the granting of the research contract on which this thesis is based, and Mr. G.M. McNeil and Major W. Port of the Military Vehicles and Engineering Establishment, Christchurch, for their motivation in arranging the contract and their advice throughout.

The author is indebted to Dr. W. F. Anderson and Dr. A. J. Watson for their supervision and assistance, and to Dr. R. Kay of the Department of Probability and Statistics for his advice on statistical analysis.

The skills of the technical staff were much appreciated, particularly those of Mr. T. Robinson, whose help in fabrication and testing was invaluable. In addition, the work of Mrs. D. Hutson in producing photographic prints is appreciated, as is the typing ability of Miss J. Stacey.

Constructive critisms from my colleagues were the basis of many ideas expressed in this thesis : my thanks go particularly to Mr P. O'hEachteirn, Mr. A. Sanderson, Mr. P. Bull, Mr. B. Archer and Mr. R. Cubison.

It is not possible to list all of the people contributing to this work, so my thanks and apologies are extended to all those not mentioned.

Finally, I express my gratitude to my family, and particularly my wife Christine, for their support during my research.

CONTENTS

LIST OF TABLES

LIST OF FIGURES

LIST OF PLATES

LIST OF SYMBOLS

A	empirical coefficient
A_1 to A_4	functions of projectile and target properties
A_p	cross-sectional area of projectile
a	constant; cavity radius; aggregate particle radius; acceleration
a_{max}	maximum cavity radius
B_1, B_2	functions of target material properties
b	beam width; constant
b_o to b_{44}	coefficients in the fitted response surface
C	degree of rock particle comminution
CRH	calibre radius head
C_1 to C_3	target material constants
c	dilatational wave velocity
c_l	damping constant
c_{cr}	elastic wave front propagation velocity through granular medium subjected to crushing stress, σ_{cr}
c_d	aerodynamic drag coefficient
D	measured normal penetration depth
$\bar{D}$	mean normal penetration depth
D'	measured penetration path length
D_p	predicted normal penetration depth
D_p'	predicted penetration path length
d	measured instantaneous normal penetration depth; beam depth
d_b	burrow/crater diameter
d_c	critical instantaneous penetration depth
d_o	normal penetration after indentation stage
d_p	projectile or penetrator diameter
d_{pe}	effective d_p for non-circular penetrator

E	Young's Modulus
E_p	reference value of E_{pl}
E_{pl}	Young's modulus of penetrator
E_{sec}	secant modulus
E_t	Young's modulus of target, during strain hardening
e	strain
e_{le}	locked elastic strain
e_{lp}	locked plastic strain
e_u	residual value in the u^{th} observation of a design for response surface analysis
F_i	impact force
F_{n_1,n_2}	value in statistical F distribution corresponding to degrees of freedom n_1 and n_2
f_{bt}	tensile failure stress
f'_c	cylinder concrete compressive strength
G	function of penetrator depth and penetrator diameter
k	constant
k_A	attenuation coefficient
l	span of beam; length
l_n	projectile nose length
M	bending moment
m	mass
N_o to N_3	nose performance coefficients of varying definition
n	porosity
n_1, n_2	degrees of freedom for statistical F distribution
n_o	initial porosity
n_{cr}	porosity at crushing
P	load; force
p_i	cavity pressure due to inertial effects

p_s	cavity pressure due to static effects
p_t	total cavity pressure
Q_1 to Q_n	functions of soil properties
R	modulus of rupture
RD	relative density
S	target material constant
s	distance
T_c	cure temperature
T_s	temperature at testing
t	specimen thickness; time; form of statistical probability distribution; panel thickness
t_m	minimum thickness necessary for containment at a given confidence level.
t_p	specimen thickness necessary to prevent perforation
t_s	thickness necessary to prevent scabbing; specimen age
u	function of CRH; observation number (1 to n) in an experiment design
V_b	burrow/crater diameter
v	instantaneous velocity
v_c	critical velocity
v_o	impact velocity
v_p	particle velocity
v_r	residual velocity
w	moisture content
x_1	percentage resin by weight
x_2	percentage rock aggregate by weight
x_3	sieve sizes passing and containing rock aggregate
x_4	polymer hardness
x_{iu}	level of i^{th} factor in the u^{th} observation
Y	yield stress
y_u	response from the u^{th} observation

$\bar{y}_u$	mean value of y_u
y_p	predicted value of y_u
Z	section modulus

α	coefficient; function of target material properties
α_1 to α_3	functions of target material properties
β	function of target material properties; positive constant
γ	function of target material properties
δ	function of target material properties; central deflection
$\tan\delta$	material loss tangent
η	function of target material properties
λ	pulse wavelength

ρ	density
ρ_o	initial target density
ρ_l	locked target density
ρ_{le}	locked elastic target density
ρ_{lp}	locked plastic target density
σ	stress; standard deviation
σ_f	unconfined compressive strength of soil
σ_F	uniaxial compressive strength
σ_{cr}	crushing stress
$\bar{\tau}$	time of a past stressing event
ϕ'	angle of shearing resistance of soil
ϕ	half nose angle of cone; response surface function

GLOSSARY OF TERMS

Burrow : a narrow, elongated crater.

Calibre Radius Head (CRH) : ratio of radius of nose curvature, R, to projectile diameter, d_p.

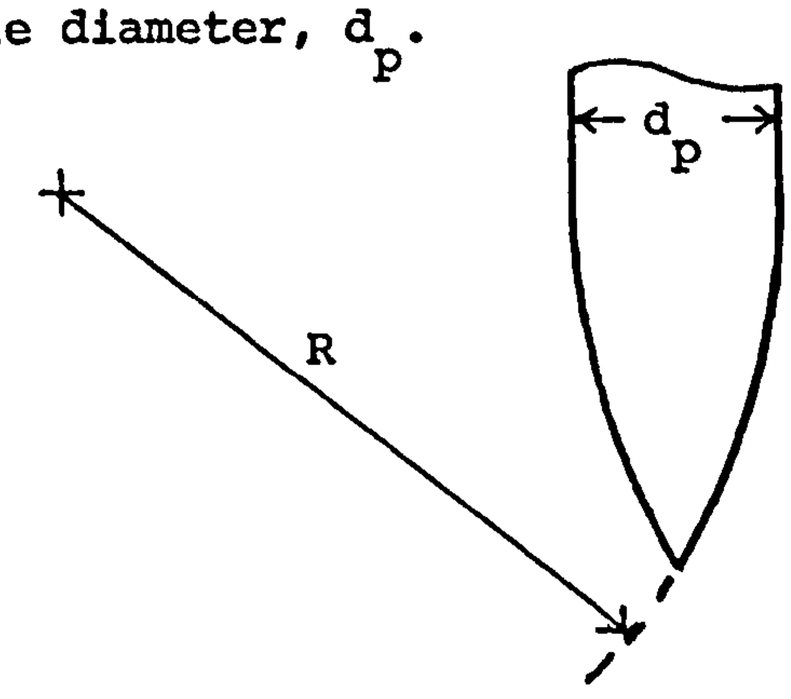

Cratering : failure of front free surface caused by crushing and displacement during impact and penetration of projectile. Normally crater cross section is larger than projectile entry hole cross section.

Penetrator : body intended to penetrate a target due to kinetic energy.

Penetration : movement of a penetrator within a target.

Penetration Path Length : cumulative length of a series of secants measured along the curved path of a penetrator within a target.

Perforation : occurs when a penetrator exits from the back face of a target.

Projectile : Penetrator designed for efficient penetration of a target.

Normal Penetration : Normal distance from front face of target to penetrator tip.

Scabbing : tensile failure of rear free surface caused by large displacement of rock aggregate particles during penetration of a penetrator.

CHAPTER 1

INTRODUCTION

An interest in the protection of buildings and other structures against small arms fire led Gibbs and Prescott (1974) to undertake a limited experimental study into the behaviour of dry gravel armour. Their tests showed that a theoretical approach to find the optimum gravel particle size, using "billiard ball" theory, was not valid because of the high degree of comminution of the gravel particles. The effectiveness of the armour, however, was proven.

A major problem in using gravel is containment of the material. A flexible binder is desirable because of the extensive fracture which occurs in brittle material on impact. Hence the idea arose of using a cold curing rubbery polymer as the binder, and this thesis details the investigation into the resultant composite.

Initially a very detailed literature survey was carried out and the most relevant details are given in Chapter 2. This survey, plus initial attempts at a theoretical approach, showed that too many simplifying assumptions would have to be made for any theory developed to be valid. Efforts were therefore concentrated on a experimental study to optimise the variables in cost/effective terms.

At an early stage it was realised that a two phase mixture of elastomer (rubbery polymer) and rock particles would be very expensive because of the large percentage voids which had to be filled with high cost elastomer. Hence sand was included in the mix to act as a filler and reduce cost. A wide range of elastomers of varying costs were commercially available, and a survey of these and initial testing on the most promising were carried out. Details of the materials and equipment used are given in Chapter 3.

Having narrowed down the field of potentially useful materials, plans were made for the main test programme. Originally it had been proposed

that firing tests would be carried out on targets by the Ministry of Defence. However, the change in emphasis from theoretical to experimental meant an increase in the number of firing tests, making this arrangement impractical. No previous studies of this nature had been undertaken at the University, so it was necessary to construct a firing range. An indoor range was built, along with ancilliary facilities, at the University research station at Harpur Hill, Buxton, to Royal School of Infantry specifications.

The number of variables involved in the study, their interdependence, and the range of values possible for each variable meant a full parametric study was not feasible. Use was made of response surface theory, detailed in Chapter 4, to try to identify trends leading to optimum mixes. This method, normally used in the fields of chemistry and biology, is a very efficient method of experimental research which has been neglected in engineering. This thesis provides an example of its use in the examination of the properties of a new composite, and the adaption of the theory of specific circumstances.

Altogether, almost 700 target specimens were tested. In addition, limited bending, compression, and creep tests were carried out to provide information on the behaviour of the composite under normal conditions. The test results are given in Chapter 5, and discussed in Chapter 6. Conclusions and recommendations for further study are listed in Chapter 7.

In addition, some preliminary work was done on the ricochet characteristics of the composite and its response to contact explosive charges. This is considered beyond the scope of this thesis; for details see Anderson et al (1980).

CHAPTER 2

LITERATURE SURVEY

2.1 Introduction

The composite which was being investigated was an unusual one because of the relatively low elastic modulus of the matrix. No published information on the penetration resistance of this type of composite material could be found, although there was a limited amount of information available about rigid polymer concretes whose matrix elasticity was higher.

The literature survey therefore concentrated on closely related topics and these have been separated into relevant information about

(i) penetration mechanics

and (ii) mechanical properties of materials at high strain rates, including stress waves and fracture

2.2 Penetration Mechanics

Penetration is the movement of a body within a target. Military research has undoubtably provided the main avenue of advancement for the understanding of penetration mechanics, with metals being the most common target. Until the recent development of layered and composite armour, steel armour plate was extensively used for protection against damage by various types of projectile. Also, from a theoretical point of view, metals are easily understood because of their homogeneity and deformation characteristics. However, due to the behavioural differences between metals and rock or elastomers, and the fact that metal targets are usually thin, this area of the literature is not documented in detail, except where directly relevant. Good reviews of the penetration characteristics of metals are those by Backman and Goldsmith (1978) and Jonas and Zukas (1978).

The second main body of literature on projectile penetration relates to targets of earth materials, ice and concrete and since this is of more relevance to the present study some historical background is given.

From studies of projectile penetration into earth materials Robins (c1742) and Euler (c1750) proposed the first penetration equation of the form

$$-\frac{dv}{dt} = \gamma \qquad \ldots 2.1$$

where v = instantaneous velocity

t = time

γ = a positive constant

This was used to assess the protective capabilities of earth embankments against ball ammunition. Poncelot (c1829/35) suggested a higher order equation

$$-\frac{dv}{dt} = \alpha v^2 + \gamma \qquad \ldots 2.2$$

where α is a positive constant

Résal (c1895) modified the equation to

$$-\frac{dv}{dt} = \alpha v^2 + \beta v \qquad \ldots 2.3$$

where β is a positive constant

These equations are all special forms of a more general equation, namely

$$-\frac{dv}{dt} = \alpha v^2 + \beta v + \gamma \qquad \ldots 2.4$$

The only experimental data available to test these equations consisted of the final penetration depth, D, and v_o, the impact velocity. If D was known as a function of v_o, then α, β, and γ may theoretically have been evaluated. However, large experimental scatter caused this to be very difficult. More details of this early work are given by Goldsmith (1960).

With the advancement of experimental methods, Allen et al. (1957a) were able to measure the velocity histories of steel penetrators (i.e. bodies intended to penetrate) of various nose cone angle during the penetration of contained dry quartz sand. Impact velocity was approximately 700 m/s, and penetrator mass approximately 80 g.

This initial theoretical work was based on equation 2.4 and they assumed that the sand medium could be treated as a fluid, with an aerodynamic drag coefficient of c_d. Values of α, β, γ, and c_d were evaluated for the differing cone angles.

However, a typical velocity penetration graph (Figure 2.1) showed an apparent transition point at d_c and v_c, the critical depth and velocity. This transition was related to a physical transition at d_c between a diffuse trail in the sand before d_c, and a distinct trail afterwards. Thus separate equations describing both regions were proposed. These were

$$v_o > v > v_c : -\frac{dv}{dt} = \alpha v^2 \qquad \ldots 2.5$$

$$v_c > v > 0 : -\frac{dv}{dt} = \alpha_1 v^2 + \gamma \qquad \ldots 2.6$$

From these relationships, equations of penetration depth were produced

$$v_o > v > v_c \qquad d - d_c = \frac{1}{\alpha} \ln \frac{v_c}{v} \qquad \ldots 2.7$$

$$v_c > v > 0 \qquad d = d_c + \frac{1}{2} \ln \frac{\alpha_1 v_c^2 + \gamma}{\alpha_1 v^2 + \gamma} \qquad \ldots 2.8$$

Thus the final penetration D, was given by

$$D = d_c + \frac{1}{2\alpha_1} \ln \frac{\alpha_1 v_c^2 + \gamma}{\gamma} \qquad \ldots 2.9$$

where d_c, v_c, α, α_1, γ were obtained from graphs similar to Figure 2.1.

The physical significance of constants α, α_1 and γ used above was discussed. The term m γ, where m was the projectile mass, was considered to be the force necessary to overcome, by grain fracture, the structural framework formed by the sand grains resisting the motion of the penetrator when moving

at negligible velocity. The terms αv^2 and $\alpha_1 v^2$ were interpreted as the acceleration of the penetrator due to target inertia.

Allen et al. (1957a) suggested that the transition of penetration behaviour was related to the local velocity of sound in the target medium. However, later work by the same authors (1957b) failed to prove this. In this latter study, the relationship between initial kinetic energy of the penetrator and sand comminution was also examined. Figure 2.2 shows the relationship obtained, which confirmed earlier work by Morrison and Allen (1955) concerning the comminution of crushed limestone due to projectile penetration.

The step in the plot in Figure 2.2 corresponds to a significantly higher value of v_c than that determined from the penetration depth - velocity plot.

Maurer and Rinehart (1960) also used the method of fitting simple relationships to experimental data. They investigated the cratering and burrow formation by spherical steel balls in sandstone and granite for various impact angles assuming an implied semi-infinite target. A burrow is considered to be a narrow elongated crater. Impact velocities ranged from approximately 90 to 1800 m/s. Behavioural differences were evident between the two rock types. Normal impact (that is at right angles to the impact face) into the softer sandstone yielded a cup shaped crater surrounding a narrow burrow. This is illustrated in Figure 2.3. Under similar conditions granite yielded only the cup with no burrow.

The formula used to calculate penetration path length was based on a form of equation 2.4

$$- \frac{dv}{dt} = \beta v \qquad \ldots\ldots 2.10$$

This yielded a final penetration

$$D = C_1 \frac{m}{A_p} (v_o - v_c)$$

where C_1 is a target material constant

m is the projectile mass

A_p is the projectile cross sectional area

v_c in this case is the critical value of v_o at which cratering begins to occur.

Figures 2.4 and 2.5 show the D vs $\frac{mv_o}{A_p}$ for granite and sandstone respectively.

The relationships between C_1 and tensile strength, compressive strength, shear strength and the quantity $\rho_o c$ (where c is the dilational wave velocity and ρ_o is the initial target density) were experimentally examined. It was found that $1/C_1$ was proprotional to shear strength, and to $\rho_o c$. These conclusions were based on only 4 rock types and may not hold for all rock types. The ratios of the values of C_1 (effectively the penetration ratios) for sandstone, tuff, potash, and granite were approximately 1 : 0.83 : 0.52 : 0.22.

Other experimental relationships found to be linear in this study were:

(i) cup depth vs v_o

(ii) cup radius squared vs v_o

(iii) cup surface area vs v_o

(iv) cup volume vs v_o^2

A quantity called impact force, F_i, was defined as

$$F_i = \frac{A_p}{C_1} (v_o - v_c) \qquad \ldots 2.11$$

This represented the force over and above that necessary to initiate failure. It was found that the ratio (impact force/surface area of cup) was independent of impact velocity for all rock types. This was a logical outcome from equation 2.11, and relationship (iii) above. Kinetic energy per unit crater volume,i.e. specific energy,was also found to be independent of impact velocity for granite, but to increase with impact velocity for sandstone.

Vanzant (1963) carried out penetration studies on cement and marble for various projectile geometries and velocities. He assumed penetration could be expressed thus

$$D = C_2 v_o^a m^b \qquad \ldots 2.12$$

where a, b and C_2 are constants

Similar expressions were fitted to the data relating impact energy, crater volume, and penetration depth.

Thompson (1966) examined the penetration of particulate media by using available continuum and constitutive equations for the target media, along with known boundary conditions, to try to produce an analytical solution to substantially reduce testing programmes. The soil medium was treated as viscoplastic but it was stated that the constitutive equations would not be valid when communution occurred, as a great deal of energy is absorbed in this way.

Initial tests were carried out on a two dimensional model, with needle roller bearings between plexiglass plates representing the target medium, to enable displacements to be monitored. For the three dimensional tests various projectiles, target materials, and impact velocities were used, and typical results are shown in Figures 2.6 and 2.7. Large-scale field tests were also undertaken, with accelerometers in the projectiles giving the required information.

The theoretical treatment was concluded by reducing the governing relationships down to four differential equations; two first order and two second order. No solution was achieved, and Thigpen (1974) reported the equations still unsolved.

Young (1969) extended the empirical approach by proposing a general equation of the form

$$D = f_1(N_o)\ f_2(A_p)\ f_3(m)\ f_4(v_o)\ f_5(S) \qquad \ldots 2.13$$

where f_n denotes 'function of'

S is a target material constant

N_o is a nose performance coefficient

On experimental evidence, this was modified to

$$D = f_1(N_o)\ f_6\left(\frac{m}{A_p}\right)\ f_7(v_o)\ f_8(S) \qquad \ldots 2.14$$

A method was developed to enable many existing test results, obtained under varying conditions, to be used to determine the functions within equation 2.14. The method, called normalisation, is essentially an iterative technique, and used the following equation for the first iterative step

$$D = \frac{m}{A_p}\ \frac{C_3}{2313} \log_{10}\left[\ 1 + \frac{v_o^2}{19974}\ \right] \qquad \ldots 2.15$$

where C_3 is an empirical target material constant determined in imperial units, and converted to SI units by its denominator.

Young decided on a set of standardised values for N_o, $\frac{m}{A_p}$, v_o and S, and using equation 2.15, calculated what the experimentally determined penetration depths would have been if $\frac{m}{A_p}$, v_o and S had been at his standardised values. Thus an equation in N_o only was obtained. This process was carried out for $\frac{m}{A_p}$, v_o and S in turn, representing the first iterative step. The normalisation was then repeated until sufficient convergence occurred.

A transition in the velocity function was found, and hence two penetration equations resulted

$$D = 6.08 \times 10^{-3} \times S\ N_o\ \left(\frac{m}{A_p}\right)^{\frac{1}{2}} \ln\left(1 + 2.15 \times 10^{-4} v_o^2\right)$$

for $v < 61$ m/s $\qquad \ldots 2.16$

$$D = 1.17 \times 10^{-4} \; S \; N_o \; (\frac{m}{A_p})^{\frac{1}{2}} \; (v_o - 30.48)$$

for $v > 61$ m/s ... 2.17

where m, A_p and v_o are in SI units, and S and N_o are as described by Young (1969).

The equations above, often called the Sandia Corporation Empirical Formulae, showed a significantly improved fit to the data over equation 2.15.

Using equations 2.16 and 2.17, a nomograph was presented to calculate predicted penetration depth. This is illustrated in Figure 2.8. A method for applying the equation to layered soils was also discussed.

This method shows the usefulness of empirical relationships if formulated with care. A comparative analysis of five predictive methods by Hadala (1975) showed Young's equation to be very useful and this work will be discussed in more detail later.

Ross and Hanagud (1969) developed dynamic spherical cavity expansion theory after it was initially adapted from the static case by Goodier (1964).

The theory was based on a determination of the pressure necessary to cause the expansion of a spherical cavity of radius a within the target medium at a velocity and acceleration of $\dot{a}$ and $\ddot{a}$ respectively. This was then related to the force acting on a projectile, with a hemispherical forward surface. The projectile was assumed to be rigid, axisymmetric, and penetrating normally. Only normal stresses were assumed to be acting on the projectile nose, a limitation in the theory.

Hanagud and Ross (1971) used the theory to describe deep penetration into a compressible, strain hardening target material, specifically aluminium. Volumetric and shear characteristics were simplified as shown in Figure 2.9. The concept of 'locking' was used, where the material kept a constant strain over a wide range of stresses.

Figure 2.10 shows the state of the material around a cavity undergoing expansion. The pressure in the cavity, p_t, and hence the normal stress on the

projectile nose comprised two components

$$p_t = p_s + p_i \qquad \ldots 2.18$$

where p_s is the static resistance term, assumed to be independent of projectile size, which would not be true for granular targets

p_i is the inertial resistance term

The static pressure was shown to be

$$p_s = -\frac{2}{3} Y.\ln\delta + \frac{4}{9} E \left[1 - e^{-3\beta}\right] + \frac{2}{27}\pi^2 E_t - \frac{4}{9} E_t \eta \qquad \ldots 2.19$$

where $\delta = 1 - \frac{\rho_o}{\rho_{lp}} e^{-3\beta}$

$$\beta = \frac{Y}{2E} - \frac{e_{le}}{3}$$

$$\eta = \sum_{n=1}^{\infty} \frac{\delta n}{n^2}$$

Y = yield stress of target material

E = Young's modulus of target material

E_t = modulus after yield of target material

ρ_o = original target density

ρ_{lp} = locked plastic density

e_{le} = locked elastic strain

The dynamic inertial pressure was

$$p_i = \rho_{lp} (B_1 \ddot{a}\ddot{a} + B_2 \dot{a}^2) \qquad \ldots 2.20$$

where $B_1 = 1 - \delta^{\frac{1}{3}}$

$$B_2 = \frac{3}{2} - (2 + \frac{\rho_o}{\rho_{lp}}) \delta^{\frac{1}{3}} + \frac{1}{2} \delta^{\frac{4}{3}}$$

From these expressions an equation of motion was determined, leading to an expression for penetration depth of the form

$$D = d_o + \frac{3}{4}\left[\frac{(\frac{m}{A_p}) + B_1 (\frac{d_p}{3}) \rho_{1p}}{B_2 \rho_{1p}}\right] \ln\left[\frac{p_s + \frac{2}{3} B_2 \rho_{1p} v_o^2}{p_s}\right] \quad \ldots 2.21$$

where d_o = the penetration depth at the end of the indentation stage, i.e. assuming a hemispherical indent of d_p, then $d_o = d_p/2$

The method was extended by Ross and Hanagud (1971) to enable it to cope with a layered medium; ice with snow cover. The material properties assumed, however, were even further simplified from those in Figure 2.9.

Rohani (1972) applied cavity expansion theory to the normal impact of right circular cylindrical penetrators into controlled laboratory soil targets at velocities between 305 and 1525 m/s. Brass and steel penetrators were used; soil types were compacted and uncompacted sand and highly plastic clay.

Variations in penetration with soil type, penetrator type and impact velocity were examined, along with the damage to the penetrator. Figure 2.11 shows the variation in penetration with impact velocity for both types of penetrators. Possible reasons were given for the reduction in penetration at high impact velocities, which could not be explained by the theory.

From equation 2.21, for a given impact situation, nine parameters need defining to enable cavity expansion theory to be applied, namely ρ_{1p}, ρ_o Y, E, E_t, e_{1e} for the target, and m, d_p and v_o for the penetrator. The first term is the equation d_o (or $d_p/2$) was ignored.

E, E_t, Y, e_{1e} and ρ_{1p} were estimated by idealising the volumetric and uniaxial stress-strain curves for the target materials into the same form as Figure 2.9. Unfortunately, the confining pressure used was apparently chosen rather arbitrarily. ρ_{1p} was determined from the relationship

$$\rho_{1p} = \rho_o \frac{1}{1 + \varepsilon_{1p}} \quad \ldots 2.22$$

The rest of the nine parameters needed were easily measured. The degree of agreement between theory and experiment was reasonable for the six combinations of penetrator and target at the lower end of the velocity range. However, cavity expansion theory is independent of pressure and deformation rate, and hence predicts the same resistance to penetration at any impact velocity. In addition, it fails to cater for penetrator deformation. Hence it was not capable of predicting the decreasing depth of penetration which was noticeable in Figure 2.11 at the higher impact velocities.

Riparbelli and Brown (1972) described a method of predicting crater profiles for penetrators entering water and earth materials. Impact velocities were between 914 and 2438 m/s. The analysis was based on the idea that, at subsequent stations along the penetration line, small amounts of target material were compressed and then expanded, overshooting the radius of the penetrator because of inertial effects. These stations were considered as sources of spherical fronts which were described using a one dimensional numerical program, WONDY II, which took into account the correct Hugoniot pressure-volume function for the target material. From their results a predictive numerical program CRATER was developed, and reasonable correlation with experimental results was achieved.

Dunlap (1972) attempted to determine which soil properties were relevant to Young's soil constant, S. He assumed that a blow count for a certain penetration of a dynamic cone penetrometer into in-situ soils reflected the behaviour during penetration by a projectile. After some preliminary analyses, a multiple linear regression analysis was carried out by computer, the program having the facility to drop the least important variables and leave only those exhibiting the required significance. The sand variables affecting blows per unit penetration at the 95% confidence level were the in-situ unit weight, depth of soil below surface, angle of shearing resistance and $\tan^2 (45 + \phi'/2)$. For clays and silts the variables similarly remaining were the soil cohesion,

clay content and $\tan^2(45 + \phi'/2)$. The results were not considered very useful even by the author himself.

Murff and Coyle (1973), by fitting data to the generalised polynomial given in equation 2.23 below, obtained the simplified equation 2.24 by initially fitting data ignoring projectile mass and impact velocity effects

$$m \frac{d^2d}{dt^2} = A_1 + A_2 d + A_3 \frac{dd}{dt} + A_4 d^2 + A_5 d \frac{dd}{dt} \quad \ldots 2.23$$

$$m \frac{d^2d}{dt^2} = A_1 + A_2 d + A_3 \frac{dd}{dt} \quad \ldots 2.24$$

where A_n are functions of projectile and soil properties.

A big advantage of equation 2.24 is that it can be directly intergrated to produce final penetration depth, thus making numerical procedures unnecessary.

Next, the effects of projectile diameter and nose length (l_n) to diameter ratio were examined by curve fitting, producing an equation of the form

$$m \frac{d^2d}{dt^2} = Q_1 d_p^2 \left(\frac{l_n}{dp}\right) \frac{dd}{dt} + Q_2 d_p^2 \frac{dd}{dt} + Q_3 d_p d + Q_4 d_p^2 \quad \ldots 2.25$$

in which Q_n are functions of soil properties. These were determined from data with all other variables, except soil parameters, kept constant. Q_n were assumed to be functions of unconfined compressive strength, σ_f, for clays and relative density, RD, for dry sand. The final fitted equations for clay and dry sand respectively were

$$m \frac{d^2d}{dt^2} = -10.27\, \sigma_f d_p^2 - (0.572\, \sigma_f + 340)\, d_p d + \left[42.6\, d_p^2 - 9.67\, d_p^2 \left(\frac{l_n}{d_p}\right)\right] \frac{dd}{dt} \quad \ldots 2.26$$

and

$$m \frac{d^2d}{dt^2} = -238\, d_p^2\, RD - 162\, d_o\, RD\, d + \left[37.3 \left(\frac{l_n}{d_p}\right) - 86.6\right] d_p^2\, RD \frac{dd}{dt} \quad \ldots 2.27$$

Excellent correlation was achieved between the predictions of the above equationsand the experimental results. However, the impact velocities used were low (up to approximately 60 m/s).

Gibbs and Prescott (1974) investigated the response of dry gravel armour to impact by small arms ammunition. Having determined the coefficient of restitution of steel on rock, an optimum rock particle mass was determined which removed the maximum kinetic energy, 50%, from the projectile by momentum transfer. This determination was based on simple elastic impact. After 7 collisions, the projectile energy remaining was less than 1% of the original kinetic energy, and after 10 collisions, the remaining energy was less than 0.1%. From considerations of collision probability and aggregate packing, a target thickness could be calculated for a given confidence level.

However, the evidence of the experimental work carried out was that a large degree of gravel particle fragmentation occurred which invalidated the assumptions in the theory. In addition, the asymptotic nature of the solution meant it was difficult to rationally chose what number of collision to use for the target thickness determination.

Description of the penetration process using numerical methods in computer programs has been carried out for the past 20 years, but it is in the past 10 years that this method has been widely used. Thigpen (1974) established governing equations, constitutive relations and boundary conditions for penetration into two rock materials, and used a 2-dimensional Langrarian (computational grid fixed in the material) computer code, TOODY II, for his analysis. The target material was treated as an elastic-plastic continuum, which was incorrect in that rock deformation involves crack formation and crushing or sliding of grain boundaries rather than plastic flow. However, the model readily lent itself to analysis. Comparison between predicted penetration into limestone and an actual test result yielded a large error of 44%,

highlighting the difficulty in using such simplified assumptions as were necessary for the analysis. Even with these simplifications, computer-run times were measured in hours: the high cost of this is obvious.

Rohani (1975) utilised a computer code based on cavity expansion theory in an elastic-plastic, strain hardening, compressible, layered material. He summarised theoretical results for penetration into concrete and rock, and compared them with results from other accepted predictive methods. In the case of concrete, good agreement with two common empirical relationships was obtained. The effect of varying target compressibility was considered. In the case of rock, reasonable agreement of predicted velocity history, deceleration and penetration depth was noted with a finite difference deformable body calculation, and with actual results from field tests. The effect on predicted penetration of varying the experimental parameters was discussed.

Butler (1975) discussed the practical use of cavity expansion theory in the penetration of projectiles into rock. The penetration parameters were discussed in detail. Methods of obtaining the necessary material constants from classifications based on standardised tests were discussed, as well as the correlations between simple in-situ tests and material constants e.g. Schmit hardness vs yield stress, Y, for various dry unit weights.

In addition, Butler proposed a modification function to the basic cavity expansion theory for a given nose projectile, to be used as a multiplier to p_i. This was

$$N_1 = \frac{2}{u^2} \int_0^{\psi=\phi(u)} \left[\sin^2 \psi + \frac{\sin^3\psi \cos^2\psi}{1-(1-u)\cos\psi} \right] (\cos \psi - 1+u)\, d\psi \quad \ldots 2.28$$

where $u = \frac{1}{2CRH}$

$$\phi(u) = \tan^{-1} \left(\frac{2u-u^2}{1-u}\right)$$

and CRH is the calibre radius head.

This equation, given without derivation or reference, was plotted as a graph of N_1 vs CRH (Figure 2.12), where CRH, the calibre radius head, is the ratio of the nose curvature radius to the projectile diameter. A computerised method of treating multi-layer targets was detailed.

Hadala (1975) compared the performance and ease of use of five predictive methods, as well as giving a good critical review of the assumptions behind each. The two methods which were most favoured were two already discussed, spherical cavity expansion theory and Sandia Corporation Empirical Formula. Only penetration of large projectiles into soil and rock was considered.

Bernard (1975) offered a deep penetration cavity expansion theory capable of dealing with multi-layer targets, and conical or ogival nose shapes, the latter being considered in a different way to Butler (1975). This was a generalised method, superceding the shallow penetration theory of Barnard and Hanagud (1975). The specific target materials discussed were snow with ice cover, frozen soil, concrete and aluminium.

Equation 2.20 was modified as follows so that target particle motion need not necessarily be normal to the cavity surface

$$p_i = \rho_{1p} (B_1 a \ddot{a} + B_2 v_p^2) \qquad \ldots 2.29$$

where v_p = target particle velocity, with normal and tangential components

The particle velocity in this equation was then related to the projectile velocity through a nose shape function, N_2.

For projectiles with a nose cone in the homogenous target, N_2 was developed as a function of the projectile dimensions and, in addition, target material properties. Ogive noses were considered as equivalent cones. For layered

targets, the value of N_2 was also influenced by the material properties of the next target layer.

The functional forms of N_2 were empirically obtained, but considered applicable to all rigid penetrators in all cohesive targets.

Shoiya et al.(1976) discussed the penetration of small steel spheres into thick epoxy targets, with impact velocities up to,and above,the dilational wave velocity of the resin. A system of wires cast into the target was used to determine the velocity history of the projectile, and a simple force law approach was used to analyse the data presented.

Kar (1978) examined the penetration problem empirically, and its implications for buried concrete structures. Penetrators of various cross sectional shapes were considered. A general relationship of the following form was proposed.

$$D = f(d_{pe}, m, v_o, N_3, E_p, \sigma_F) \qquad \ldots 2.30$$

where d_{pe} is the effective penetrator diameter, equal to

d_p for a solid cylinder

N_3 is a nose performance coefficient

E_p is the penetrator elastic modulus

σ_F is the uniaxial compressive strength of the target

Using regression analysis on existing results, an equation was obtained which was used to determine penetration depth. However, extra terms appeared in this equation, and their origin was not explained.

For earth materials and a solid cylindrical penetrator the equation given was

$$G_{(D/d_p)} = \frac{\alpha_2}{\sigma_F^{0.5}} \cdot N_3 \cdot \left[\frac{E_{pl}}{E_p}\right]^{1.25} \cdot \frac{m}{d_{pe}^{2.31}} \cdot \left[\frac{v_o}{1000}\right]^{1.25} \qquad \ldots 2.31$$

where $G_{(D/d_p)} = \left(\frac{D}{2d_p}\right)^2$ for $\frac{D}{d_p} \leq 2$

and $G_{(D/d_p)} = \left(\frac{D}{d_p} - 1\right)$ for $\frac{D}{d_p} \geq 2$ ... 2.32

α_2 is an empirical coefficient

E_{pl} is the actual penetrator elastic modulus as compared to the reference modulus of E_p

Relationships for N_3 were given for closed end and hollow circular (pipe) missiles, as well as equivalent circular forms for non-circular projectiles. Methods for the calculation of residual velocity were discussed, yielding a new impact velocity onto a buried structure, v_r.

From the fitting of a similar function to equation 2.30, for a solid cylindrical projectile penetrating concrete, Kar obtained

$$G_{(D/d_p)} = \frac{\alpha_3}{f'_c} \cdot N_3 \cdot \left[\frac{E_{pl}}{E_p}\right]^{1.25} \cdot \frac{m}{d_{pe}^{2.8}} \cdot \left[\frac{v_r}{1000}\right]^{1.80} \quad \text{... 2.33}$$

where $G_{(D/d_p)}$ is as defined earlier in equation 2.32

f'_c is the concrete compressive strength of a cylindrical specimen

Various equations for N_3 were given for different missile types.

For the concrete buried structure, the thickness of concrete necessary to prevent scabbing (t_s) or perforation (t_p) were discussed separately. Scabbing is defined as tensile failure of the rear target face, and perforation is the exit of the penetrator from the rear face of the target. For $3 \leq \frac{t_p}{d_p} \leq 18$, the following equations were given

$$t_p = a + 1.32d_p + 1.24D \quad \text{... 2.34}$$

$$t_s = a + d_p \left[\frac{E_p}{E_{pl}}\right]^{0.2} \cdot \left[2.12 + 1.36 \left(\frac{D}{d_p}\right)\right] \quad \text{... 2.35}$$

where a is half the maximum aggregate size

From the results of the tests given by Kar, the fit of all of these equations appears to be good.

Yew and Stirbis (1978) modified the dynamic cavity expansion theory. They considered a rigid conical penetrator, of half angle ϕ, whose tip produced a series of spherical cavity expansions as it moved through the target medium. The radii of the final cavities were governed by the nose geometry of the penetrator; that is, the envelope of the cavities conformed to the nose shape of the penetrator. This can be seen in Figure 2.13, where cavities initiated at O_1 and O_2 were considered to have reached the given size when penetration was d. The maximum cavity radius, a_{max}, occurred when the nose cone formed a tangent to the cavity at the nose cone corner. Thus a gap was predicted between the earth and the penetrator behind the nose cone: there is some experimental evidence suggesting this to be the case.

Three stages of penetration were considered

(i) Entry of the conical part of the penetrator

$$0 \leqslant d \leqslant l_n + \frac{d_p}{2} \tan \phi$$

(ii) Subsequent penetration

$$l_n + \frac{d_p}{2} \tan \phi \leqslant d \leqslant \text{target thickness}$$

(iii) Entering the interface between targets

Target material properties were assumed as in Figure 2.9, except that a single locking strain, e_1, was adopted for the target with an equivalent density of ρ_1.

Equations of motion for these three cases were developed. For a homogeneous target, the equation of motion for stage (ii) led to the following equation, from which depth of penetration may be obtained. (Stage (i) was considered negligible).

$$\frac{p_s}{2\rho_1 \sin^2 \phi B_2} \left[1 + \frac{2\pi\rho_1 \sin^2 \phi B_1 d_o{}^2 D}{m} \right] 8 \frac{B_2}{B_1}$$

$$= v_o{}^2 + \frac{p_s}{2\rho_1 \sin^2 \phi B_2} \qquad \ldots 2.36$$

where ϕ = cone half angle

$$B_1 = 1 - \frac{\alpha}{\delta^{2/3}},$$

$$B_2 = \frac{3}{2} - \frac{\alpha}{\delta^{2/3}}\left[2 - \frac{(1-\delta)^2}{(1-\alpha)}\right] + \frac{1}{2}\delta^{4/3}\left[1 - \frac{(1-\frac{\alpha}{\delta})^2}{(1-\alpha)}\right],$$

$$p_s = \frac{2}{3} Y \ln \delta + \frac{4}{9} E_t \left[\frac{\pi^2}{6} - \sum_{k=1}^{\infty} \frac{\delta^4}{k^2}\right] + \frac{4}{3} \beta E;$$

in which $\alpha = - e_{1p}$; $\delta = \alpha + 3\beta$ and $\beta = \frac{Y}{2(E-E_t)}$.

The obvious problem with this adaption of dynamic cavity expansion theory is that the a_{max} assumption is no longer valid with ogive noses. Comparisons with other predictive methods were carried out for two tests using large penetrators impacting tuff and limestone. The noses of these projectiles were ogival, and though not stated, it is apparent from the $\frac{l_n}{d_p}$ values given that the cone included by the ogive was used to calculate this. This approximation is likely to be reasonable for ogives with large CRHs, as the longer the ogival nose, the closer it becomes to a cone. Figure 2.14 shows the deceleration- depth predictions for two other methods, as compared to the above method and the experimental results for the limestone.

2.3 Stress Waves and Material Behaviour at High Strain Rates

This section is intended to give a general review of the type of behaviour to be expected from the constituent materials of the composite, under conditions similar to those existing during impact.

2.3.1 Viscoelastic Materials

Elastomers form part of a group of materials which are described as viscoelastic, because of the combination of viscous and elastic properties they exhibit. The relevant aspects of their behaviour can be summarised as follows (Davey and Payne, 1964)

(i) Very high strains are possible, which makes elastomers

efficient energy storers. For example, vulcanised rubber can store over 150 times more strain energy per unit weight than a hardened and tempered spring.

(ii) The modulus of elasticity increases with strain rate, and decreases with temperature. Four regions of behaviour exist. At very high temperatures or low strain rates, the elastomer exhibits a region of flow. With lowering temperature or increasing strain rate, the elastomer then displays, in sequence, rubbery elastic behaviour, transitional behaviour, and finally glassy behaviour.

(iii) Over a loading cycle, there is a hysteresis loss.

(iv) These properties vary with the amount of plasticisers and fillers present, and with the type of elastomer itself.

Much of the dynamic experimental work has been limited to the response to small repeated strains, i.e. vibration, which is not strictly applicable to this study of an elastomeric composite.

Linear viscoelastic models were developed as early approximations to viscoelastic behaviour. They are based on combinations of spring and dashpot models. The characteristic equations of these two elements are, respectively,

$$\sigma = Ee \qquad \ldots 2.37$$

$$\sigma = c_1 \frac{de}{dt} \qquad \ldots 2.38$$

where σ = direct stress

e = direct strain

E = Young's modulus of elasticity

c_1 = damping constant

t = time

A simple explanation of the various models is given by Goldsmith (1960).

The properties of materials at high strain rates are well illustrated by their response to stress waves. Obviously, linear propagation simplifies the analytical problems involved, and so much of the literature is concerned with this. The most popular types of linear experimental work use

(i) Cylindrical test specimen. This gives a means of finding propagation mechanisms in the material.

(ii) Disc shaped test specimen, sandwiched between cylinders of known properties. This gives a simple stress/strain/strain rate correlation.

(iii) Filamentous specimen. This allows both longitudinal and lateral strain waves to be examined.

Kolsky (1949) measured the stress/strain behaviour of rubber by method (ii) for a stress pulse of 20μs duration. Experimental and theoretical results are shown in Figure 2.15.

To obtain the theoretical curve, Kolsky used the equation

$$\sigma = Ee + A\int_0^t \exp\left[\frac{-(t-\bar{\tau})}{\alpha}\right]\frac{de}{d\bar{\tau}}\,d\bar{\tau} \qquad \ldots 2.39$$

where α and A are coefficients chosen for best fit, as is Young's modulus E, and $\bar{\tau}$ is the time of a past stressing event.

As can be seen from Figure 2.15 the fit of data to theory was not good.

Kolsky (1956) attempted to describe the propagation of stress pulses in three plastics. He showed that if the input stress pulse is sinusoidal, the changing pulse shape can be predicted by means of a numerical Fourier synthesis, assuming that the effects of the lateral inertia of the rod are negligible. Also if the damping is constant and small, the effects of damping and velocity change can be combined into a single parameter, which applies to all such viscoelastic solids.

His theoretical treatment was for one-dimensional propagation in bars,

but some experimental results were obtained for spherical waves in blocks of varying thickness.

In recent years the mathematics of non-linear viscoelasticity have been developed, but its inherent complexity and difficulty of application is high. Consequently, the non-linear interpretation of real viscoelastic behaviour is still in the empirical state, and therefore is not reviewed here.

2.3.2 Rock and Particulate Media

Selig (1964) discussed the relevance of past theory and experiment in wave propagation to soil media. The basic theories considered were elastic, viscoelastic, plastic, locking and non-linear inelastic.

Experiments were carried out involving the dynamic loading of a column of uniformly graded sand with varying confining pressure and density, using a pendulum and shock wave apparatus. The pendulum experiment showed that stresses above the static yield strength could be developed by dynamic loading. The stress-strain curve was essentially the same as for static loading, but slightly steeper.

From the shock tube experiments, wave velocity, peak stress attenuation, and slope change of the shock front were obtained. The author discussed the relevance of the wave theories to the experiments, and concluded that the non-linear inelastic model provided the best option. The method of impulses was used to calculate predicted wave profiles and attenuation, which were compared to the experimental results. Rate dependent effects were not included in the theory, and the comparison with the experimental results suffered because of this.

Silverstein (1969) considered the impact of a rigid body with a rigidly contained granular bed. He described well the quasi-static stress-strain behaviour of granular materials. Typical results are shown in Figure 2.16. The precrush region corresponds to deformations at the contact points between the grains. The transition region begins with the fracture of the

grains into smaller particles. These then slide into the interstices between the grains. Once a more compact configuration is reached, the postcrush region prevails.

By assuming the following equations, an analytical model was developed. Although they refer to the quasi-static case, they are assumed to apply to the dynamic case also.

$$\text{Precrush } e = \frac{n_o - n}{1-n} = a n_o \left(\frac{\sigma}{E}\right)^b \qquad \ldots 2.40$$

$$\text{Postcrush} \qquad \frac{\sigma}{\sigma_{cr}} = A \exp\left[k \frac{(n_{cr} - n)}{n} \right] \qquad \ldots 2.41$$

where e is axial strain

n is porosity

n_o is initial porosity

n_{cr} is porosity at crushing

σ is compressive stress

σ_{cr} is compressive stress at which particles are crushed

A, k, a, b are bed constants

The equations governing impact, based on a rigid-plastic hypothesis, were developed. From these, equations were found relating distance along the sand bed to porosity after the impact transients had ended. The effect of such an impact on porosity can be seen in Figure 2.17.

The theoretical model is only valid if $v_c << v << c_{cr}$, where v_c is the critical velocity at which crushing is initiated and c_{cr} is the propagation velocity of an elastic wave front through the granular bed when subjected to crushing stress, σ_{cr}.

Grain crushing was propagated furthest for an impact velocity of 61 m/s. At impact velocities above this, the length of the damaged region decreased because the increase in bed density in the damaged region more than offset the incorporation of previously undamaged particles into the

damage zone.

The author admitted that the predicted porosities were likely to be low, as strain-rate effects were not taken into account.

Ricketts and Goldsmith (1970) determined by experiment the static and dynamic properties of rock materials and concrete-like composites. Transient loadings were achieved by the impact of a steel ball on a ballistically suspended Hopkinson bar composed of the material in question. Impact velocities ranged up to 254 m/s. The results were, in summary,

(i) some rocks caused virtually no change in pulse shape

(ii) attenuation to an increasing degree was observed in volcanic rocks, with little change in wave profile.

(iii) sandstone caused a marked change in pulse shape

(iv) artificial composites behaved similarly to normal concrete, with only minor attenuation and no dispersion of the transient.

Lovel et al.(1974) investigated the effect of a point impulse on spheres and thin discs of perspex. By geometrical means, they predicted fairly accurately the fracture of spheres by the reinforcement of tensile stress waves. The thin disc was found not to be analagous to the sphere, because the plane end surfaces of the disc received most of the energy and did not transmit it in the same manner.

Daniel and Rowlands (1975) used high speed photography, strain gauges and isochromatic fringe methods to investigate wave and fracture propagation in rock media. The effects were produced by detonating a small charge at the centre of the edge of a rectangular specimen.

Wave propagation velocities were confirmed by the experiments. The pulse was found to exhibit appreciable attenuation without dispersion, and this attenuation was separated into material and geometrical parts. This enabled the material loss tangent, tan δ, to be found from the relation

$$\tan \delta = \frac{k_A \lambda}{\pi} \qquad \ldots 2.42$$

where k_A = an attenuation coefficient

λ = pulse wavelength

Strain-depth and displacement-depth results were obtained from the experiments. The propagation of the fracture zone did not, however, agree with predictions. The reason suggested for this was that except very locally to the explosion, the failure was caused by the tensile tail of the pulse.

Lundburg (1976) attempted to evaluate the energy absorbed in dynamic rock fragmentation. From measured pulses in a split Hopkinson bar he determined the various energies involved (incident energy, reflected energy, transmitted energy) and hence calculated the absorbed energy. This was found to increase when the stress reached a critical value. For Bohus granite the critical stress was 1.8 times the static compressive strength, and for Solenhofer limestone the factor was 1.3. Rigid-plastic and linear-elastic models were analysed. The first model gave the best correlation with experimental results when the degree of fragmentation was low and the second when the degree was high. It is interesting to note that the mechanisms of brittle failure can be simply represented by analogy with plasticity theory.

2.4 Applicability of Existing Work to the Composite

Descriptions of penetration mechanics have used the following approaches

(i) empirical

(ii) assumed force law

(iii) analytical

(iv) numerical (using computer codes)

The first two categories represent quite straightforward methods of gaining penetration predictions. The parameters must be determined from penetration experiments, and application of the resultant formulae is not valid in any other context. This is because the parameters are not defined explicitly in terms

of the constitutive properties of the medium and projectile characteristics. However, such methods usually show good results within these bounds.

In the analytical approach, constitutive and continuum equations are used to describe the event, and, ideally, are solved in a closed form to produce predictions of depth, deceleration,etc. However, this type of solution has not been achieved without a high degree of simplification, such as in dynamic cavity expansion theory.

Numerical approaches are much favoured at present, but require a high degree of expenditure in time and money. However, for situations using materials with well defined properties offering a high degree of reproduceability, their value is apparent.

The latter two methods have only been developed so that they can cope with homogenous materials, possibly in layers. Heterogenous materials such as concrete have been considered, but have been treated as homogeneous; generally, the projectile sizes used have been orders of magnitude larger than the aggregate size. In the case of the composite in this study, the aggregate size used was similar or about one order of magnitude larger in terms of mass than the projectile. This meant that the situation could not realistically be simplified as homogenous or at the other extreme, layered.

Hence it was necessary to use either an empirical or force law approach. In the literature, functions of impact velocity were normally used to describe deceleration. By varying impact velocity, or observing the velocity history in the target, answers could be obtained for deceleration and penetration depth.

However, the widely differing material properties of the two main constituents of the composite meant that a deceleration history averaged between motion in these two constituents would be of limited use from any theoretical viewpoint. Also, in practice, the material thickness would be based on a maximum impact velocity (near point blank range, high velocity ammunition).

Hence penetration variation for a given impact velocity are of prime importance. The complex effects of the possible target variables on penetration was examined using response surface theory, a method whereby these variables could be altered within a framework planned for multiple polynomial regression analysis. This method is described in detail in Chapter 4.

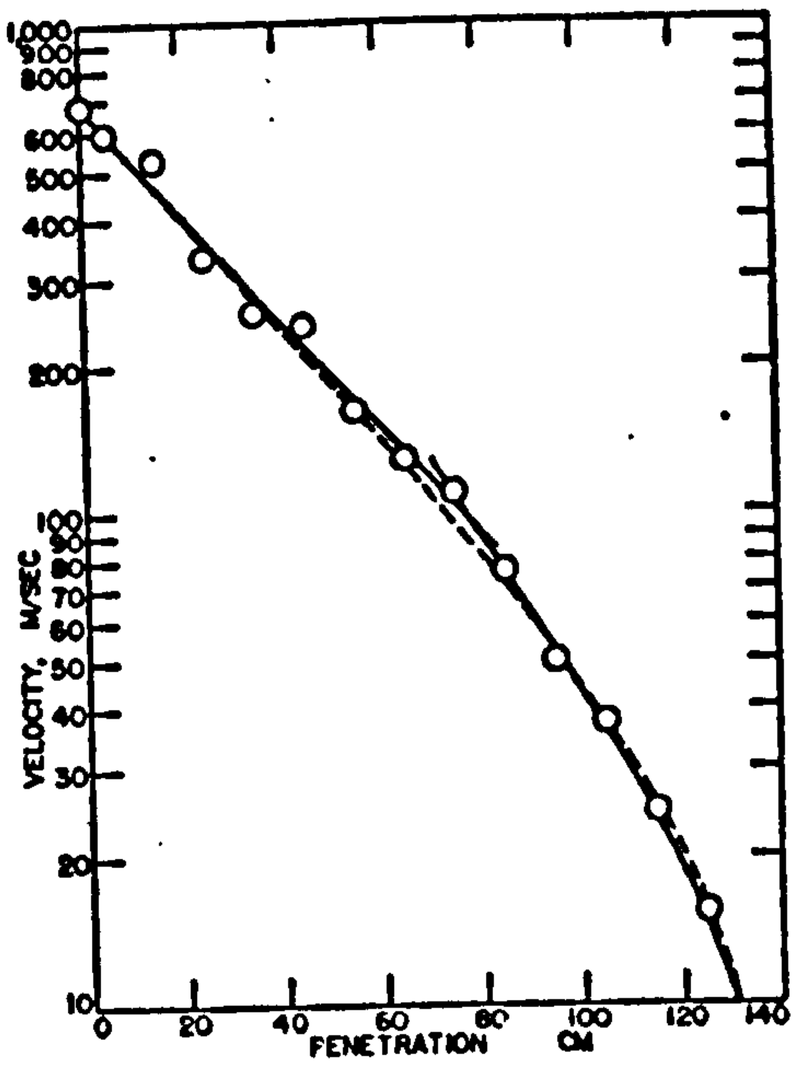

FIGURE 2.1 VELOCITY vs PENETRATION FOR CONVENTIONAL (DOTTED LINE) AND PROPOSED (SOLID LINE) THEORIES
After Allen et al (1957a)

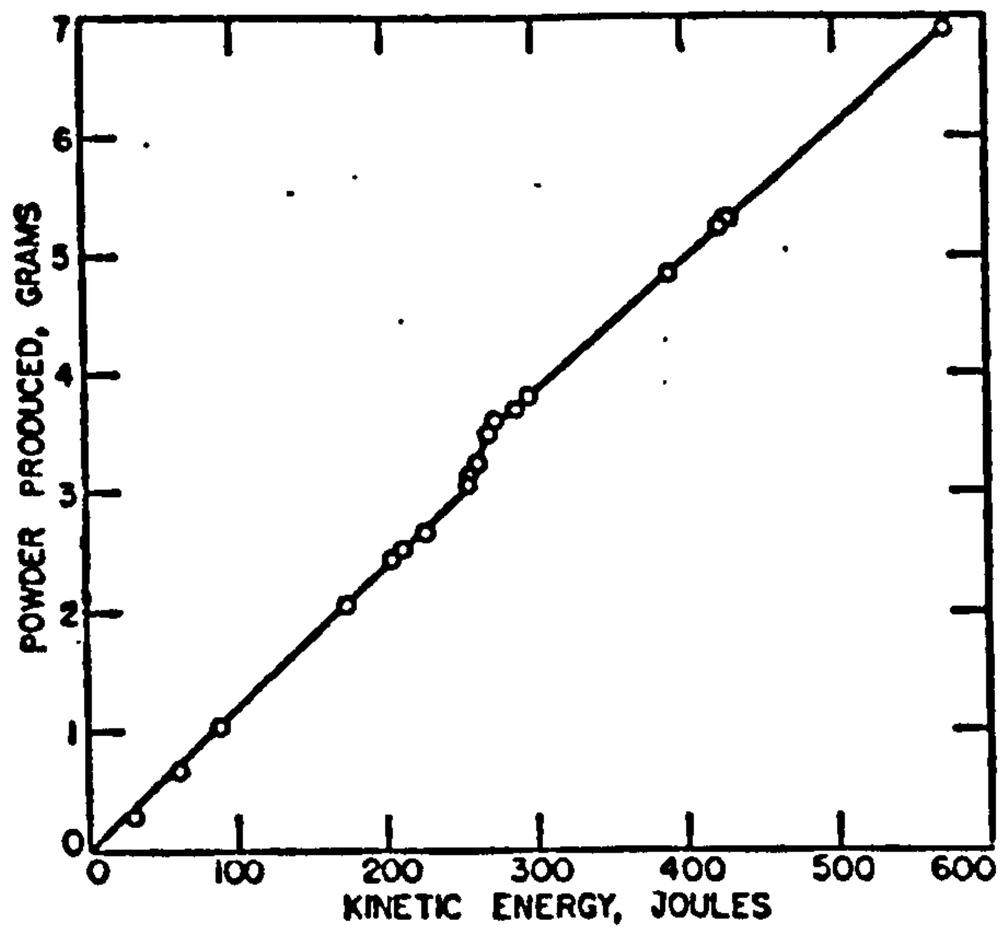

FIGURE 2.2 POWDER PRODUCED DURING PENETRATION vs INITIAL KINETIC ENERGY OF PROJECTILE
After Allen et al (1957b)

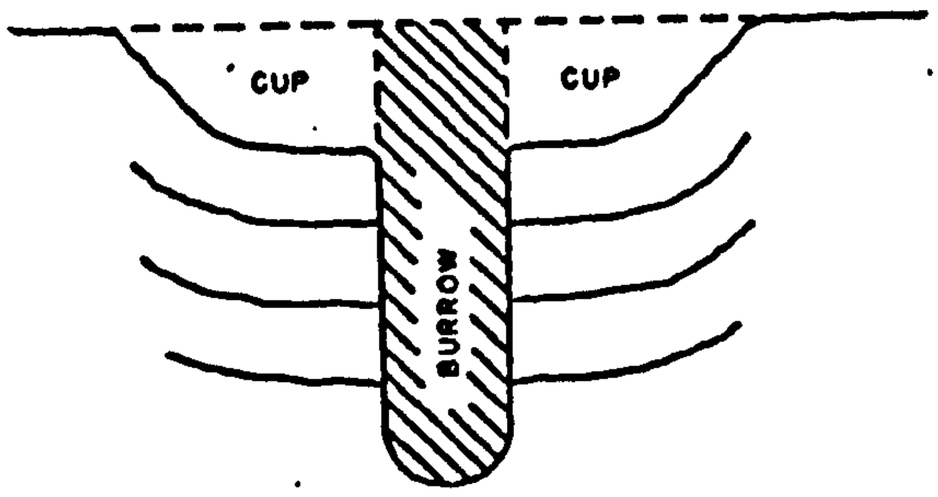

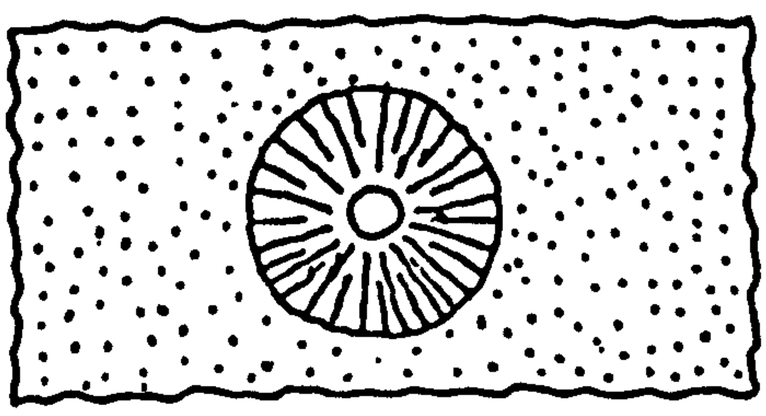

FIGURE 2.3 CRATER IN SANDSTONE FROM SPHERICAL STEEL PROJECTILE
After Maurer & Rinehart (1960)

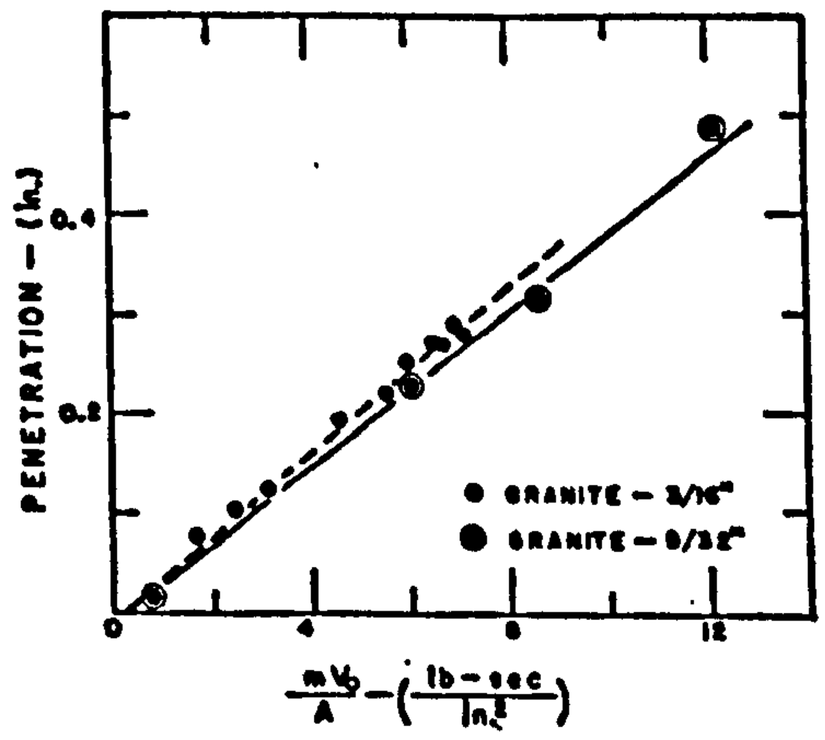

1 in. = 25·4 mm.
1 lb-sec/in^2 = 7·05 × 10^{-4} kg-sec/mm^2

FIGURE 2.4 PENETRATION vs mv_o/A_p FOR CRATERS PRODUCED BY SPHERICAL STEEL PROJECTILES
After Maurer & Rinehart (1960)

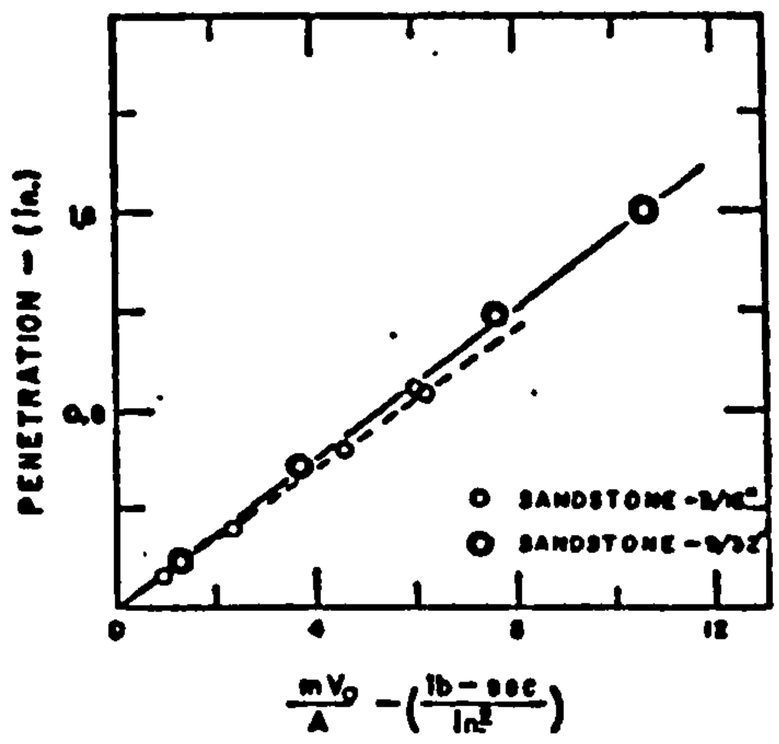

CONVERSION FACTORS AS FIGURE 2.4

FIGURE 2.5 PENETRATION vs mv_o/A_p FOR CRATERS PRODUCED BY SPHERICAL STEEL PROJECTILES. After Maurer & Rinehart (1960)

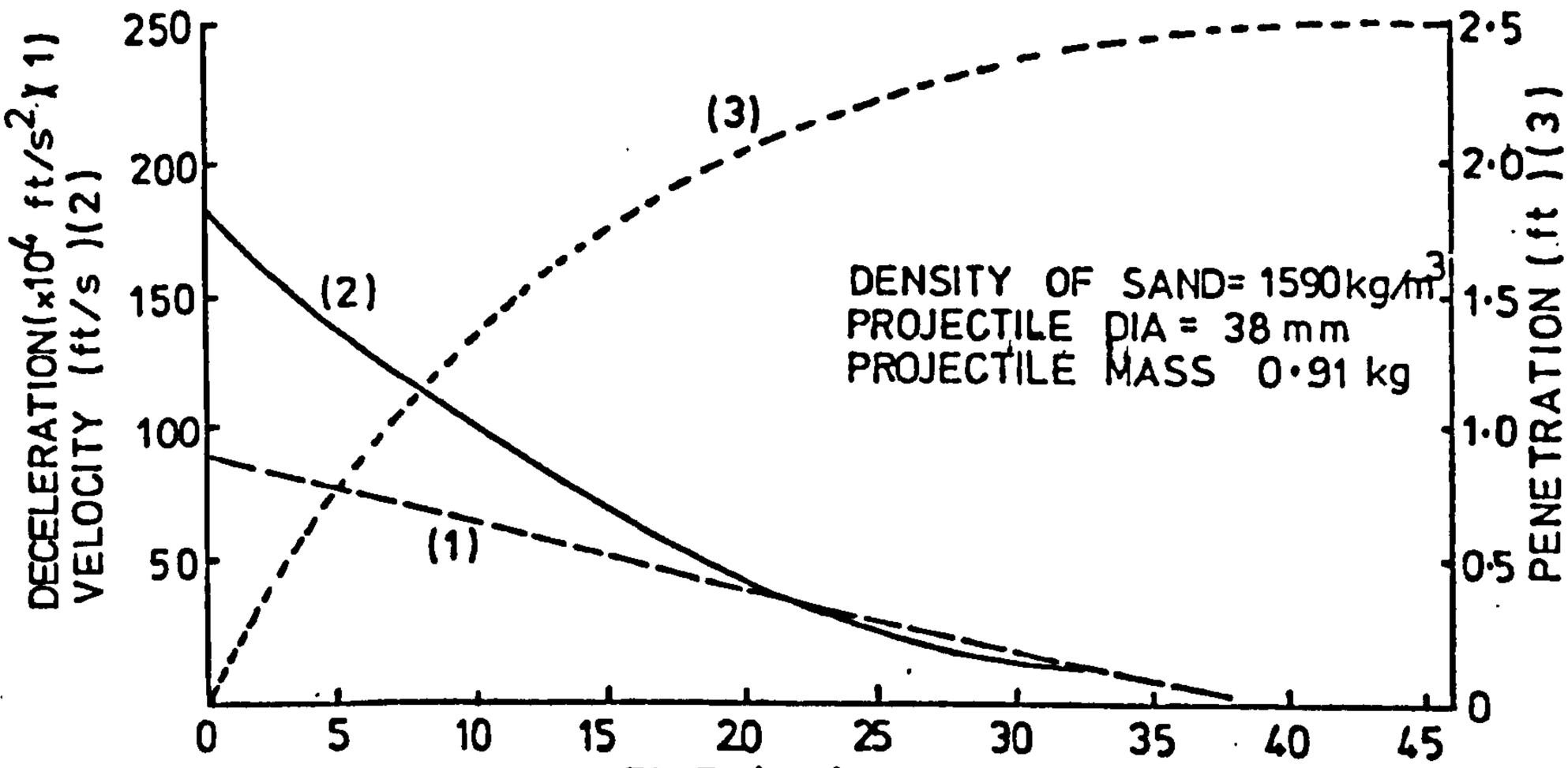

FIGURE 2.6 GRAPHS OF DECELERATION, VELOCITY, AND PENETRATION FOR SAND. After Thompson (1966)

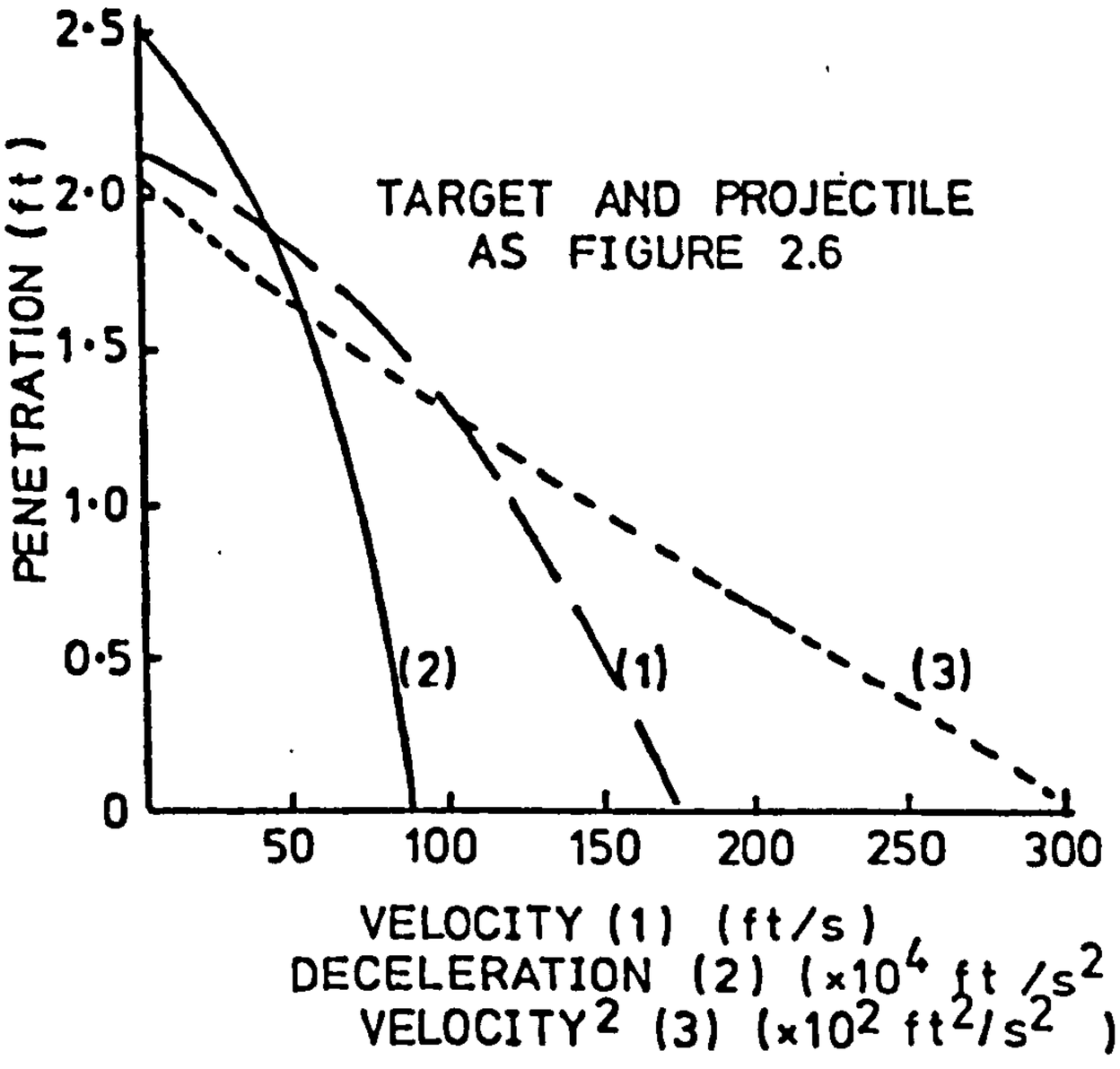

TARGET AND PROJECTILE AS FIGURE 2.6

1 ft = 0·305m
1 ft/s = 0·305m/s
1 ft²/s² = 0·093m²/s²
1 ft/s² = 0·305m/s²

FIGURE 2.7 GRAPHS OF VELOCITY, DECELERATION, AND VELOCITY² AGAINST PENETRATION FOR SAND
After Thompson (1966)

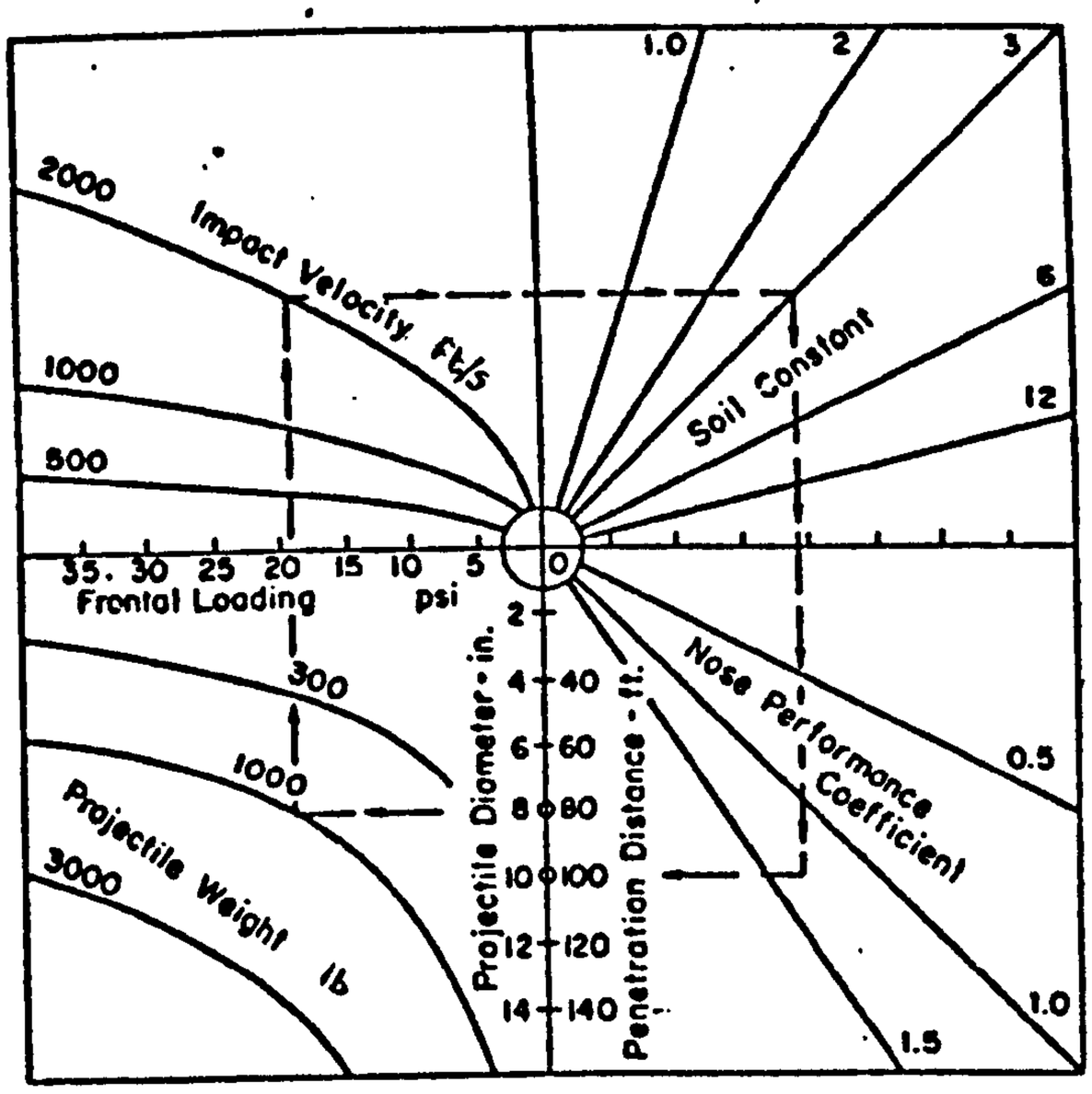

1 lb = 0·454 kg
1 psi = $4 \cdot 38 \times 10^{-3}$ N/mm^2
1 ft = 0·306 m
1 in = 25·4 mm
1 ft/s = 0·305 m/s

FIGURE 2.8 PENETRATION PREDICTION NOMOGRAM
After Young (1969)

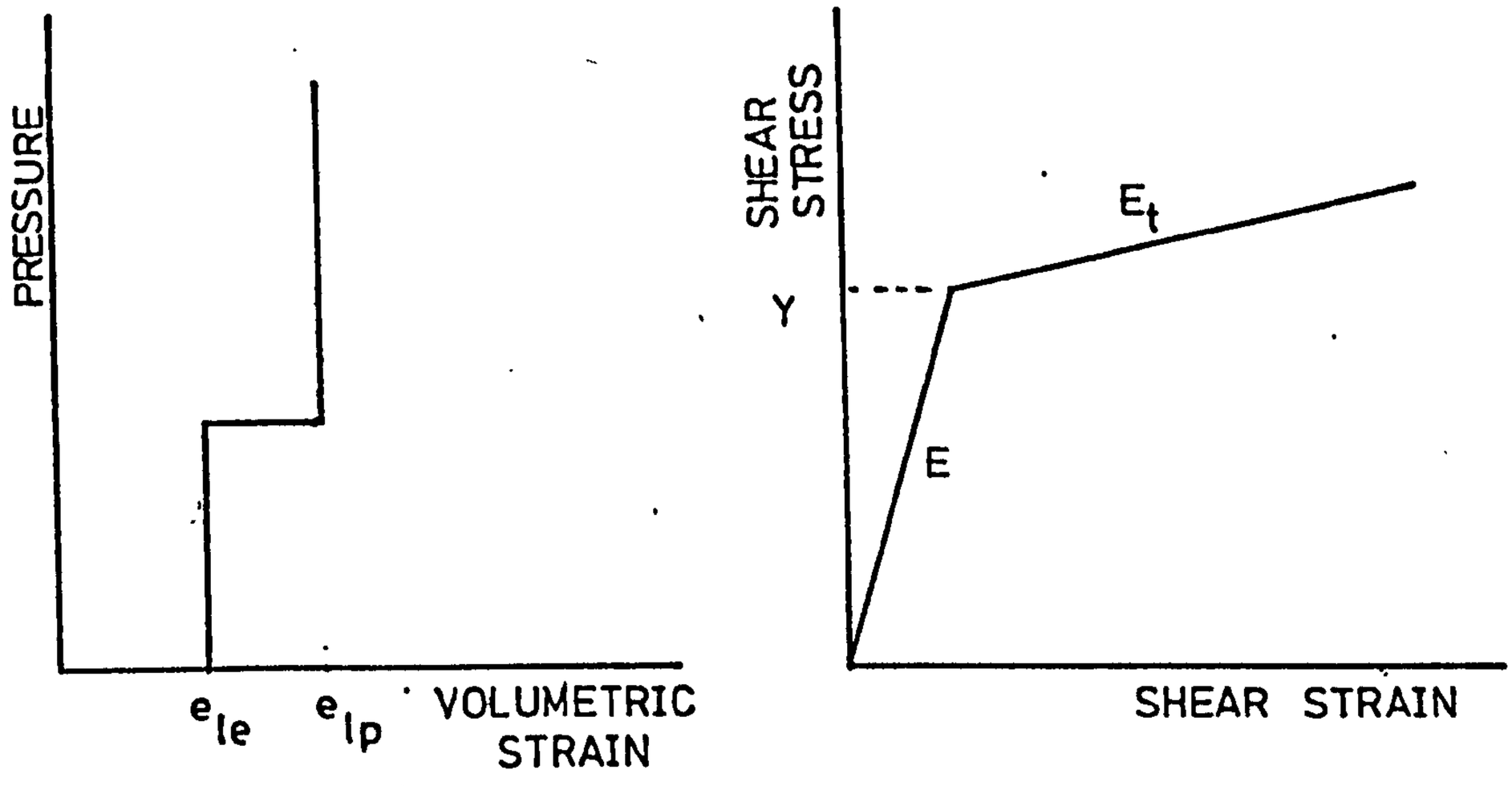

DILATATION SHEAR

FIGURE 2.9 IDEALISED STRESS-STRAIN CHARACTERISTICS FOR A LOCKING ELASTIC-PLASTIC MATERIAL
After Hanagud & Ross (1971)

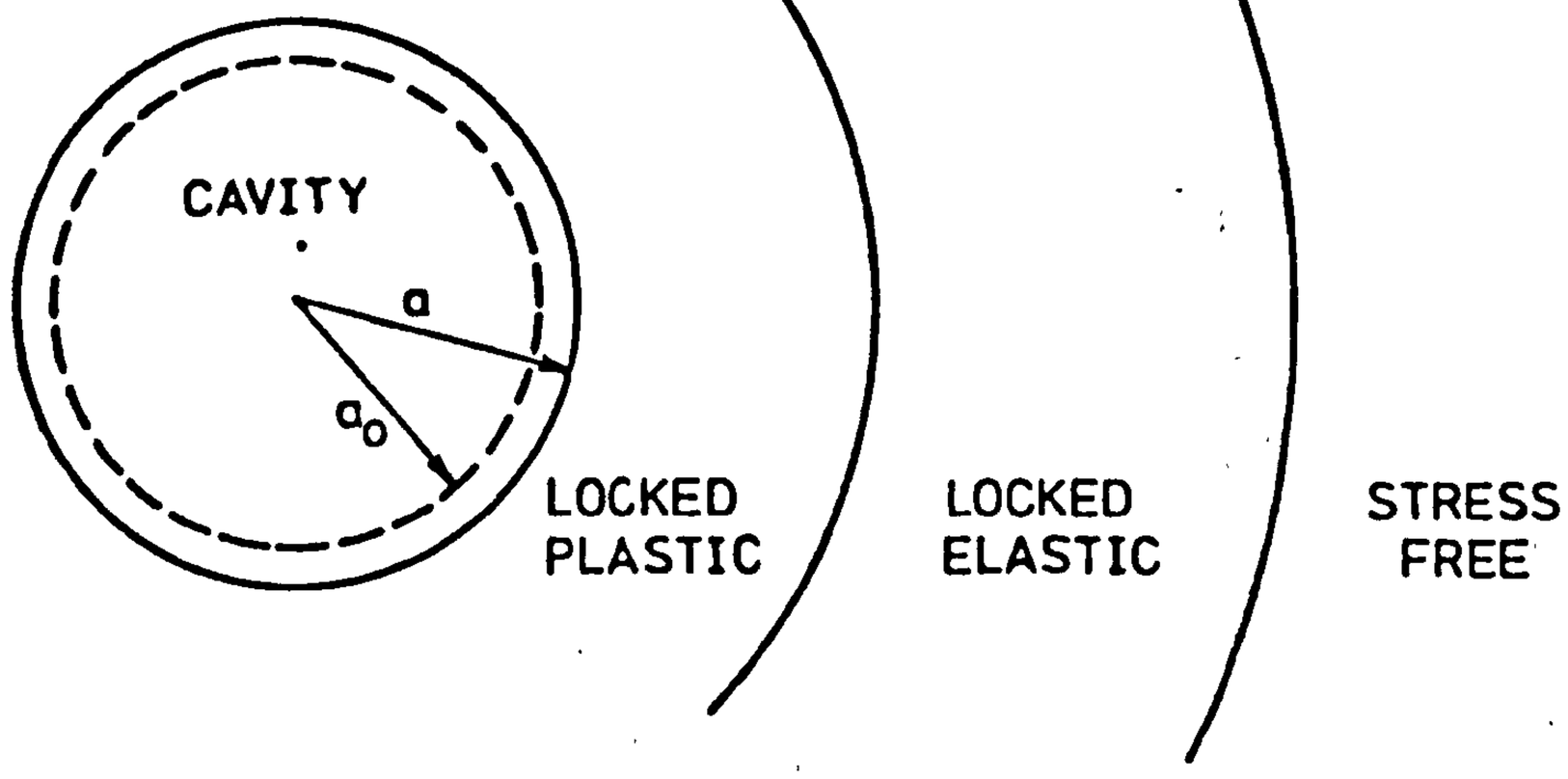

FIGURE 2.10 DYNAMIC CAVITY EXPANSION PROBLEM FOR A LOCKING ELASTIC PLASTIC MATERIAL
After Hanagud & Ross (1971)

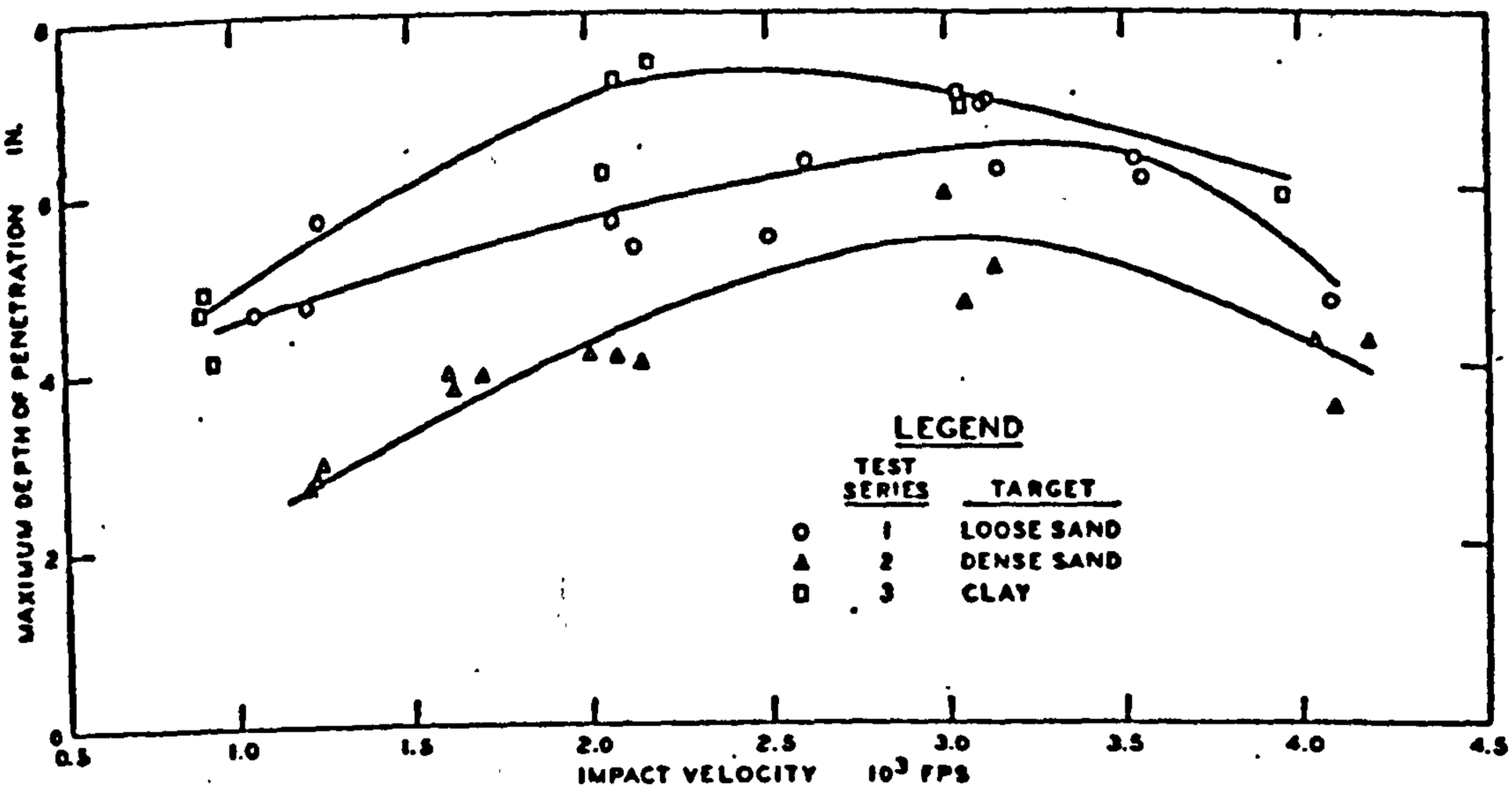

STEEL FRAGMENTS

1 in = 25·4 mm
1 ft/s = 0·305 m/s

BRASS FRAGMENTS

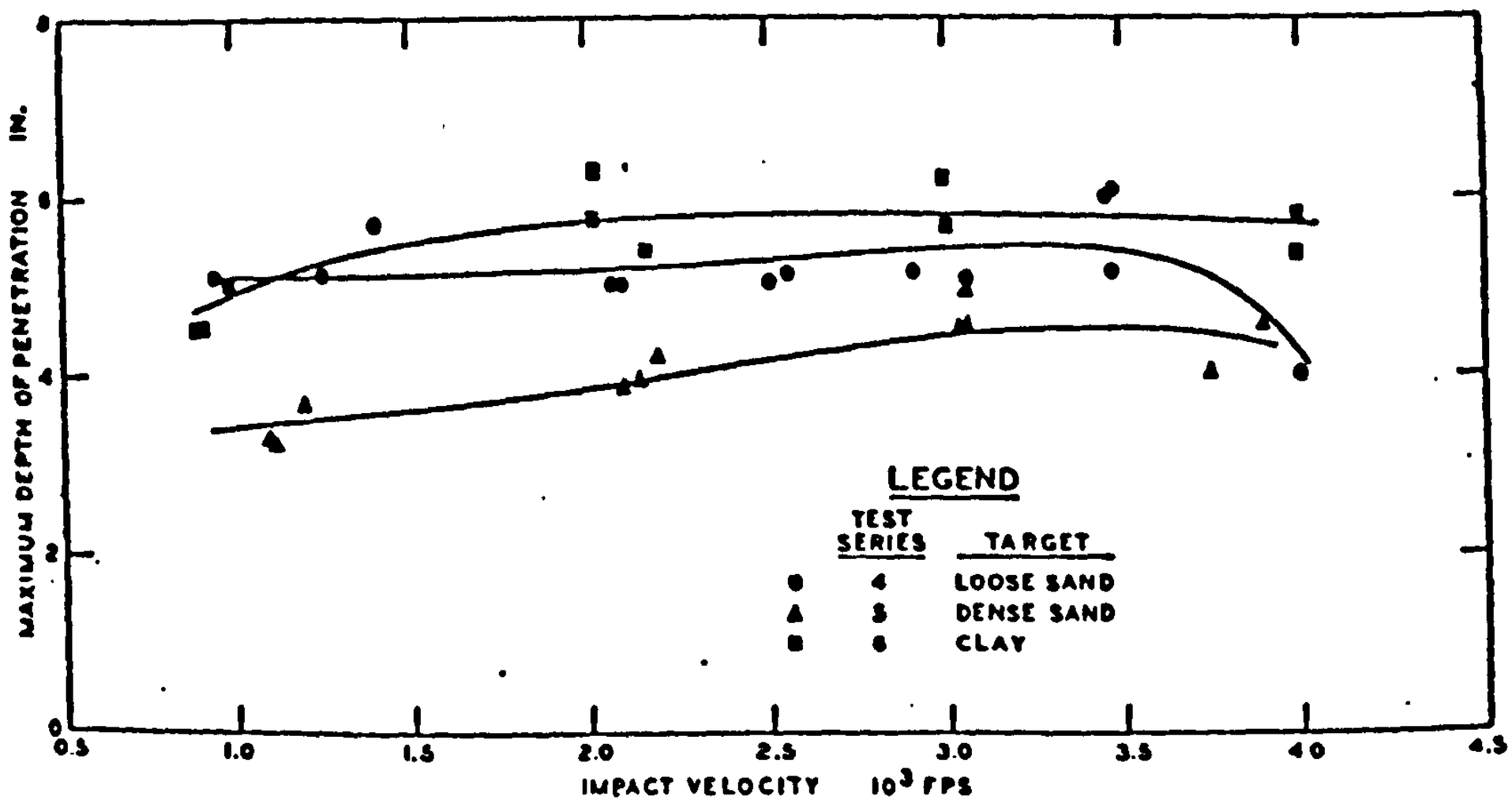

FIGURE 2.11 MAXIMUM DEPTH OF PENETRATION vs IMPACT VELOCITY FOR STEEL AND BRASS FRAGMENTS
After Rohani (1972)

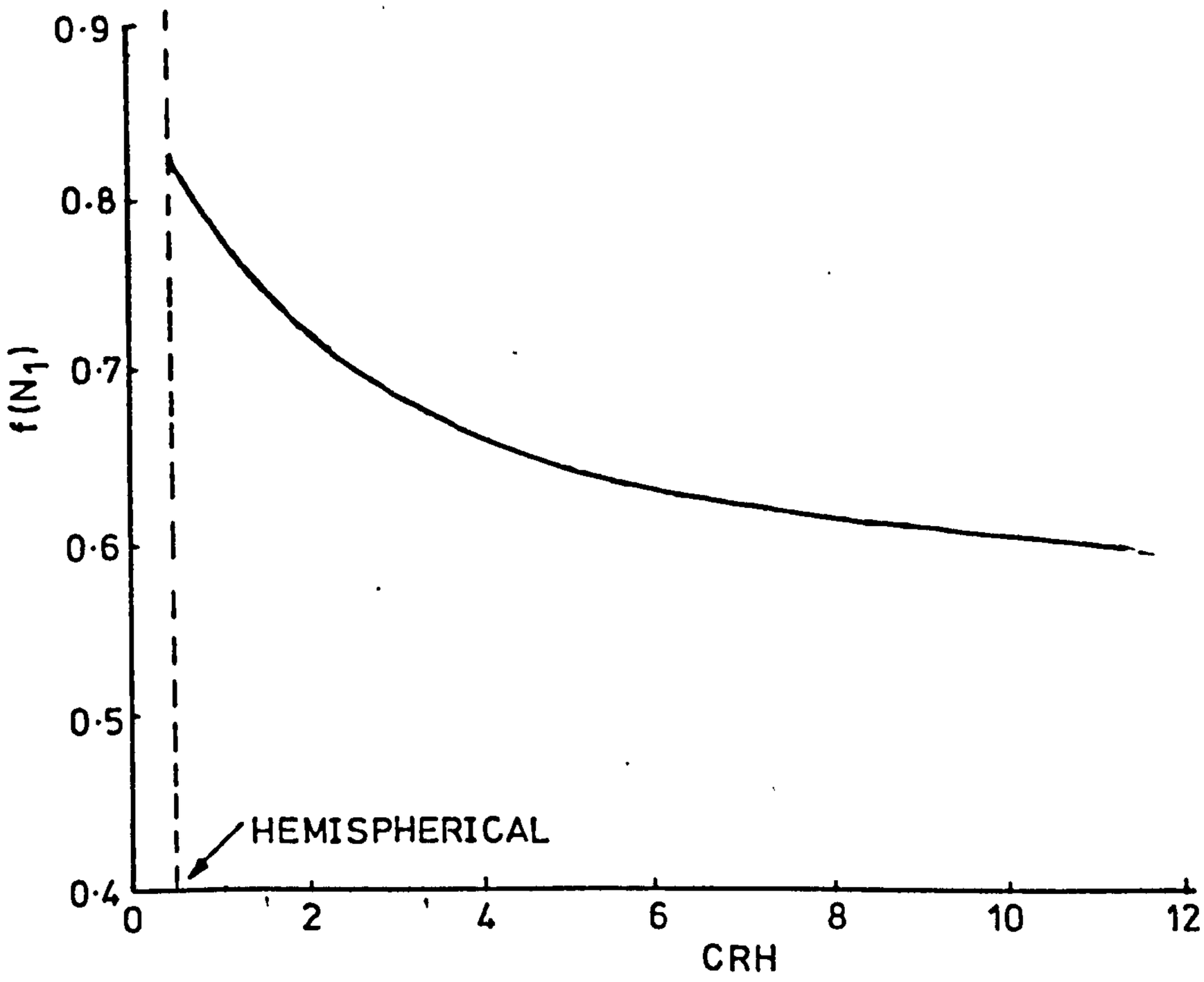

FIGURE 2.12 EFFECT OF CALIBRE RADIUS HEAD ON NOSE PERFORMANCE COEFFICIENT. After Butler (1975)

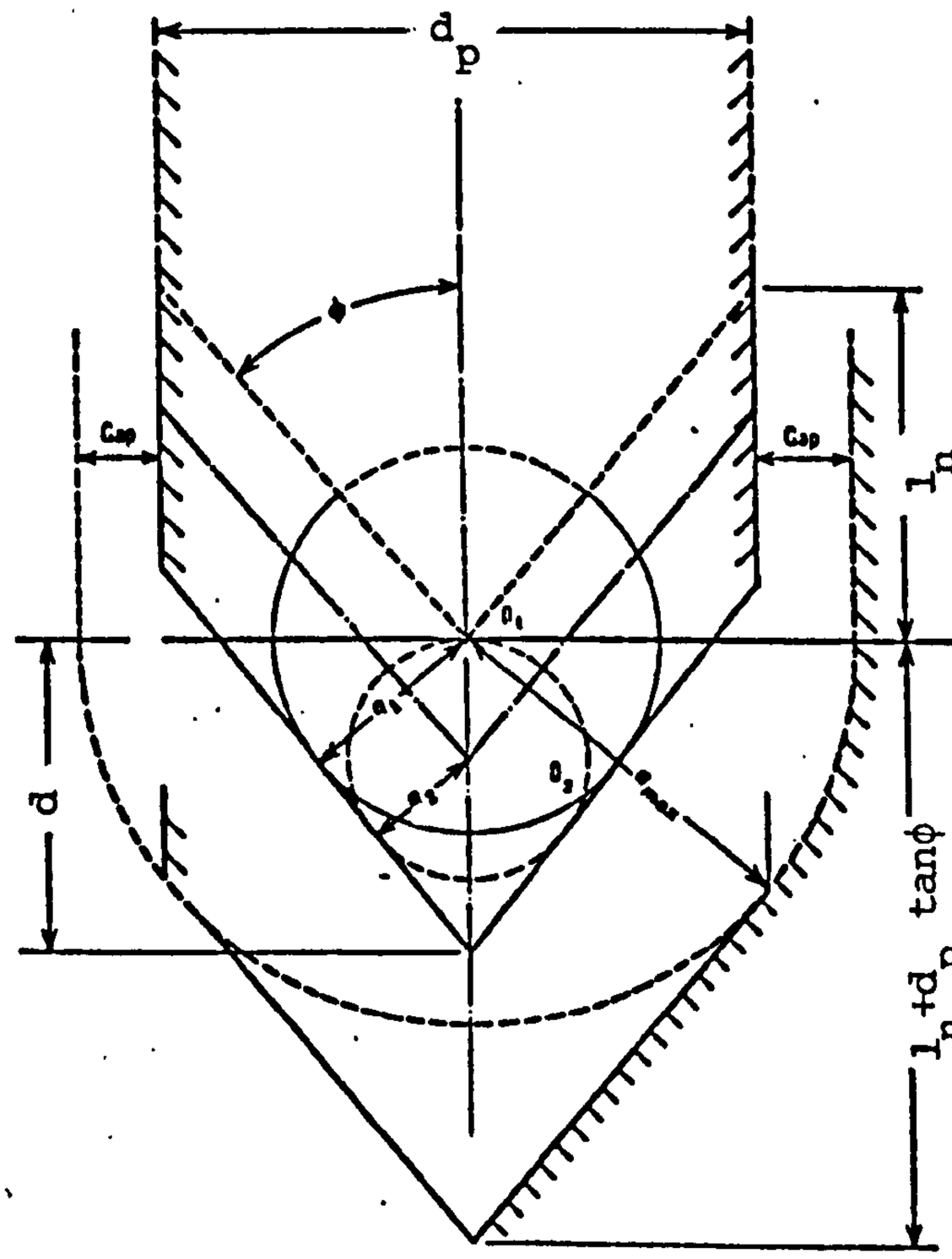

FIGURE 2.13 PENETRATION MODEL
After Yew & Stirbis (1978)

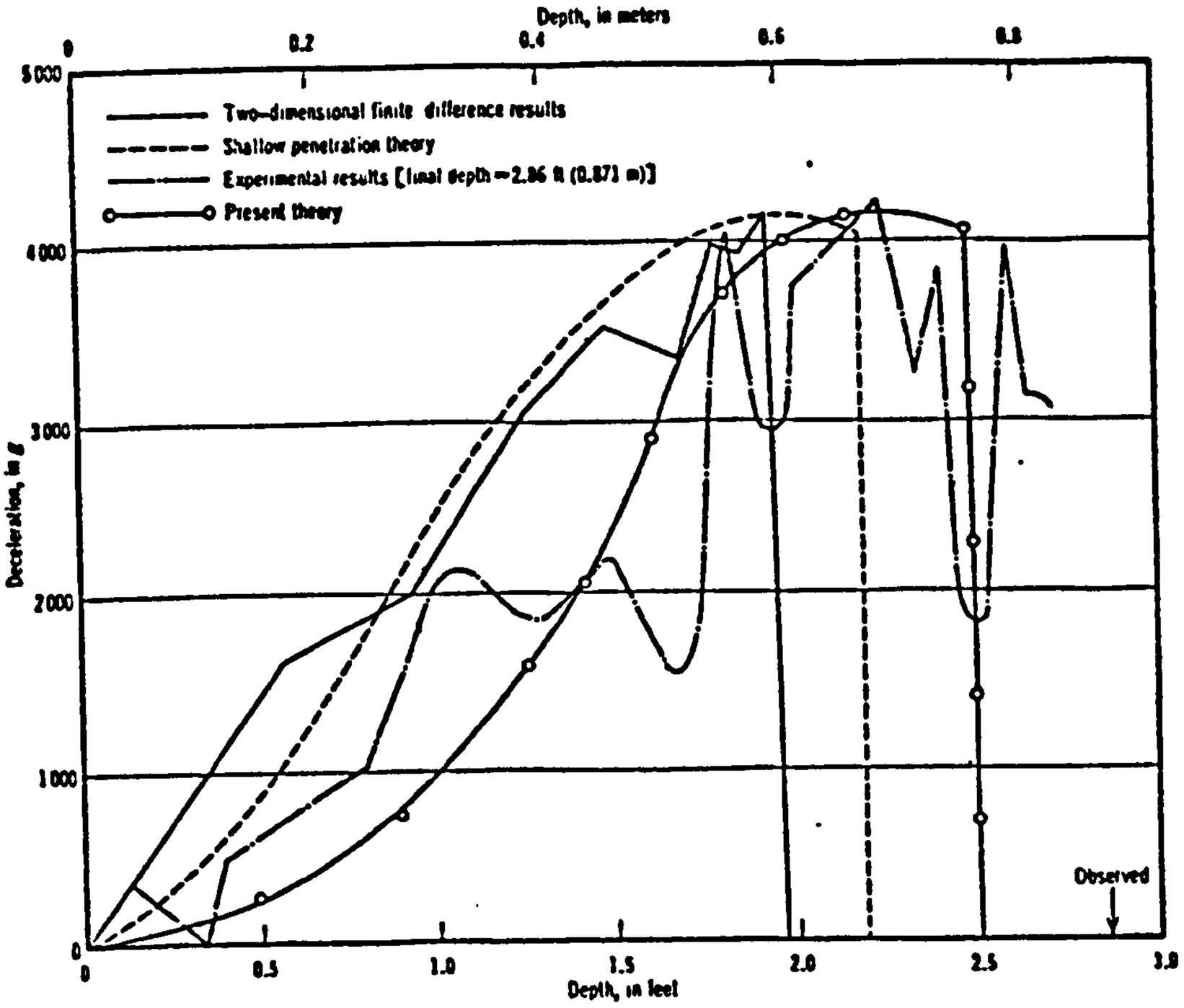

FIGURE 2.14 PROJECTILE DECELERATION vs DEPTH IN MADERA LIMESTONE. After Yew & Stirbis (1978)

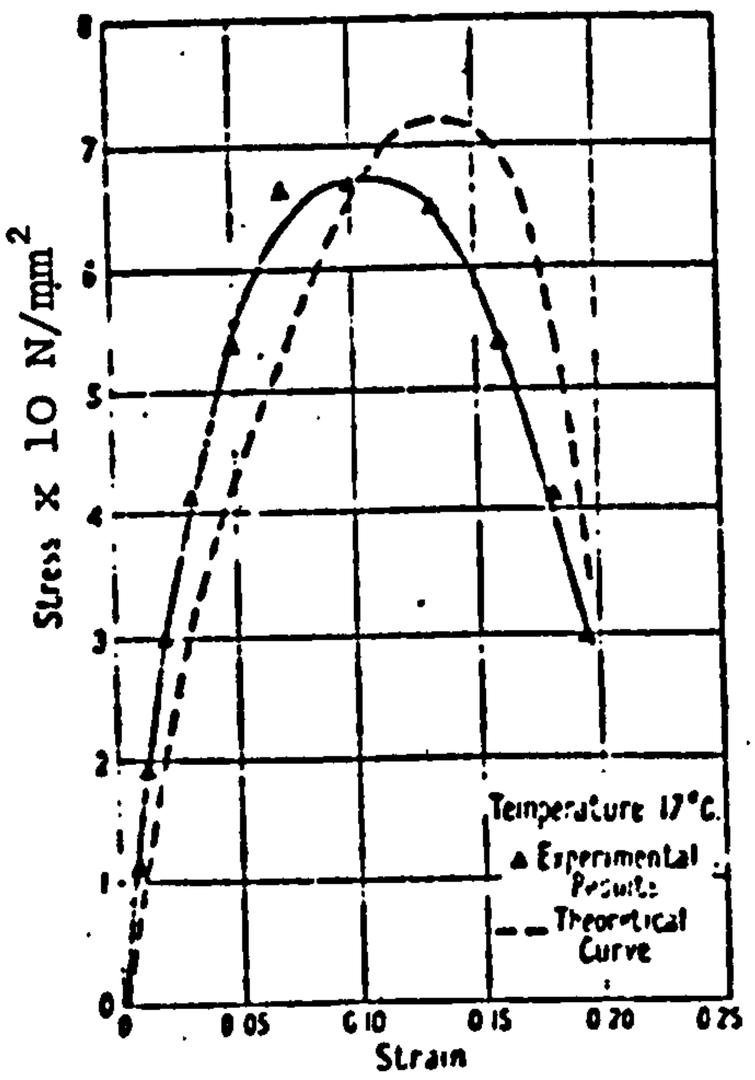

FIGURE 2.15 DYNAMIC STRESS-STRAIN CURVE FOR NATURAL RUBBER
After Kolsky (1949)

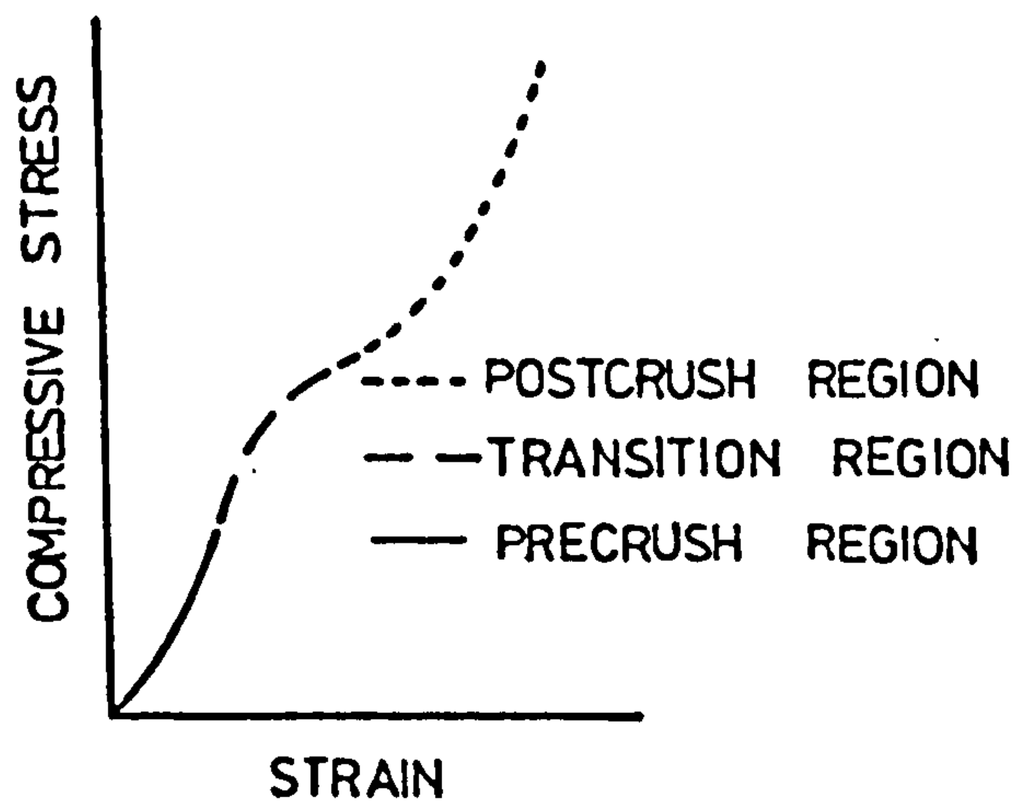

FIGURE 2.16 GENERAL SHAPE OF STRESS-STRAIN CURVE FOR GRANULAR MATERIALS IN ONE DIMENSIONAL COMPRESSION
After Silverstein (1969)

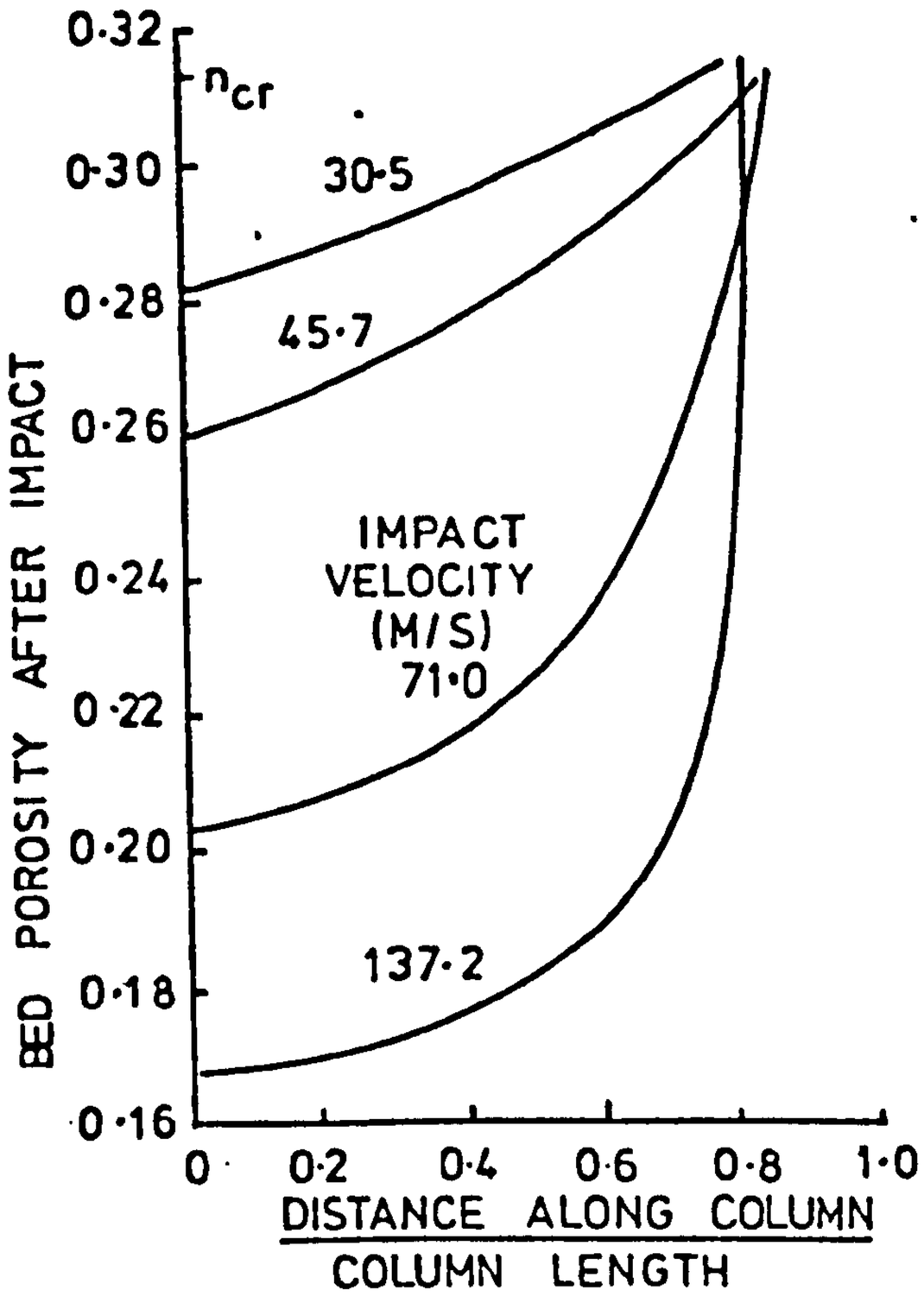

FIGURE 2.17 BED POROSITY DISTRIBUTION AFTER IMPACT FOR 20 - 40 MESH OTTAWA SAND. After Silverstein (1969)

CHAPTER 3

MATERIALS, EQUIPMENT AND PROCEDURES

3.1 Test Materials

The composites examined were produced by mixing varying proportions of fines, rock aggregates and polymers (elastomers).

3.1.1 Fines

The fines used in the composite were Zone II or Zone III sand, specifications for which are given in BS 822 : Pt 2 : 1973.

3.1.2 Rock Aggregate

The types of rock aggregate used were rounded river gravel, crushed basalt, crushed limestone and, to a limited extent, crushed hornfels. The relevant BS 812 : Pt 2 : 1975 values for these aggregates are shown in Table 3.1. All of these values were obtained from the suppliers, except for % voids. This was determined by experiment using a cylinder, 300 mm diameter and 300 mm high, and the method given in BS 812 : Pt 2 : 1975. In addition, similar tests to find the % voids were carried out using 152 mm (6") cube moulds which were used in target preparation. These tests showed an increase in measured voids resulting from using a smaller container size than the standard; the 152 mm cube moulds had only 0.16 of the volume of the vessel used to obtain the BS value of % voids.

Obvious rock properties for comparison with penetration behaviour are tensile and compressive failure stresses, and modulus of elasticity. Attempts were made to directly measure the elastic properties of the basalt and limestone. Samples of the rock, approximately 0.005 to 0.01 m^3, were obtained from the quarries after blasting, but before crushing, and 25 mm diameter rock cores taken from them. Unfortunately, all of the cores were found to be badly cracked, and those tests were abandoned. It is likely that this cracking was the result of the stress waves produced by quarry blasting, hence making it impossible to obtain unweathered samples without these faults. However, such faults are unlikely to seriously weaken the crushed rock as they would form natural failure planes during the crushing process. Hence properties of the aggregate, not the parent rock, had to be used.

The values of aggregate crushing value, impact value, and specific gravity for the rock types used may be put into perspective by comparison with the ranges of values in Table 3.2 taken from Road Note 24 (1959). These values were determined from a large number of samples of a wide range of rock types.

The river gravel was predominately quartzite and quartz, with small proportions of other rock types including flint, sandstone and limestone. The particles of the predominant rock types were rounded or irregular, but the minority rock type particles were of all shapes. A detailed description of the aggregate is not feasible because of its variability. Very little dust was present, because of the aggregate's mode of deposition from moving water which carried away the fines. The gradings supplied were 6-20 mm, 20-30 mm and 30-40 mm. Subsequent sieving, described later in the chapter, showed these gradings to be very approximate, as were the gradings of all the other rock types supplied.

The crushed basalt was a fine grained olivine basalt, dark greyish green in colour. The aggregate particles were angular. There was a significant amount of dust present, but much of it was removed by subsequent sieving. The rock was obtained in gradings as follows: 6-10 mm, 10-14 mm, 14-20 mm, 20-28 mm. 28-40 mm.

The crushed limestone was a fine grained sedimentary rock, mid grey in colour and angular in shape. The amount of dust present was similar to the basalt, and the gradings obtained were also as above.

The crushed hornfels was obtained in one relatively small sample. It was a diabase hornfels, metamorphic in origin, and dark greenish grey in colour. The particles were angular in shape. A small amount of dust was present, but much less than with the basalt and limestone. The size obtained was the maximum size available: 16-22 mm.

3.1.3 Elastomers

Synthetic polymers are divided into two classes, thermoplastic and thermosetting. The former can be softened repeatedly by the addition of heat, whereas the latter cannot. In elastomeric forms of both polymer types, the

high extensions possible are mainly due to uncoiling and unfolding of long chain molecules. In thermoplastic elastomers, these chains are bonded to each other by Van der Waals forces, which are overcome by heating, yet re-assert themselves on cooling. Thermosetting chain molecules, however, are linked by covalent bonds, which cannot be reverseably overcome.

This study required a commercially available cold curing polymer, and all of those examined were of the thermosetting variety. The types which were examined, but for various reasons not used in the main penetration test program, are listed in Table 3.3, with general manufacturers' and observed data. In addition, the reasons why they were unsuitable are given.

The 'ideal' material should have the following properties

(i) low cost

(ii) low viscosity

(iii) gel time adequate for casting

(iv) thereafter, a short time to cure at room temperature

(v) elastic behaviour at strain rates occurring during impact, even at low temperature

(vi) moderate mechanical properties under normal conditions

In practice, all of these points were not attainable by any one of the materials examined. The best overall behaviour came from polyurethanes. These were available in two types: polyester and polyether. The best of these types, adopted after some preliminary tests described in Chapter 4, are listed with their properties in Tables 3.4 and 3.5. The mechanical properties should be treated with caution, because the cure conditions are different when the elastomers are used in the composite, the rock and sand providing a heat sink for the heat of reaction. The Diorez 570 strength values are likely to be misleading because the values given relate to a mix where extra ingredients and more catalyst were used. It was decided to seek more appropriate information only if Diorez 570 proved superior in its behaviour during penetration tests to the 2851 resin blend. Tests carried out during the project were limited to

the properties of the composite as a whole. General properties are further discussed below.

Diorez 570 is a linear mixed glycol polyester polyurethane. At room temperature the viscosity of the prepolymer is qualitatively between that of thick oil and syrup. However, when mixed with the other liquid constituents, this viscosity reduced to that of a thick oil, approximately 60 poise. These other ingredients are 1-4 butane diol to improve mechanical properties, Isonate 143L (an isocyanate)to effect the cure, and Stanclere TL (dibutyl tin dilaurate), a catalyst.Mix proportions to obtain differing hardnesses are given in Table 3.6. Sufficient catalyst could not be added to give the full mechanical properties possible in this resin because the gel time was reduced too much for adequate mixing and casting to be possible. Hence a compromise was sought and found at around 4 drops per mix of 8-9 kg of composite. It was kept at this level for all resin percentages, as a slightly higher cure rate was thought necessary with a low resin (rock + sand) ratio to counter the extra effective heat sink thus present. Tests had progressed using this method when the decision was made to use the 2851 resins,where the catalyst was already included in with the prepolymer. Hence catalyst levels varied in different ways for the two resin types.

The 2851/304 and 2851/219 were polyether polyurethanes, blended in various ratios to give a range of hardnesses. When used this way they are called here the 2851 resins. The mix proportions for different hardnesses are shown in Table 3.7. Initially, LS480 described in Table 3.3 was to be used as the polyether polyurethane, but after preliminary tests the manufacturer withdrew it from the market because of chemical instability. After initial trials with the 2851 resins described in Chapter 4, they were adopted instead. Both 2851 prepolymers (which also included the catalyst and diol) had a viscosity similar to liquid paint. The prepolymers were mixed with 2875/003 isocyanate to effect the cure. The resultant viscosity was approximately 20 poise. The lower value

of the hardness range represented a physical boundary; the upper value (80 Shore A^{O}) was based on an estimate of where brittle behaviour was likely to occur, following the behaviour of a 95 Shore A^{O} specimen under impact, described in Section 4.2. This behaviour was deemed unacceptable because of brittle cratering under impact, and the possible scabbing in thinner specimens.

Both types of elastomers were very sensitive to moisture, and ingredients had to be stored in airtight containers. Also, the sand and rock aggregate had to be thoroughly dried, as described in Section 3.2.

3.1.4 Ammunition

Two standard NATO ammunition types were used in the test program, both of 7.62 mm calibre. The first type was ball, designed for use against personnel and light material targets. The second was armour piercing (A.P.) for use against high strength targets. Manufacturers' data are given in Tables 3.8 and 3.9. Experimental velocity and accuracy results are presented in Chapter 5.

3.2 Specimen Preparation

Each rock aggregate type was separated into single size material by sieving through the relevant BS sieves, which included 37.5, 26.5, 19.0, 13.2, 9.5 and 6.7 mm sizes. Sieve diameter was 300 mm. Sand and aggregate was oven dried in trays for 24 hours at 105^{O}C, and allowed to cool before use.

All specimens cast were small, and the maximum mix weight required was 12 kg. Hence a model A200 Hobart food mixer was used, with a mixing arm fabricated from 19 mm square steel bar. The mixer, with arm and mixing bowl, is shown in Plate 3.1.

For the main penetration tests, 152 mm concrete cube moulds were used to their full depth. Compaction of the composite was achieved with a tamping bar to BS 1881 : Pt 3 : 1970. To reduce the thickness of the specimen where required, an adjustable levelling bar, shown in Plate 3.2, was used to allow a flat specimen surface to be formed below the level of the mould top.

For compression and creep tests, standard 102 diameter x 203 mm long cylinder moulds were used, and for bending tests, 500 x 100 x 100 mm prism

moulds were used. Shutter oil was found superior to silicon grease for ease of demoulding.

Mixing was carried out as follows

(i) The resin constituents were mixed for a minimum of 30 seconds, or until they appeared blended, in the Hobart machine.

(ii) The rock aggregate and sand were added, and the mixing continued for a further minute.

(iii) The composite mixture was then tipped and scraped into the mould/moulds, and tamped as follows:

152mm square x 50 to 100mm thick - 2 layers - 35 tamps/layer

152mm square x 100 to 152mm thick - 3 layers - 35 tamps/layer

102 dia. x 203mm long cylinders - 4 layers - 20 tamps/layer

Beam specimens, 500x100x100mm - 2 layers - 100 tamps/layer

Specimens of less than 152 mm thickness in the cube moulds were levelled with the adjustable bar shown in Plate 3.2.

(iv) To avoid modification of the mix, as much of the residue as possible was scraped from the bowl.

(v) Steps (i) to (iv) were repeated as necessary

(vi) Specimens could be demoulded after a minimum of 1 hour for 2851 resins, and 1½ hours for Diorez 570.

(vii) The specimens' masses and dimensions were measured and recorded.

3.3 Penetration Tests

These tests were carried out using the ammunition described in Section 3.1.4 with a remote control solenoid firing system in an approved firing range with a gun to target distance of 20 m.

3.3.1 Gun, Mounting Frame and Solenoid Firing System

Projectiles were fired using a number 3 pressure housing and 7.62 mm proof barrel which had previously fired some 11,000 rounds. The accuracy, given in Chapter 5, was found to be adequate.

This rigid gun mounting frame is shown in Plate 3.3 and detailed in Figure 3.1. The firing solenoid, detachable trigger linkage, and pressure housing are shown in Plate 3.4.

The electrical firing system, shown in Figure 3.2, comprised a firing box with arming key and off biased switch, connected to the firing solenoid which was a Philips Control type 32 solenoid, rectified for mains use. It had an 11.4 kg pullout 18 mm stroke length. Connection wires were coaxial and a capacitor was used across the switch to reduce electrical interference with the velocity measuring rig described in Section 3.3.3.

3.3.2 Target Specimen Holder and Mounting Frame

These are shown in Figure 3.3. The target was held in place by two elastic straps on a rigid frame bolted to the floor, as pictured in Plate 3.5, enabling rapid changing of targets. The holder provided support around the rear perimeter with minimal lateral restraint due to the use of small locating studs.

3.3.3 Projectile Velocity Measurement

Standard velocity tables were available, but a rig was designed and built to measure actual velocities. The effects of batch to batch variation, propellant temperature (control of this was not practical), the extent of barrel wear, and the stiffness of the mounting frame were uncertain, and the frequency of freak velocity values was unknown.

The velocity measuring rig, shown in Plate 3.6, and Figure 3.4 consisted of two bases, each comprising primarily a light source, lens, slit, lens, and photodiode. Details of the components are given in Table 3.10. As the projectile passed through each light beam, the intensity of the light on the photodiode dropped some 13%, and the resultant voltage change, amplified by the circuit given in Figure 3.5, was sufficient to activate a Racal Dana 9903 electronic timer. With two rig bases, two voltage pulses were available to start and stop the timer. With a known base distance of 1 m, the resultant time interval was used to calculate the velocity. A general layout diagram

of the rig is given in Figure 3.6. The results of velocity measurements are summarised in Chapter 5. The velocity was measured at 1.5 m uprange from the impact point, and hence gives a slightly high estimate of impact velocity.

3.3.3.1 Development Stages, and Relevant Problems

The slit beams formed by the rig had to be of sufficient depth to encompass the spread of the projectile trajectories due to inherent inaccuracy; also the voltage fluctuation caused by the partial interruption of the beam by the projectile had to be sufficiently large to trigger the timers, and be above the level of interference.

To encompass projectile trajectory variations, a 60 mm beam height was required, and hence good quality lenses of the order of 65 mm diameter were used. The photodiodes used in the rig had the drawback of having a very small light sensitive area of 1 mm^2. Hence a light souce with a filament of 1 mm length was needed to enable proper focussing on the photodiode.

Having built the rig with this equipment, the optimum slit width was determined experimentally at 3 mm with the light source near its working voltage. This width was considered low enough not to introduce significant measurement errors.

During the commissioning of the rig, the following problems were encountered.

(i) Interference from the firing circuit. This was overcome by installing a capacitor across the firing switch, using coaxial cable to power the firing solenoid, fitting a transient suppressor between the supply and the timers, and keeping the firing box as remote as possible from the velocity measuring equipment.

(ii) Initially, a Racal 835 timer was used, and was found to be still very sensitive to interference even after the measures listed above had been taken. However, the Racal-Dana 9903 used later was much superior. Towards the end of the experiment a success rate of 90-95% could be obtained on velocity measurements.

(iii) The electrical supply in the test laboratory was unusually 'noisy' and because of this all intermittent electrical equipment in the laboratory was switched off just before each test whilst the Racal 835 was in use. With the Racal Dana 9903, however, this was found not to be necessary.

The design of the velocity rig was such that considerable adjustment could be made, as focussing of the light beam was anticipated as a possible problem. In practice, the rig provided more adjustment than was really necessary.

3.3.3.2 Installation and Initial Adjustments

The following steps were taken

(i) The frame supporting the velocity rig was installed, using rawlbolts in the concrete floor, so that its longitudinal centreline was under the line of fire, i.e. the average trajectory. In addition, it was levelled so that, upon fixing of the velocity rig, the probable line of fire passed midway up to height of the light beams.

(ii) With the light bulb supply connected, each base of the rig was adjusted by eye so as to produce a parallel slit beam, which could be focussed into the photodiode.

(iii) The two bases were then clamped onto the frame so that the distance between the light beam centres was 1000 mm. Finally, the slit in each lens cap was checked for verticality.

(iv) For each base of the rig in turn, the power supplies to the photodiode circuit were connected, and the output leads connected in turn to a Solatron digital voltmeter (DVM).

The DVM reading was noted with zero voltage across the bulb. The bulb brightness was then increased until the DVM reading had reduced by 5V. This light intensity was well below the level at which flooding (saturation) of the photodiode occurred. Slight refocussing was then carried out until the reading on the DVM reached a minimum, indicating optimum focussing. If apparent insensitivity had been noted following a large reduction in the DVM reading, it would have been prudent to reduce the bulb voltage and repeat the procedure in case flooding had occurred.

(v) The timer was set up with a DC trigger offset of around 0.75V on each channel.

3.3.3.3 Regular Adjustments

Final adjustments to the rig were carried out before each day of testing as follows.

(i) Any dust was carefully removed from the light bulb, lenses, and photodiode.

(ii) The power supplies were connected to the rig, the bulb supply being set at 3V. For each base of the rig in turn, the output leads were connected to the DVM. The resistance of R_1, Figure 3.6, was then decreased from its maximum until a change in the DVM reading ceased, i.e. flooding of the photodiode was occurring. R_2, Figure 3.5, was then used to adjust this reading to zero.

(iii) The photodiode circuit outputs were connected to the timer.

(iv) The operation of the rig was checked using a pencil held horizontally to break each beam in turn.

(v) The penetration tests were carried out as described in Section 3.3.4.

(vi) Before each subsequent test, each photodiode output was checked using the DVM and, if necessary, rezeroed. Slight drift of this voltage was attributed to dust and vibration from the impact.

3.3.4 Penetration Test Procedure

Before each day's testing

(i) The velocity measuring rig was set up as described in Section 3.3.3.3.

(ii) The tightness of bolts on gun and all mounting frames were checked.

(iii) The barrel was fitted to the pressure housing.

(iv) The base length of the velocity measuring rig was checked and, if necessary, adjusted.

Before each test, in the firing range

(i) The trigger mechanism was cocked, safety catch engaged, and the trigger mechanism unscrewed.

(ii) The bolt was removed and, except for the first test, the spent cartridge removed.

(iii) The target specimen was then changed.

(iv) A live round was placed in the gun, the bolt replaced, trigger mechanism screwed tight, solenoid linkage attached, and the safety catch disengaged.

In the control room

(v) Output voltages from the velocity measuring rig were checked as described in Section 3.3.3.3.

(vi) The timer was zeroed

(vii) Using the firing curcuit described in Section 3.3.1, the round was detonated.

After a day's testing

(i) The base distance of the velocity measuring rig was rechecked.

(ii) The barrel was cleaned and removed for safe storage.

3.4 Specimen Sectioning

The projectile path and sometimes projectile fragments were located within each target specimen by sectioning the specimen parallel to the impact face at various distances from it. A Clipper EW1-X-1 247 cutting machine was used for this purpose, initially with a 450 mm circular fibre blade. This is shown in Plate 3.7. At a later stage a diamondblade was used and found to be superior. The orientation of the saw cuts, discussed in more detail in Chapter 4,is shown in Figure 3.7.

3.5 Specimen Temperature Control

As described in Section 4.5.3, penetration tests were carried out on hot and cold target specimens. A domestic freezer was used to attain a temperature of -18°C, and a laboratory oven to attain +45°C. After transportation in insulated sacks to the firing range, and just before testing, the temperature of one specimen at each temperature level was determined by inserting a mercury thermometer into a small hole cast near a corner of the block. Measured temperatures were -8 and + 34°C. The effect of the temperature gradients within the blocks, and heat loss from the blocks during transport, make the temperatures at the block centres uncertain, but they should be between the bounds of the original and measured temperatures.

3.6 Static Tests

Although secondary in importance to the investigation of penetration characteristics, a brief static test programme was carried out to give a

reasonable estimate of the behaviour of the composite when used, for example, as protection for buildings. All static tests were carried out on optimised composite ingredient levels, except for rock aggregate size. In order to obtain meaningful results from the small static test specimens used, the rock aggregate size was limited to the 13.2 to 19.0 mm range.

3.6.1 Uniaxial Compression Tests

The large viscous element in the behaviour of the elastomer meant that any compression test could not be stopped for readings to be taken, or relaxation of stress or creep would occur.

It was decided to use 102mm diameter x 203mm long cylinders in these tests, and to monitor load and displacements electrically, using a Maynes Type 103 100 kN load cell and 25mm travel Novatech Type 102 resistance displacement transducers respectively. Input voltages were all 10v, and output voltages were recorded on a portable Solartron 3430 datalogger, with a scan interval of approximately 5 seconds. Constant displacement rate loading was achieved using a Denison T26E 50 ton testing machine, and a spherical seating was included in the system.

The relatively large displacements occurring meant that the mountings for the longitudinal transducers could not be rigidly fixed onto the specimen. This was overcome by locating the mounting rings with sliding locating pins, compressed onto the specimens with rubber bands. The mounting rings are detailed in Figure 3.8

In addition to the four longitudinal transducers, three transducers were used to monitor lateral displacements, i.e. the barrelling effect of the specimen during loading. These were located symmetrically at mid height around the perimeter of the specimen using magnetic clamps.

The test rig is pictured in Plate 3.8 with a schematic plan given in Figure 3.9. A circuit diagram is given in Figure 3.10.

After curing, specimens used needed some preparation prior to insertion in the loading machine. The top, as cast, was levelled initially using the

Clipper cutting machine. Later, however, a surface grinding machine was found to give a better finish.

The finished length of the specimens was 196 to 200mm. The central circumference was found, and circumferences at 33 mm at each side marked (i.e. $\frac{1}{3}$ total length between them). On these, at ¼ points around the circumference, the positions of the locating pins were marked.

The mounting rings with transducers were then attached, and the specimen placed in the testing machine and the lateral transducers positioned. The testing machine was then started, and adjusted to the correct strain rate. When the loading head was some 2 mm away from the specimen, the data logger was started, the supply voltage having been set previously by running the data logger until the reading from the supply monitor channel read 10 V.

3.6.2 Creep Tests

Short term creep tests were carried out on identical specimens to those in the uniaxial compression tests. The displacements were monitored using a 50 mm Demec gauge. Three pairs of Demec points were fixed equidistant around the central circumference to measure longitudinal displacements. Loading was achieved through a spherical seating from a dead load rig which utilised a system of levers to magnify the applied load by a factor of 117.4. Readings were taken at time multiples of 4 to 6, namely 0s (unloaded), 30s, 2 mins, 10 mins, 1 hr, 5 hrs, 24 hrs, 5 days (20 days). The 20 day reading was only taken where circumstances allowed.

The temperature at testing was $21^{\circ}C \pm 2^{\circ}C$, and specimens were left overnight between casting and testing to attain this temperature. The test arrangement is shown in Plate 3.9.

3.6.3 Bending Tests

To give an acceptable estimate of bending characteristics the modulus of rupture test, described in BS 1881 : Pt 3 : 1970, was adopted. Beams of 100 x 100 x 500 mm were used and loading was carried out in the as-cast

position. The loading apparatus was an ELE 50 kN flexure and transverse frame, the loading rate being 4000 N/min. The Solartron datalogger with one of the displacement transducers from the compression rig was used to monitor the central deflection of the beam, whilst still wired into the circuit shown in Fig. 3.10. The test arrangement is shown in Figure 3.11.

Information about suppliers or manufacturers of materials and equipment described in this chapter is given in Appendix A1.

	Crushed limestone	Crushed basalt	River gravel	Crushed hornfels
*Oven dry specific gravity	2.67	2.75	2.57	2.75
*Saturated, surface dry specific gravity	2.68	2.82	2.60	2.77
*Aggregate crushing value, %	23	17	not available	12
*Aggregate impact value, %	23	17	16	11
*10% fines load (kN)	160	250	377	not available
% voids - compacted 26.5-37.5 mm aggregate	43%	43.8%	35%	insufficient material
% voids - uncompacted 26.5-37.5 mm aggregate	49.3%	49.4%	39.4%	insufficient material
% voids - compacted 152.4 mm cube mould, 26.5-37.5 mm aggregate	44%	46%	39.1%	44.2% +
% voids - uncompacted 152.4 mm cube mould, 27.5-37.5 mm aggregate	52.1%	49.4%	43.7%	51.8%+

* Obtained from suppliers

+ 16.0-22.0 mm aggregate used

Table 3.1

Relevant BS 812 (1975) properties for rock aggregate, including % voids values from tests using penetration specimen moulds

Distribution of test values for the different rock-groups

(a) Aggregate crushing test

Rock group	Aggregate crushing value*										
	10	12	14	16	18	20	22	24	26	28	30
	Percentage of samples having lower value:										
Hornfels	16	67	89	98							
Prophyry	8	26	59	83	92						
Basalt	9	21	44	77	87	93					
Quartzite		6	31	61	77	87	93				
Gritstone	7	16	29	46	63	72	85	91	95		
Flint				15	74	88	94				
Granite		7	13	23	41	60	72	80	87	91	95
Limestone					5	13	30	47	68	82	90
Artificial							7	13	23	47	68
All groups+	5	12	24	38	52	62	69	76	83	90	95

(b) Aggregate impact test

Rock group	Aggregate impact value*										
	10	12	14	16	18	20	22	24	26	28	30
	Percentage of samples having lower value:										
Hornfels	19	62	83	93							
Porphyry	6	25	52	77	88	95					
Basalt	7	17	43	76	89	95					
Granite		18	33	43	54	64	73	81	87	92	
Gritstone		9	17	28	49	67	80	86	90	93	95
Quartzite			5	12	24	45	63	75	84	90	95
Limestone						19	51	72	84	92	
Flint						5	35	77	91		
Artificial						5	10	17	34	71	84
All groups+		12	21	32	45	53	71	81	88	93	

*In these tests, a numerically lower result indicates a higher resistance in the test

+Including results from unclassified samples

Table 3.2 a&b

Aggregate crushing value and aggregate impact value for various rock types

(From Road Note 24, 1959)

(c) Specific gravity

Rock group	Specific gravity										
	2.95	2.90	2.85	2.80	2.75	2.70	2.65	2.60	2.55	2.50	2.45
	Percentage samples having a higher specific gravity										
Hornfels	22	29	36	43	56	100					
Basalt		15	36	59	75	85	92				
Prophyry			12	24	39	56	73	88			
Granite	6	7	9	12	18	29	51	95			
Gritstone			5	10	22	47	70	87			
Artificial				5	12	30	67	88			
Limestone						22	66	85	94		
Quartzite							12	78			
Flint								3	63	87	95
All groups		5	10	17	27	42	58	75	90		

Table 3.2c

Specific gravity for various rock types

(From Road Note 24, 1959)

Polymer Type	Viscosity	General Mechanical Properties	Cost	Comments
Polysulphide rubber	Low	Low Strength Elastomer	High	Too expensive
Polyurethane	High	High Strength Elastomer	High/ average	Most sorts too viscous
Unsaturated polyester resin	Low	Medium Strength low extension	Low	Brittle
Epoxy resin	Medium	Very High Strength low extension	Average	Brittle
Neoprene latex	Low	Medium Strength Elastomer	Low	Water based colloid slow cure
Polythixon	Low	Low Strength elastomer, or high strength with low extension	High	Too expensive
Silicone rubber	High	Medium Strength medium extension	Very high	Too expensive
Hydroxyl terminated polybutadiene	High	Low/medium strength elastomer	Average	Too viscous
Butadiene	High	Low Strength Elastomer	Average	Too viscous
LS 480 (polyether polyurethane)	Low	Medium/high strength	Average	Discontinued by manufacturer because of chemical instabilities

Table 3.3

Relative properties of rejected polymers

	Ingredient parts		Range of cured elastomer properties @ 24 hrs and room temperature	
	2851/304 & 2851/219 prepolymer blend	2875/003 isocyanate		
Viscosity (poise)	27.5 @ 24°C	2.0 @ 25°C	-	-
Specific gravity	1.35	1.22	1.32	1.32
Hardness (Shore A)	-	-	80	60
Tensile Strength (N/mm^2)	-	-	8.36	4.15
Elongation at break (%)	-	-	210	350
Storage requirements	Airtight 0-25°C	Airtight 0-25°C	-	-
Storage Time	officially, 6 months, but probably 12 months unopen		-	-

Table 3.4

Polyether type polyurethane ingredients and resultant properties of 2851/304 and 2851/219 resin blend at the extremes of the hardness range used, from manufacturer's data

	Ingredient parts			Cured elastomer properties @ 24 hrs and room temperature*
	Diorez 570 prepolymer	Isonate 143L	1-4 butane diol	
Viscosity (poise)	75	0.3	0.3	-
Specific gravity	1.13	1.22	1.10	-
Hardness (Shore A)	-	-	-	50
Tensile Strength (N/mm^2)	-	-	-	6.5
Elongation at break (%)	-	-	-	550
Storage requirements	Airtight 0-50°C	Airtight 20-30°C	Airtight 20-30°C	-

* The only data available was for a low hardness mixture with filler, plasticiser, dessicant, extra catalyst, and without 1-4 butane diol. As this resin type did not give the best results in the penetration tests, more relevant properties were not sought.

Table 3.5

Polyester type polyurethane ingredients and resultant properties of Diorez 570, from manufacturer's data

Shore A hardness(nominal)*	65	70	75	80	85
Diorez 570 prepolymer (%)	72.20	70.05	66.53	63.25	59.31
Isonate 143L (%)	23.83	25.22	27.94	30.36	33.21
1-4 butane diol %	3.97	4.73	5.52	6.39	7.47
Stanclere TL	Approx 1 drop per 200g of rest of liquid mix				

* Because a low catalyst level had to be used to retard the gel time and allow time for casting, it is unlikely that these hardnesses were actually achieved. Nominal values given are manufacturers specification for correct amount of catalyst.

Table 3.6

Mix proportions for various hardnesses of Diorez 570

Shore A hardness	60	65	70	75	80
2851/304 prepolymer etc(%)	86.21	74.25	58.75	47.68	36.18
2851/219 prepolymer etc(%)	0	10.41	24.47	34.53	44.95
2875/003 isoyanate (%)	13.79	15.34	16.78	17.79	18.87

Table 3.7

Mix proportions for various hardnesses of 2851 resin blend

General description	The cartridge consists of a cartridge case, a bullet, a primer and propelling charge. The complete assembly weighs 24.4 grams, with an overall length of 71.05 mm
Bullet	Bullet jacket - Tombac 90/10 Lead alloy core Overall length 29.25 mm Mass = 9.3 grams
Ballistics	Velocity = 849 m/s at 5 m Accuracy = vertical + horizontal error < 150 mm at 150 m

Table 3.8

Manufacturer's data for 7.62 mm NATO ball ammunition

General description	The cartridge consists of a cartridge case, a bullet, a primer and propelling charge. The complete assembly length is 71.12 mm
Bullet	Bullet jacket - 90/10 guilding metal Bullet length = 33.30 mm Mass = 9.60-9.90 g
Core of bullet	Material - hardened steel Length - 23.8 mm Diameter - 6.10 mm Mass - 3.74 g
Propellant	2.9 g ball powder PRB
Ballistics	Velocity = 825 m/s at 20 m at 21^{o}C

Table 3.9

Manufacturer's data for 7.62 NATO armour piercing (AP) ammunition

Component	Specification
Lenses	65 mm diameter. Focal length 150 mm
Fixed resistors	High stability carbon film
Variable resistors	Phodiode circuit - 25 kΩ wirewound Light bulb circuit - 10 Ω wirewould
Light sources	0.25a RLP 11B m.e.s. capped. From RLP Miniature Bulb Co.

Table 3.10

Velocity rig component specifications

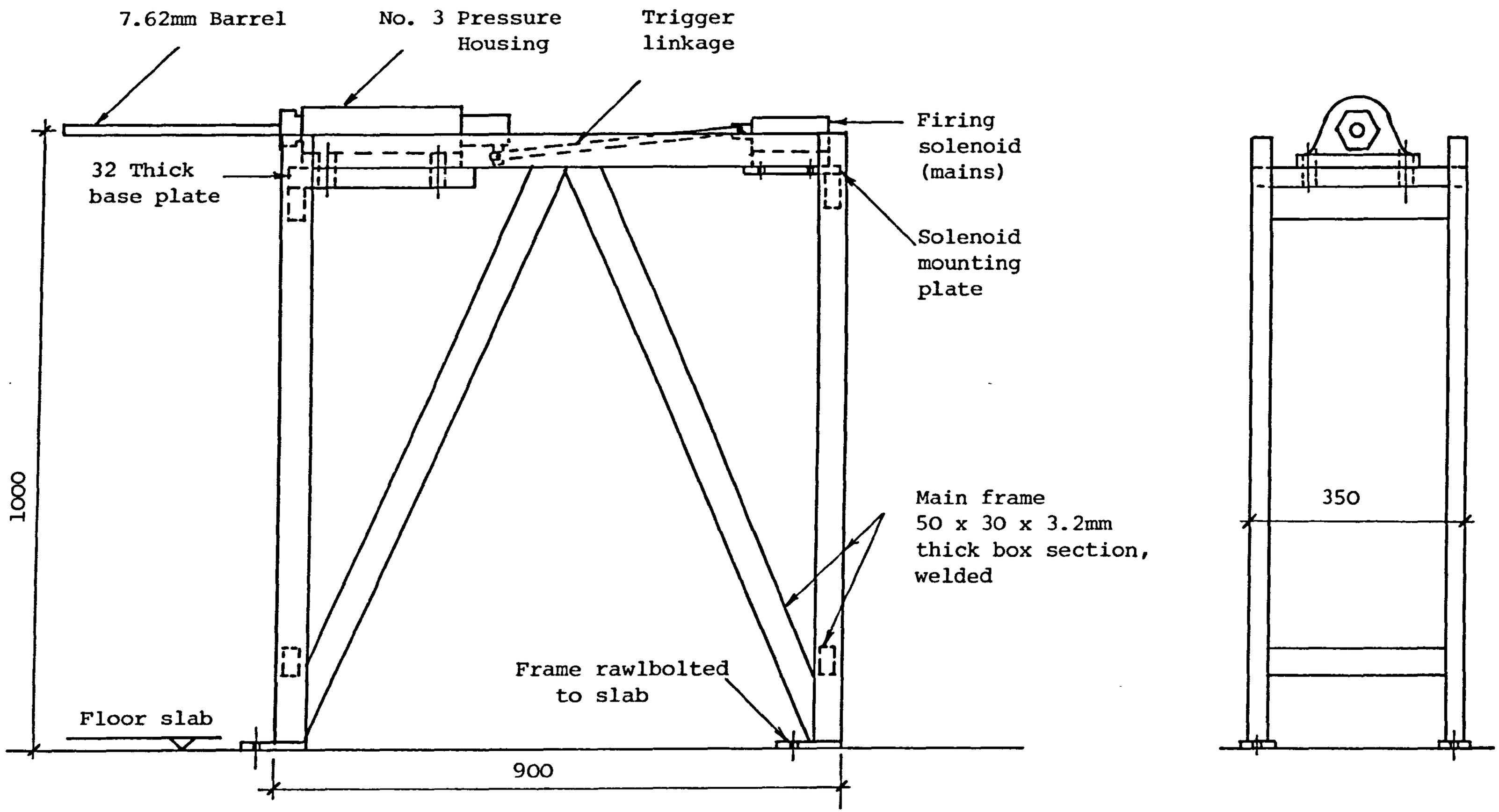

SIDE ELEVATION

FRONT ELEVATION

all dimension in mm

FIGURE 3.1 MOUNTING OF GUN AND FIRING SOLENOID

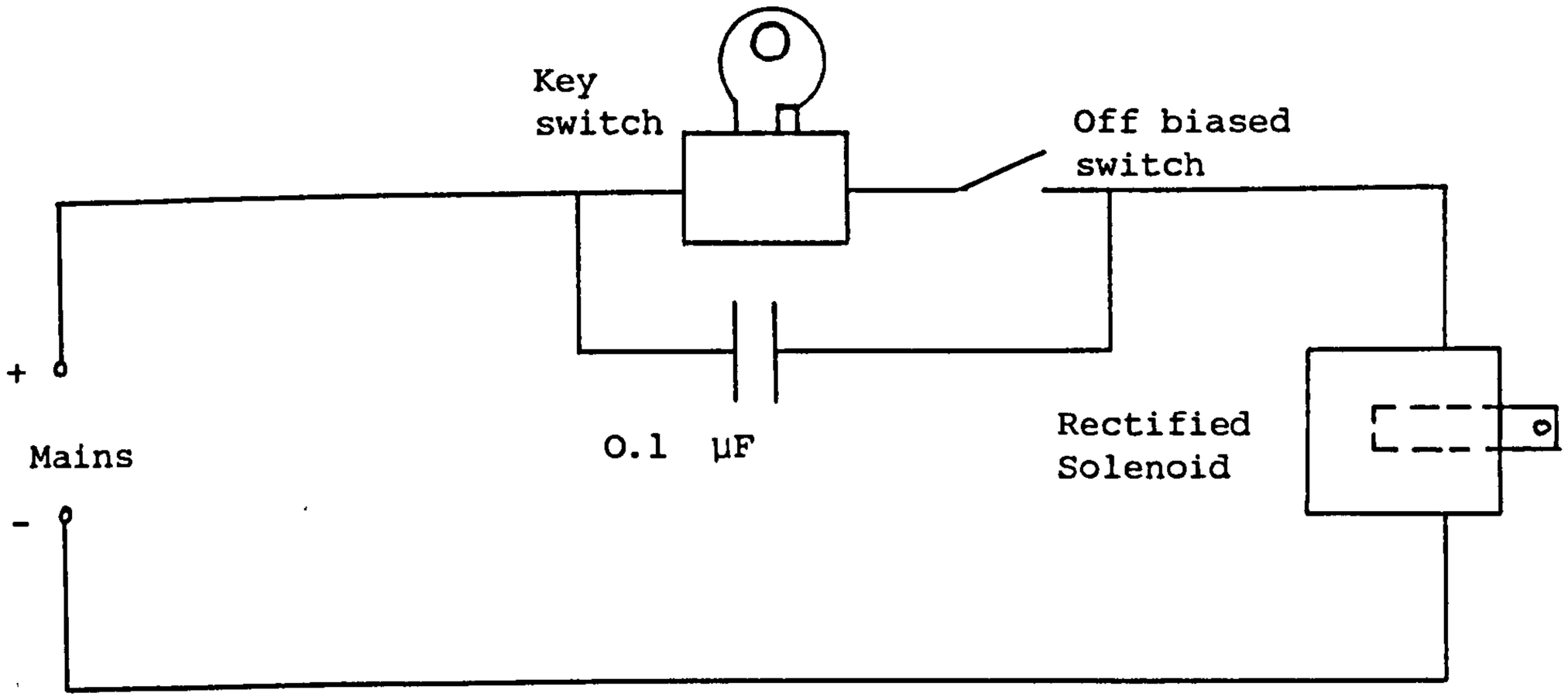

FIGURE 3.2 SCHEMATIC DIAGRAM OF ELECTRICAL FIRING CURCUIT
(earth lead excluded)

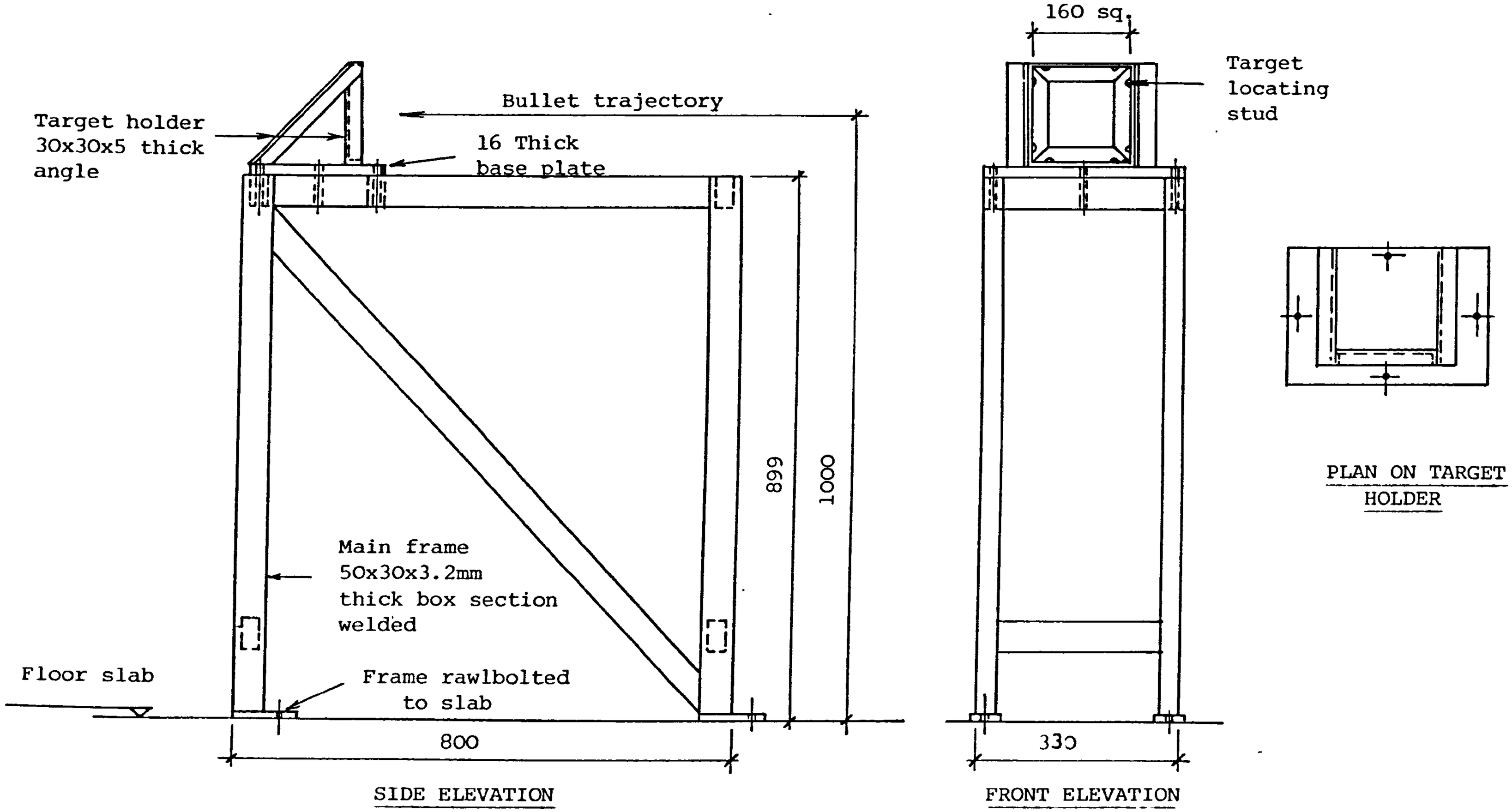

all dimensions in mm

FIGURE 3.3 DETAILS OF TARGET HOLDER AND MOUNTING FRAME

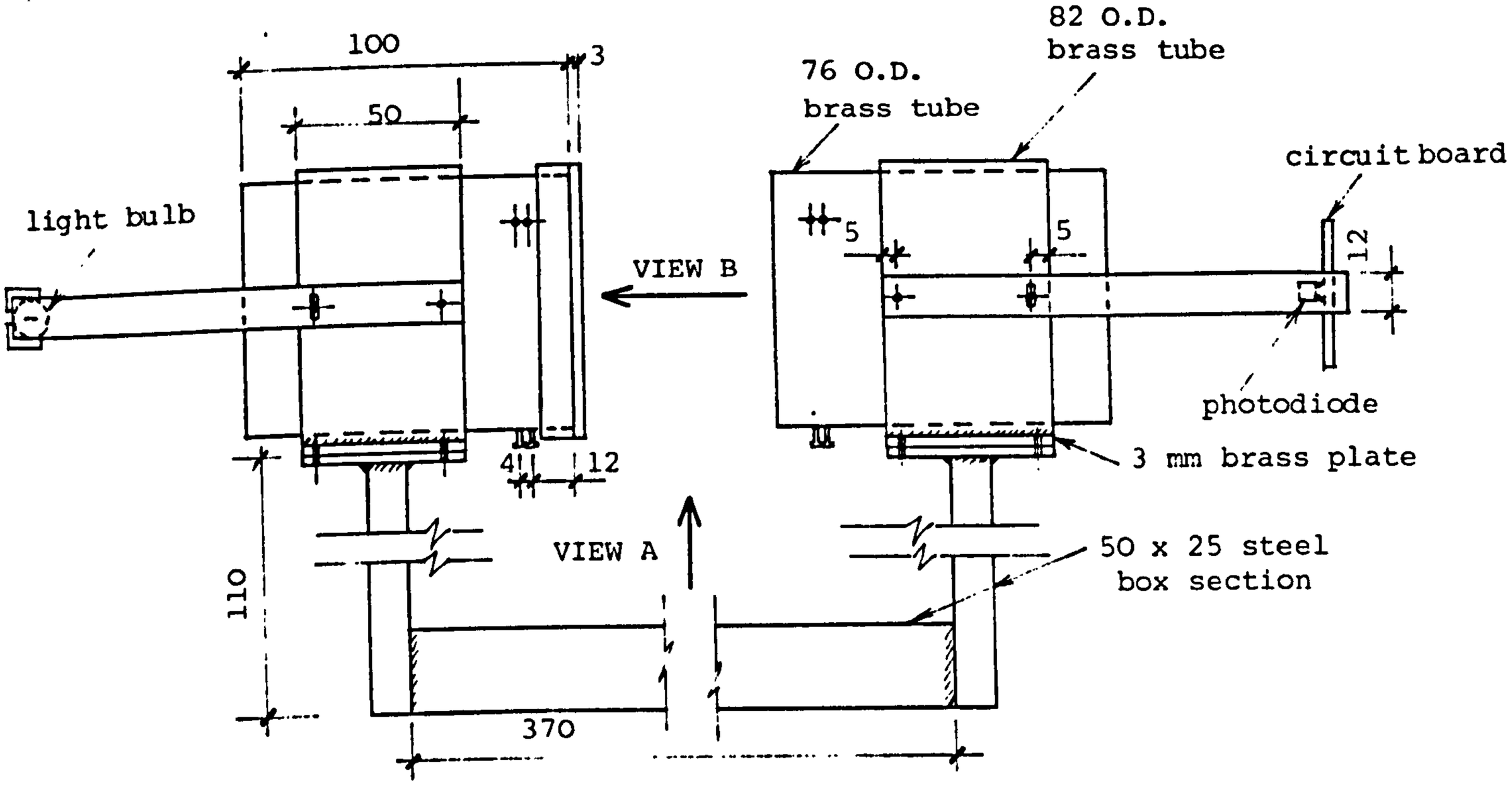

ELEVATION

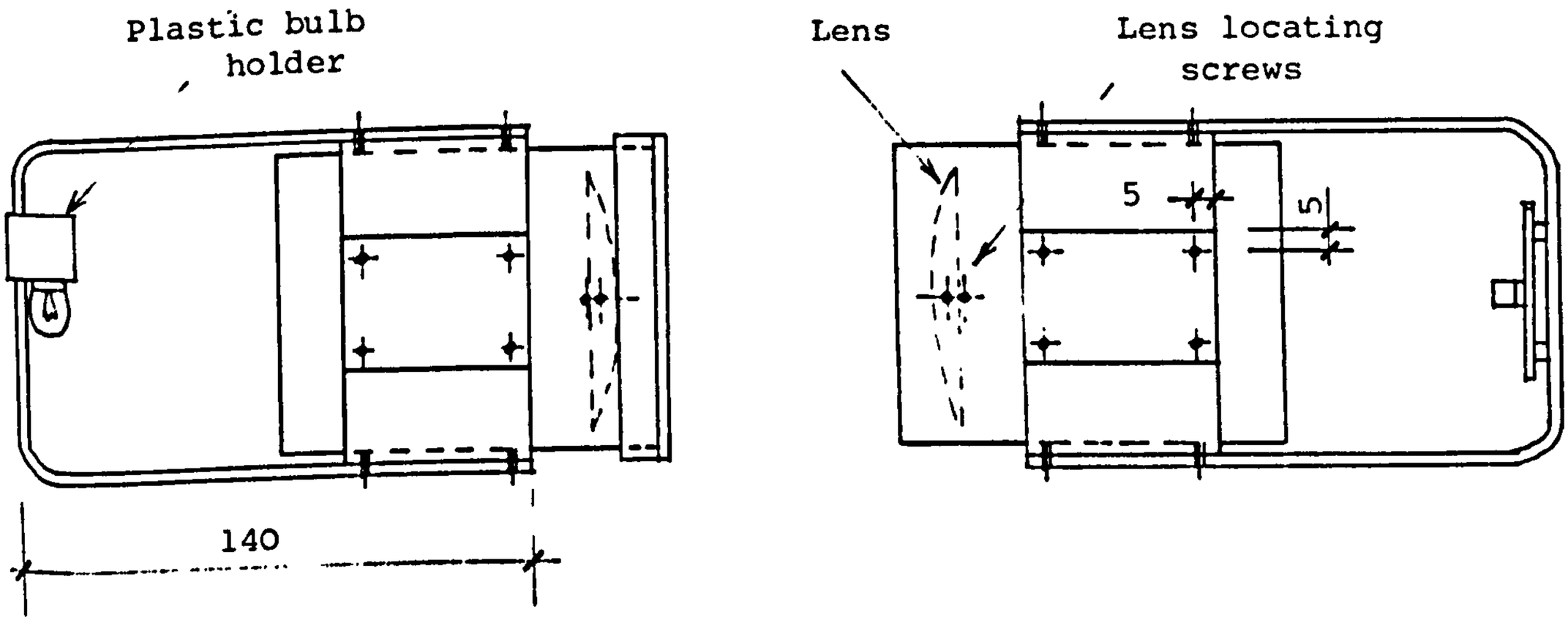

VIEW A

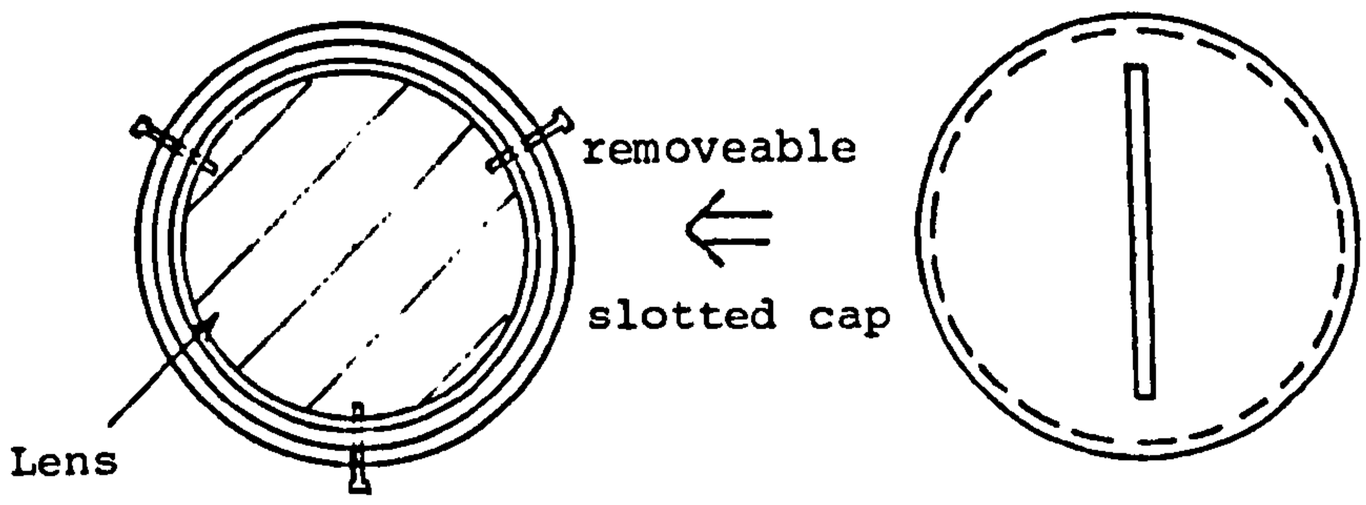

VIEW B

FIGURE 3.4 DETAILS OF VELOCITY MEASURING RIG

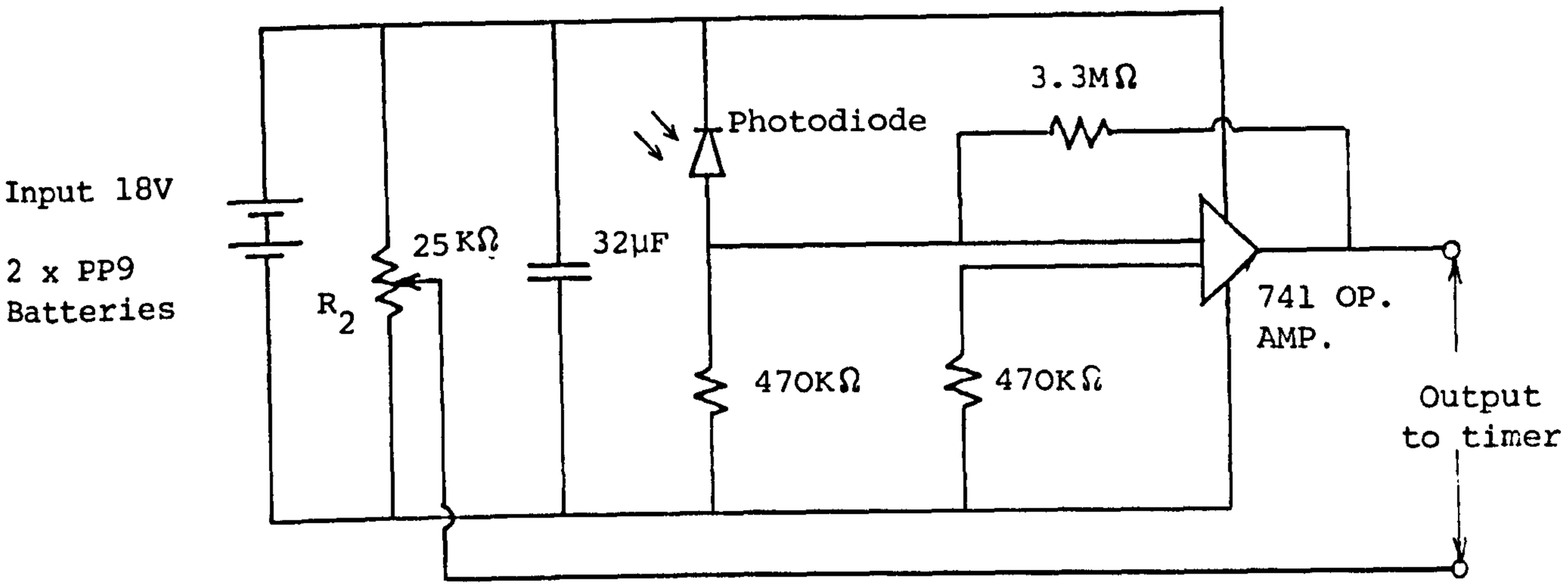

FIGURE 3.5 DIAGRAM OF PHOTODIODE CIRCUIT

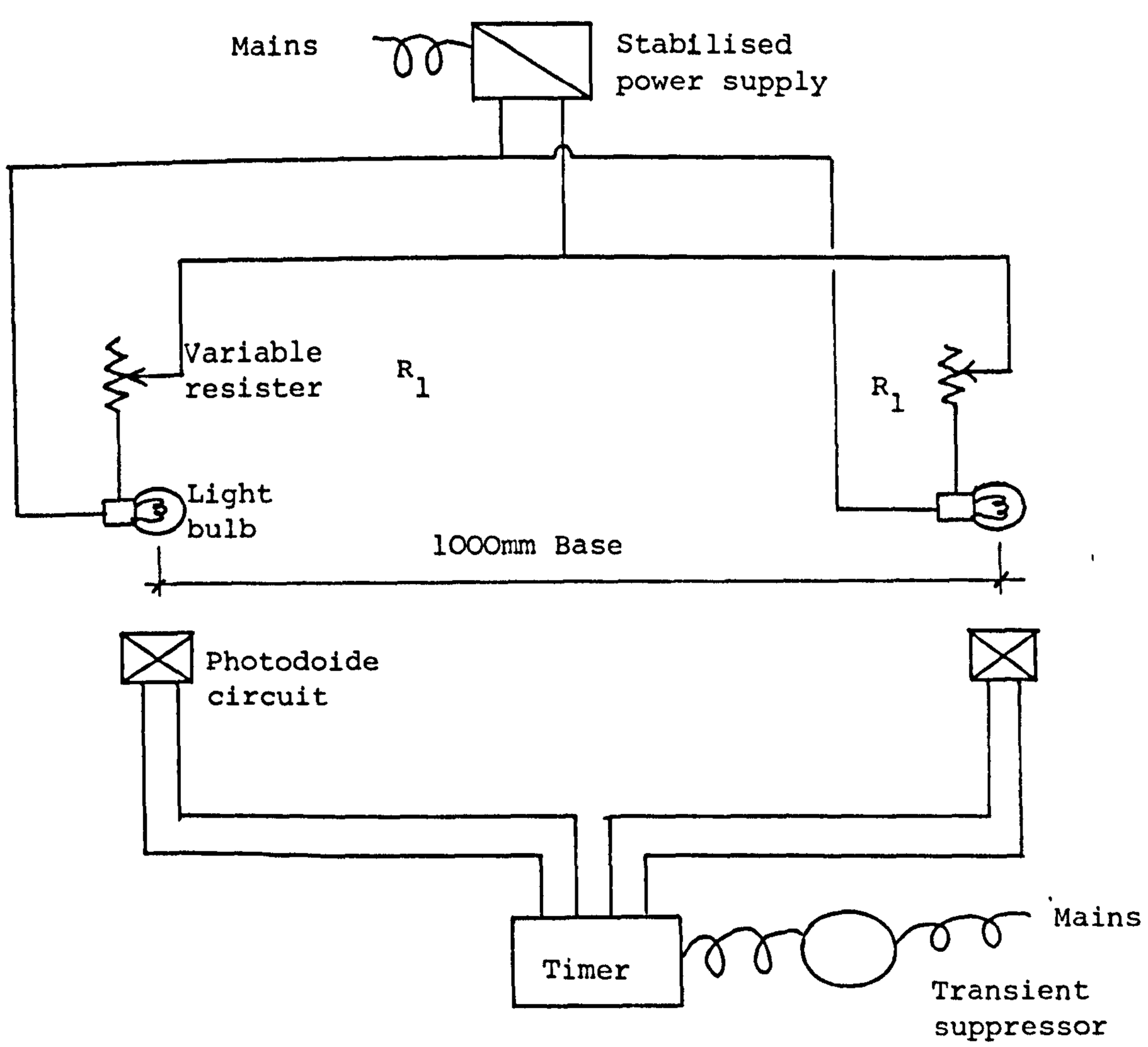

FIGURE 3.6 SCHEMATIC DIAGRAM OF VELOCITY MEASURING RIG

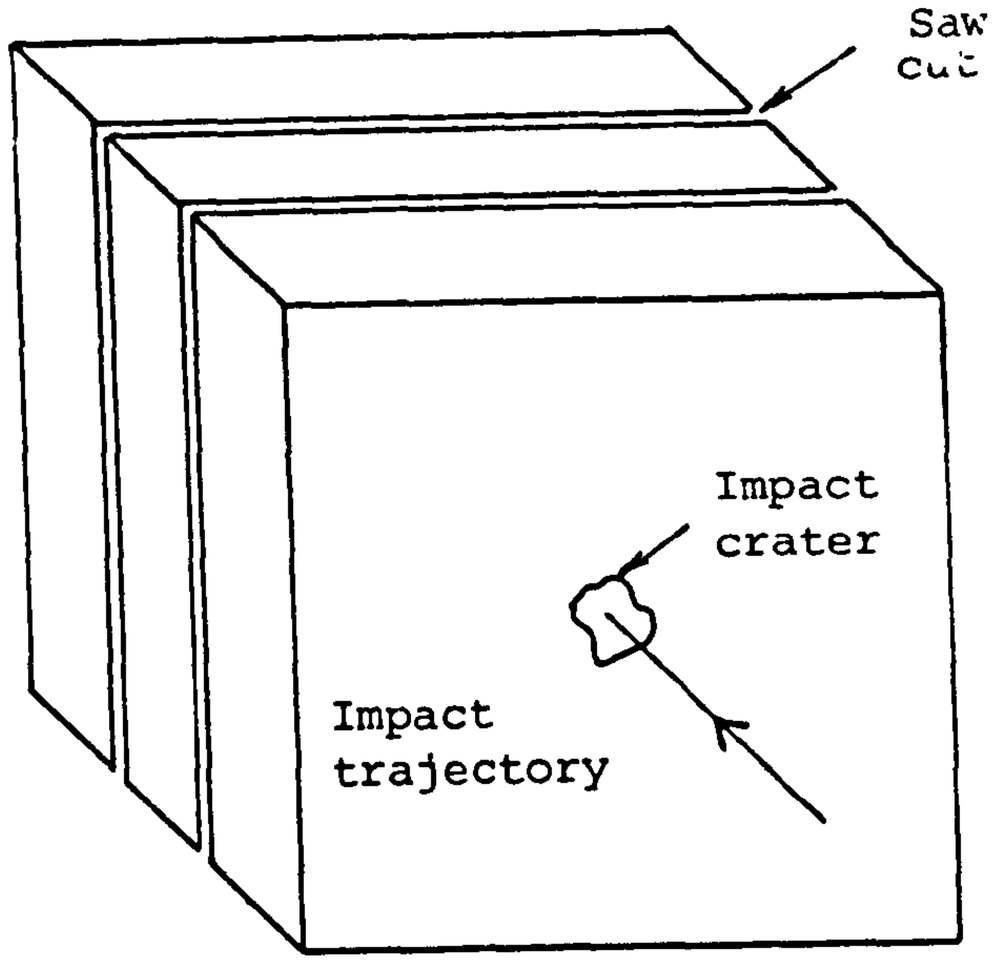

FIGURE 3.7 ORIENTATION OF SAW CUTS

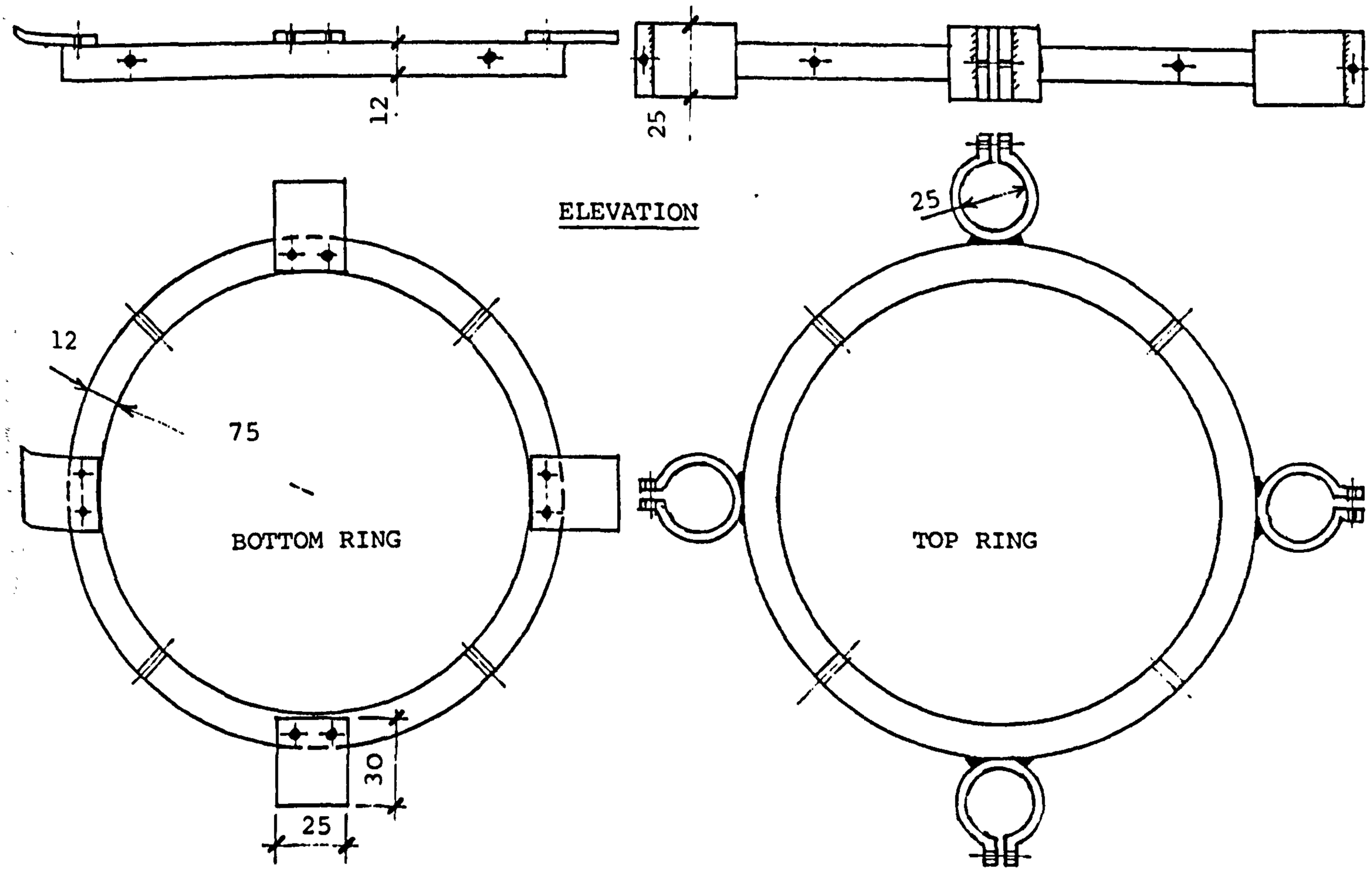

FIGURE 3.8 DETAILS OF MOUNTING SYSTEM FOR LONGITUDINAL DISPLACEMENT TRANSDUCERS IN UNIAXIAL TEST RIG

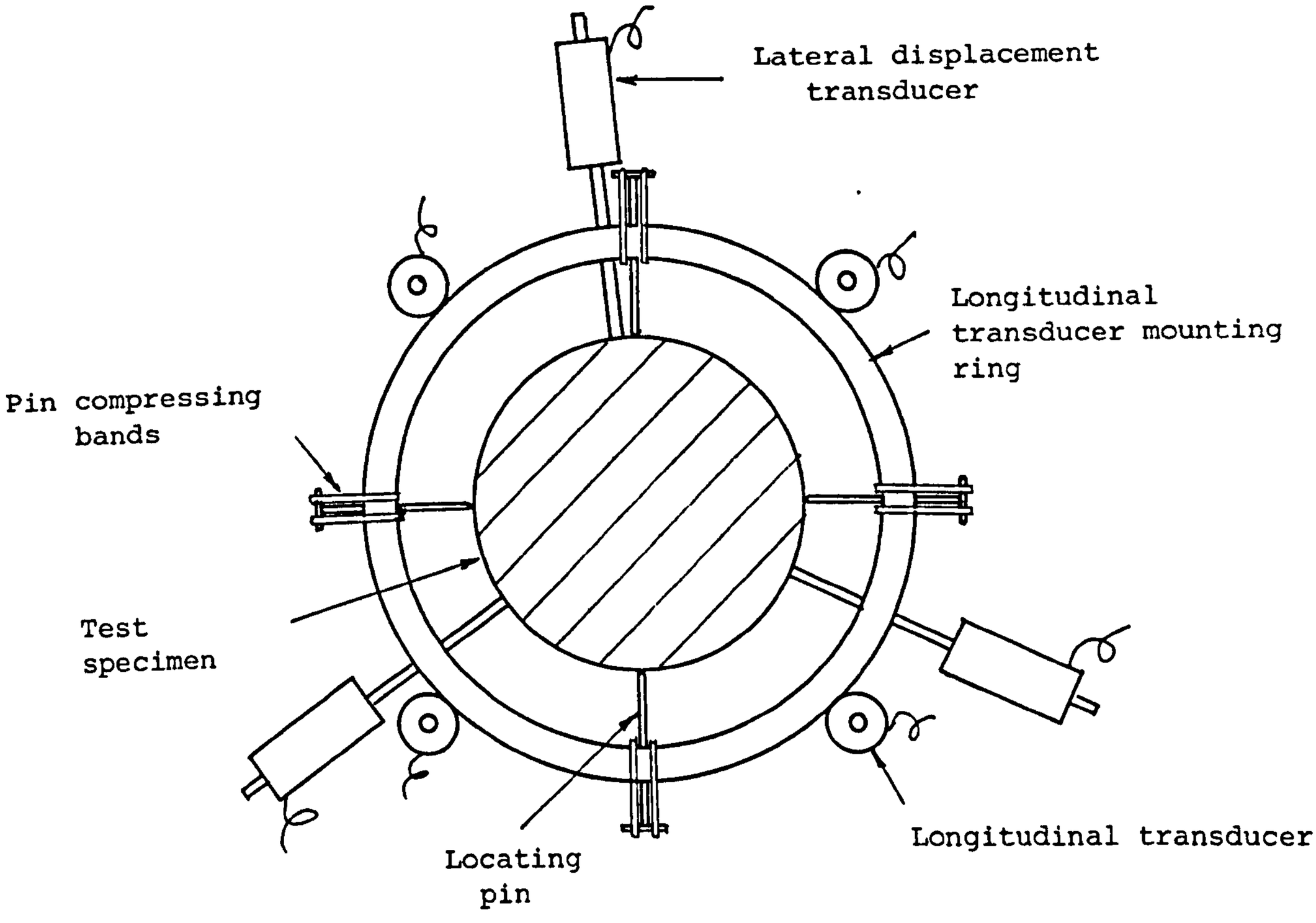

FIGURE 3.9 PLAN OF UNIAXIAL COMPRESSION RIG

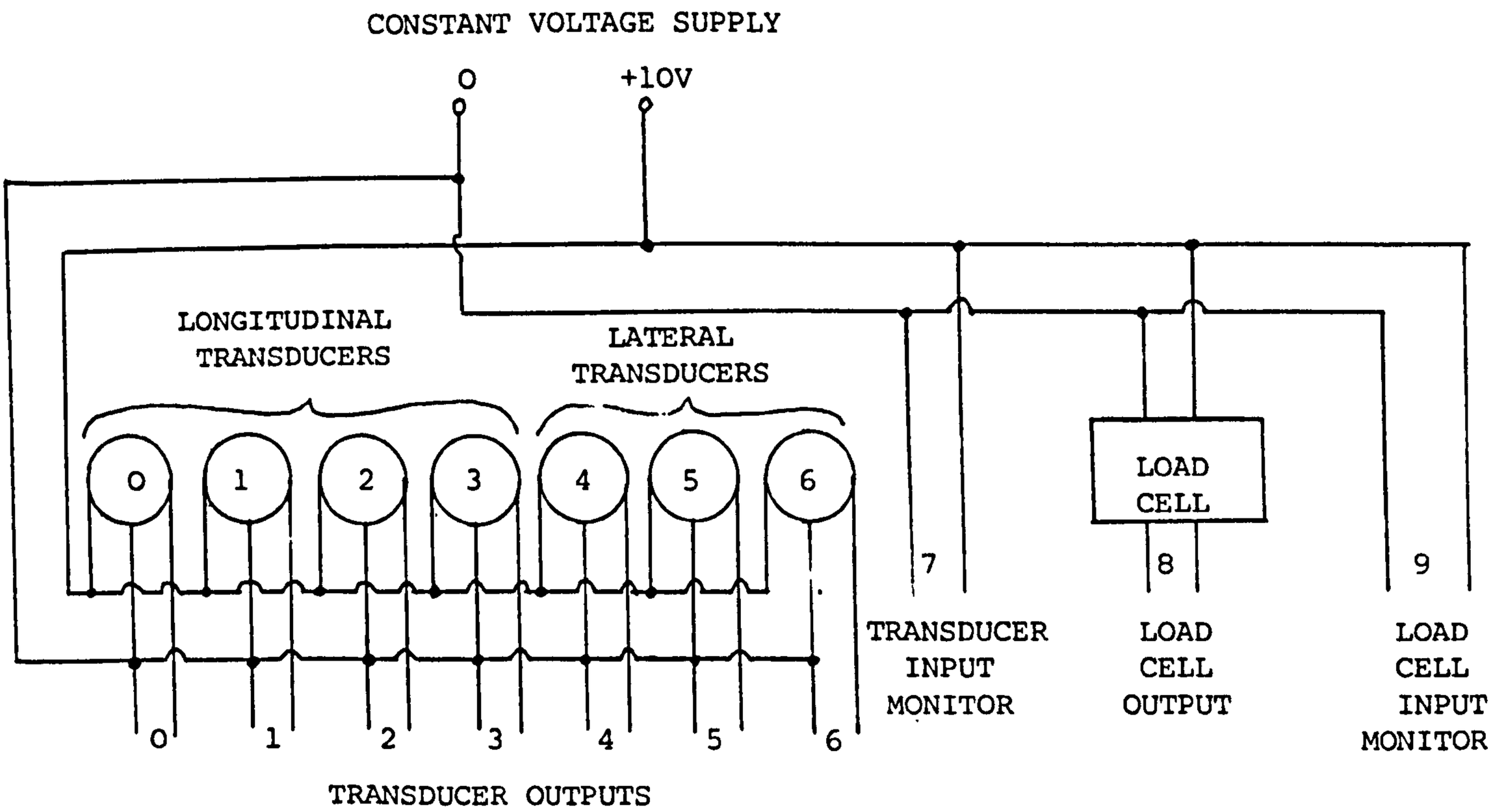

FIGURE 3.10 SCHEMATIC CIRCUIT DIAGRAM OF UNIAXIAL COMPRESSION TEST RIG

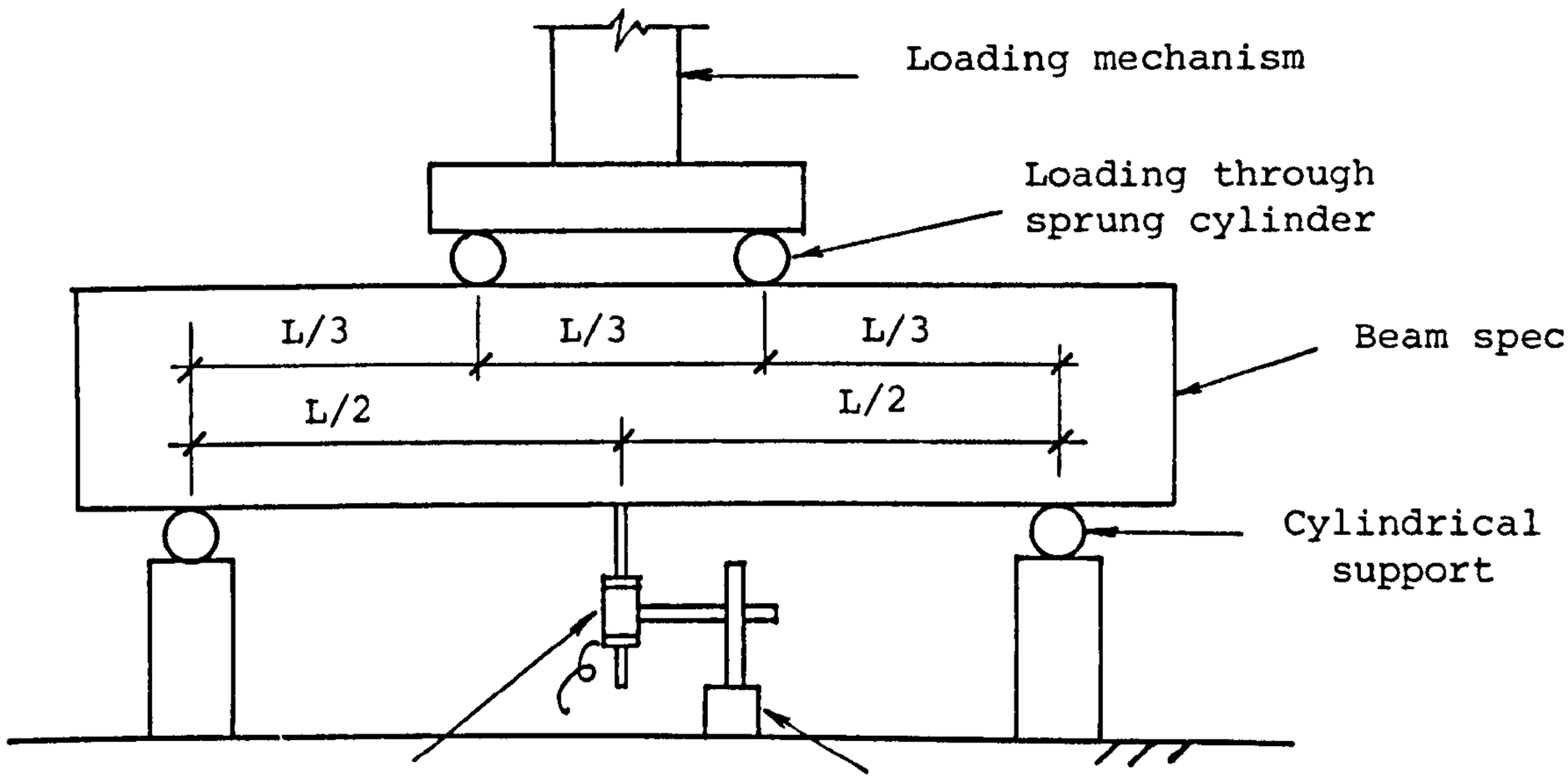

FIGURE 3.11 ARRANGEMENT OF BEAM BENDING TESTS

PLATE 3.1 HOBART MIXING MACHINE AND BOWL, WITH FABRICATED MIXING ARM

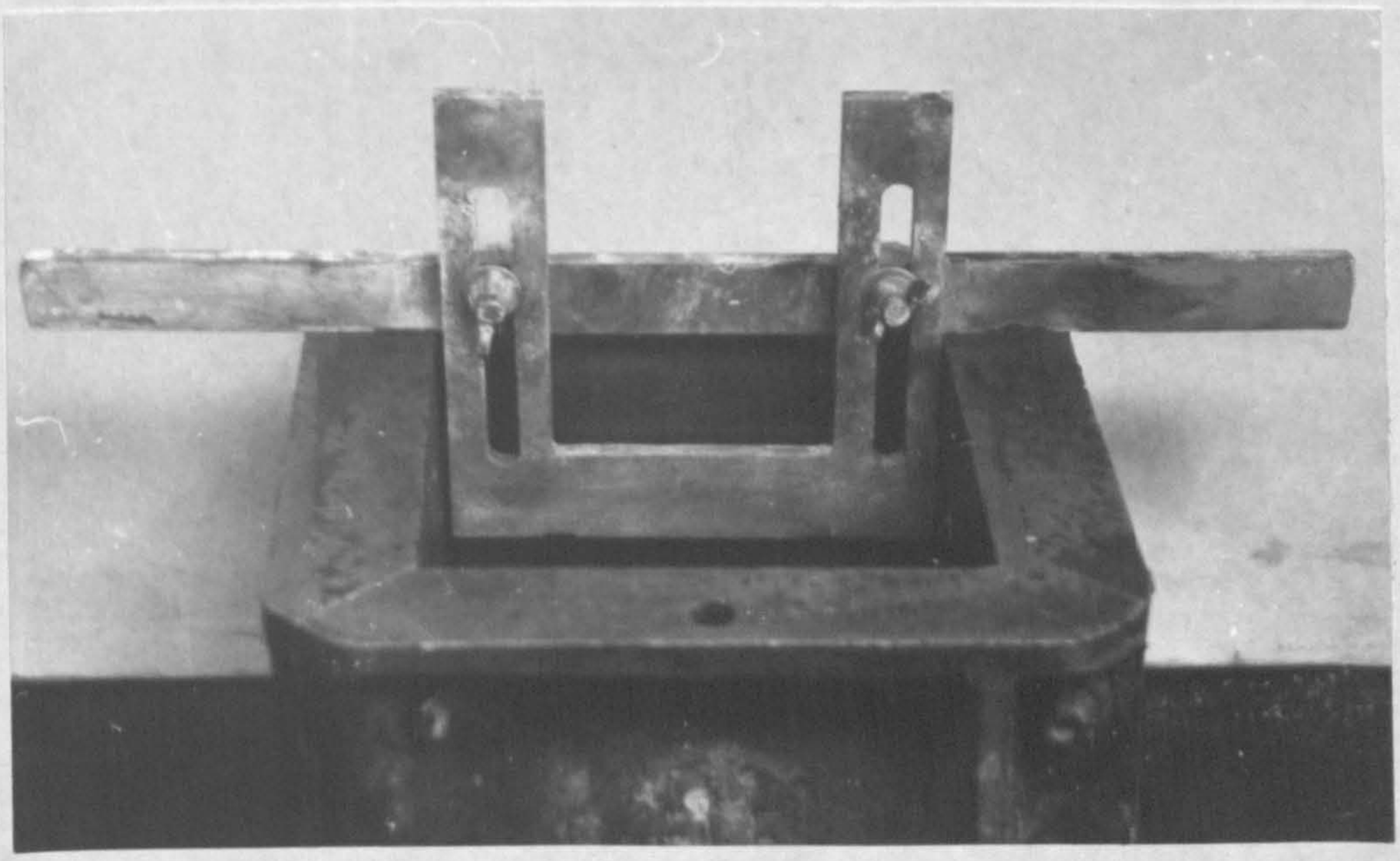

PLATE 3.2 ADJUSTABLE LEVELLING BAR

PLATE 3.3 GUN AND MOUNTING FRAME

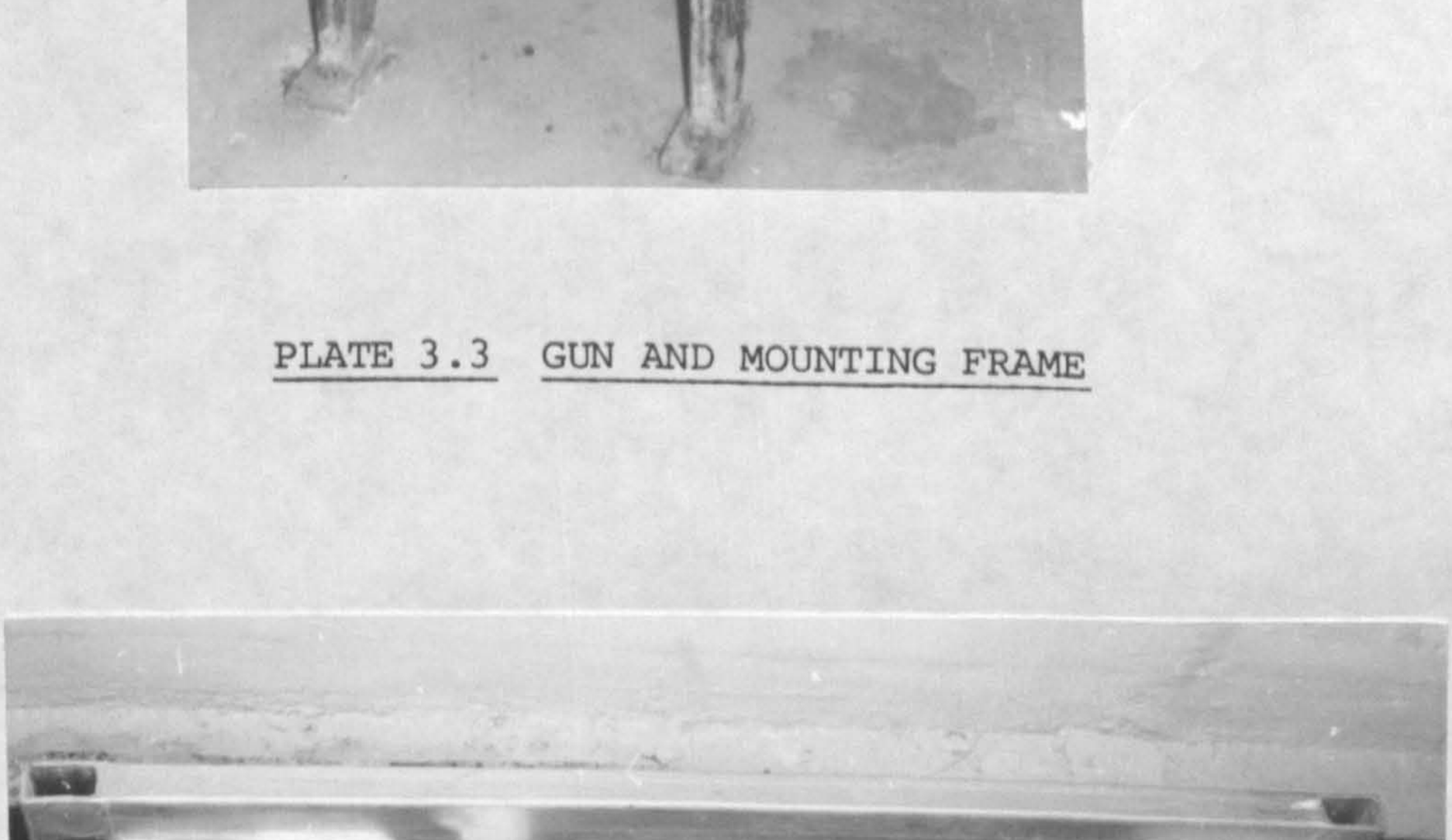

PLATE 3.4 FIRING SOLENOID, LINKAGE, AND NO. 3 PRESSURE HOUSING

PLATE 3.5 TARGET SPECIMEN HELD IN POSITION WITH ELASTIC STRAPS

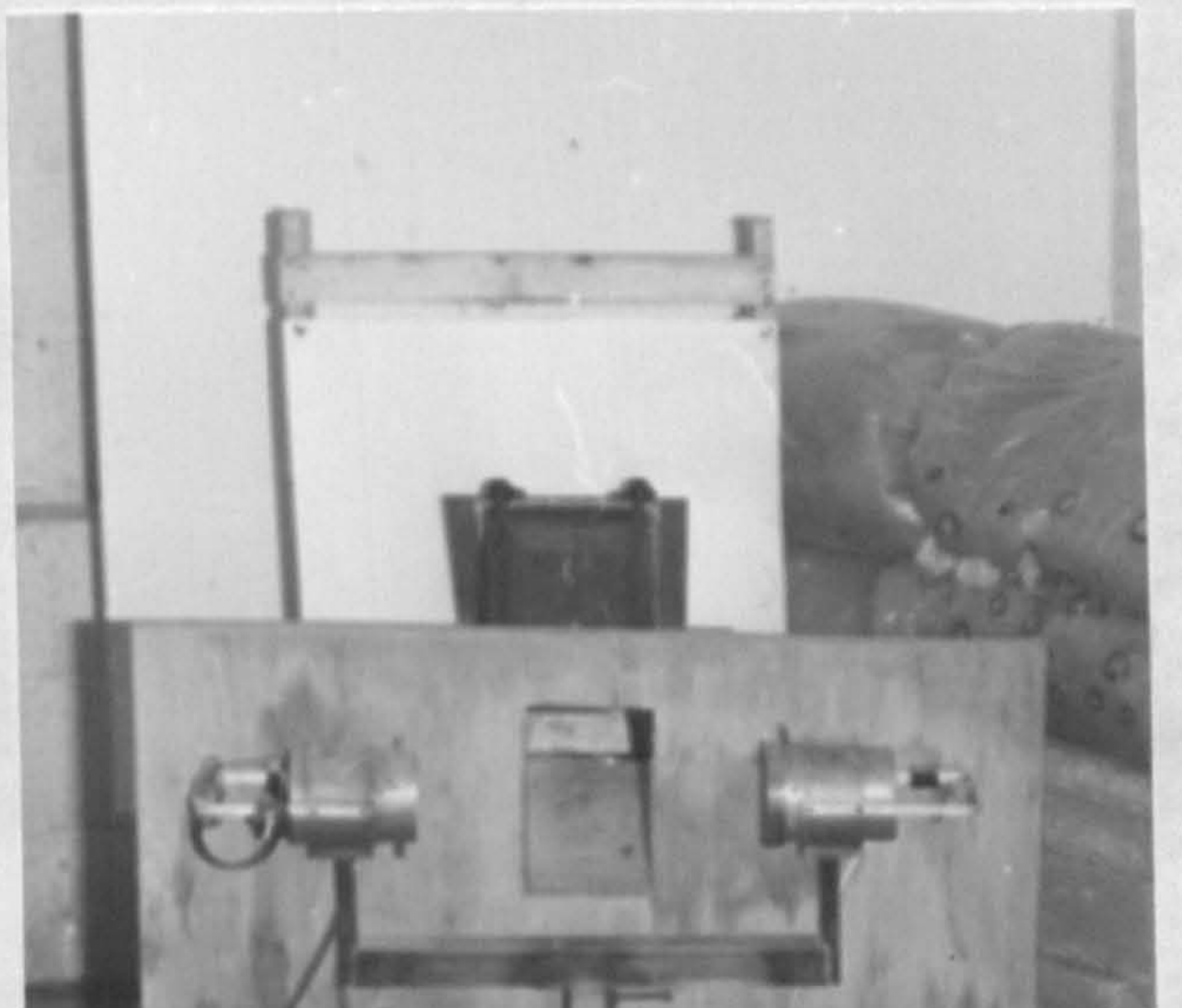

PLATE 3.6 VELOCITY MEASURING RIG, VIEWED FROM ABOVE FIRING LINE

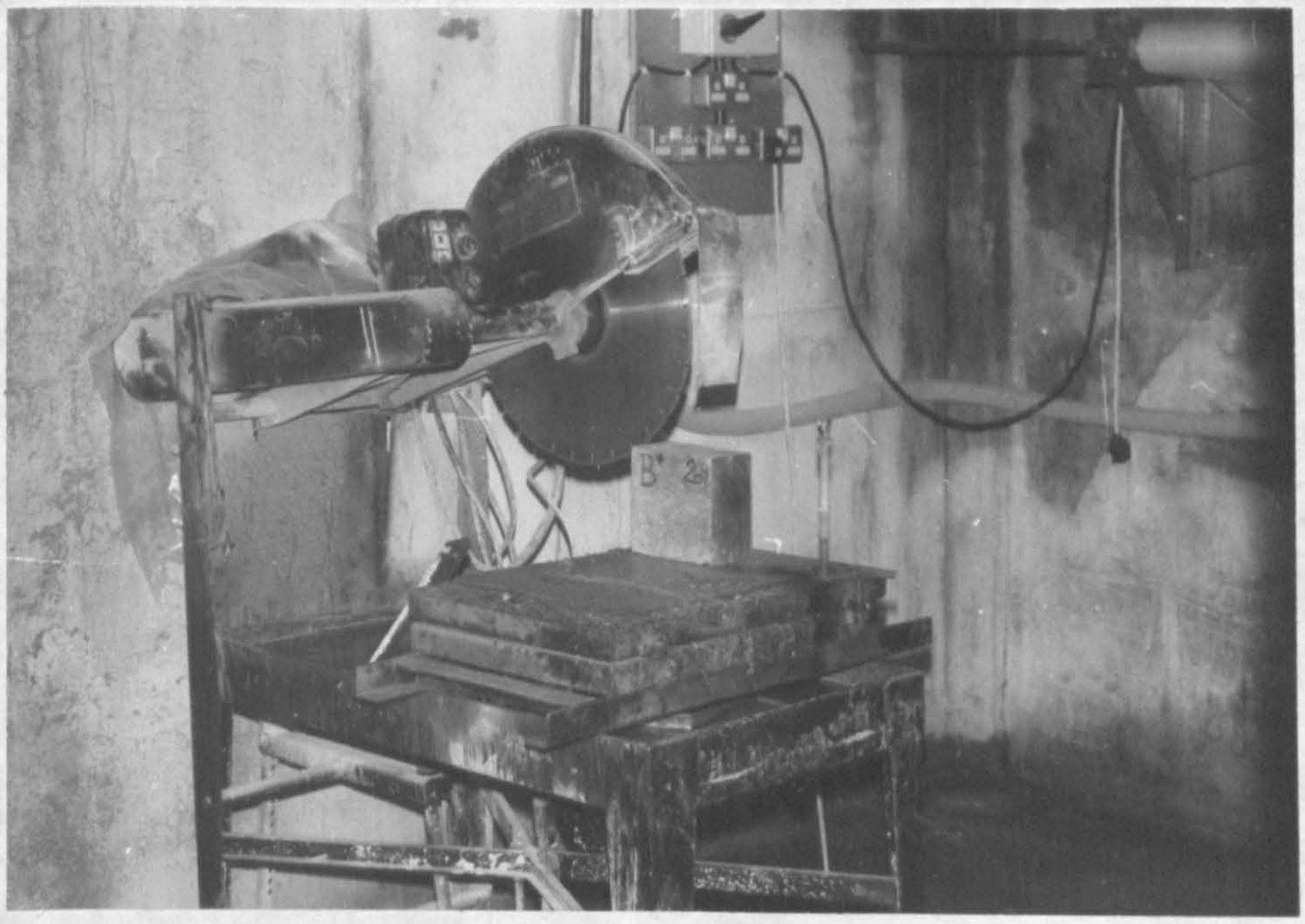

PLATE 3.7 CLIPPER CUTTING MACHINE WITH SPECIMEN, PRIOR TO CLAMPING

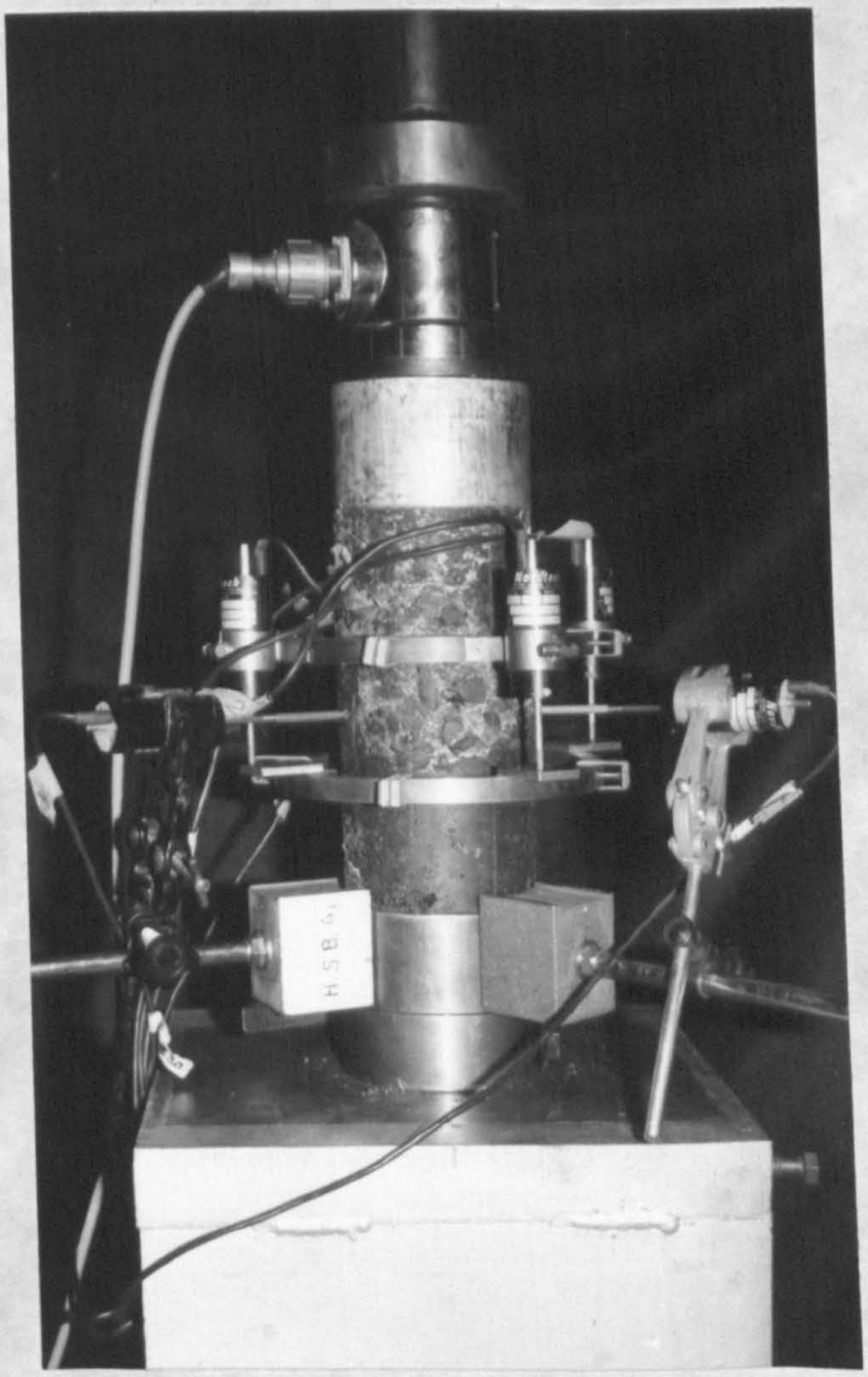

PLATE 3.8 UNIAXIAL COMPRESSION TEST RIG

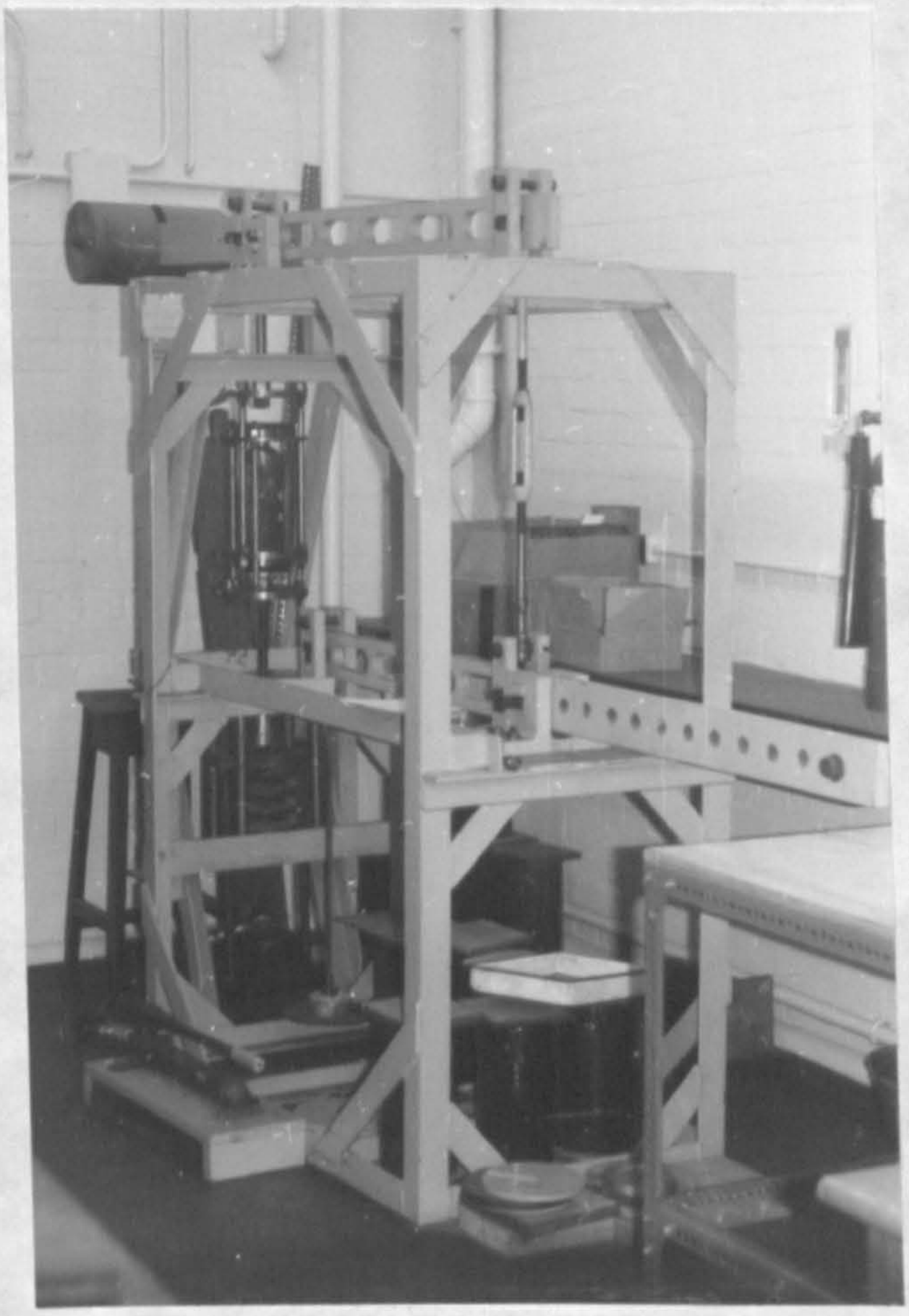

PLATE 3.9 CREEP TEST RIG, WITH SPECIMEN IN POSITION

CHAPTER 4

EXPERIMENTAL PROGRAMME AND METHODS OF ANALYSIS

4.1 Penetration Tests - General

4.1.1 Method of Approach

The various available theoretical and semi-empirical approaches to the mechanics of penetration were discussed in Chapter 2, and all were found to be inapplicable in the case of the composite. It was thus necessary to develop a new approach tailored to the specific circumstances arising from the nature of the composite. At this stage it is useful to tentatively discuss the likely progression of events during the penetration process of an armour piercing projectile into the composite.

When the projectile collides with the composite, the initial stages of penetration are likely to be in the polyurethane/sand matrix. Compressive stress waves will be set up in the visco-elastic material leading to limited compressive damage and radial cracking due to circumferential tensile stresses. Heat generation, which will continue throughout the penetration event, will begin due to friction. Erosion of the projectile sheath begins, mainly due to the abrasive nature of the sand in the matrix.

Next the projectile encounters a rock particle, probably at an oblique angle. If this was a simple elastic collision, between two unrestrained bodies, then the behaviour could be predicted; the projectile would transfer momentum to the rock particle and begin to tumble (i.e. rotate about a radial axis through its centre of gravity). The momentum gained by the rock particle would also include a rotational component.

However, because of the high impact velocity, the collision is not an elastic one. The impact generates intense compressive stress waves. These will cause crushing in the rock particle, some radial cracking due to tangential

tensile stresses, and other tensile failure following stress wave reflection from the rock particle boundaries. This reflection will also partially or wholly destroy the rock/polymer bond for the particle in question. Only relatively weak compressive waves are likely to reach adjacent rock particles through the polymer matrix because of the differing rock/polymer modulii, but points of contact between the rock particles would give points of transmission for compressive waves. Local crushing is possible at these points of contact. Some tensile failure in the adjacent particles is also likely in the same way as in the impacted particle.

The projectile will also incur damage. The soft sheath will be partly stripped from the hard core over the area of impact. Serious compressive damage of the core is unlikely because of its very high strength; instead tensile stress waves set up may cause its breakup. For a given projectile, the extent of this breakup will depend on the orientation of the collision, and upon the modulus and compressive strength of the rock material. The non-symmetry of the impact will tend to cause a trajectory change and tumbling of the projectile. Unless the projectile is shattered, it will tend to restabalise when in the softer polymer matrix.

Collisions with further rock particles add to the complexity of the situation. As the projectile is further showed by energy expended is in momentum transfer, comminution of rock particles, projectile damage, heat etc., the elastic component of the collisions will become of greater importance.

Theoretical analysis of this highly complex situation described above was considered to be impossible within the time available and after much deliberation, an empirical approach was chosen based on response surface theory, more normally used in the fields of chemistry and biology. This method helped determine the correct proportions of the composite components to give the best end product i.e. to aid optimization. Before describing this method of experimental planning, the variables of possible interest are examined.

4.1.2 Examination of Variables

Table 4.1 gives a list of quantitative dependent variables. The average surface diameter and volume of the burrow/crater were of limited interest, because target damage was hoped to be kept to a reasonable level, and below this level was not considered important. Much of the projectile's energy was likely to have been expended in comminution of the aggregate particles, but the practical problem of separating rock and polymer once cast to measure this would have meant much time being spent with results being of dubious value.

The fundamental aim of the project was to minimise the target thickness necessary to resist perforation, whilst keeping the cure time and the impact damage to the composite to an acceptable level. Thus the normal penetration or penetration path length were considered as alternatives for the design criterion. The former was used initially but replaced by the latter because of its greater physical significance: a projectile internally deflected through 90^{o} would show no further increase in normal penetration. This would give a misleading impression of the target's penetration resistance. Target specimen damage by excessive cratering, cracking, or even fragmentation,is not considered in the optimisation procedure described later, but the occurrance of these effects in the optimised composite under normal conditions was deemed unacceptable. In addition,the thickness of optimized composite necessary to resist perforation with a given confidence level was examined.

Qualitative independent variables examined were rock type, type of fines, polymer type and bullet type. All except type of fines were considered of marked importance. Zone II or Zone III sand to BS 822: Pt 2 : 1973 was used as fines in the composite for reasons of availability. Variation of this was not thought likely have any great influence on penetration. Details of the other three qualitative independent variables are given below:

(i) rounded river gravel, crushed basalt and limestone represented,in general terms, high strength, medium strength, and low/medium strength rock types respectively. In addition, limited tests on hornfels, a very high

strength rock, were carried out late in the project for comparison purposes only. The properties of these rocks, and their relationships with the total available range of properties, have been discussed in Chapter 3.

(ii) of all the resins surveyed, polyester (Diorez 570) and polyether (2851) polyurethanes were the only ones whose properties were acceptable and warranted detailed studies.

(iii) 7.62 mm armour piercing (A.P.) and ball ammunition were the standard NATO types used in this project.

Quantitative independent variables are given in Table 4.2. These were subdivided into primary and secondary variables. Primary variables were those which determined the composite mix proportions and ingredient characteristics used. Thus they were % polymer by weight, x_1, % rock aggregate by weight, x_2, rock aggregate size, x_3, and polymer hardness, x_4. These primary variables were used in the optimization procedures. Secondary variables were those whose effect needed only to be investigated using optimized primary variable levels. The levels of the secondary variables were kept as constant as possible during optimization of the primary variables. These levels are also given in Table 4.2.

4.2 Preliminary Penetration Tests

Preliminary target specimens P1 to P3 were cast from three types of polyurethane elastomers: LS480 polyether, 2851/201 polyether and Diorez 570 polyester.

The mixes used, given in Table 4.3, were chosen after trial castings to determine what intuitively seemed to be the correct proportions. The levels used at this stage were not critical as only general information was needed from these tests. The specimens were freestanding during testing, with a concrete block placed on top of them to give greater stability on impact.

It was hoped that four spaced penetration tests could be carried out on each of these specimens of 152 mm square frontal area. However, the

impact face damage which occurred, shown in Plates 4.1 to 4.3, led to the conclusion that only one test was possible for each specimen, i.e. a central impact.

The normal penetrations measured, also given in Table 4.3, suggested that a specimen thickness of 125 mm was a good estimate to try in initial tests.

The 2851/201 resin used for the block shown in Plate 4.2, was not considered suitable because of the excessive damage occurring.

Diorez 570, the lowest viscosity polyester polyurethane found during the materials research, was considered satisfactory for further testing.

LS480 was thought at this stage to be the likely polyether polyurethane to be tested. Unfortunately, it was subsequently withdrawn from the market due to chemical instability in storage. Hence an alternative polyether polyurethane had to be used, and after discussion with the manufacturers of LS480, 2851/304 and 2851/219 polymers were recommended as the best alternatives. These could both be used with either of two isocyanates; 003 or Isonate 143L. The latter was also used with Diorez 570, and needed a storage temperature of over 20^{o}C. Six central impact penetration tests were carried out, with mixes based on the 2851/304 and 2851/219 polyurethanes, and results are given in Table 4.4. An 85 mm diameter conical crater was formed in specimen P4. This was considered unacceptable, both because it represented a large damage radius and because it suggested the likelihood of rear face scabbing in thinner specimens due to brittle behaviour. Hence the remaining tests used 2851/304 resin with both isocyanates. The penetration path lengths from these very limited tests suggested 003 isocyanate to be superior. Added to its lower cost and less critical storage requirements, this was considered sufficient information on which to decide on this isocyanate. To give a range of polymer hardnesses, a blend of 2851/304 and 2851/219 resins, henceforth called 2851 resins, with 003 isocyanate was used.

Table 4.5 gives a summary of the resins and ammunition types used in the preliminary and main tests.

4.3 Optimization of Penetration Resistance - Experimental Design and Analysis

4.3.1 Description of Method

As discussed in Section 4.1, it was necessary to optimize the four primary quantitative (x) variables,% resin, % rock, rock size and polymer hardness,in terms of penetration. Normally, this would be carried out by keeping three variables constant, varying the fourth, and repeating this procedure for all four variables. Thus sets of fitted equations would be obtained, each in only one x variable. From this stage, optimization can only be achieved by examining general trends, and carrying out experiments on a trial and error basis.

Response surface theory was used to overcome these difficulties. It enabled a unified equation to be obtained for any qualitative variable combination, relating penetration path length or normal penetration to all four x variables at once. At first standard designs were used (Cochran and Cox, 1959); later these were adapted to the particular requirements of this project. Details of the theory are given in Appendix A.2, but it is worthwhile describing it briefly here and giving the terminology used.

Each x variable, or factor, was examined at various values, or levels. These levels may be simplified by translating them into coded levels. For example, a factor at levels 70, 80 and 90 may be coded to -1, 0, +1. The effect on the dependent variable, i.e. penetration,of varying the factor levels is called the response. The response surface is the unified equation mentioned above relating the penetration to the four x variables. This equation is a polynomial which may theoretically be of any degree (linear, quadratic, cubic, etc) and is fitted to the experimental data by multiple regression. In practice the degree of the fitted polynomial is usually limited to 2, i.e. a quadratic expression. To physically represent a response surface with more than 3 x variables is very difficult. A simple example of a quadratic response surface in two x variables, with a response y, may be represented as a contour

map, as shown in Figure 4.1. This figure is drawn to show a minimum value of y.

A fitted response surface does not normally coincide exactly with the experimental points. The difference between the actual and predicted levels is the residual. This is composed of lack of fit, experimental or measurement errors e.g. actual penetration path length, and random error. Tests are described in Appendix A.2 which determine whether the lack of fit is significantly larger than the sum of the experimental and random errors.

4.3.2 Linear Polynomial Fitting

Experimental designs (Cochran and Cox, 1957) were used for linear response surface fitting, to enable an initial estimate of the response magnitude to be obtained, and the relative importance of the four x variables to be examined. These tests used the three main rock types (limestone, basalt, river gravel) with Diorez 570 and A.P. ammunition. The 2851 resins were not available at this stage. The three resultant test series were denoted as series 1 to 3.

The fitting of a linear polynomial required that each x variable was set at 3 levels. The experimental design used is given in Table 4.6. It consisted of a half replicate of a 2^4 factorial i.e. half of all combinations of x_1 to x_4 at two coded levels +1 and -1, with three repeated tests at the centroid $x_1 = x_2 = x_3 = x_4$ = coded level 0 to give an estimate of experimental error.

The actual factor levels corresponding to the coded ones are given in Table 4.7, and represented what were considered to be practical ranges, with intervals of a significant size.

The form of the fitted equation is

$$D_p \text{ or } D_p' = b_o + b_1x_1 + b_2x_2 + b_3x_3 + b_4x_4 \qquad \ldots 4.1$$

depending on which dependent variable is used, and with

x_i in the coded scale

D_p = predicted normal penetration

D_p' = predicted penetration path length

b_o = mean penetration, i.e. predicted penetration with x values at coded level O.

b_1 to b_4 = numerical coefficients

The explanation of the procedure will continue using penetration path length only.

It can be shown that the coefficient b_i may be evaluated from the following equations

$$b_o = \frac{\sum_{1}^{11} D_i'}{11} \quad \ldots 4.2$$

$$b_1 = \frac{\sum_{1}^{4} D_i' - \sum_{5}^{8} D_i'}{8} \quad \ldots 4.3$$

$$b_2 = \left(\frac{D_1' + D_2' + D_5' + D_6' - D_3' - D_4' - D_7' - D_8'}{8}\right) \quad \ldots 4.4$$

$$b_3 = \left(\frac{D_1' + D_3' + D_5' + D_7' - D_2' - D_4' - D_6' - D_8'}{8}\right) \quad \ldots 4.5$$

$$b_4 = \left(\frac{D_1' + D_4' + D_6' + D_7' - D_2' - D_3' - D_5' - D_8'}{8}\right) \quad \ldots 4.6$$

where D_i' is the measured penetration path length into the i^{th} specimen of the test series

The next step was to determine whether the fit of the linear polynomial was adequate. This process is described in Appendix A.2.

The test was passed in all cases. Normally the fitted equation would then be used to determine the line of steepest ascent or descent, to try to approach the maximum or minumum of the actual response surface and, once there, to use a quadratic design. However, the low repeatibility evident from the results meant that the number of useful increments of variables over the practical variable range was of the region of 5-6 for all x variables. Hence it was decided to move directly to a quadratic analysis.

4.3.3 Quadratic Polynomial Fitting - Main Test Series

Fitting of these polynomials was carried out on each of seven qualitative variable combinations. Six of these were all the combinations of the basalt, limestone, and river gravel with the Diorez 570 and 2851 resins, using A.P. ammunition.

It was strongly suspected that the ball ammunition would give lower penetrations than A.P., so only one test series was carried out using ball, i.e. rounded river gravel/2851 resins/ball ammunition. These tests series were denoted as series 4 to 10.

The main experimental design for quadratic polynomial fitting is given in Table 4.8, as tests 1 to 31. It is composed of a full 2^4 factorial, (all combinations of x_1 to x_4 at coded levels +1 and -1) with seven repeated points at $x_1 = x_2 = x_3 = x_4 = 0$. In addition, to give the necessary range for quadratic fitting, 8 points were included with each variable taking ± 2 in turn, with all others at zero. These latter points can be visualised as extending the basic cubic shape of the design into a star shape: hence the name 'star design' which is normally used. The dependent variable used as the response was penetration path length, D'.

Having been tested, each specimen was sectioned parallel to the impact face using the equipment described in Section 3.4. Initially these cuts were made at regular intervals from the impact face: 25 mm, (37.5), 50, 62.5, 75, 87.5 etc. The bracketed figure was included when a low penetration was expected. However, this amount of sectioning was very time consuming; later the section spacing was decided upon depending upon experience of similar target specimens.

The calculation of the penetration path length, D', is shown in Figure 4.2

The choice of the five necessary levels of each factor was relatively simple because of physical limitations, and it was hoped that the combination of factor levels giving a minimum penetration path length would be near to the centre of these ranges. The equivalent real factor levels to coded factor levels may be seen in Tables 4.9 and 4.10 for Diorez 570 and 2851 resins respectively. The % resin, x_1, is higher, and % rock, x_2, lower, for Diorez 570 to overcome the effect of its greater viscosity. The differing hardnesses, x_4, are the result of material property constraints.

The experiments resulted in a value of penetration path length for each specimen within each test series, and for seven such test series in all.

Fitting of the quadratic response surface to these values of penetration path length was carried out using part of an available program, SPSS (Statistical Package for Social Sciences). The steps necessary to use this package in a program called PENET, are given in Appendix A.3

The fitted equation, with all x variables in the coded scale, takes the form

$$D_p' = b_o + b_1x_1 + b_2x_2 + b_3x_3 + b_4x_4$$
$$+ b_{12}x_1x_2 + b_{13}x_1x_3 + b_{14}x_1x_4$$
$$+ b_{23}x_2x_3 + b_{24}x_2x_4 + b_{34}x_3x_4$$
$$+ b_{11}x_1^2 + b_{22}x_2^2 + b_{33}x_3^2 + b_{44}x_4^2 \qquad \ldots 4.7$$

where b_o is the predicted penetration with all coded x levels at zero.

b_1 to b_{44} are x term coefficients

Checks for lack of fit of the response surface are given in Appendix A.2. A three step mathematical procedure was used to locate and describe the stationary point on the response surface. A minimum predicted penetration was hoped for.

(i) The response surface equation was differentiated with respect to each x variable in turn, giving four simultaneous equations.

(ii) These equations were solved to give the x_n coordinates of the stationary point, using a matrix inversion program MATINV. (Appendix A.3)

(iii) The cancnical transformation of the response surface was found, to enable the nature of the stationary point to be truly determined (i.e. maximum, minimum, or complex

saddle point) using a method described by Davies (1954) supplemented by the program EIGEN (Appendix A.3) which found the eigenvalues of the resultant determinant. These eigenvalues were the coefficients of the transformed equation.

Unfortunately, no minimum was found to exist on the surfaces and the above procedures were hence abortive, and are therefore not described in detail.

It was thus necessary to numerically scan the response surface, to locate the variable combinations giving the lowest values of D_p', whilst still considering cost effectiveness and practicality of manufacture. A program CODEFIT was written which calculated D_p' for each of the 625 possible combinations of the four x variables at the five levels used. See Appendix A.3

As mentioned earlier, a star design was used for the main quadratic analysis. Figure 4.3 shows, for two x variables, the area covered by the star design and that covered by a numerical computer scan such as CODEFIT. The combinations of x variable levels outside the experimental area gave equated values of D_p', but these were only examined for trends: their numerical values could not be relied upon because of the inaccuracy of quadratic equations when extrapolated.

4.3.4 Corner Filling in the Quadratic Design-First Stage

In all cases examined, low values of D_p' were indicated in a corner of the scan, i.e. at one of the 16 corner combinations of $x_1 = \pm 2$, $x_2 = \pm 2$, $x_3 = \pm 2$, $x_4 = \pm 2$. As discussed in section 4.3.3, the actual predicted values of D_p' in these areas are open to doubt, so extra tests were carried out in the most promising corners of some test series. Tests 32 to 38 in Table 4.8 show the extra variable level combinations used where the corner of interest was, as an example, $x_1 = -2$, $x_2 = x_3 = x_4 = +2$.

As implied above, some test series were excluded from 'corner filling'. The results for both resin types for the basic design are compared in Chapter 5, with 2851 resins showing superiority. Hence only the combination of the best rock type, rounded river gravel, was used with Diorez 570 for corner testing. The three series with 2851 resins and A.P. ammunition were continued. The low penetrations obtained from the ball ammunition into 2851 resins with rounded river gravel meant that this series could be discontinued before corner testing, as A.P. ammunition would give more significant results.

The inherent assumptions above of inferior performance by Diorez 570 and ball ammunition are discussed in more detail in Chapter 5.

Having carried out the extra corner tests, PENET was repeated, giving a modified version of equation 4.7. CODEFIT was then applied again.

In the case of the best rock/polymer type combination with A.P. ammunition, i.e. rounded river gravel with 2851 resins, a solution was obtained at this stage and the optimization procedure was complete. However, for the other test series the results were still contradictory, and further corner filling of other corners was necessary, as described below.

4.3.5 Corner Filling-Second Stage

Examination of predicted penetrations (see results in Chapter 5) for corners of the x variable field shows that large extrapolation errors are evident. When one corner in each series was the subject of further tests i.e. corner filling-first stage, this removed the extrapolation error from this corner. However, the lack of symmetry which now existed in the experiments had the effect of indicating another corner as giving lower penetrations. Thus other corners needed extra tests. The total number of corners was 2^4 i.e. 16, of which one had already been examined. To examine the other 15 would have been too time consuming, and so certain assumptions were made. These were

(i) that values of x_3 (rock aggregate size) below coded level zero are not of interest. This assumption was backed up by an isolated series of seven tests using smaller limestone aggregate with 2851 resins and A.P. ammunition. The penetration path lengths obtained were very large.

(ii) that values of x_1 (% polymer) greater than coded level zero were not cost effective. Based on the results which had obtained at this stage of the analysis, this assumption was a reasonable one.

Thus the number of corners to be tested was 2^2 i.e. four, minus the one already examined, leaving three. Three tests, representing a quarter of the possible combinations, were carried out in each of these 3 corners.

In the example given in Table 4.8, these second stage corner tests are represented by tests 39 to 47.

After the second stage corner tests, PENET was used again to refit the response surface, and CODEFIT to scan the x level combinations to find those giving low values of D_p'.

The solutions obtained were then tested on target specimens of a realistic thickness, as described in the next section.

4.4 Determination of Minimum Target Thickness

The penetration tests described earlier used a nominally 152 mm thick specimen, intended to be perforated only very rarely,if at all. Thus, in most cases, the effect of the rear face as a free surface was likely to be small. However, when the best, or most cost effective, combination of x variables had been found i.e. the optimum mix, it was necessary to determine the value of the specimen thickness, t_m,which would contain the bullet with a given degree of confidence.

The first stage was to determine, by testing specimens of varying thickness,

the thickness at which perforation began to occur. From these results, a thickness which contained 80-90% of the projectiles was sought, and further tests carried out at this thickness for confirmation purposes. Thus, for a series of 20 tests at the thickness, 2 to 4 perforations would be expected. Also, the mean penetration, plus the required number of standard deviations, should also correspond to this thickness. With a perforation nominally given a penetration value, D , equal to the thickness, t, + 10 mm and the values of D determined for the rest of the specimens by sectioning, an estimate of a protection level of 97.5 to 99% was obtained by increasing the specimen thickness by a relevant multiple of the standard deviation of D. Normal penetration D was used instead of penetration path length D_p' because it included the element of random variation due to non-normal penetration. Also, if the estimated 80-90% confidence thickness was not satisfied by the thickness tested, this thickness could be calculated by again applying the correct multiple of the standard deviation.

In the composite giving the best results, the thickness calculated for 97.5 to 99% confidence level was tested.

4.5 Supplementary Penetration Tests

4.5.1 Limited Testing of Another Rock Aggregate

As expected, the test results indicated lower penetration with increasing aggregate strength. A limited number of tests were therefore carried out on a very hard aggregate, hornfels. Seven tests were carried out at $x_1 = x_2 = x_3 = x_4 = 0$ (coded) to compare with the repeated tests at the centre of the main quadratic designs, using 2851 resins and A.P. ammunition.

4.5.2 Target Temperature Effects

In practical use, the composite may be subjected to extremes of temperature. The polymer,especially,is very temperature sensitive, and liable to brittle behaviour at low temperatures. Accordingly, limited penetration tests were carried out on the 80-90% confidence level thickness, 80 mm, for the best rock/polymer combination,rounded river gravel with 2851

resin, at its optimum mix. The initial temperatures were -18°C and +45°C, but these were expected to change during specimen transportation. Age at testing was 3 days, to allow the cure to have reached a high level before changing the temperature. Testing after 1 day, as in the normal penetration tests,would have confused the cure and temperature effects. Twenty tests were carried out at each temperature.

4.5.3 Effect of Cure Temperature

For 2851 resins the manufacturers suggest that a temperature rise of 10°C will approximately double the cure rate, and a similar drop in temperature will approximately half the cure rate.

For Diorez 570, the material can only reach a proper level of cure at an elevated temperature. This temperature can normally be achieved by the heat of reaction. However, the reaction speed necessary to produce this heat meant an insufficient time for casting. Low catalyst levels were therefore used to retard the cure rate and the required high temperature for full cure was not achieved in the composite. This is a likely explanation for the inferior performance of Diorez 570 composites when compared with the 2851 resin composites.

4.5.4 Effect of Cure Time

The main evidence on the variation of properties with time came from the beam bending tests described later. However, a comparison of 1 day and 3 day penetration resistance was carried out for rounded river gravel, 2851 resin blend, and A.P. ammunition. Twenty tests on 80 mm thick specimens at the optimum mix were carried out at each time, and the number of perforations and mean vertical penetration of those bullets contained, were compared. Normal penetration D was used for comparison purposes instead of penetration path length, D_p', because the former was of more relevance in thickness tests.

4.5.5 Effect of Moisture

Significant quantities of water in the mix have a catastrophic effect on the curing reaction, resulting in a soft, spongy material.

The manufacturers suggest that small amounts of water may be compensated for, with 2851 resins, by adding 15 g of isocyanate for every 1 g of water in the rock or sand. However, it is likely that this procedure would distort the final properties considerably, and, if possible, dry materials should be used, with a moisture content of less than 0.01%.

4.6 Static Tests

Since penetration tests showed that 2851 resins gave a superior performance, static tests were only carried out on composites based on these.

4.6.1 Bulk Density Tests

Compacted and uncompacted bulk density tests were carried out as described in Chapter 3 to enable the percentage voids to be calculated as described in BS 812 : Pt 2 : 1975. This was useful for comparison with the optimum mixes arrived at Chapter 5. A sample of the sectioned specimens for each main rock type were used to determine the voids in the final mixes by tracing the section onto graph paper, and counting the area of the rock particles.

4.6.2 Uniaxial Compressive Tests

One possible use envisaged for the composite was to form an exterior blockwork skin to a structure. Hence basic information concerning the compressive properties of the optimum mixes was determined. Using the equipment described in Chapter 3, the following information could be determined for each optimum mix.

(i) stress-strain characteristics under uniaxial loading conditions,

(ii) the effect of strain rate on the above,

(iii) maximum compressive stress,

(iv) Poisson's ratio.

Three tests on each of the three main rock types at each of three displacement rates (1.27, 2.54, 5.08 mm/min) were carried out, giving a total of 27 tests in all.

4.6.3 Creep Tests

These tests, described in Section 3.6.2, were carried out because of the

susceptability of polymers to creep due to the large viscous element in their behaviour. The tests were carried out on identical specimens to those described in the previous section: two tests for each main rock type, with an additional test for river gravel, because of its superior behaviour in the penetration tests.

It was considered unlikely that the composite would ever be used in a load bearing situation. Hence, an estimate of working load was obtained by estimating the stress due to self weight over a 10 m height of composite, equivalent to three storeys.

Values of strain, evaluated from each of the three pairs of Demec points, were averaged to eliminate bending effects.

4.6.4 Beam Bending Tests

The beam bending tests were carried out to assess the maximum size of panel of the composite which could be transported and handled without failure occurring.

The arrangement described in Section 3.6.3 yielded deflection-time data, and failure load. In addition, loading rate was known. In all cases failure occurred between the loading points, so the BS 1881 : Pt 3 : 1970 formula could be used to calculate tensile stress:

$$f_{bt} = \frac{P.l}{bd^2} \qquad \ldots 4.8$$

where f_{bt} = tensile stress (N/mm^2)

P = total applied load (N)

b = beam width (mm)

d = beam depth (mm) and l = beam span (mm)

A full stress-strain plot was obtained as follows

(i) Points were chosen spaced throughout the deflection-time datalogger output.

(ii) Knowing the failure load and loading rate, the loads corresponding to the above deflection readings were calculated.

(iii) Using the central deflection formula for the above loading case

$$\delta = \frac{23Pl^3}{108bd^2E_{sec}} \qquad \ldots 4.9$$

where δ is the central deflection

l is the span

E_{sec} is the secant modulus,

the value of E_{sec} was calculated at each point considered.

(iv) Equation 4.8 was used to calculate f_{bt} at each load from (ii).

(v) knowing the stress and secant modulus at each point, the strain e could easily be calculated from

$$E = \frac{\sigma}{e} \qquad \ldots 4.10$$

Three tests were carried out for each of the three main rock types at an age of one day. In addition, to examine the variation of properties with time, the tests with rounded river gravel were repeated, again in triplicate, at ages of 3 hrs, 8 hrs, 3 days and 9 days.

Maximum panel size was evaluated from the failure stress (modulus of rupture, R) results in the following way

(i) Assume maximum allowable stress during handling is R/3.

(ii) Assume worst loading condition, the unstable equilibrium where a beam with u.d.l. is balanced centrally.

Thus maximum bending moment

$$M = \frac{Ptl^2}{8} \qquad \ldots 4.11$$

where P = material density

l = maximum panel length

t = panel thickness

$$\text{Also} \quad \frac{R}{3} = \frac{M}{Z} = \frac{6M}{t^2} \qquad \ldots 4.12$$

Eliminating M from equations 4.11 and 4.12

$$1 = \sqrt{\frac{4}{9}\frac{tR}{\rho}} \qquad \ldots\ 4.13$$

Variable	Symbol	Units
* Normal penetration (thick target)	D	mm
* Penetration path length (thick target)	D'	mm
Average surface diameter of burrow/crater	d_b	mm
Volume of burrow/crater	V_b	mm^3
Degree of comminution of rock aggregate particles	C	-
* Min. target thickness for a given confidence level for containment	t_m	mm

* Variables used

Table 4.1

Quantitative dependent variables in the penetration experiments

Variable	Symbol(Units)	Value in optimization programme
*% polymer by weight in mix	x_1	variable
*% rock aggregate by weight in mix	x_2	variable
* rock aggregate size	x_3 (mm)	variable
* polymer hardness (fixed by ingredient proportions)	x_4 (Shore A°)	variable
+ specimen cure temperature	T_c (°C)	ambient
+ specimen temperature at testing	T_s (°C)	ambient
+ age of specimen	t_s (days)	1
+ specimen thickness	t (mm)	152
+ moisture content of sand and rock	w	0
bullet velocity	v m/s	approx 810

* Primary quantitative variables considered in the optimization programme.

+ Secondary quantitative variables whose effects were examined on one or more qualitative variable combinations at optimum primary quantitative variable levels.

Table 4.2

Quantitative independent variables in the penetration tests

Specimen Number	P1	P2	P3
% weight polymer	14	14	14
% weight 20-28 mm limestone aggregate	54	54	54
% weight sand	32	32	32
Polymer type	LS480 polyether polyurethane	2851/201 polyether polyurethane	Diorez 570 polyester polyurethane
Mechanical props.- fully cured	Fairly Good	Poor	Good
Target specimen thickness t (mm)*	130	100	120
Vertical penetration D (mm)	Shot 1 Ball 80 2 A.P. 100 3 A.P. 85	1 Ball (P) 2 A.P. (P)	1 Ball 78 2 A.P. 75 (S) 3 A.P. 100 (S)

* Block thickness dependent upon polymer sample availablity
(S) indicates exit from side of specimen at this depth
(P) indicates perforation

Table 4.3

Preliminary Target Specimen Data

Specimen Number	P4	P5	P6	P7	P8	P9
% weight of polymer (x_1)	17	11	15	13	13	11
% weight of rock aggregate (river gravel) (x_2)	52	52	60	56	56	52
Aggregate size (mm) (x_3)	26.5	26.5	13.2	19	19	26
% weight of sand	31	37	25	31	31	37
Type of polymer	219	304	304	304	304	304
Type of isocyanate	2875/003	2875/003	2875/003	2875/003	Isonate 143L	Isonate 143L
Hardness of polymer (Shore A°) (x_4)	95	68	68	68	68+	68+
Vertical penetration D (mm)	37	40	64	51.5	51.5	76.5

Target size 152 mm cube

Table 4.4

Tests on 2851/304 and 2851/219 based composites to find an alternative to LS480 polyether polyurethane

Test group	Resin type	Ammunition type	Rock type	Impact condition
Preliminary tests (Section 4.2) Specimens P1-P3	Diorez 570 210 LS480	A.P. & Ball	Limestone	multiple, spaced impact Target freestanding
Tests for replacement polyether resin (Section 4.2) Specimens P4-P9	2851/219 2851/304	A.P.	River gravel	single central impact Target rear perimeter supported
Main tests (Section 4.3)	2851/219 & 2851/304 blended → called 2851	A.P. & Ball	River gravel crushed limestone crushed basalt crushed hornfels	single central impact Target rear perimeter supported

Table 4.5

Summary of preliminary and main penetration test materials

Target block no. (within a test series)	1	2	3	4	5	6	7	8	9,10,11
Resin % wt. x_1	1	1	1	1	-1	-1	-1	-1	0
Rock aggregate % wt. x_2	1	1	-1	-1	1	1	-1	-1	0
Rock size (mm) x_3	1	-1	1	-1	1	-1	1	-1	0
Pure polymer hardness x_4	1	-1	-1	1	-1	1	1	-1	0

Table 4.6

Combinations of coded values of variables

comprising a test series for linear fitting of results

Value (coded scale)		-1	0	+1
Levels	Resin % wt. x_1	11	13	15
(actual scales)	Rock aggregate % wt.(LIMESTONE, RIVER GRAVEL) x_2	51	55	59
	Rock aggregate % wt. (BASALT) x_2	52	56	60
	Rock size (mm) x_3	9.5 to 13.2 Nominally 13.2	13.2 to 19.0 Nominally 19.0	19.0 to 26.5 Nominally 26.5
	Pure polymer final hardness (Shore A degrees) x_4	75	80	85

Table 4.7

Actual variable levels corresponding to coded levels

Test Number	x_1	x_2	x_3	x_4
1	-1	-1	-1	-1
2	+1	-1	-1	-1
3	-1	+1	-1	-1
4	+1	+1	-1	-1
5	-1	-1	+1	-1
6	+1	-1	+1	-1
7	-1	+1	+1	-1
8	+1	+1	+1	-1
9	-1	-1	-1	+1
10	+1	-1	-1	+1
11	-1	+1	-1	+1
12	+1	+1	-1	+1
13	-1	-1	+1	+1
14	+1	-1	+1	+1
15	-1	+1	+1	+1
16	+1	+1	+1	+1
17	-2	0	0	0
+*18	+2	0	0	0
*19	0	-2	0	0
20	0	+2	0	0
+*21	0	0	-2	0
22	0	0	+2	0
*23	0	0	0	-2
24	0	0	0	+2
25	0	0	0	0
26	0	0	0	0
27	0	0	0	0
28	0	0	0	0
29	0	0	0	0
30	0	0	0	0
31	0	0	0	0
32	-1	+2	+2	+1
33	-1	+2	+1	+2
34	-1	+1	+2	+2
35	-2	+2	+2	+2
36	-2	+2	+1	+1
37	-2	+1	+2	+1
38	-2	+1	+1	+2
39	-2	-2	+2	+2
40	-2	-1	+2	+1
41	-2	-2	+1	+2
42	-2	+2	+2	-2
43	-2	+1	+2	-1
44	-1	+2	+1	-2
45	-2	-2	+2	-2
46	-2	-1	+2	-1
47	-1	-2	+1	-2

Table 4.8

Example for total experiment design for one polymer/bullet/rock combination

Tests 1-31 - main quadratic design common to all series

Tests 32-38 - example of first stage corner filling -
* tests ignored in polynomial fitting at this stage

Tests 39-47 - example of second stage corner filling -
+ tests ignored in polynomial fitting at this stage

Value (coded scale)		-2	-1	0	1	2
Values (real)	Resin % wt. x_1	9	11	13	15	17
	Rock aggregate % wt. x_2	44	48	52	56	60
	Rock size (mm) x_3	9.5	13.2	19.0	26.5	37.5
	Pure polymer final hardness (Shore A degrees) x_4	65	70	75	80	85

Table 4.9

Equivalent real variable values and coded values for mixes using Diorez 570 resin

Value (coded scale)		-2	-1	0	1	2
Values (real)	Resin % wt. x_1	7	9	11	13	15
	Rock aggregate % wt x_2	44	49	54	59	64
	Rock size (mm) x_3	9.5	13.2	19.0	26.5	37.5
	Pure polymer final hardness (Shore A degrees) x_4	60	65	70	75	80

Table 4.10

Equivalent real variable values and coded values for mixes using 2851 resins

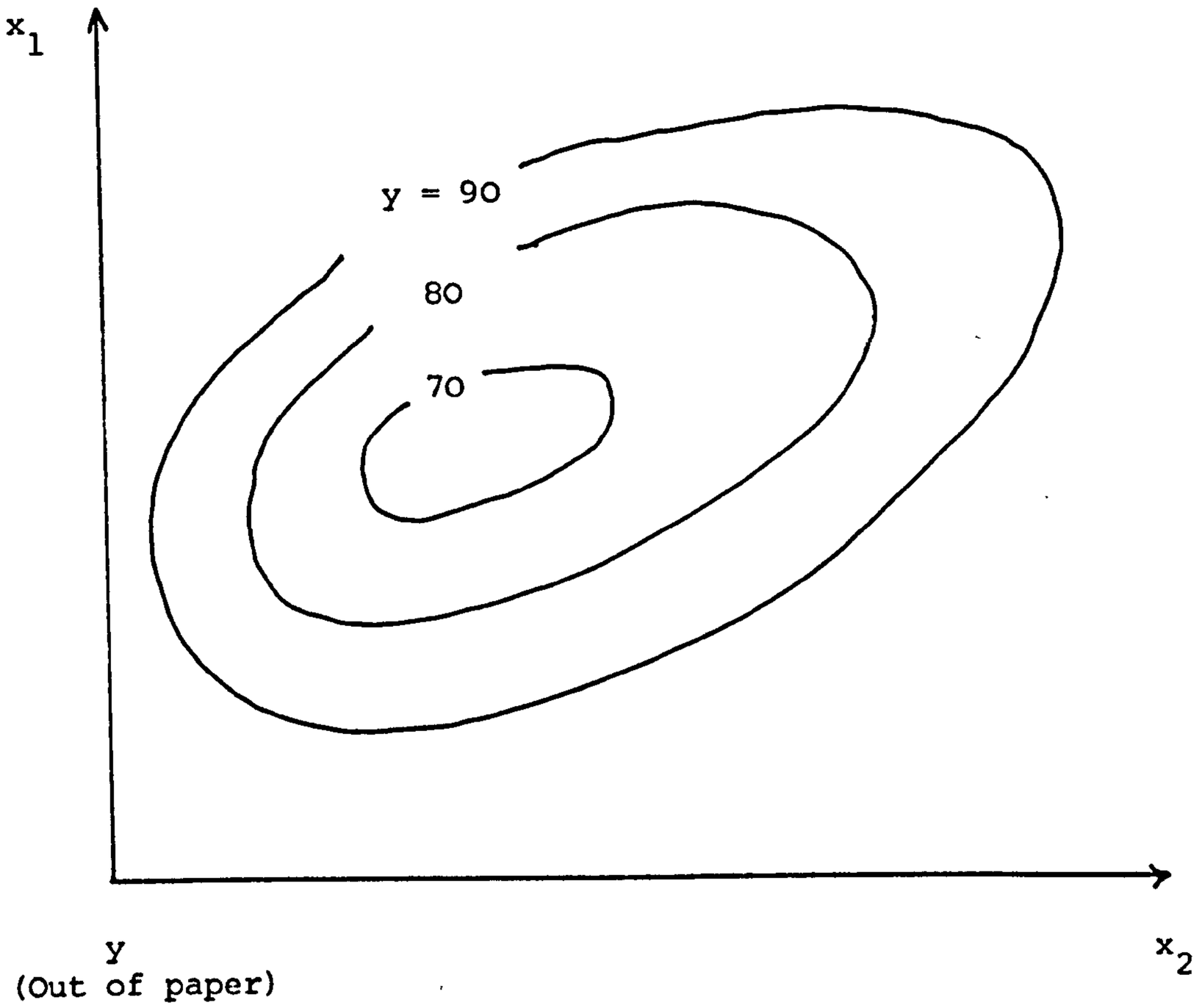

FIGURE 4.1 RESPONSE SURFACE REPRESENTED AS A CONTOUR MAP FOR TWO x VARIABLES

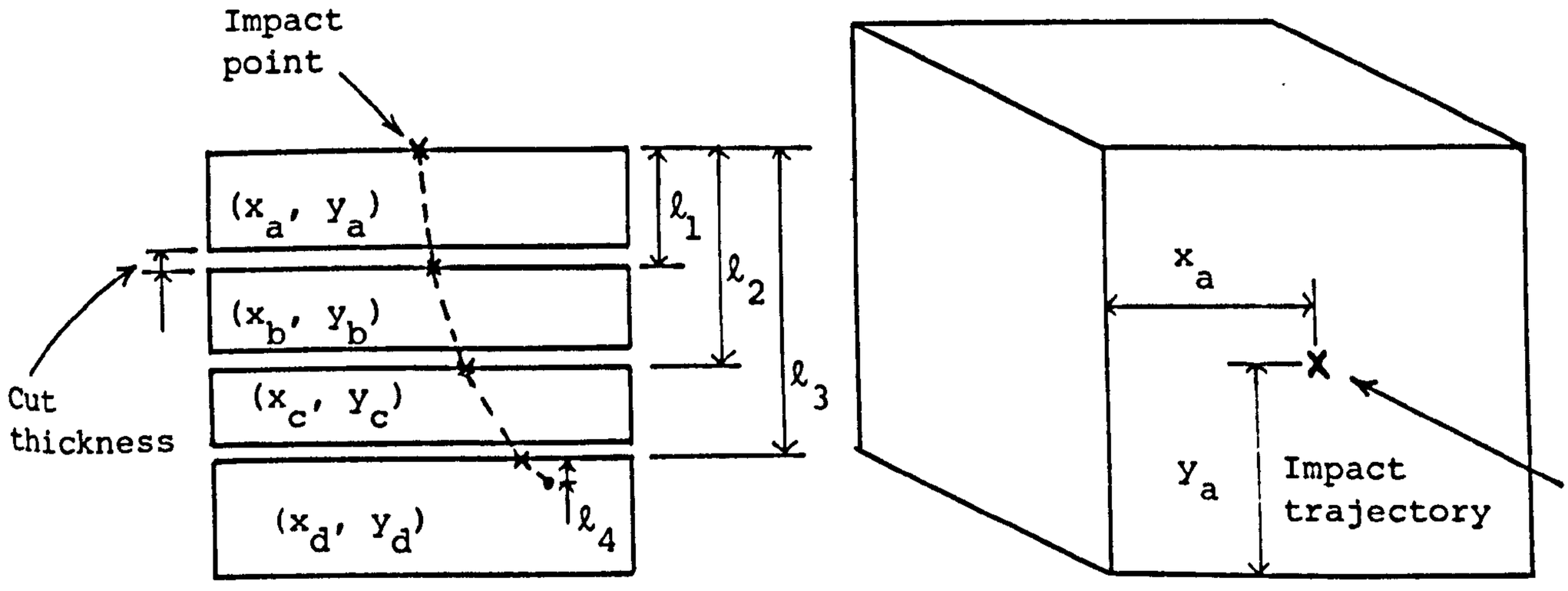

PLAN ON SECTIONED SPECIMEN

ISOMETRIC ELEVATION ON IMPACT FACE

$$D' = (\ell_1^2 + (x_b - x_a)^2 + (y_b - y_a)^2)^{\frac{1}{2}} + ((\ell_2 - \ell_1)^2 + (x_c - x_b)^2 + (y_c - y_b)^2)^{\frac{1}{2}}$$

$$+ ((\ell_3 - \ell_2)^2 + (x_d - x_c)^2 + (y_d - y_c)^2)^{\frac{1}{2}} + \ell_4$$

FIGURE 4.2 CALCULATION OF PENETRATION PATH LENGTH, D'

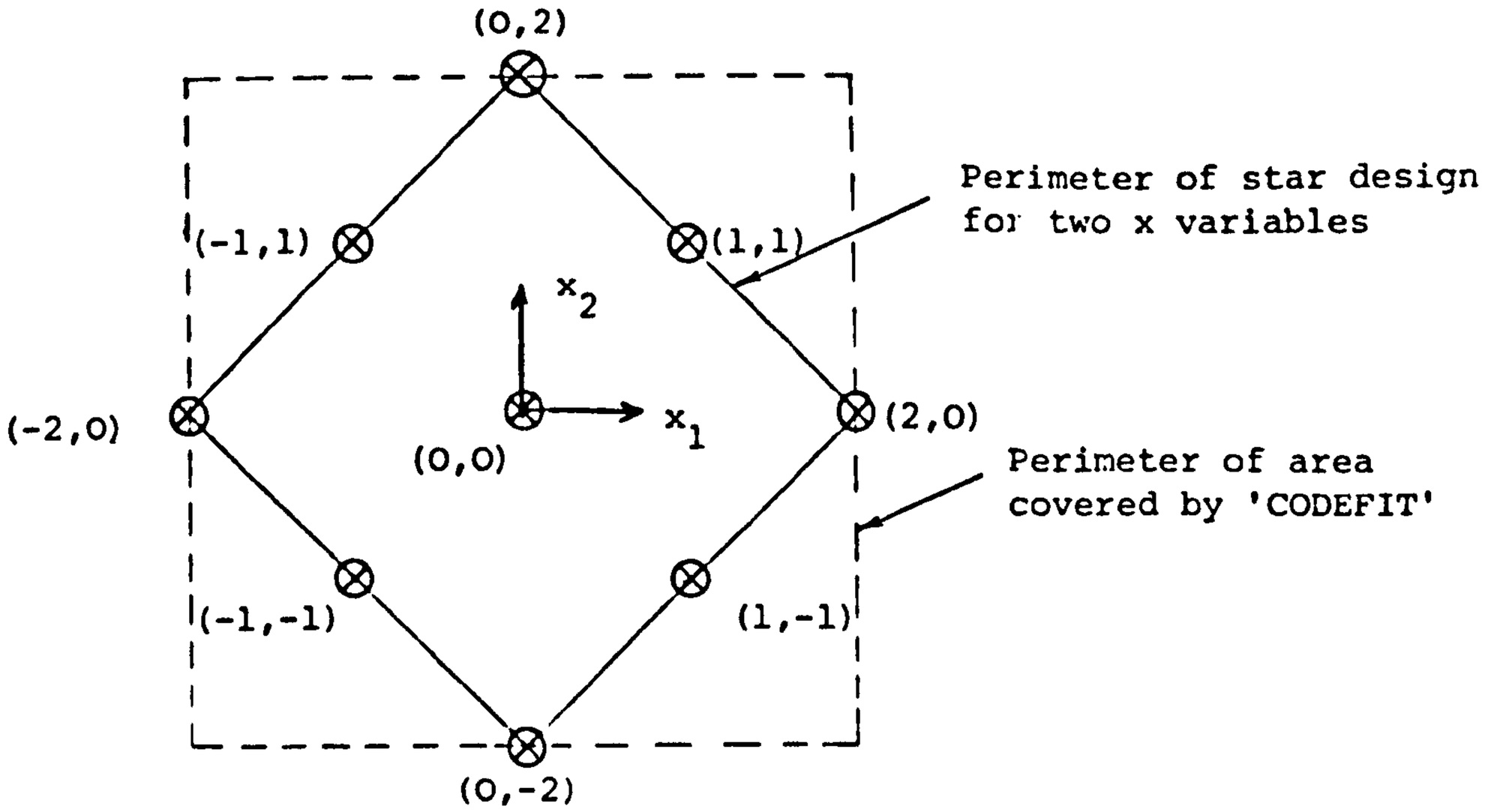

FIGURE 4.3 STAR DESIGN WITH THE EXTENT OF ANALYSIS BY 'CODEFIT' FOR AN EXAMPLE USINC TWO x VARIABLES

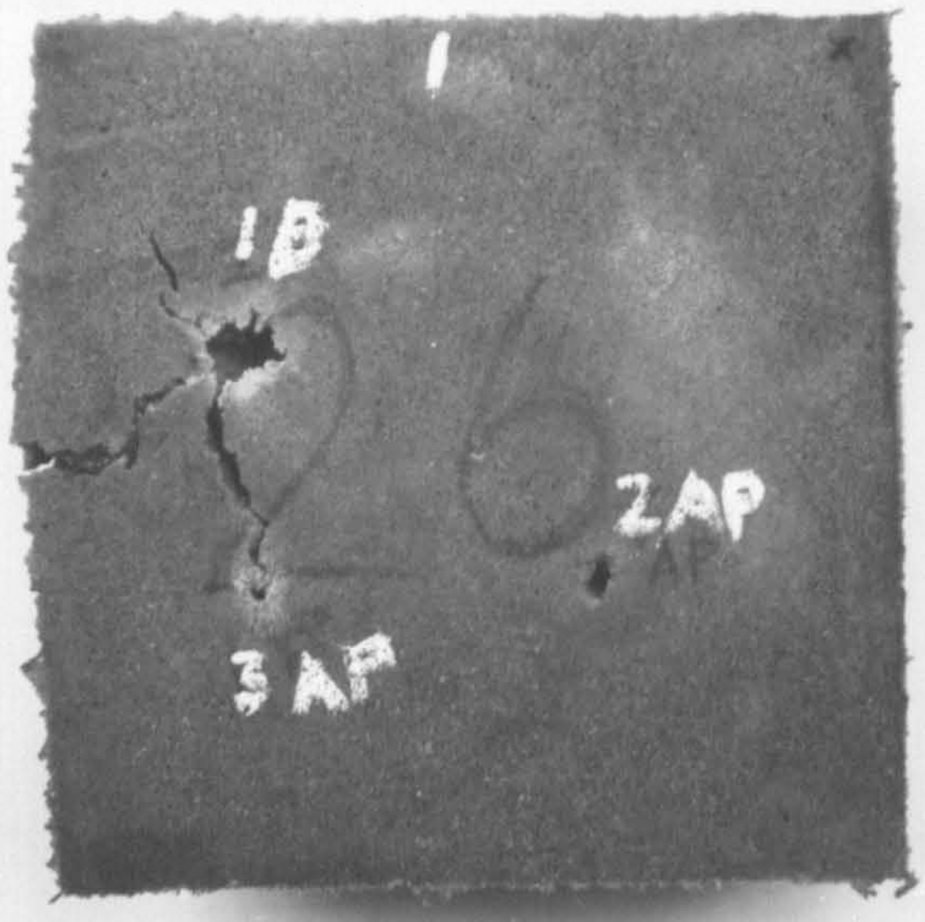

PLATE 4.1 PRELIMINARY TARGET SPECIMEN P1-LS480 RESIN, LIMESTONE, SAND

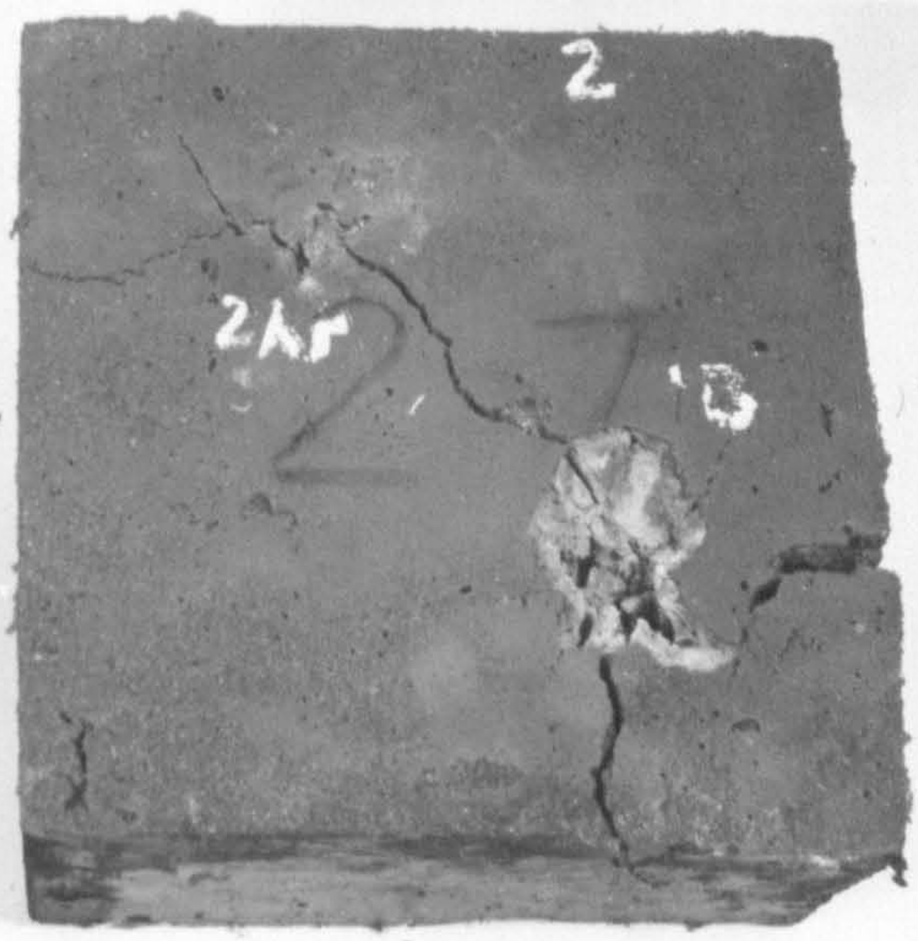

PLATE 4.2 PRELIMINARY TARGET SPECIMEN P2-2851/201 RESIN, LIMESTONE, SAND

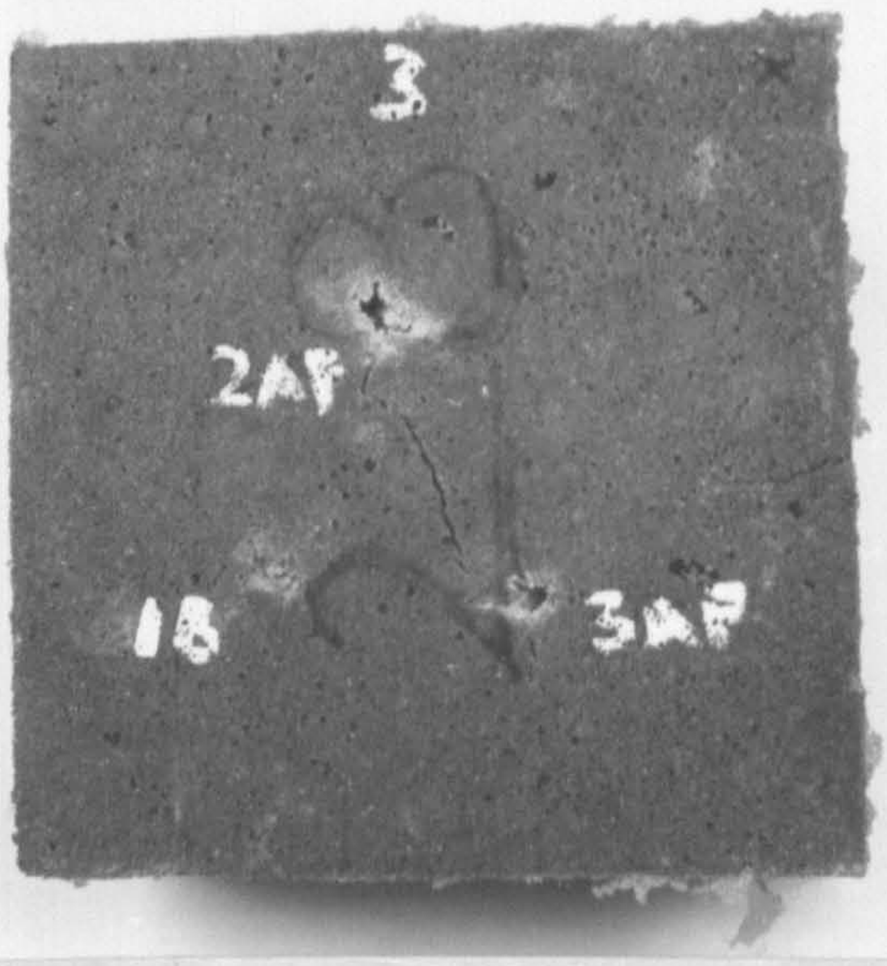

PLATE 4.3 PRELIMINARY TARGET SPECIMEN P3-DIOREZ 570 RESIN, LIMESTONE, SAND

CHAPTER 5

EXPERIMENTAL RESULTS AND ANALYSIS

5.1 Measured Velocity and Accuracy of Projectiles

Manufacturer's data for velocity and accuracy was given in Tables 3.8 and 3.9.

From all of the velocity readings obtained using the velocity measuring rig, values of mean velocity and standard deviation were calculated for each bullet type. These values are given in Table 5.1. In addition, histograms of the velocity distribution are given in Figure 5.1. A.P. ammunition was used during the cold winter period, with the firing range unheated,and it was noticeable that most of the group of lower velocities shown on the histogram were obtained during this period. Hence, on the A.P. velocity histogram, those readings obtained during the winter period are marked, and a separate distribution is apparent. Ball ammunition was not used during this period. It should be noted that velocity was measured at 18.5 m, whereas the target was at 20 m.

Reasons for the variation in velocity are discussed in Chapter 6.

Occasionally minor re-aiming was carried out on the gun stand, thus altering the firing line, so only 20 sets of impact coordinates were used to estimate accuracy for each type of ammunition. Means and standard deviations were calculated for both vertical and horizontal inaccuracy. These are also given in Table 5.1.

5.2 The Optimization of Composite for Minimum Penetration

5.2.1 Linear Polynomial Fitting using Measured Normal Penetration(D)

The normal penetration depths for the three main rock types (rounded river gravel, crushed basalt, and crushed limestone)with Diorez 570 resin and armour piercing (A.P.) ammunition are listed in Table 5.2. Specimen number refers to the number of the specimen within each test series, in this case 1 to 11. By this means, Table 5.2 can be related to Tables 4.6

and 4.7 to determine which combination of coded factor levels is represented in each test, and their equivalent actual levels.

The high incidence of perforation or side exits in series 1 led to this series being ignored; the evidence of the series for limestone and river gravel was considered to be sufficient on which to make a decision concerning further experimentation.

Using equations 4.2 to 4.6, for the limestone, series 2, the coefficients of the linear response surface for normal penetration were

$$b_o = 87.8,\ b_1 = -3.6,\ b_2 = +10.3,\ b_3 = -15.8,\ b_4 = -19.0$$

Thus the equation of the response surface was, from equation 4.1,

$$D_p = 87.8 - 3.6x_1 + 10.3x_2 - 15.8x_3 - 19.0x_4 \qquad \ldots 5.1$$

where x_1 = % resin by wt.

x_2 = % rock by wt.

x_3 = rock aggregate size

x_4 = polymer hardness

D_p = predicted normal penetration

Similarly, for the river gravel, series 3, the equation was

$$D_p = 65.6 + 2.4x_1 + 12.4x_2 - 18.6x_3 - 8.6x_4 \qquad \ldots 5.2$$

It is again emphasised that both of these equations are in the coded scale of x_n.

The test for the validity of linear fit, Appendix A.2, was applied to the results of test series 2 and 3 and it was found that both series passed for linear fit at the 5% significance level.

5.2.2 Linear Polynomial Fitting using Measured Penetration Path Length (D')

Having observed large deviations from normal penetration in some of the

target specimens, it was decided to evaluate the penetration path length D', as shown in Figure 4.2. The analysis was carried out using this dependent variable for series 2 and 3 to observe the differences in the fitted equations from equations 5.1 and 5.2.

Using equations 4.1 to 4.6 for series 2, limestone,and series 3, rounded river gravel, the response surfaces were respectively

$$D_p' = 99.4 + 0.3x_1 + 11.0x_2 - 22.7x_3 - 22.6x_4 \quad \ldots 5.3$$

$$D_p' = 71.6 - 0.4x_1 + 10.2x_2 - 23.1x_3 - 10.4x_4 \quad \ldots 5.4$$

Using the test for lack of fit, Appendix A.2, for both series it was again found that the lack of fit was not significantly higher than pure error.

5.2.3 Quadratic Polynomial Fitting to Main Quadratic Design

The main experimental design for the fitting of a quadratic response surface was described in Section 4.3.3. It consisted of a series of 31 tests for each combination of rock type, polymer type, and projectile type, which was of interest. The assumption of inferior penetration capability for ball ammunition was confirmed later (cf section 5.3) on one rock/polymer combination. Thus the number of test series was (3x2)+1 = 7.

Penetration path length was used as the dependent variable because of its greater physical significance over normal penetration. The combinations of coded factor levels in the main test series, represented by each specimen number in each series, were shown in Table 4.8. The analysis was carried out using PENET, detailed in Appendix A.3.

The values of D' and D_p' for each rock type using 7.62 mm A.P. projectiles and Diorez 570 are given in Table 5.3 as series 4 to 6. Similarly the values of D' and D_p' for each rock type using 7.62 mm A.P. projectiles and 2851 resins are shown in Table 5.4 as series 7 to 9, along

with the values for the single test series, numbered 10, for 7.62 mm ball ammunition with 2851 resins and rounded river gravel. The test number in each series in Tables 5.3 and 5.4 may be compared with those in Table 4.8 to find coded values for each test. These may then be related to actual values of the variables using Tables 4.9 and 4.10.

The analysis of the results was described in Chapter 4 and Appendix A.2. The computing necessary in this analysis is described in Appendix A.3. To summarise, the six stages of the analysis on each of the main quadratic designs were:-

(i) Determination of the response surface, using PENET.

(ii) Check on lack of fit of response surface.

(iii) Determination of location of stationary point on surface, using MATINV.

(iv) Calculation of coefficients of the canonical transformation of the response surface, using EIGEN, to determine the nature of the stationary point: maximum, minimum, or complex.

(v) If necessary, stepwise scan of predictions of response surface using CODEFIT over the range of possible variable combinations, and examination of the results for low and cost effective values of D_p'.

(vi) If necessary, the identification of extra tests needed in the 'corners' of the design, and the repetition of the previous stages.

The analysis of the seven test series with the steps denoted as above, are now presented.

For rounded river gravel, 7.62 mm A.P. projectiles and Diorez 570 (Series 4)

(i) The response surface was

$$D_p' = 75.18 + 4.20x_1 - 0.08x_2 - 18.79x_3 - 9.82x_4$$
$$+ 4.35x_1x_2 - 5.36x_1x_3 - 2.28x_1x_4 - 1.98x_2x_3 + 8.64x_2x_4 + 5.83x_3x_4$$
$$- 6.29x_1^2 - 0.59x_2^2 + 0.30x_3^2 + 1.40x_4^2 \qquad \ldots 5.5$$

(ii) Lack of fit calculations of this and other first quadratic fits below, given in Table 5.5, were based on equation A.2.5, from Appendix A.2. Column 8 in Table 5.5 shows positive results for all series and therefore lack of fit is not significantly greater than random error.

(iii) Differentation of equation 5.5 resulted in

$$\begin{bmatrix} -12.58 & 4.35 & -5.36 & -2.28 \\ 4.35 & -1.18 & -1.98 & 8.64 \\ -5.36 & -1.98 & 0.60 & 5.83 \\ -2.28 & 8.64 & 5.83 & 2.80 \end{bmatrix} \begin{bmatrix} x_1 \\ x_2 \\ x_3 \\ x_4 \end{bmatrix} = \begin{bmatrix} -4.20 \\ 0.08 \\ 18.79 \\ 9.82 \end{bmatrix}$$

Solution by MATINV gave stationary points

$$x_{1S} = -1.46,\ x_{2S} = -1.37,\ x_{3S} = 2.60,\ x_{4S} = 1.15$$

(iv) The coefficients of the transformed equation, found using EIGEN, were

$$B_1 = -7.99,\ B_2 = -5.01,\ B_3 = 2.30,\ B_4 = 5.52$$

Because there is a mixture of signs in these coefficients, a complex stationary point existed, and recourse was made to CODEFIT.

As mentioned in Chapter 4, this scan extended into the corners of the variable field, to coded values ±2, beyond the area covered by the experiments, and hence was prone to large errors. It was assumed, however, that where a

solution did not exist within the experimental field of investigation, the trends, if not the values, of D_p' in the 'corners' were valid.

The two possible areas of interest in this case were:

$x_1 = 2$, $x_2 = -2$, $x_3 = 2$, $x_4 = 2$ giving $D_p' = -45.48$ mm

and $x_1 = -2$, $x_2 = 2$, $x_3 = 2$, $x_4 = -2$ giving $D_p' = -42.92$ mm

Because of the lower resin content, the latter is more attractive from a cost-effective point of view, and hence extra tests were carried out in this 'corner'. The negative values of D_p' are obviously not possible, but are compared because of the trends.

For crushed basalt, 7.62 mm A.P. projectiles, and Diorez 570 resin (Series 5)

(i) $$D_p' = 91.67 + 3.85x_1 - 10.37x_2 + 1.30x_3 - 2.14x_4 + 5.21x_1x_2$$
$$+ 0.08x_1x_3 - 0.89x_1x_4 - 11.71x_2x_3 + 1.09x_2x_4 + 23.31x_3x_4$$
$$+ 4.65x_1^2 + 1.91x_2^2 + 8.11x_3^2 + 3.34x_4^2 \quad \ldots 5.6$$

(iii) MATINV yielded

$x_{1S} = -1.79$, $x_{2S} = 2.77$, $x_{3S} = -0.62$, $x_{4S} = -1.77$

(iv) Coefficients of the transformed penetration equation were

$B_1 = -8.16$, $B_2 = 1.40$, $B_3 = 6.01$, $B_4 = 18.78$

Hence there was no minimum.

(v) CODEFIT yielded the following interesting variable combination

$x_1 = -2$, $x_2 = +2$, $x_3 = +2$, $x_4 = -2$ giving $D_p' = -26.97$ mm

Hence extra tests were carried out in this corner.

For crushed limestone, 7.62 mm A.P. projectiles, and Diorez 570 resin (Series 6)

(i) $D_p' = 122.49 - 12.01x_1 - 5.91x_2 - 7.16x_3 + 4.99x_4$

$- 12.54x_1x_2 - 0.64x_1x_3 - 8.28x_1x_4 + 5.61x_2x_3 - 9.26x_2x_4 - 4.33x_3x_4$

$- 9.50x_1^2 - 6.47x_2^2 - 8.05x_3^2 - 7.21x_4^2$ ... 5.7

(iii) MATINV yielded

$x_{1S} = -7.49$, $x_{2S} = 14.42$, $x_{3S} = 6.65$, $x_{4S} = -6.61$

(iv) Coefficients of the transformed equation were:

$B_1 = -17.95$, $B_2 = -9.68$, $B_3 = -3.73$, $B_4 = 0.14$

Hence there was no minimum.

(v) CODEFIT yielded the following favourable variable combinations

$x_1 = 2$, $x_2 = 2$, $x_3 = 2$, $x_4 = 2$ giving $D_p' = -160.37$ mm

$x_1 = -2$, $x_2 = -2$, $x_3 = +2$, $x_4 = -2$ giving $D_p' = -113.77$ mm

Again because of the lower resin content the second combination is better from a cost-effective point of view: hence extra tests were carried out in that area.

For rounded river gravel, 7.62 mm A.P. projectiles, and 2851 resins (Series 7)

(i) $D_p' = 49.56 + 3.75x_1 - 5.72x_2 - 0.94x_3 - 1.81x_4$

$+ 0.23x_1x_2 + 2.33x_1x_3 - 1.60x_1x_4 + 0.29x_2x_3 - 3.16x_2x_4 - 3.09x_3x_4$

$+ 1.40x_1^2 + 5.21x_2^2 + 3.70x_3^2 - 0.80x_4^2$ ... 5.8

(iii) MATINV yielded

$x_{1S} = -2.20$, $x_{2S} = 0.38$, $x_{3S} = 0.52$, $x_{4S} = -0.68$

(iv) Coefficients of the transformed penetration equation were

$B_1 = -3.32$, $B_2 = -0.03$, $B_3 = 4.82$, $B_4 = 8.03$

Hence there was no minimum.

(v) CODEFIT yielded the following interesting variable combinations

$x_1 = -2$, $x_2 = 2$, $x_3 = 2$, $x_4 = 2$ giving $D_p' = 35.49$ mm

$x_1 = -1$, $x_2 = 1$, $x_3 = 1$, $x_4 = 2$ giving $D_p' = 31.07$ mm

Hence the one corner represented by both of these combinations was the subject of further tests.

For crushed basalt, 7.62 mm A.P. ammunition, 2851 resins (Series 8)

(i) $$D_p' = 103.24 + 0.10x_1 - 0.65x_2 - 6.52x_3 - 5.54x_4 - 5.99x_1x_2 - 6.71x_1x_3 - 9.21x_1x_4 - 3.04x_2x_3 + 5.16x_2x_4 + 2.34x_3x_4 + 5.63x_1^2 + 2.13x_2^2 + 0.21x_3^2 - 7.53x_4^2 \quad \ldots 5.9$$

(iii) MATINV yielded

$x_{1S} = -0.72$, $x_{2S} = -0.75$, $x_{3S} = -0.22$, $x_{4S} = -0.22$

(iv) The coefficients of the transformed penetration equation were

$B_1 = -9.24$, $B_2 = -2.92$, $B_3 = 2.88$, $B_4 = 9.72$

Hence there was no minimum.

(v) CODEFIT yielded the following interesting variable combinations

$x_1 = 2$, $x_2 = 2$, $x_3 = 2$, $x_4 = 2$ giving $D_p' = 9.97$ mm (first combination)

$x_1 = -1$, $x_2 = -2$, $x_3 = -2$, $x_4 = 2$ giving $D_p' = 42.11$ mm (second combination)

It was difficult to believe the second combination: the evidence of the experiments of other test series had suggested large rock particles (x_3 positive) to be superior in performance. Hence, initially only the first combination was the subject of further tests.

For crushed limestone, 7.62 mm A.P. ammunition 2851 resins (Series 9)

(i) $$D_p' = 100.03 + 7.29x_1 - 0.94x_2 - 7.96x_3 - 8.10x_4$$
$$+ 5.97x_1x_2 + 1.48x_1x_3 + 5.63x_1x_4 - 4.93x_2x_3 - 4.80x_2x_4 + 7.16x_3x_4$$
$$- 6.23x_1^2 + 0.59x_2^2 - 3.02x_3^2 - 1.28x_4^2 \qquad \ldots 5.10$$

(iii) MATINV yielded

$$x_{1S} = 3.82,\ x_{2S} = 3.04,\ x_{3S} = 1.47,\ x_{4S} = 3.65$$

(iv) The coefficients of the transformed equation were:

$$B_1 = -8.90,\ B_2 = -5.76,\ B_3 = 0.21,\ B_4 = 4.52$$

Hence there was no minimum.

(v) CODEFIT yielded the following interesting combinations

$x_1 = -2$, $x_2 = 2$, $x_3 = 2$, $x_4 = 2$ giving $D_p' = -50.12$ mm

Hence this corner was the subject of further tests.

For rounded gravel, 7.62 mm ball projectiles, 2851 resins (Series 10)

(i) $$D_p' = 44.64 - 0.96x_1 - 0.55x_2 - 2.78x_3 - 2.89x_4$$
$$- 0.02x_1x_2 - 0.52x_1x_3 + 1.83x_1x_4 - 1.39x_2x_3 - 2.89x_2x_4 - 2.67x_3x_4$$
$$- 3.83x_1^2 - 1.51x_2^2 - 1.75x_3^2 + 0.16x_4^2 \qquad \ldots 5.11$$

(iii) MATINV yielded

$$x_{1S} = 0.02,\ x_{2S} = 0.00,\ x_{3S} = 1.03,\ x_{4S} = 0.31$$

(iv) Coefficients of the transformed equation were:

$$B_1 = -4.10,\ B_2 = -3.31,\ B_3 = -0.92,\ B_4 = +1.40$$

Hence there was no minimum.

(v) CODEFIT yielded a lowest penetration at

$x_1 = -2$, $x_2 = 2$, $x_3 = 2$, $x_4 = 2$ giving $D_p' = -26.59$ mm

Because of the generally low levels of D', the assumption of inferior penetration by ball ammunition was confirmed, and no corner tests carried out.

5.2.4 First Stage Corner Tests; Second Stage Quadratic Analysis

It has been shown in the previous section that optimum variable combinations were indicated in corners of the variable fields which were not covered by the main quadratic design. Hence extra penetration tests were necessary in these corners.

Comparison of results in Tables 5.3 and 5.4 for the two resin types showed, generally, higher penetrations with Diorez 570 than with 2851 resins. A straight comparison of penetrations was not possible between the two types because of the differing real variable levels, which were given in Tables 4.9 and 4.10. However, by comparing real variable levels in these tables it can be seen that the point equivalent to $x_1 = x_2 = x_3 = x_4 = 0$ (i.e. centroid) in the coded Diorez 570 scale is $x_1 = 1$, $x_2 = -0.4$, $x_3 = 0$, $x_4 = 1$ in the coded 2851 resin scale.

Thus, by substituting these values into equations 5.8 to 5.10, comparisons can be made between the predicted penetrations at the centroid of the Diorez 570 design, and the point in the 2851 resin design giving the same real variable levels. The results of this comparison are given in Table 5.6, and show a clear advantage for 2851 resins. However, this comparison is of points close to, or at, the design centres and, because optimum levels were likely to be in the corners of the variable field, Diorez 570 was not dropped entirely from the study. Instead, further tests were carried out for all three main rock types and 2851 resins, but only the best rock type, river gravel, was combined with Diorez 570 for futher study.

Hence the four qualitative variable combinations to be subjected to corner tests were 2851 resins with A.P. ammunition and all three main rock types, (series 7 to 9) as well as Diorez 570 with A.P. ammunition and rounded river gravel (series 4). Because of the series to series variation in the corners considered, the extra test plans are shown separately in Table 5.7.

This table also gives the values of D' for the extra tests in the first combination of the crushed basalt/A.P./2851 resins. These series 8 values of D', compared to those in Table 5.4, did not give the expected improvement in performance and were considered too high to justify the cost of the high resin content. Consequently, no further analysis was carried out on these results and an alternative corner was sought. The other corner which CODEFIT indicated to be of interest for this series was the second combination of $x_1 = -1$, $x_2 = -2$, $x_3 = -2$, $x_4 = 2$. This was assumed to be unlikely because of the small rock aggregate size indicated.

Further confirmation of this assumption came when penetration tests were carried out with small size limestone aggregate and 2851 resins (cf section 5.2.5). Thus the extrapolations of the surface which gave the aforementioned first and second combinations of variables for the basalt/A.P./2851 resins were regarded as very dubious.

On the basis of the evidence from the corner fitting of the limestone and river gravel/A.P./2851 series, a third combination, $x_1 = -2$, $x_2 = 2$, $x_3 = 2$, and $x_4 = 2$, was chosen for corner fitting of the basalt/A.P./2851 series. Details of coded values in this corner are given in Table 5.8.

The values of D' equated from the corner tests, along with those from the parts of the main test series used, are given in Table 5.9. Also included are the values of D_p' equated by PENET. The fitted equations are given below, along with results from CODEFIT. Lack of fit tests for these series are given in Table 5.10. The positive results in column 8 of this table indicated that lack of fit is not significantly greater than random error for all series.

For rounded river gravel 7.62 mm ammunition and Diorez 570 (Series 4)

$$D_p' = 74.13 + 8.23x_1 - 0.50x_2 - 17.77x_3 - 6.83x_4$$
$$+ 0.15x_1x_2 - 8.48x_1x_3 + 0.34x_1x_4 + 2.56x_2x_3 + 4.99x_2x_4 + 0.10x_3x_4$$
$$- 3.22x_1^2 - 0.89x_2^2 - 1.36x_3^2 + 4.61x_4^2 \quad \ldots 5.12$$

The lowest CODEFIT prediction in the corner of the variable field subjected to further tests was

$x_1 = 0$, $x_2 = 0$, $x_3 = 2.0$, $x_4 = 0$ giving $D_p' = 33.16$ mm

A better cost effective combination was

$x_1 = -2.0$, $x_2 = 0$, $x_3 = 2.0$, $x_4 = 0$ giving $D_p' = 37.73$ mm

However, lower values of D_p' were obtained in other untested corners. The lowest was when $x_1 = 2.0$, $x_2 = -2.0$, $x_3 = 2.0$, $x_4 = 2.0$ giving $D_p' = -23.97$ mm.

This value of D_p' was somewhat higher than the value of -45.48 mm which was found applying CODEFIT to the first quadratic fit. It was obvious that high inaccuracies may exist in untested corners so extra tests were carried out as detailed in the next section.

For rounded river gravel, 7.62 mm A.P. ammunition and 2851 resins (Series 7)

$$D_p' = 48.49 + 6.80x_1 - 4.82x_2 - 2.05x_3 - 0.87x_4$$
$$- 2.63x_1x_2 + 3.94x_1x_3 - 4.83x_1x_4 - 1.31x_2x_3 - 1.39x_2x_4 - 2.97x_3x_4$$
$$+ 7.83x_1^2 + 4.53x_2^2 + 0.91x_3^2 + 0.19x_4^2 \quad \ldots 5.13$$

CODEFIT yielded lowest values in the corner where the extra tests were carried out. Lowest values were when

$x_1 = -1$, $x_2 = 1$, $x_3 = 2$, $x_4 = 2$ giving $D_p' = 34.91$ mm

and $x_1 = 0$, $x_2 = 1$, $x_3 = 2$, $x_4 = 2$ giving $D_p' = 29.47$ mm

Making the assumption that the composite cost was proportional to resin content (which, considering the relatively high cost of the resin, is reasonable), the optimum cost/effective point was sought.

The increments in CODEFIT were therefore reduced from 1.0 to 0.2, giving the following lowest predicted penetration results for each x_1 (resin) level

when $x_1 = -1.0$(9%) $x_2 = 0.8$ $x_3 = 2$ $x_4 = 2$ $D_p' = 34.79$ mm,

when $x_1 = -0.8$(9.4%) $x_2 = 0.8$ $x_3 = 2$ $x_4 = 2$ $D_p' = 32.56$ mm,

when $x_1 = -0.6$(9.8%) $x_2 = 1$ $x_3 = 2$ $x_4 = 2$ $D_p' = 30.85$ mm,

when $x_1 = -0.4$(10.2%) $x_2 = 1$ $x_3 = 2$ $x_4 = 2$ $D_p' = 29.76$ mm,

when $x_1 = -0.2$(10.6%) $x_2 = 1$ $x_3 = 2$ $x_4 = 2$ $D_p' = 29.30$ mm.

Each adjacent pair of combinations, from the minimum penetration combination, was examined in turn using the simple argument that when the percentage decrease in penetration became greater than the percentage increase in resin content, then an improvement in cost effectiveness had been achieved i.e. resin percentage may be reduced at the expense of higher penetration if

$$\frac{x_1(\text{high})}{x_1(\text{low})} \times \frac{D_p'(\text{at } x_1 \text{ high})}{D_p'(\text{at } x_1 \text{ low})} > 1 \qquad \ldots 5.14$$

Applying equation 5.14 to each adjacent pair of combinations from the minimum penetration combination

$$\frac{10.6}{10.2} \times \frac{29.30}{29.76} = 1.023 > 1 \quad \therefore \text{ reduce } x_1$$

$$\frac{10.2}{9.8} \times \frac{29.76}{30.85} = 1.004 > 1 \quad \therefore \text{ reduce } x_1$$

$$\frac{9.8}{9.4} \times \frac{30.85}{32.56} = 0.988 < 1$$

Therefore the optimum cost/effective mix for this combination of qualitative variables is

$x_1 = -0.6(9.8\%)$, $x_2 = 1.0(59\%)$, $x_3 = 2.0(26.5\text{-}37.5\text{mm})$, $x_4 = 2.0(80)$

Thus no further optimising experiments were required.

For crushed basalt, 7.62 mm A.P. ammunition and 2851 resins (Series 8)

$$D_p' = 105.53 - 1.76x_1 + 0.71x_2 - 6.89x_3 - 8.67x_4$$
$$- 2.88x_1x_2 - 2.61x_1x_3 - 4.49x_1x_4 - 5.98x_2x_3 + 3.47x_2x_4 + 0.47x_3x_4$$
$$- 1.03x_1^2 - 0.29x_2^2 - 0.59x_3^2 - 3.67x_4^2 \quad \ldots \quad 5.15$$

In the corner subjected to further tests, CODEFIT yielded the following lowest value of D_p'

when $x_1 = 0$, $x_2 = 2$, $x_3 = 2$, $x_4 = 2$, $D_p' = 49.43$ mm

This was because of the strong trend to the $x_1 = x_2 = x_3 = x_4 = 2$ corner, which gave the lowest D_p' in the first quadratic fit. However, lower values were obtained in an untested corner where

$x_1 = 0$, $x_2 = -2$, $x_3 = -2$, $x_4 = 2$ giving $D_p' = 42.65$ mm

This anomaly meant extra tests were necessary, as described in the next section.

For crushed limestone, 7.62 mm A.P. ammunition and 2851 resins (Series 9)

$$D_p' = 95.52 + 10.01x_1 - 4.26x_2 - 6.03x_3 - 11.67x_4$$
$$+2.61x_1x_2 - 4.10x_1x_3 + 2.17x_1x_4 - 1.13x_2x_3 - 2.41x_2x_4 + 13.94x_3x_4$$
$$- 2.16x_1^2 + 3.19x_2^2 - 2.64x_3^2 + 4.41x_4^2 \quad \ldots \quad 5.16$$

The lowest CODEFIT prediction in the corner of the variable field subjected to further tests was when

$x_1 = -2$, $x_2 = 2.$, $x_3 = 0$, $x_4 = 2.$ giving $D_p' = 36.69$ mm

However, lower values of D_p' were predicted in other untested corners such as when

$x_1 = -2$, $x_2 = 2$, $x_3 = -2$, $x_4 = 2$ giving $D_p' = -29.46$ mm

This value of D_p' is close to the predicted value of -24.39 mm for this variable level combination in the first quadratic analysis, when the lowest prediction in the corner where the extra tests were subsequently carried out was -50.12 mm. Hence it is apparent that large inaccuracies exist in the corners, and removing the inaccuracy from one naturally points to the other, leading to the anomalous results. Further corner tests were carried out to confirm this point and these are discussed in the next section.

5.2.5 Second Stage Corner Tests : Third Stage Quadratic Analysis

In the analysis of the main quadratic design for basalt/A.P./2851 resins (series 8), a variable combination with a low x_3 (small aggregate size) was indicated as being cost effective. In addition, after the first stage corner fitting for limestone/A.P./2851 resins, a combination with a low x_3 was also indicated, although in this case the result was almost certainly due to the non-symmetry introduced into the design by the corner tests. To confirm the assumption that these predictions were invalid, and due to large prediction errors in the variable field corners not covered by experiment, a set of seven tests was carried out in the in $x_1 = -2$, $x_2 = 2$, $x_3 = -2$, $x_4 = 2$ corner for limestone/A.P./2851 resins combinations. These tests and their results are detailed in Table 5.11 and it can be seen that high penetrations and perforations occurred, comfirming the assumption that small aggregate size was unsuitable.

A solution was obtained for the optimum cost/effective mix for rounded river gravel/A.P./2851 resins. For the other qualitative variable combinations, however, no such solution was obtainable, because of the high errors evident in extrapolating values of D_p' into the corners of the design not so far

subjected to further tests. Based on the assumptions listed in Section 4.3.5. extra tests were carried out in the three corners assumed to be of interest for these combinations. These extra, second stage, corner tests are listed in Table 5.12.

The analysis procedure was repeated to include these extra test results. x_n combinations at the opposite ends of the variable field to these assumed to be of interest were omitted. The values of measured penetration path length, D', used in the PENET analysis are given in Table 5.13 along with the predicted penetration path length D_p'

Lack of fit test results are given in Table 5.14 and the positive values in column 8 indicate that lack of fit is not significantly greater than random error. The fitted equations for the three qualitative variable combinations examined in this section are given below, along with results from CODEFIT.

<u>For rounded river gravel, A.P. ammunition, and Diorez 570</u> (Series 4)

$$D_p' = 70.8 + 5.73x_1 + 1.17x_2 - 15.26x_3 - 10.30x_4$$
$$+ 3.78x_1x_2 - 7.93x_1x_3 - 2.60x_1x_4 - 1.05x_2x_3 - 1.04x_2x_4 + 3.05x_3x_4$$
$$- 2.02x_1^2 - 0.10x_2^2 - 0.16x_3^2 + 2.79x_4^2 \quad \ldots \quad 5.17$$

The most cost effective x variable combination from CODEFIT was when

$x_1 = -2(9\%)$, $x_2 = 2(60\%)$, $x_3 = 2(26.5$ to $37.5mm)$, $x_4 = 0(75$ Shore $A^o)$

giving $D_p' = 35.21$ mm

Only the CODEFIT output with $x_1 < 0$ and $x_3 > 0$ were considered i.e. low resin content and larger aggregate size, because the other areas were excluded from extra experimentation as detailed earlier.

For crushed limestone, A.P. ammunition and 2851 resins (Series 9)

$$D_p' = 92.3 + 7.64x_1 + 0.05x_2 - 3.68x_3 - 8.35x_4$$
$$+ 4.50x_1x_2 - 4.17x_1x_3 + 6.09x_1x_4 - 3.02x_2x_3 + 0.69x_2x_4 + 10.02x_3x_4$$
$$- 0.31x_1^2 + 2.03x_2^2 - 0.79x_3^2 + 3.16x_4^2 \quad \ldots \quad 5.18$$

The most effective, and cost effective, x variable combination from CODEFIT was when

$x_1 = -2(7\%)$, $x_2 = 2(64\%)$, $x_3 = 2(26.5\text{-}37.5\text{mm})$, $x_4 = 0.2(69 \text{ Shore } A^\circ)$, giving $D_p' = 59.99$ mm.

From the evidence of tests 39 to 45 in this series, detailed in Table 5.11 only values of rock size coded $x_3 = +2$ were examined, as a bias exists towards small rock aggregate sizes which these tests showed to be unrealistic.

For crushed basalt, A.P. ammunition and 2851 resins (Series 8)

$$D_p' = 98.53 + 0.25x_1 - 0.92x_2 - 8.90x_3 - 6.10x_4$$
$$- 4.76x_1x_2 - 1.55x_1x_3 - 3.61x_1x_4 - 4.11x_2x_3 - 1.97x_2x_4 - 0.41x_3x_4$$
$$- 0.51x_1^2 + 5.12x_2^2 - 0.07x_3^2 - 1.97x_4^2 \quad \ldots \quad 5.19$$

The most cost effective x variable combination from CODEFIT was when

$x_1 = -2(7\%)$, $x_2 = -0.4(52\%)$, $x_3 = 2(26.5 \text{ to } 37.5\text{mm})$, $x_4 = -2(60 \text{ Shore } A^\circ)$

giving D_p' 74.7 mm

However, a value of D_p' almost as low was obtained when

$x_1 = -2(7\%)$, $x_2 = +0.4(56\%)$, $x_3 = +2(26.5 \text{ to } 37.5\text{mm})$, $x_4 = +2(80 \text{ Shore } A^\circ)$

giving $D_p' = 76.2$ mm.

The latter was chosen because of the greater experimental detail in that area of the design, and because harder resin was indicated as better in the river gravel/A.P./2851 resins most cost effective mix already obtained in the previous section.

A summary of the coefficients in the equations for all of the response surfaces examined is given in Tables 5.15 and 5.16. The optimized mixes for the relevant qualitative variable combinations, arrived at in the previous sections, are summarised in Table 5.17.

The next requirement was to determine the thickness of specimen necessary to prevent perforation at a given confidence level, based on the mixes given in Table 5.17.

5.3 Thickness Tests

In the previous two sections, values of penetration path length were predicted for mixes which were shown to be the most cost effective, based on stated assumptions. The next requirement was to determine the thickness of specimen based on these mixes necessary to resist perforation at a given confidence level. The thickness necessary for each combination of rock, bullet and polymer was different from the value of predicted path length, D_p', given, for four reasons

(i) Inaccuracy in the fitted equation.

(ii) The high scatter of experimental results, and the number of standard deviations from the mean necessary to gain the required confidence level for containment.

(iii) D and not D' is the relevant measured quantity for protective thickness

(iv) The effect of the increased proximity of the rear surface of the target specimen due to decreased thickness from the optimization tests.

Two confidence levels were obtained for the protective capability of the composite. The first, 80-90% containment, was thought to be applicable where the composite was to be used for protecting an existing reasonably strong structure, e.g. brickwork. Most of the projectiles would be contained, but those that were not would have their kinetic energy greatly decreased. The second confidence level, 97.5-99%, was considered sufficient where the composite was to be used alone, or over a weak structure.

Preliminary tests were carried out with target specimens of varying thickness to determine the general trends in the protective capability with thickness. These tests are not documented here, as they were only instrumental in obtaining the thickness used in the tests presented. The normal penetration depth is used here rather than penetration path length, because, once the composite optimization has been achieved, it is this component of the penetration which is of interest. Specimens were tested after 1 day unless otherwise stated.

The progression of the thickness tests was as follows

(i) The most favourable rock type / polymer type combination was examined first, namely rounded river gravel with 2851 resins, at x_1 = 9.8%, x_2 = 59%, x_3 = 26.5 to 37.5mm, x_4 = 80 Shore A^o, the optimum mix. It was still assumed that A.P. ammunition would give greatest penetration and was therefore used in all these tests. From the preliminary thickness tests, the 80-90% confidence level for containment was expected to be attained with a specimen thickness of 80 mm, and hence this thickness was used. The results given in Table 5.18 from series 11 confirm this depth as adequate. The mean + (z x standard deviation) calculations for this 80-90% confidence level gave a penetration of 69.9 to 76.2mm which is near to 80 mm,and the percentage of bullets actually retained

was 85%. When calculating means, etc, perforation was considered as nominal thickness +10mm. Typical entry holes for this series are shown in Plate 5.1. When perforation occurred, scabbing at the rear surface of the target was as shown in Plate 5.2.

(ii) To check the assumption of the higher penetration of A.P. ammunition the above series was repeated using ball ammunition. The results, given in Table 5.18 series 12, show lower penetrations, indicating that this assumption was valid. Plate 5.3 shows entry holes for this series and indicates more front face cratering with ball ammunition than with A.P.

(iii) The effect of cure time on the composite is examined using 'static' bending tests later in this chapter. However, the effect on normal penetration depth of specimen age was also examined by repeating series 11 with a specimen age of 3 days instead of 1 day. The results are given as series 13 in Table 5.18 showing a slight, but not significant, increase in mean penetration and standard deviation.

(iv) From the mean and standard deviation results for series 11, the thickness for 97.5 to 99% confidence was estimated to be 100 mm. Results of tests carried out on specimens of this thickness are given in series 14, Table 5.18 and the mean and standard deviation were similar to series 11. No perforations occurred, although on one test the tip could be seen protruding slightly from the rear face of the target specimen.

(v) The best cost effective mix for basalt with 2851 resins and A.P. ammunition was indicated in section 5.2.5 to be

x_1 = 7%, x_2 = 56%, x_3 = 26.5 to 37.5mm, x_4 = 80 Shore A^o. This combination was tested at a thickness of 110 mm, and the results given as series 15 in Table 5.19. The penetrations in the first ten tests were high, and also extensive damage occurred to many of the target specimens as shown in Plate 5.4. The series was therefore discontinued and the resin percentage, x_1, was nominally increased to 9%, and the optimum mix at this level tested. This optimum mix was found,from a detailed scan of equation 5.19 using the program CODEFIT, to be when

x_1 = -1(9%), x_2 = +0.8(58%), x_3 = +2(26.5 to 37.5mm),

x_4 = +2(80 Shore A^o), giving D_p'=65.7 mm

The results obtained using this mix are shown as series 16 in Table 5.19.Damage was reduced to an acceptable level (Plate 5.5) and the values of mean and standard deviation indicated the 110 mm thickness as adequate for the 80-90% confidence level. The thicknesses for 97.5-99% confidence levels were projected as 131.6 to 141.2, nominally 130-140mm.

With the basalt the resin percentages had to be increased for the integrity of the target specimen to be maintained. The predicted path length was decreased with this change, although the higher resin percentage was predicted as being less cost effective. In reality, the performance was improved more than was indicated by the predicted path lengths.

(vi) For limestone/A.P./2851 resin combinations the optimum had been predicted with a low resin content (x_1 = 7%, x_2 = 64%, x_3 = 26.5 to 37.5mm and x_4 = 69 Shore A^o). When targets

110 mm thick were prepared to this mix and tested (series 17, Table 5.20) penetrations were large and damage was excessive. Plate 5.6 shows typical damage, although slightly exaggerated by subsequent slicing of the targets. The Series was discontinued after ten tests and another series, number 18, was started with a 9% resin content. Again penetrations were large and excessive damage occurred (Plate 5.7), so the series was discontinued.

Although predicted penetration path lengths were decreasing with decreasing resin content and hence becoming more cost effective, it was intuitively felt that penetration resistance could be improved by increasing the resin content in a similar way to the basalt series. CODEFIT gave a mix for 11% resin content of x_1 = 0(11%), x_2 = 1(59%), x_3 = 2(26.5 to 37.5 mm) and x_4 = 2(80 Shore A^O) giving D_p' = 115.18 mm. A full series of tests (series 19) was carried out on 120 mm thick blocks of this mix. The results are given in Table 5.20. This gave thicknesses of 95.1 to 106.1 mm for 80-90% confidence and 123.9 to 134.4 mm for 97.5-99% confidence. Damage in this series was minimal, typical blocks being shown in Plate 5.8.

(vii) As mentioned in Section 5.2.4,the behaviour of Diorez 570 was inferior to the 2851 resins, and only the best rock type , river gravel, was examined after the main test series for the first quadratic analysis had been completed. The optimized mix for Diorez 570 with river gravel using A.P. ammunition was found in Section 5.2.5 to be x_1 = 9%, x_2 = 60%, x_3 = 26.5 to 37.5 mm, x_4 = 75 Shore A^O giving a predicted penetration path length of 35.21 mm. A series

of tests (series 20) was carried out on 80 mm thick blocks prepared with this mix,and the results are compared with the optimum river gravel/2851 resin mix results (series 11) in Table 5.21. This shows an inferior peformance from the Diorez and hence confirms earlier findings and predictions. Surface damage was minimal in this series as shown by the two blocks in Plate 5.9.

A summary of the mixes considered to be an acceptable compromise between general target damage and penetration resistance for the best resin (2851) and main rock types is given in Table 5.22.

5.4 Supplementary Penetration Tests

5.4.1 Limited Testing of Another Rock Aggregate, Hornfels

Seven tests,denoted as series 21,were carried out using a very hard aggregate, diabase hornfels, at $x_1=x_2=x_3=x_4=0$, using 2851 resins and A.P. ammunition as described in Section 4.5.1. The results are given in Table 5.23. Also given in the table for comparison are the results of the corresponding tests with the other rock types.

5.4.2 Target Temperature Effects

The results of the tests carried out on cold and hot targets of the final river gravel/2851 resin mix (cf Table 5.22) prepared as described in Section 4.5.2 are given in Table 5.24 as series 22 and 23 respectively. Also included in the table are the results of similar tests (A.P. ammunition and 80 mm thick target at 3 days) at ambient temperature (series 13).

The standard deviations for all series are very similar. The mean penetrations of the normal and hot targets were similar. The cold specimens gave a lower mean penetration, but fracturing of the target was excessive (Plate 5.10) when compared with that at normal temperature. This low temperature brittleness is a problem inherent in the polymer type. In most

cases, penetration depth could not be obtained by sectioning of the cold specimens, because of the degree of fracturing. However, the penetration depth could be found by splitting the specimen along its fractures and locating the burrow and projectile fragments.

Damage to the hot targets was minimal as shown in Plate 5.11.

5.5 Static Tests

The mixes used in these tests were as given in Table 5.22 except that the aggregate size was reduced (x_3 = 13.2% 19 mm, not 26.5 to 37.5 mm).

5.5.1 Uniaxial Compressive Tests

The results of the uniaxial compressive tests discussed in Section 4.6.2 are given graphically in Figures 5.2 to 5.6 as stress - longitudinal strain and stress - Poisson's ratio plots. Ultimate stresses and strains are compared in Table 5.25, along with values of tangent modulus at zero stress, and secant modulus at 1/3 maximum stress.

The results imply the following general trends

(i) Strength and modulus increasing with increasing strain rate. The strains corresponding to maximum stress were fairly consistent.

(ii) Angular aggregates (ie basalt and limestone) give lower strength and modulus values than rounded aggregate (river gravel) at a similar resin content, but failure occurs at similar strains.

(iii) The mix proportions given in Table 5.22 show that the two angular aggregate composites, basalt and limestone, have different resin percentages. If it is assumed that the rock type has little effect on the behaviour in the static tests then it can be seen that increase in resin content leads to an increase in strength, strain at failure, tangent modulus and secant modulus.

5.5.2 Creep Tests

The results of the creep tests are presented graphically in Figure 5.7, the time axis being logarithmic. The low stress level used led to the creep strains being small, and consequently there was a significant scatter in the

readings. This was due to the relative inaccuracy of the Demec gauge, over the small strains measured. Also, varying the pressure on the Demec gauge could give slightly different readings, because of the flexible nature of the composite.

The tests were relatively short in duration, and so it was not possible to use anything more complex than a simple linear-logarithmic creep rate.

The results, summarised in Table 5.26, show a large variation within each rock type, both in terms of initial strain, and creep rate.

5.5.3 Beam Bending Tests

These tests were carried out on final mixes of all three main rock types and produced a failure load and a central deflection - time history. Also examined were the effects of increasing cure time for the river gravel composite. From the results, stress strain histories were derived, as described in Section 4.6.4. The plots of these are given in Figures 5.8 to 5.14. The deflection at failure, stress, strain and secant modulus at 1/3 failure stress are given in Table 5.27. The secant modulus value represents a safe working stress, applicable during handling of panels constructed from the composite.

For rounded river gravel, in a composite 80 mm thick, the maximum panel dimension may be calculated using the 1 day failure stress from Table 5.27 and equation 4.13. Density is estimated from target specimen weights and dimensions

$$l = \sqrt{\frac{4}{9} \times \frac{0.08 \times 3.95 \times 10^6}{21000}} = 2.59 \text{ m}$$

For the weakest composite, using basalt as in series 16 at 110 mm thickness

$$l = \sqrt{\frac{4}{9} \times \frac{0.11 \times 2.76 \times 10^6}{20210}} = 2.58 \text{ m}$$

5.6 Voids Measurement - Cast Specimens

The results of the voids measurement from sectioned specimens are given in Table 5.28. The method of measurement was described in Section 4.6.1.

Ammunition type (7.62 mm)	Variable	Distance from gun (m)	Mean	Standard deviation	Number of readings
A.P.	Velocity	18.5	807.2 m/s	9.8 m/s	366
Ball	Velocity	18.5	793.6 m/s	7.6 m/s	48
A.P.	Vertical(y) Coordinate	20	77.4 mm	6.2 mm	20
A.P.	Horizontal(x) Coordinate	20	80.3 mm	4.7 mm	20
Ball	Vertical(y) Coordinate	20	74.1 mm	6.9 mm	20
Ball	Horizontal(x) Coordinate	20	80.0 mm	6.4 mm	20

Table 5.1

Measured velocity and accuracy information

Rock type/ Series No/ Nominal thickness (mm)	Specimen No.	Normal penetration D (mm)	Predicted normal penetration D_p (mm) (Eqs.5.1 &5.2)	Penetration path length D' (mm)	Predicted Penetration path length D_p' (mm) (Eqs.5.3 & 5.4)
Crushed basalt/ Series 1/ Nominal thickness 125*	1	59	-	-	-
	2	91			
	3	97			
	4	(P)			
	5	100(S)			
	6	(P)			
	7	78			
	8	109			
	9	84			
	10	72			
	11	(P)			
Crushed limestone/ Series 2/ Nominal thickness 155	1	58	59.5	63.1	65.5
	2	133	135.5	155.0	156.1
	3	53	77.0	56.0	88.6
	4	93	70.5	110.8	88.8
	5	130	107.5	132.1	110.0
	6	77	101.0	77.6	110.2
	7	40	42.5	41.7	42.8
	8	117	118.5	131.0	133.4
	9	115	89	125.5	99.4
	10	70	89	97.5	99.4
	11	93	89	103.0	99.4
Rounded river gravel/ Series 3/ Nominal thickness 155	1	52	53.2	55.3	53.3
	2	127	107.6	127.9	114.9
	3	40	45.6	44.0	48.3
	4	65	65.6	72.7	73.7
	5	65	65.6	68.6	69.6
	6	80	85.6	90.7	95.0
	7	41	23.6	41.4	27.5
	8	77	78.0	102.5	95.2
	9	53	65.6	53.0	71.6
	10	65	65.6	73.5	71.6
	11	58	65.6	58.5	71.6

*

Note :- thickness changed after this series due to occurrance of perforation.

(P) indicates perforation

(S) indicates side exit

Table 5.2.

Penetration results and linear polynomial fitting predictions using Diorez 570 and A.P. ammunition.

Test Number	Measured penetration, path length, D', and predicted penetration path length D_p' (mm)					
	Rounded river gravel-series 4		Crushed basalt Series 5		Crushed limestone Series 6	
	D'	D_p'	D'	D_p'	D'	D_p'
1	82.1	103.7	139.1	134.2	75.2	81.9
2	131.3	118.7	135.1	133.1	74.9	100.8
3	70.7	81.5	138.9	124.2	141.9	102.5
4	94.6	113.9	141.0	144.0	66.5	71.2
5	56.5	69.1	127.0	113.4	65.0	66.3
6	51.7	62.7	102.3	112.6	80.6	82.7
7	31.3	39.1	73.9	56.6	83.8	109.3
8	51.1	50.0	96.8	76.7	84.5	75.5
9	58.0	59.7	71.1	82.8	138.3	135.6
10	51.8	65.6	51.6	78.2	146.3	121.4
11	61.5	72.1	78.3	77.3	120.6	119.2
12	107.4	95.3	88.2	93.4	67.8	54.8
13	46.2	48.4	149.0	155.3	106.8	102.7
14	43.1	32.8	144.7	151.0	58.2	85.9
15	39.7	52.9	109.3	102.9	146.3	108.7
16	54.8	54.7	105.2	119.4	47.8	41.7
17	70.8	41.6	82.2	102.6	88.2	108.5
18	51.3	58.4	139.2	117.9	69.7	60.5
19	81.9	73.0	139.9	120.0	130.0	108.4
20	85.8	72.7	59.6	78.6	52.1	84.8
21	129.4	114.0	133.0	121.5	88.1	104.6
22	45.4	38.8	116.1	126.7	81.4	76.0
23	124.0	100.4	79.2	109.4	98.1	83.7
24	59.6	61.1	131.9	100.8	78.1	103.6
25	77.8	75.2	88.3	91.7	149.2	122.5
26	54.6	"	90.5	"	72.1	"
27	90.9	"	98.6	"	113.6	"
28	96.0	"	79.0	"	92.9	"
29	59.7	"	64.4	"	92.7	"
30	85.6	"	108.4	"	176.9	"
31	63.7/53.0 117.1/53.4*	"	112.5	"	160.0	"

* Extra tests carried out in error, but included in the analysis. Specimen size 152 x 152 x 155 thick (nominal due to slight swelling)

Table 5.3

Values of measured and predicted penetration path length for three rock types with Diorez 570 and A.P. projectiles-first quadratic analysis

Test Number	Values of D' and D_p' (mm)							
	AP projectiles						Ball projectiles	
	Rounded river gravel-series 7		Crushed basalt series 8		Crushed limestone series 9		Rounded river gravel series 10	
	D'	D_p'	D'	D_p'	D'	D_p'	D'	D_p'
1	61.4	58.8	107.0	98.8	115.7	110.1	36.4	39.2
2	74.0	64.4	141.0	142.9	119.6	98.9	37.5	34.7
3	69.0	52.6	101.0	105.3	124.1	116.1	46.0	46.7
4	46.1	59.1	130.7	125.4	119.1	128.1	46.1	42.2
5	40.1	57.8	78.5	100.6	116.6	86.8	55.9	42.8
6	81.7	72.7	133.3	117.8	76.2	81.5	34.0	36.3
7	39.6	52.9	121.3	94.9	63.5	73.1	45.6	44.7
8	81.4	68.7	69.6	88.1	131.0	90.9	38.1	38.1
9	60.5	70.9	96.1	91.2	68.1	77.9	45.0	40.9
10	85.3	70.1	76.2	98.3	99.3	89.3	45.5	43.7
11	45.1	52.1	107.0	118.3	70.5	64.7	41.7	36.9
12	72.3	52.2	110.0	101.5	99.6	99.2	30.6	39.6
13	72.6	57.6	101.2	102.3	92.7	83.3	32.5	33.9
14	52.1	66.1	73.3	82.6	122.7	100.5	39.4	34.6
15	32.7	39.9	105.5	117.2	59.9	50.3	25.5	24.2
16	48.7	49.3	69.7	73.6	85.6	90.7	30.3	24.9
17	60.6	47.7	126.4	125.6	51.5	60.5	25.0	31.3
18	45.3	62.7	134.5	126.0	68.0	89.7	27.0	27.4
19	79.3	81.8	122.4	113.1	78.3	104.3	33.0	39.7
20	57.1	59.0	110.5	110.5	95.8	100.5	37.5	37.5
21	51.6	66.2	118.7	117.1	103.4	103.9	44.1	43.2
22	72.7	62.5	98.8	91.0	41.8	72.0	24.5	32.1
23	49.0	50.0	75.2	84.2	86.3	111.1	47.0	51.1
24	39.3	42.7	80.4	62.0	72.8	78.7	36.9	39.6
25	43.5	49.6	73.6	103.2	117.9	100.0	53.6	44.6
26	49.6	"	116.6	"	109.4	"	42.8	"
27	59.7	"	108.3	"	122.1	"	44.6	"
28	49.7	"	122.5	"	61.5	"	45.3	"
29	39.9	"	106.1	"	117.8	"	43.9	"
30	37.7	"	122.4	"	108.6	"	37.6	"
31	66.8	"	73.2	"	62.9	"	44.7	"

Specimen size 152 x 152 x 155 thick (nominal due to slight swelling)

Table 5.4

Values of measured and predicted penetration path length for 2851 resin blend for three rock types with A.P. projectiles and one rock type with ball projectiles - first quadratic analysis

		$\Sigma(D'-D_p')^2$ (1)	$\Sigma(D'-\bar{D}')^2$ at $x_1=x_2=x_3=x_4=0$ (2)	(1)-(2) (3)	Degrees of freedom for residuals (4)	No. of points at $x_1=x_2=x_3=x_4=0$ (5)	$\frac{(3)}{(2)} \times \left[\frac{(5)-1}{(4)-(5)+1}\right]$ (6)	$F^{+}_{(4)-(5)+1,(5)-1}$ (7)	(6)<(7)? (8)
A.P. DIOREZ 570	Rounded river gravel Series 4	8498	4314	4184	19*	10*	0.873	$F_{10,9} = 3.14$	Yes
	Crushed basalt Series 5	7863	1679	6184	16	7	2.210	$F_{10,6} = 4.06$	Yes
	Crushed Limestone Series 6	18723	9459	9264	16	7	0.588	$F_{10,6} = 4.06$	Yes
A.P. 2851 RESIN BLEND	Rounded river gravel Series 7	4018	670	3348	16	7	3.00	$F_{10,6} = 4.06$	Yes
	Crushed basalt Series 8	6216	2731	3485	16	7	0.767	$F_{10,6} = 4.06$	Yes
	Crushed limestone Series 9	11109	4145	6963	16	7	1.008	$F_{10,6} = 4.06$	Yes
BALL, 2851 RESIN BLEND	Rounded river gravel Series 10	689	134	555	16	7	2.485	$F_{10,6} = 4.06$	Yes

* Due to extra tests at $x_1=x_2=x_3=x_4=0$

\+ F values obtained from standard statistical tables.

Note - Figures in brackets refer to the contents of the enclosed column number.

Table 5.5 Lack of fit calculations for first quadratic fit.

Rock Type	D_p' from first quadratic analysis (mm).	
	Diorez 570 $x_1=x_2=x_3=x_4=0$ (coded) From equations 5.5 to 5.7	2851 resins $x_1=+1, x_2=-0.4, x_3=0, x_4=+1$ (coded) From equations 5.8 to 5.10
River gravel	75.18	56.04
Basalt	91.67	88.14
Limestone	122.49	100.22

Table 5.6 Comparison of equivalent values of D_p' for Diorez 570 and 2851 resins, using A.P. ammunition

Rounded River gravel Diorez 570:Series 4					Rounded river gravel 2851 resins:Series 7					Crushed basalt 2851 resins:Series 8 (first combination)						Crushed limestone 2851 resins:Series 9				
Test No.	Coded level x_1	x_2	x_3	x_4	Test No.	Coded level x_1	x_2	x_3	x_4	Test No.	Coded level x_1	x_2	x_3	x_4	D'	Test No.	Coded level x_1	x_2	x_3	x_4
32	-1	2	2	-1	32	-1	2	2	1	32	1	2	2	1	89.6	32	-1	2	2	1
33	-1	2	1	-2	33	-1	2	1	2	33	1	2	1	2	70.2	33	-1	2	1	2
34	-1	1	2	-2	34	-1	1	2	2	34	1	1	2	2	60.6	34	-1	1	2	2
35	-2	2	2	-2	35	-2	2	2	2	35	2	2	2	2	79.9	35	-2	2	2	2
36	-2	2	1	-1	36	-2	2	1	1	36	2	2	1	1	75.2	36	-2	2	1	1
37	-2	1	2	-1	37	-2	1	2	1	37	2	1	2	1	84.9	37	-2	1	2	1
38	-2	1	1	-2	38	-2	1	1	2	38	2	1	1	2	70.3	38	-2	1	1	2

Table 5.7 Coded levels used in first stage corner tests including penetration path length for Series 8.

Test Number	Coded level			
	x_1	x_2	x_3	x_4
39	-1	2	2	1
40	-1	1	1	2
41	-1	2	2	2
42	-2	2	2	2
43	-2	1	1	1
44	-2	2	2	1
45	-2	1	1	2

Table 5.8 Third combination of coded levels used in first stage corner fitting for Series 8, crushed basalt/AP/2851 resins.

Diorez 570			2851 resins								
Rounded river gravel - series 4			Rounded river gravel - series 7			Crushed Basalt - series 8			Crushed Limestone - series 9		
Test No.	D'	D_p'	Test No.	D'	D_p'	Test No.	D'	D_p'	Test No	D'	D_p'
1	82.1	89.8	1	61.4	53.7	1	107.0	104.5	1	115.7	121.3
2	131.3	122.2	3	69.0	54.7	3	101.0	116.7	3	124.1	114.7
3	70.7	73.4	4	46.1	64.8	4	130.7	121.7	4	119.1	143.8
4	94.6	106.4	5	40.1	50.3	5	78.5	107.0	5	116.6	91.9
5	56.5	65.9	6	81.7	86.7	6	133.3	113.0	6	76.2	94.1
6	51.7	64.4	7	39.6	46.1	7	121.3	95.3	7	63.5	80.7
7	31.3	59.8	8	81.4	71.9	8	69.6	89.7	8	131.0	93.4
8	51.1	58.9	9	60.5	70.3	9	96.1	88.3	9	68.1	70.6
9	58.0	65.3	10	85.3	71.7	10	76.2	86.8	10	99.3	98.0
11	61.5	68.8	11	45.1	65.8	11	107.0	114.4	11	70.5	54.3
12	107.4	103.2	12	72.3	56.6	12	110.0	101.3	12	99.6	92.1
13	46.2	41.8	13	72.6	55.0	13	101.2	92.5	13	92.7	96.9
14	43.1	41.7	14	52.1	72.1	14	73.3	80.7	14	122.7	107.8
15	39.7	55.6	15	32.7	45.3	15	105.5	94.8	15	59.9	76.1
16	54.8	56.1	16	48.7	51.6	16	69.7	71.3	16	85.6	97.5
17	70.8	44.8	17	60.6	66.2	17	126.4	104.9	17	51.5	66.9
20	85.8	69.6	20	57.1	57.0	20	110.5	105.8	20	95.8	99.8
22	45.4	33.2	22	72.7	48.0	22	98.8	89.4	22	41.8	72.9
23	124.0	106.2	24	39.3	47.5	24	80.4	73.5	24	72.8	89.8
25	77.8	74.1	25	43.5	48.5	25	73.6	105.5	25	117.9	95.5
26	54.6	74.1	26	49.6	48.5	26	116.6	105.5	26	109.4	95.5
27	90.9	74.1	27	59.7	48.5	27	108.3	105.5	27	122.1	95.5
28	96.0	74.1	28	49.7	48.5	28	122.5	105.5	28	61.5	95.5
29	59.7	74.1	29	39.9	48.5	29	106.1	105.5	29	117.8	95.5
30	85.6	74.1	30	37.7	48.5	30	122.4	105.5	30	108.6	95.5
31	63.7	74.1	31	66.8	48.5	31	73.2	105.5	31	62.9	95.5
31A	53.0	74.1	32	35.0	45.1	39	62.2	77.5	32	73.5	77.1
31B	117.1	74.1	33	52.8	52.7	40	88.6	87.2	33	76.5	83.8
31C	53.4	74.1	34	41.1	34.9	41	77.3	72.4	34	130.7	103.9
32	46.8	45.7	35	59.8	64.6	42	106.9	88.8	35	78.3	81.7
33	59.3	65.0	36	97.6	76.8	43	104.8	106.5	36	63.1	55.5
34	86.7	64.7	37	36.0	54.0	44	83.1	95.5	37	75.7	66.0
35	52.6	56.0	38	86.1	70.5	45	71.9	96.7	38	62.3	67.7
36	58.5	44.6									
37	39.6	48.1									
38	57.7	66.8									

Table 5.9

Values of D', with values of D_p' from

PENET, using A.P. ammunition after first stage corner tests

		$\Sigma(D'-D_p')^2$ (1)	$\Sigma(D'-\bar{D}')^2$ (2) at $x_1=x_2=x_3=x_4=0$ (2)	(1)-(2)=(3) (3)	Degrees of freedom for residual (4)	No. of points at $x_1=x_2=x_3=x_4=0$ (5)	$\frac{(3)}{(2)} \times \left[\frac{(5)-1}{(4)-(5)+1}\right]$ (6)	$F^{+}_{(4)-(5)+1,(5)-1}$ (7)	(6)<(7)? (8)
DIOREZ 570	Rounded river gravel series 4	8414	4326	4087	21	10	0.71	$F_{12,9}=3.07$	Yes
2851 RESINS	Rounded river gravel series 7	5259	670	4589	18	7	3.42	$F_{12,6}=4.00$	Yes
	Crushed limestone series 8	11114	4145	6969	18	7	0.297	$F_{12,6}=4.00$	Yes
	Crushed basalt series 9	7911	2731	5180	18	7	0.95	$F_{12,6}=4.00$	Yes

+ F values obtained from standard statistical tables

Table 5.10

Lack of fit calculations after first stage corner tests

Test Number	Coded Values				Measured penetration D' mm
	x_1	x_2	x_3	x_4	
39	-1	2	-2	1	(P)
40	-1	2	-1	2	120.9
41	-1	1	-2	2	110.2
42	-2	2	-2	2	(P)
43	-2	2	-1	1	120.9
44	-2	1	-2	1	(P)
45	-2	1	-1	2	121.6

(P) indicates perforation

Table 5.11

Coded levels and measured penetration path length

for limestone/AP/2851 resin combinations

in small aggregate size corner

Rounded river gravel Diorez 570 Series 4 cont.					Crushed basalt 2851 resins Series 8 cont.					Crushed limestone 2851 resins Series 9 cont.				
Test No.	Coded level				Test No.	Coded level				Test No.	Coded level			
	x_1	x_2	x_3	x_4		x_1	x_2	x_3	x_4		x_1	x_2	x_3	x_4
39	-2	2	2	2	46	-2	-2	2	2	46	-2	-2	2	2
40	-2	1	2	1	47	-2	-1	2	1	47	-2	-1	2	1
41	-1	2	1	2	48	-1	-2	1	2	48	-1	-2	1	2
42	-2	-2	2	2	49	-2	2	2	-2	49	-2	2	2	-2
43	-2	-1	2	1	50	-2	1	2	-1	50	-2	1	2	-1
44	-1	-2	1	2	51	-1	2	1	-2	51	-1	2	1	-2
45	-2	-2	2	-2	52	-2	2	2	-2	52	-2	-2	2	-2
46	-2	-1	2	-1	53	-2	1	2	-1	53	-2	-1	2	-1
47	-1	-2	1	-2	54	-1	2	1	-2	54	-1	-2	1	-2

Table 5.12

Coded levels used in second stage corner filling tests

Diorez 570			2851 resins					
Rounded river gravel - series 4			Crushed basalt - series 8			Crushed limestone - series 9		
Test No.	D'	D_p'	Test No.	D'	D_p'	Test No.	D'	D_p'
1	82.1	84.3	1	107.0	100.4	1	115.7	114.8
2	131.3	109.3	2	141.0	120.7	2	119.6	117.3
3	70.7	83.3	3	101.0	120.2	3	124.1	110.6
4	94.6	123.4	4	130.7	121.5	4	119.1	131.0
5	56.5	65.7	5	78.5	94.7	5	116.6	101.8
6	51.7	58.9	6	133.3	108.8	6	76.2	87.6
7	31.3	60.4	7	121.3	98.1	7	63.5	85.5
8	51.1	68.8	8	69.6	93.2	8	131.0	89.3
9	58.0	64.9	9	96.1	100.1	9	68.1	64.5
10	51.8	79.5	10	76.2	106.0	10	99.3	91.3
11	61.5	59.7	11	107.0	112.1	11	70.5	63.0
12	107.4	89.4	12	110.0	98.9	12	99.6	107.9
13	46.2	58.4	13	101.2	92.8	13	92.7	91.5
14	43.1	41.3	14	73.3	92.5	14	122.7	101.7
15	39.7	49.0	15	105.5	88.3	15	59.9	78.0
16	54.8	47.0	16	69.7	69.0	16	85.6	106.1
17	70.8	51.2	17	126.4	96.0	17	51.5	75.7
19	81.9	68.8	19	122.4	120.8	19	78.3	100.2
20	85.8	73.5	20	110.5	117.2	20	95.8	100.5
22	45.4	39.6	22	98.8	80.4	22	41.8	81.7
23	124.0	102.4	23	75.2	102.8	23	86.3	121.6
24	59.6	61.2	24	80.4	78.4	24	72.8	88.2
25	77.8	70.8	25	73.6	98.5	25	117.9	92.3
26	54.6	70.8	26	116.6	98.5	26	109.4	92.3
27	90.9	70.8	27	108.3	98.5	27	122.1	92.3
28	96.0	70.8	28	122.5	98.5	28	61.5	92.3
29	59.7	70.8	29	106.1	98.5	29	117.8	92.3
30	85.6	70.8	30	122.4	98.5	30	108.6	92.3
31	63.7	70.8	31	73.2	98.5	31	62.9	92.3
31 A	53.0	70.8						
31 B	117.1	70.8						
31 C	53.4	70.8						
32	46.8	45.1	39	66.2	85.3	32	73.5	79.4
33	59.3	73.1	40	88.6	88.7	33	76.5	83.7
34	86.7	59.4	41	77.3	65.1	34	130.7	98.9
35	52.6	48.4	42	106.9	90.2	35	78.3	74.4
36	58.5	44.1	43	104.8	114.3	36	63.1	57.8
37	39.6	46.2	44	83.1	85.9	37	75.7	72.3
38	57.7	61.6	45	71.9	89.3	38	62.3	62.6
39	41.7	44.1	46	107.5	104.4	46	114.1	128.8
40	43.6	46.1	47	76.5	89.1	47	101.0	100.8
41	42.8	46.2	48	110.5	105.5	48	117.4	108.0
42	113.9	86.4	49	132.4	104.7	49	51.5	70.9
43	46.5	65.2	50	55.1	89.3	50	77.7	71.9
44	57.4	69.2	51	115.8	116.1	51	122.8	95.9
45	77.6	74.1	52	116.9	87.4	52	138.2	136.4
46	57.9	61.1	53	60.6	84.6	53	120.6	103.3
47	64.1	79.5	54	76.0	101.4	54	137.8	131.3

Table 5.13

Values of D' with values of D_p' from PENET using AP ammunition after second stage corner tests

		$\Sigma(D' - D_p')^2$ (1)	$\Sigma(D' - \bar{D}')^2$ at $x_1=x_2=x_3=x_4=0$ (2)	(1) - (2) (3)	Degrees of freedom for residuals (4)	No. of points at $x_1=x_2=x_3=x_4=0$ (5)	$\frac{(3)}{(2)} \times \left[\frac{(5)-1}{(4)-(5)+1}\right]$ (6)	$F^{+}_{(4)-(5)+1,(5)-1}$ (7)	(6)<(7)? (8)
DIOREZ 570	Rounded river gravel series 4	12677	4326	8351	33	10	0.72	$F_{24,9}$ =2.90	Yes
2851 resins	Crushed limestone series 8	15978	4145	11833	30	7	0.71	$F_{24,6}$ =3.84	Yes
	Crushed basalt series 9	15199	2731	12468	30	7	1.14	$F_{24,6}$ =3.84	Yes

+ F values obtained from standard statistical tables

Table 5.14

Lack of fit calculations after second stage corner tests

Series No.	Rock/bullet/ resin description	Eqn. No.	D_p' with $x_n=0$	Coefficients of x terms in the response surface equation													
				b_1	b_2	b_3	b_4	b_{12}	b_{13}	b_{14}	b_{23}	b_{24}	b_{34}	b_{11}	b_{22}	b_{33}	b_{44}
4	River gravel/AP/ Diorez 570	5.5	75.18	+4.20	-0.08	-18.79	-9.82	+4.35	-5.36	-2.28	-1.98	+8.64	+5.83	-6.29	-0.59	+0.30	+1.40
5	Basalt/AP/ Diorez 570	5.6	91.67	+3.85	-10.37	+1.30	-2.14	+5.21	+0.08	-0.89	-11.71	+1.09	+23.31	+4.65	+1.91	+8.11	+3.34
6	Limestone/ AP/ Diorez 570	5.7	122.49	-12.01	-5.91	-7.16	+4.99	-12.54	-0.64	-8.28	+5.61	-9.26	-4.33	-9.50	-6.47	-8.05	-7.21
7	River gravel/AP/ 2851 resins	5.8	49.56	+3.75	-5.72	-0.94	-1.81	+0.23	+2.33	-1.60	+0.29	-3.16	-3.09	+1.40	+5.21	+3.70	-0.80
8	Basalt/AP/ 2851 resins	5.9	103.24	+0.10	-0.65	-6.52	-5.54	-5.99	-6.71	-9.21	-3.04	+5.16	+2.34	+5.63	+2.13	+0.21	-7.53
9	Limestone/ AP/ 2851 resins	5.10	100.03	+7.29	-0.94	-7.96	-8.10	+5.97	+1.48	+5.63	-4.93	-4.80	+7.16	-6.23	+0.59	-3.02	-1.28
10	River gravel/ball 2851 resins	5.11	44.64	-0.96	-0.55	-2.78	-2.89	-0.02	-0.52	+1.83	-1.39	-2.89	-2.67	-3.83	-1.51	-1.75	+0.16

Table 5.15

Coefficients in equations of response surfaces after main test series - format as Eq. 4.7

	Rock/bullet/ resin description	D_p' with $x_n=0$ (mm)	Coefficients of x terms in the response surface equation													
			b_1	b_2	b_3	b_4	b_{12}	b_{13}	b_{14}	b_{23}	b_{24}	b_{34}	b_{11}	b_{22}	b_{33}	b_{44}
Inc. first corner tests	River gravel/AP/ Diorez 570	74.13	+8.23	-0.50	-17.77	-6.83	+0.15	-8.48	+0.34	+2.56	+4.99	+0.10	-3.22	-0.89	-1.36	+4.61
	River gravel/AP/ 2851 resins	48.49	+6.80	-4.82	-2.05	-0.87	-2.63	+3.94	-4.83	-1.31	-1.39	-2.97	+7.83	+4.53	+0.91	+0.19
	Basalt/AP/ 2851 resins	105.53	-1.76	+0.71	-6.89	-8.67	-2.88	-2.61	-4.49	-5.98	+3.47	+0.47	-1.03	-0.29	-0.59	-3.67
	Limestone /AP/ 2851 resins	95.52	+10.01	-4.26	-6.03	-11.67	+2.61	-4.10	+2.17	-1.13	-2.41	+13.94	-2.16	+3.19	-2.64	+4.41
Inc. first & second corner tests	River gravel/AP/ Diorez 570	70.76	+5.73	+1.17	-15.26	-10.30	+3.78	-7.93	-2.60	-1.05	-1.04	+3.05	-2.02	-0.10	-0.16	+2.79
	Basalt/AP/ 2851 resins	98.53	+0.25	-0.92	-8.90	-6.10	-4.76	-1.55	-3.61	-4.11	-1.97	-0.41	-0.51	+5.12	-0.07	-1.97
	Limestone /AP/ 2851 resins	92.27	+7.64	+0.05	-3.68	-8.53	+4.50	-4.17	+6.09	-3.02	+0.69	+10.02	-0.31	+2.03	-0.79	+3.16

Table 5.16

Coefficients in equations of response surfaces, after first and second stage corner filling - format as Eq.4.7

From Series No.	Rock type	Resin type	% resin by weight x_1	% rock aggregate by weight x_2	Rock size (mm) x_3	Polymers hardners (Shore A^o) x_4
4	River gravel	Diorez 570	9	60	26.5 to 37.5	75
7	River gravel	2851	9.8	59	26.5 to 37.5	80
8	Basalt	2851	7	56	26.5 to 37.5	80
9	Limestone	2851	7	64	26.5 to 37.5	69

Table 5.17

Mixes obtained from optimization procedure

Series Number.	11	12	13	14
Bullet Type.	AP	Ball	AP	AP
Specimen Age (days)	1	1	3	1
Specimen thickness (mm)	80	80	80	100
Penetration, Test No. 1	30	29	52	37
" " " 2	54	37	39	68
" " " 3	40	32	90(P)	40
" " " 4	35	60	28	44
" " " 5	90(P)*	27	40	58
" " " 6	41	58	46	59
" " " 7	51	24	76	54
" " " 8	26	56	45	51
" " " 9	27	34	90(P)	38
" " " 10	43	90(P)	34	62
" " " 11	42	30	54	33
" " " 12	48	40	90(P)	47
" " " 13	45	31	30	36
" " " 14	65	22	90(P)	100
" " " 15	53	90(P)	30	41
" " " 16	39	41	61	40
" " " 17	60	27	41	38
" " " 18	90(P)	29	47	82
" " " 19	90(P)	49	32	41
" " " 20	30	31	72	54
Mean penetration, $\bar{D}$	50.0	41.9	54.4	51.2
Predicted path length, D_p'	30.85	-	-	30.85
Standard deviation	19.7	19.4	21.8	16.6
Thickness for 80-90% confidence (z=0.86 to 1.33)	66.9 to 76.2	58.6 to 67.7	73.1 to 83.4	65.5 to 73.3
Thickness for 97.5-99% confidence (z=2.09 to 2.54)	91.2 to 100.0	82.4 to 91.2	100.0 to 109.8	85.9 to 93.4

* P indicates perforation.

Table 5.18

Values of normal penetration (mm) for the optimum rounded river gravel/2851 resin combinations

(x_1 = 9.8% Resin; x_2 = 59% rock; x_3 = 26.5-37.5 mm aggregate; x_4 = 80 shore A^o hardness)

Series Number Specimen Thickness % Resin	15 110mm 7%	16 110mm 9%
Penetration, Test No. 1	120(P)*	64
" " " 2	55	78
" " " 3	120(P)	102
" " " 4	120(P)	62
" " " 5	120(P)	104
" " " 6	56	46
" " " 7	(S)	76
" " " 8	(S)	77
" " " 9	48	72
" " " 10	120(P)	60
" " " 11	+	91
" " " 12		120(P)
" " " 13		58
" " " 14		62
" " " 15		120(P)
" " " 16		106
" " " 17		60
" " " 18		49
" " " 19		110
" " " 2o		109
Mean penetration, $\bar{D}$	(94.9)	81.3
Predicted path length, D_p'	76.20	67.63
Standard deviation	(32.5)	23.6
Thickness for 80-90% confidence (z = 0.86 to 1.33)	(122.8 to 138.1)	101.6 to 112.7
Thickness for 97.5-99% confidence (z = 2.09 to 2.54)	(162.8 to 177.5)	130.6 to 141.2

* P indicates perforation, S indicates side exit
\+ test series discontinued because of number of perforations and excessive damage

Table 5.19

Values of normal penetration (mm) for crushed basalt/2851 resin combinations
(Figures in brackets are unlikely to be accurate because of limited number of tests and number of perforations)

Series Number Speciman Thickness % Resin	17 110 7	18 110 9	19 120 11
Penetration, Test No. 1	62	66	47
" " " 2	57	120(P)	53
" " " 3	120(P)*	62	89
" " " 4	46	69	70
" " " 5	50	120(P)	78
" " " 6	120(P)	80	41
" " " 7	58	70	69
" " " 8	(S)	120(P)	38
" " " 9	72	53	107
" " " 10	54	48	105
" " " 11	+	+	51
" " " 12			130(P)
" " " 13			85
" " " 14			70
" " " 15			77
" " " 16			68
" " " 17			69
" " " 18			60
" " " 19			97
" " " 20			95
Mean penetration, $\bar{D}$	(71.0)	(80.8)	75.0
Predicted path length D_p'	59.99	100.02	115.18
Standard deviation	(27.1)	(27.0)	23.4
Thickness for 80-90% confidence (z = 0.86 to 1.33)	(94.3 to 107.0)	(104.0 to 116.7)	95.1 to 106.1
Thickness for 97.5-99% confidence (z = 2.09 to 2.84)	(127.6 to 139.8)	(137.2 to 149.4)	123.9 to 134.4

* P indicates perforation, S indicates side exit.
+ test series discontinued because of perforations and excessive damage

Table 5.20

Values of normal penetration (mm) for limestone/2851 resin combinations.
(Figures in brackets are unlikely to be accurate because of limited number of tests and number of perforations)

Series Number Resin Type	11 2851	20 Diorez
Penetration, Test No. 1	30	36
" " " 2	54	90(P)
" " " 3	40	38
" " " 4	35	28
" " " 5	90(P)*	90(P)
" " " 6	41	90(P)
" " " 7	51	57
" " " 8	26	59
" " " 9	27	55
" " " 10	43	90(P)
" " " 11	42	50
" " " 12	48	90(P)
" " " 13	45	34
" " " 14	65	64
" " " 15	53	90(P)
" " " 16	39	39
" " " 17	60	90(P)
" " " 18	90(P)	55
" " " 19	90(P)	60
" " " 20	30	53
Mean penetration, $\bar{D}$	50.0	62.9
Predicted path length, D_p '	30.85	35.21
Standard deviation	19.7	21.9
Thickness for 80%-90% confidence (z = 0.86-1.33)	66.9 to 76.2	81.7 to 92.0
Thickness for 97.5%-99% confidence (z =2.09-2.54)	91.2 to 100.0	108.7 to 118.5

* P indicates perforation

Table 5.21

Comparison of results of tests with AP bullets fired at 80mm thick targets of optimum mixes of river gravel and 2851 resins and river gravel and Diorez resin

From series number	Rock type	% resin by weight x_1	% rock aggregate by weight x_2	Rock size (mm) x_3	Polymer hardness (Shore A^O) x_4	t_m for 80-90% Confidence limits (mm)	t_m for 97.5 to 99% Confidence limits (mm)
11	River gravel	9.8	59	26.5 to 37.5	80	75	100
16	basalt	9	58	26.5 to 37.5	80	110	140
19	limestone	11	59	26.5 to 37.5	80	100	130

Table 5.22

Summary of results from thickness tests using 2851 resins

Series Number Aggregate Type	21 Hornfels	7 River gravel	8 Basalt	9 Limestone
Test No. 1 (25)*	86.6	43.5	73.6	117.9
" " 2 (26)	69.3	49.6	116.6	109.4
" " 3 (27)	62.1	59.7	108.3	122.1
" " 4 (28)	44.4	49.7	122.5	61.5
" " 5 (29)	77.5	39.9	106.1	117.8
" " 6 (30)	52.3	37.7	122.4	108.6
" " 7 (31)	94.1	66.8	73.2	62.9
Mean	69.5	49.6	103.2	100.0
Standard deviation	16.7	9.8	19.8	24.3

All blocks nominally 155mm thick.

* Numbers in brackets refer to test numbers in Table 5.4

Table 5.23

Comparison of AP penetrations (mm) into hornfels/2851 resin composite and main rock types/2851 resin composites. All mixes at $x_1 = x_2 = x_3 = x_4 = 0$ (For hornfels x_1= 11% resin; x_2 = 54% rock; x_3 = 13.2 to 19.0 mm aggregate; x_4 = 70 Shore A^o hardness)

Series Number Temperature	22 -7°C	23 +34°C	13 +15°C
Penetration, Test No. 1	48	63	52
" " " 2	56	37	39
" " " 3	90(P)*	33	90(P)
" " " 4	59	36	28
" " " 5	63	61	40
" " " 6	25	90(P)	46
" " " 7	56	58	76
" " " 8	38	53	45
" " " 9	45	41	90(P)
" " " 10	40	37	34
" " " 11	46	62	54
" " " 12	90(P)	46	90(P)
" " " 13	40	36	30
" " " 14	25	38	90(P)
" " " 15	50	90(P)	30
" " " 16	20	33	61
" " " 17	24	61	41
" " " 18	33	30	47
" " " 19	41	90(P)	32
" " " 20	28	34	72
Mean penetration $\bar{D}$	45.9	51.5	54.4
Standard Deviation	19.0	19.5	21.8

* P indicates perforation

Table 5.24

Comparison of normal penetrations into targets of optimum mix river gravel/2851 resins at different temperatures

Rock Type	Rounded river gravel												Crushed basalt				Crushed limestone			
Loading head displacement rate (mm/min)	1.27				2.54				5.08				2.54				2.54			
Specimen number	1	2	3	MEAN	4	5	6	MEAN	7	8	9	MEAN	10	11	12	MEAN	13	14	15	MEAN
Maximum stress (N/mm^2)	8.20	6.36	7.10	7.22	9.33	8.36	9.40	9.03	8.75	8.79	10.59	9.38	6.11	5.72	5.73	5.85	7.40	7.10	6.73	7.08
Corresponding longitudinal strain ($x10^{-3}$)	19.24	22.78	18.80	20.27	18.78	18.48	20.36	19.21	16.66	23.80	18.60	19.69	19.16	20.45	20.88	20.16	18.67	22.19	24.16	21.67
Secant modulus at 1/3 max. stress (N/mm^2)	833	581	598	671	763	917	877	852	1053	508	698	753	544	645	516	568	851	620	571	681
Tangent modulus at zero stress (N/mm^2)	870	630	630	710	842	920	890	873	1053	661	1053	922	559	650	520	573	1111	661	615	796

Table 5.25

Stress-strain and modulus data for uniaxial compressive tests

Rock type	River gravel	Crushed basalt	Crushed limestone
Specimen No.	1 2 3	4 5	6 7
Creep strain/ $\log_{10}$ time(s) ($X10^{-5}$)	6.1 3.6 4.6 (mean = 4.8)	6.2 2.8 (mean = 4.5)	2.7 4.2 (mean = 3.5)

TABLE 5.26

Creep rate results

Rock type/ age at testing	Deflection at failure (mm)	Tensile failure stress (N/mm^2)	Strain to failure x 10^{-4}	Secant modulus at 1/3 failure stress (N/mm^2)
River gravel/ 3 hours	6.38 6.88 (6.99)* 7.72	2.94 3.05 (2.94) 2.83	193 208 (212) 234	280 272 (270) 258
River gravel/ 8 hours	7.06 8.17 (7.58) 7.51	3.96 3.77 (3.78) 3.62	207 247 (227) 227	426 400 (410) 405
River gravel/ 1 day	6.25 7.60 (7.27) 7.96	3.85 4.04 (3.95) 3.96	187 228 (219) 241	367 313 (341) 342
River gravel/ 3 days	5.55 6.58 (6.46) 7.26	4.32 4.74 (4.33) 3.92	168 195 (193) 215	694 667 (557) 309
River gravel/ 9 days	5.96 8.30 (7.26) 7.53	3.49 3.73 (3.65) 3.73	197 149 (170) 164	400 357 (362) 328
Basalt/ 1 day	4.48 5.47 (5.05) 5.20	2.92 3.08 (2.76) 2.27	132 160 (149) 154	400 306 (319) 252
Limestone/ 1 day	5.94 7.43 (7.37) 8.75	3.72 3.58 (3.70) 3.81	175 225 (221) 264	460 290 (324) 222

* Figures in brackets are mean values

Table 5.27

Summary of bending test data

	% voids for specimen number										(%) Mean	(%) Std'd Dev.
	1	2	3	4	5	6	7	8	9	10		
Series 11 River gravel	61.2	46.7	47.6	47.7	43.7	41.6	48.9	46.4	40.2	43.6	46.8	5.5
Series 16 Basalt	56.2	58.1	43.9	45.7	59.9	44.1	46.4	44.2	52.4	50.8	50.2	5.9
Series 19 Limestone	48.8	45.00	45.5	50.7	50.5	45.8	48.3	48.1	46.1	53.8	48.3	2.7

Table 5.28

Measurement of voids from sectioned specimens of optimised mixes

Notes : Only sections > 25 mm from specimen front or back used to avoid edge.

For mixes used in these test series, see Table 5.22

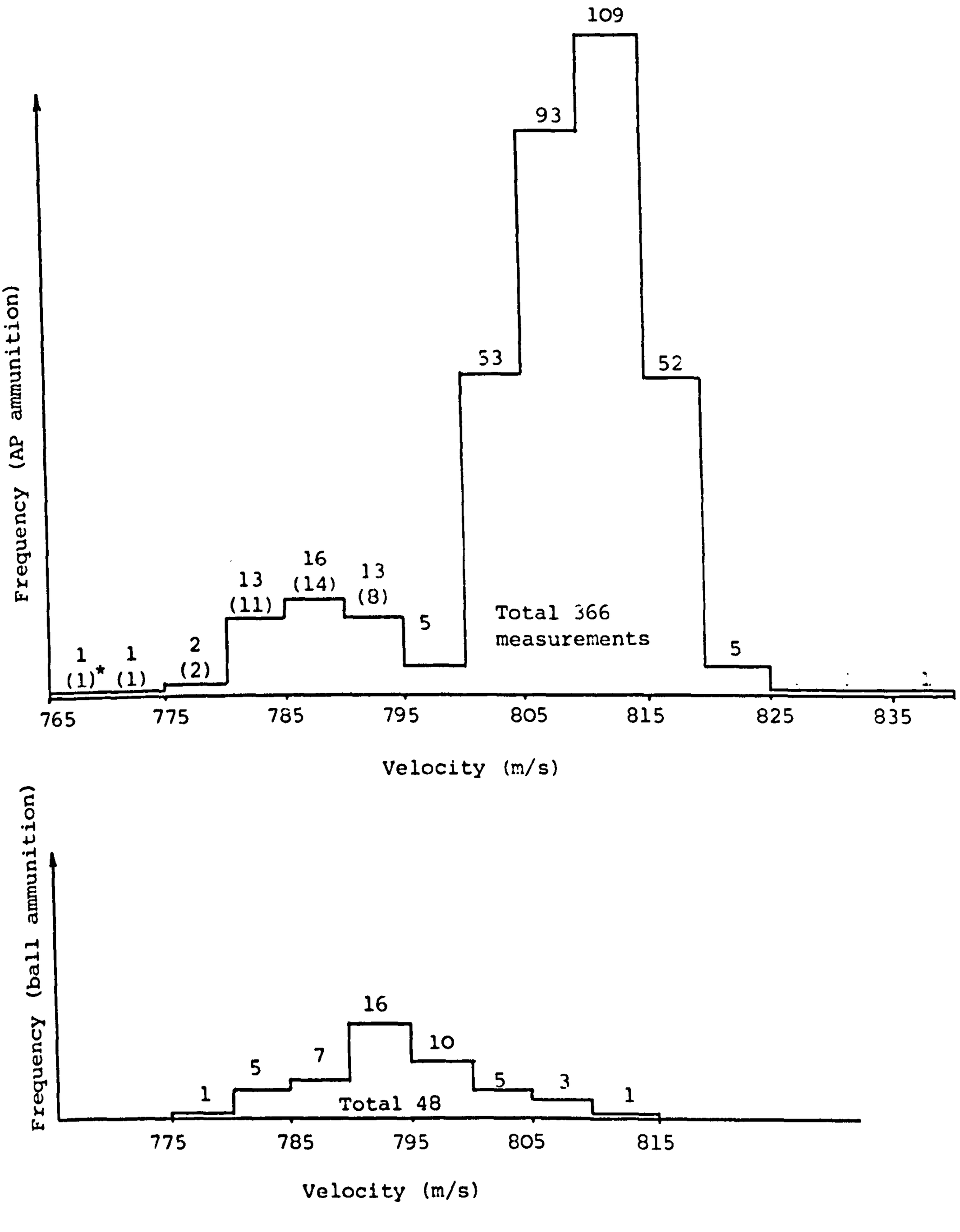

* Figures in brackets refer to measurements in unheated range during winter

FIGURE 5.1 HISTOGRAMS OF MEASURED VELOCITIES FOR BOTH 7.62mm AMMUNITION TYPES

FIGURE 5.2 UNIAXIAL STRESS STRAIN CURVES AND POISSONS RATIO PLOT-SPECIMENS 1 TO 3

River gravel 1.27mm/min displacement rate

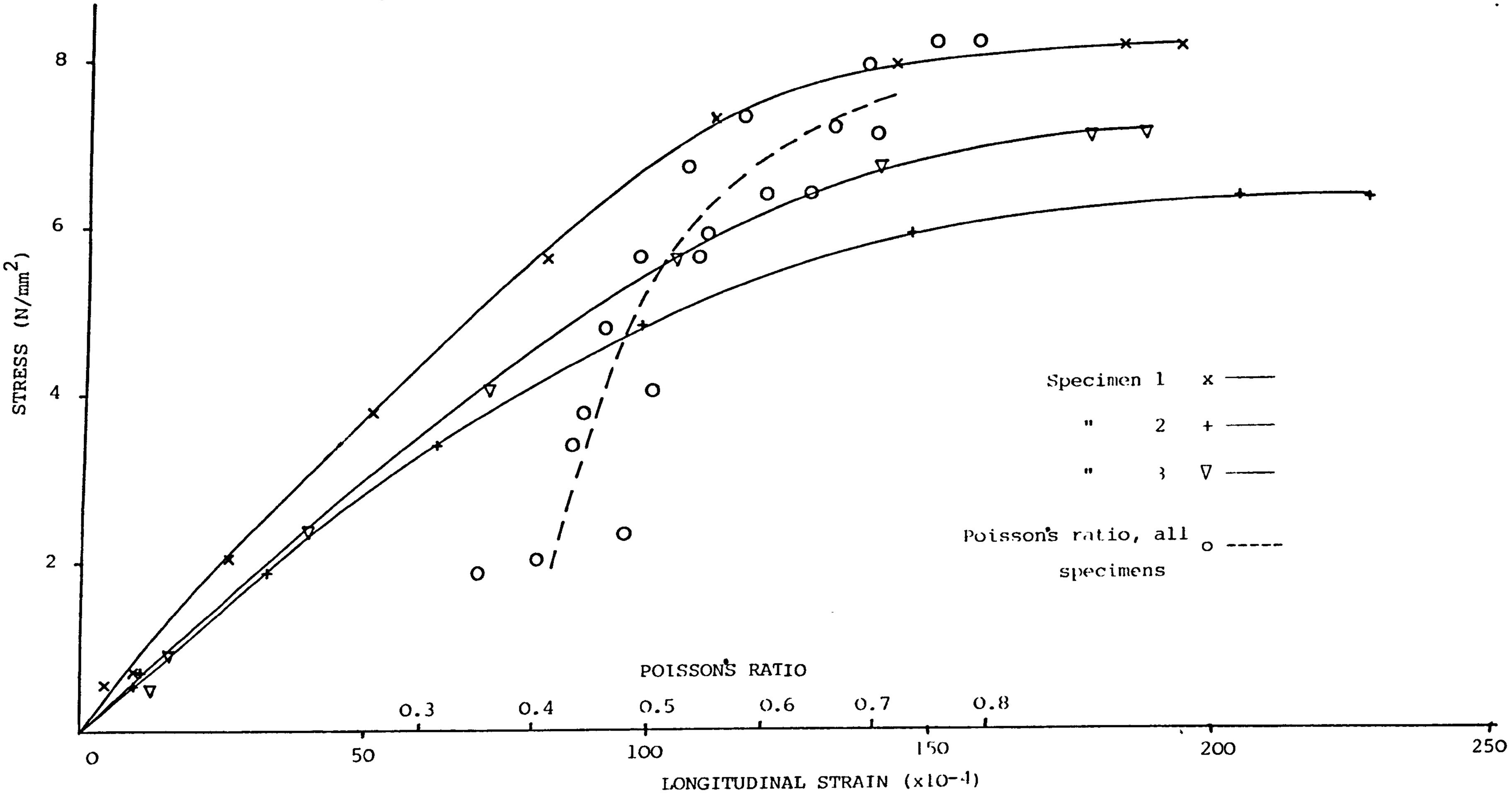

FIGURE 5.3 UNIAXIAL STRESS-STRAIN CURVES AND POISSONS RATIO PLOT-SPECIMENS 4 TO 6

River gravel 2.54 mm/min displacement rate

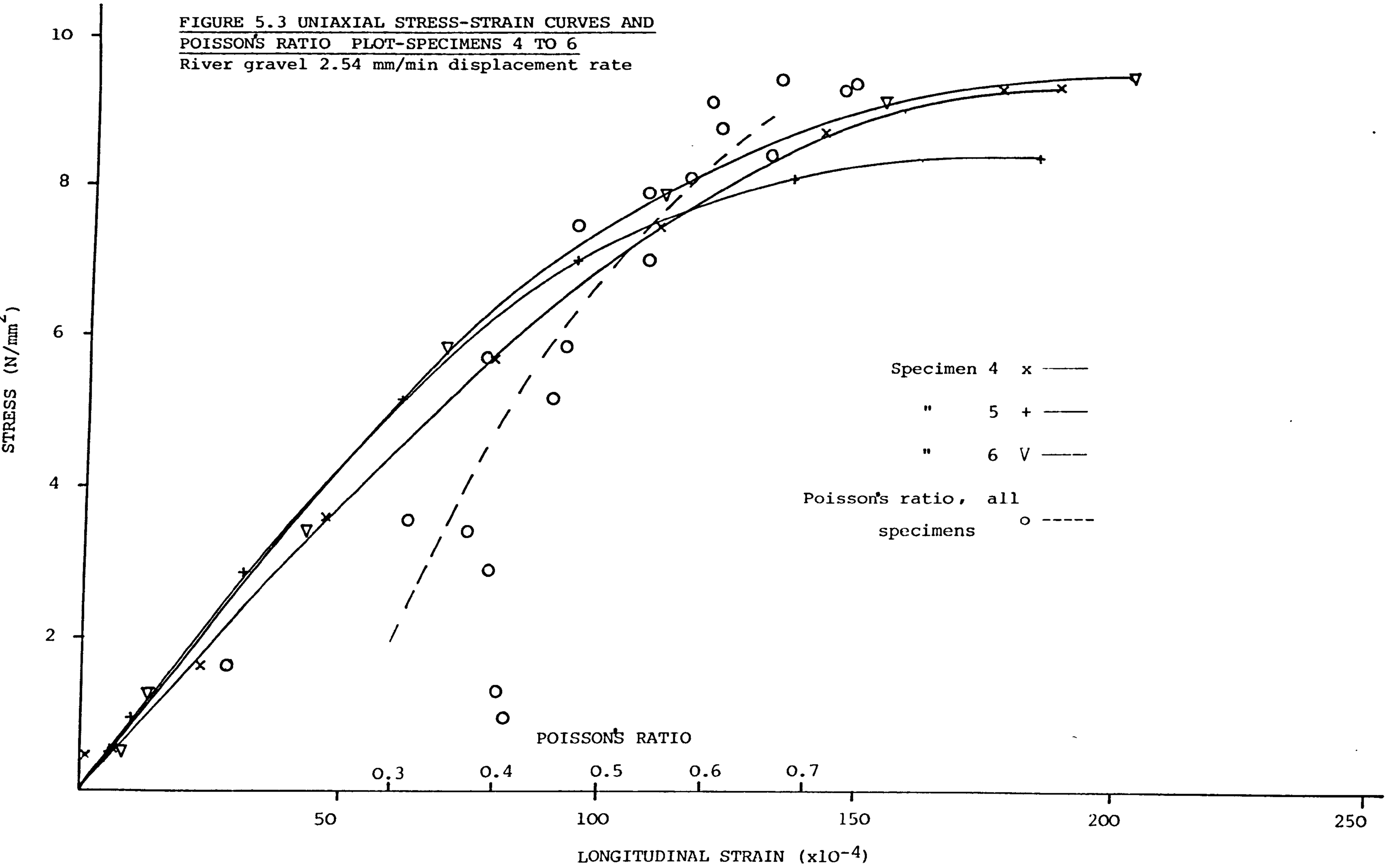

FIGURE 5.4 UNIAXIAL STRESS-STRAIN CURVES AND POISSONS RATIO PLOT-SPECIMENS 7 TO 9

River gravel 5.08 m/min displacement rate

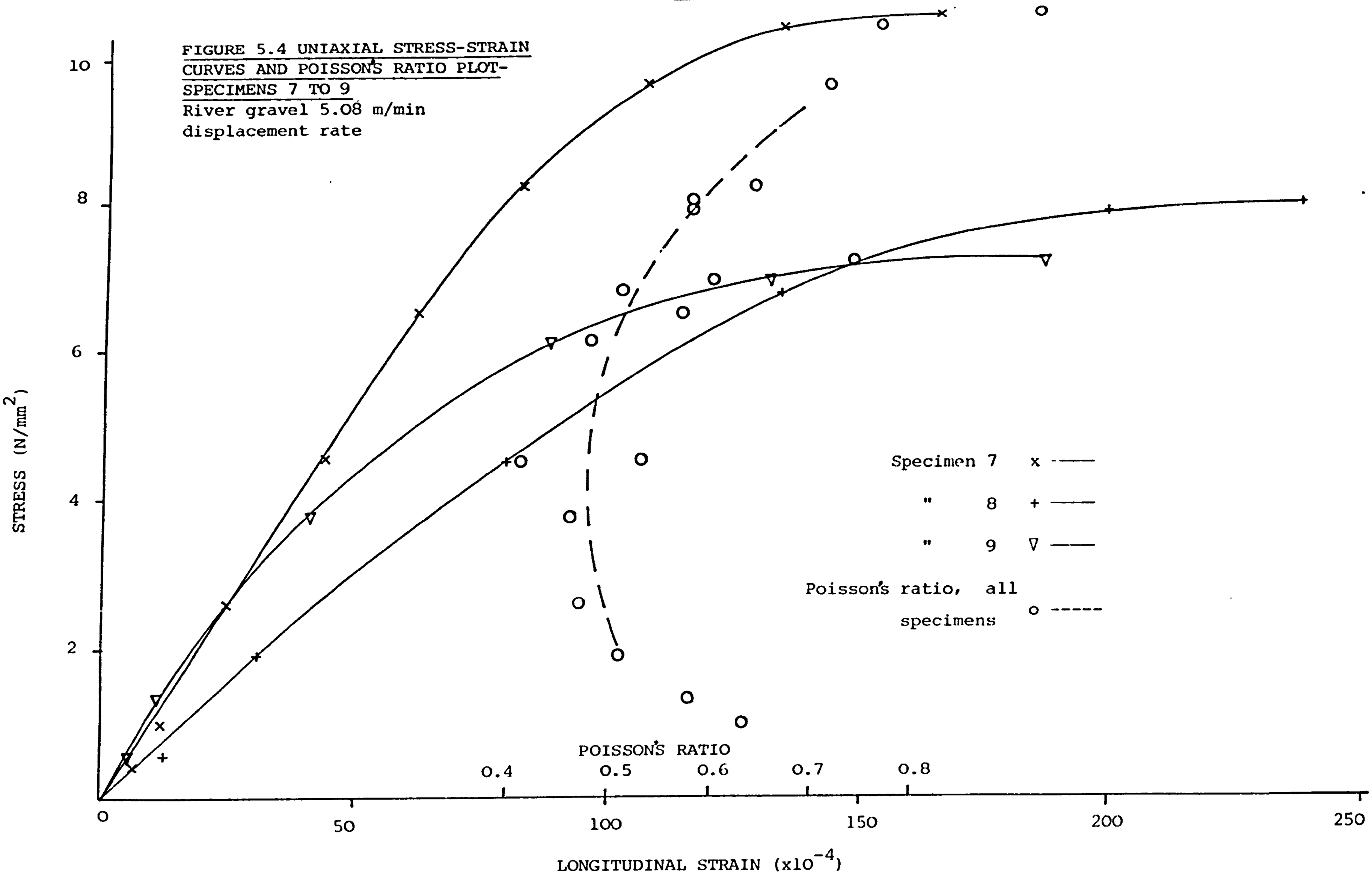

FIGURE 5.5 UNIAXIAL STRESS-STRAIN CURVES AND POISSONS RATIO PLOT-SPECIMENS 10 TO 12
Basalt 2.54 mm/min displacement rate

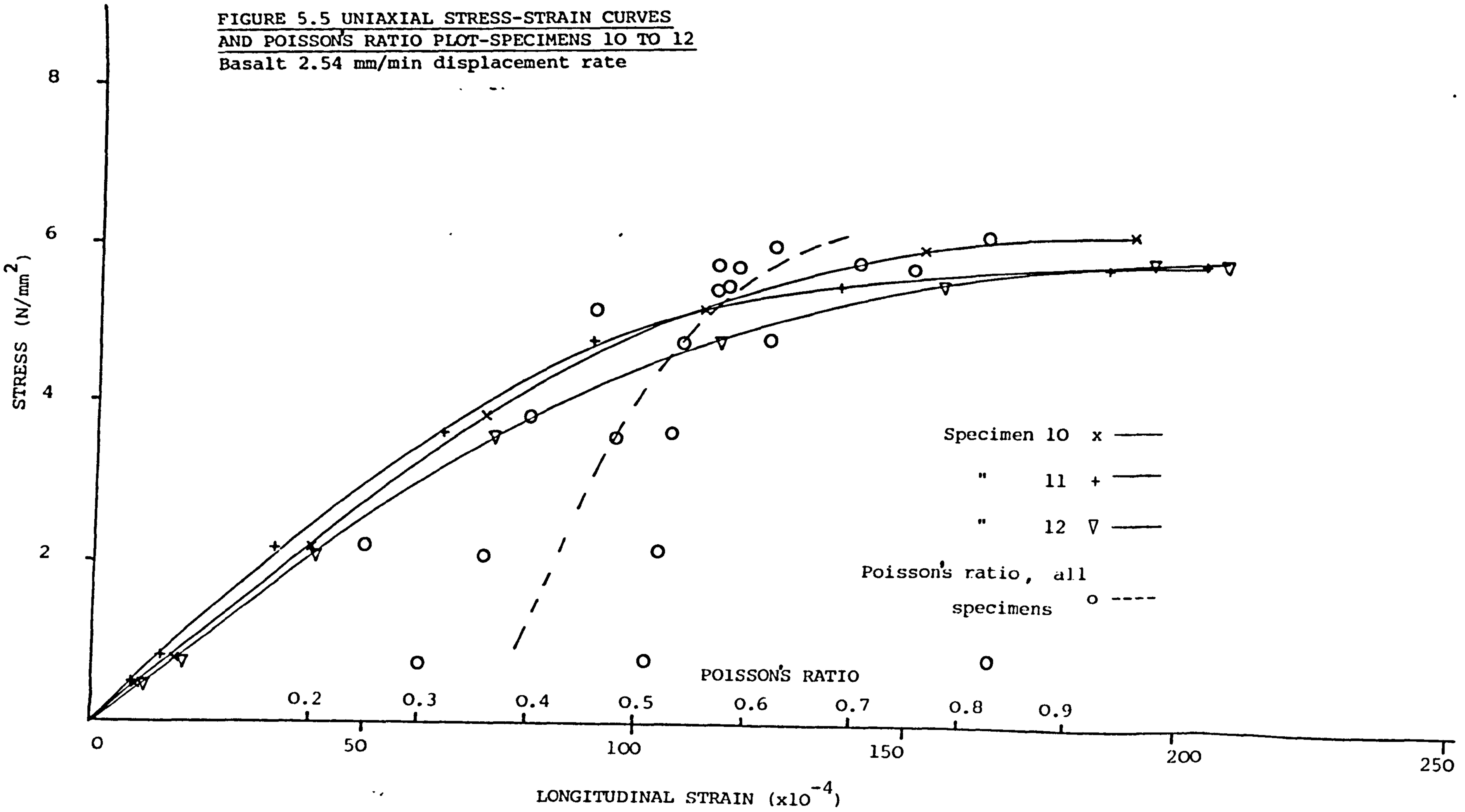

FIGURE 5.6 UNIAXIAL STRESS-STRAIN CURVES AND POISSONS RATIO PLOT-SPECIMENS 13 TO 15
Limestone 2.54 mm/min displacement rate

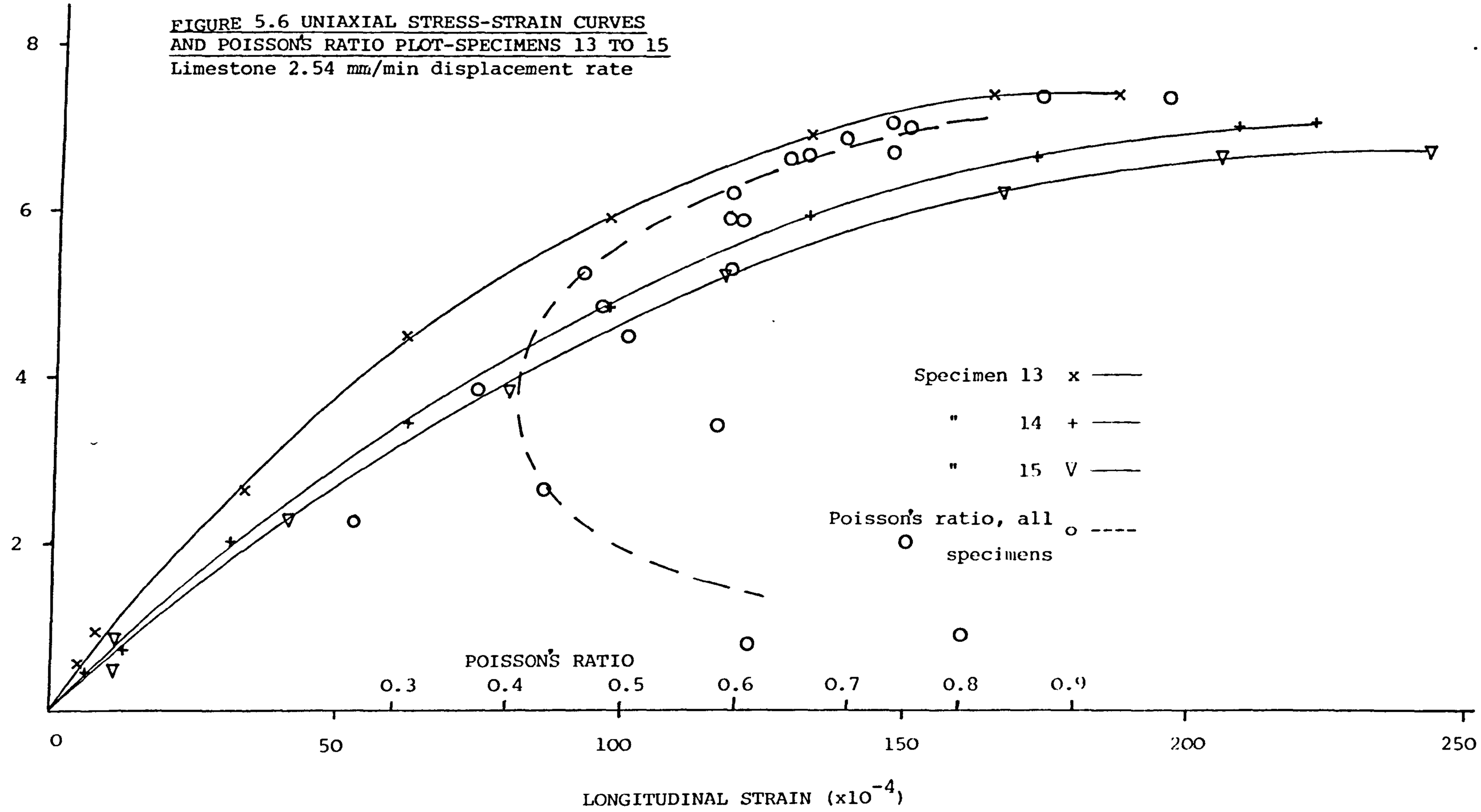

FIGURE 5.7 LONGITUDINAL STRAIN VS LOG$_{10}$ TIME FOR CREEP TESTS (2851 RESINS)

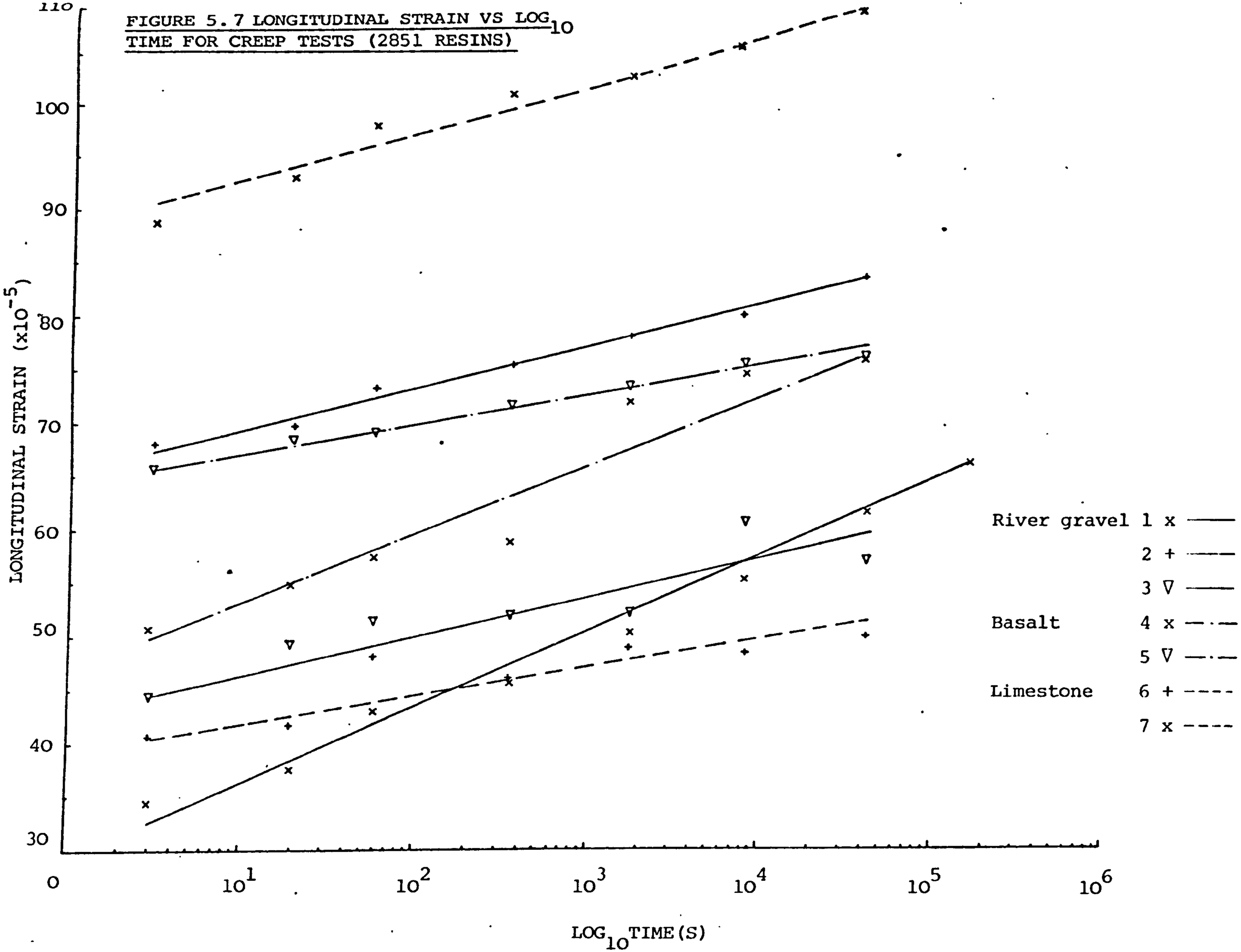

FIGURE 5.8 BENDING TEST STRESS-STRAIN CURVES-SPECIMENS 1 TO 3

River gravel. Age 3 hrs.

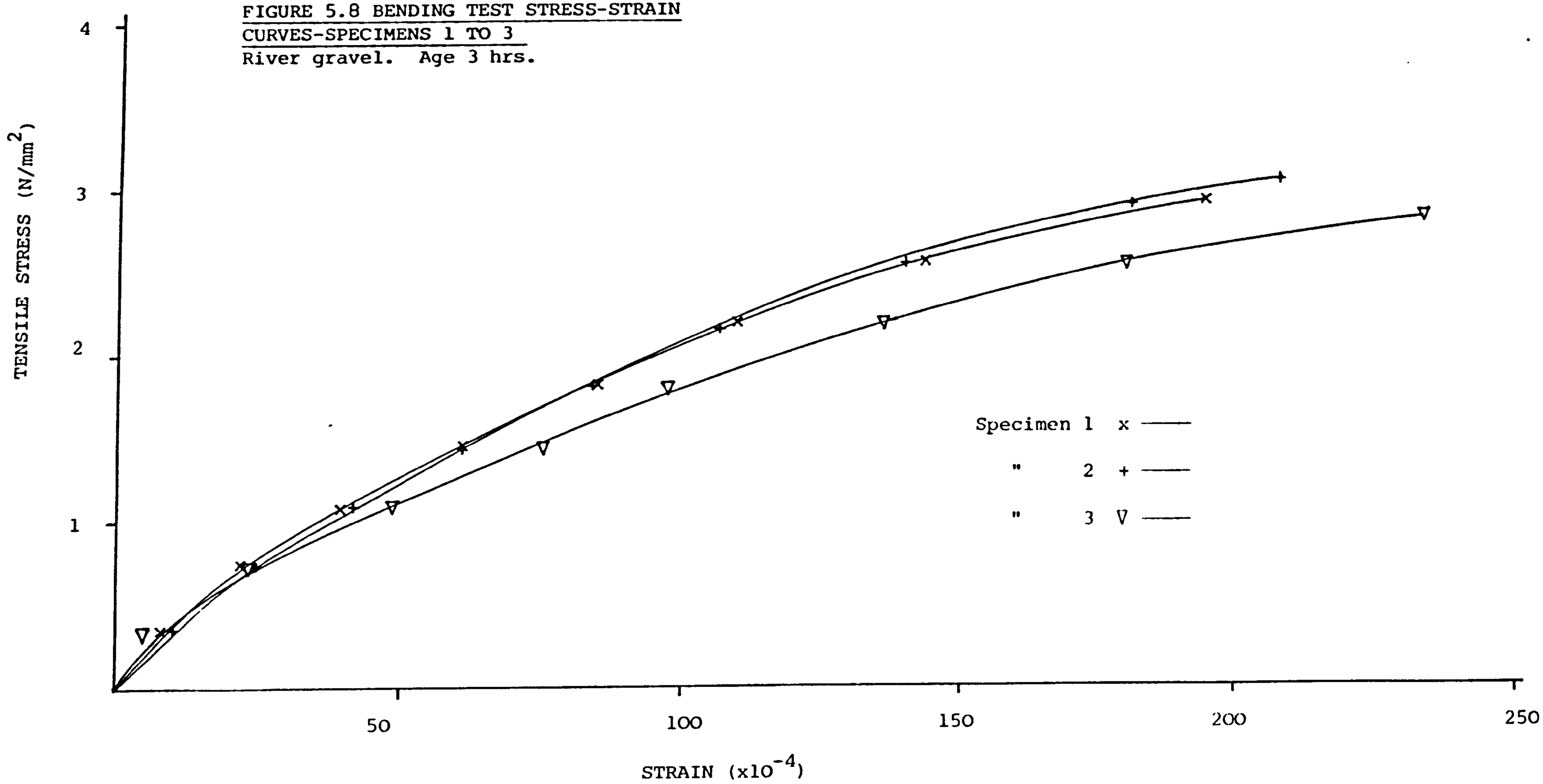

FIGURE 5.9 BENDING TEST STRESS-STRAIN CURVES-SPECIMENS 4 TO 6

River gravel. Age 8 hrs.

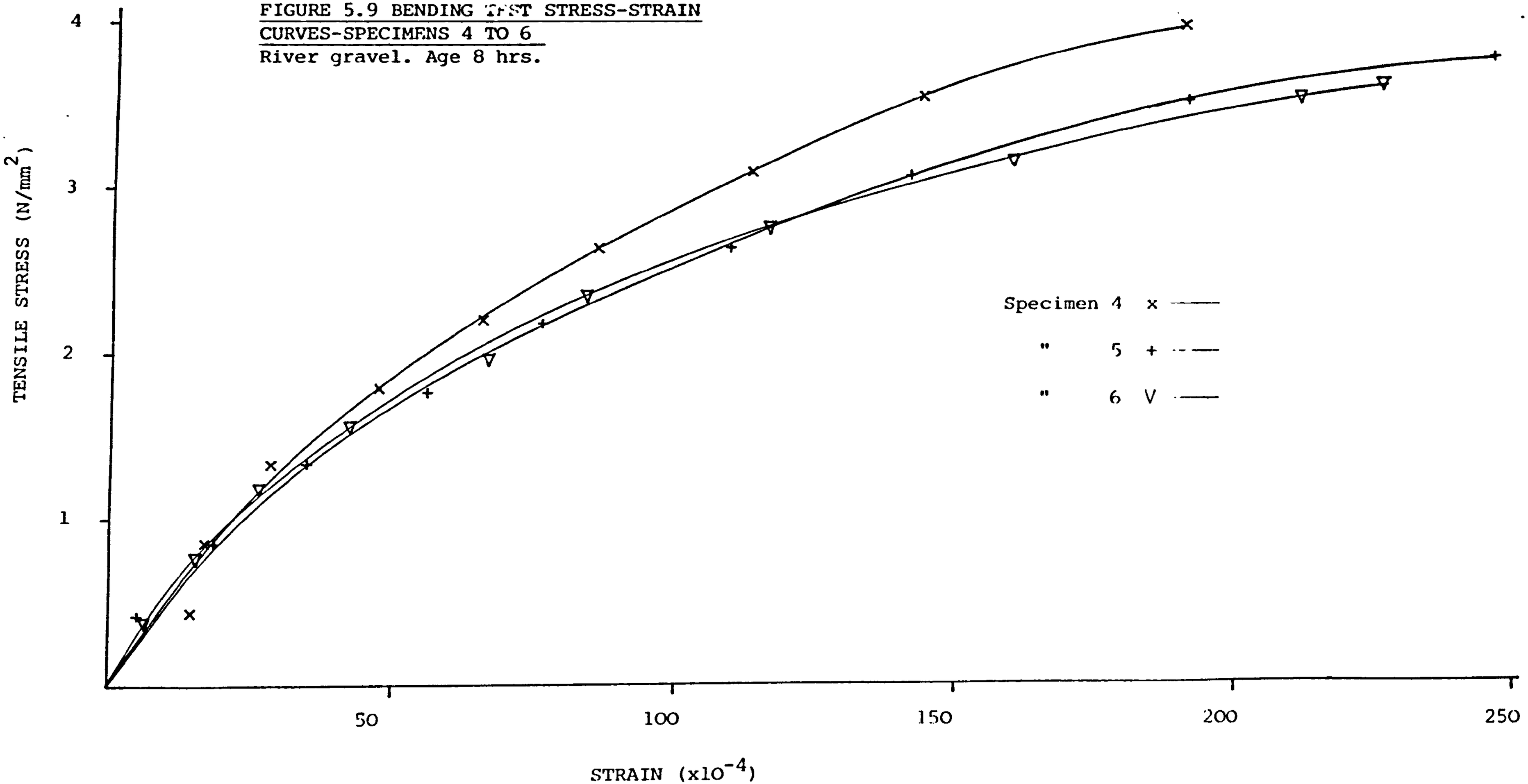

FIGURE 5.10 BENDING TEST STRESS-STRAIN CURVES-SPECIMENS 7 TO 9
River gravel. Age 1 day

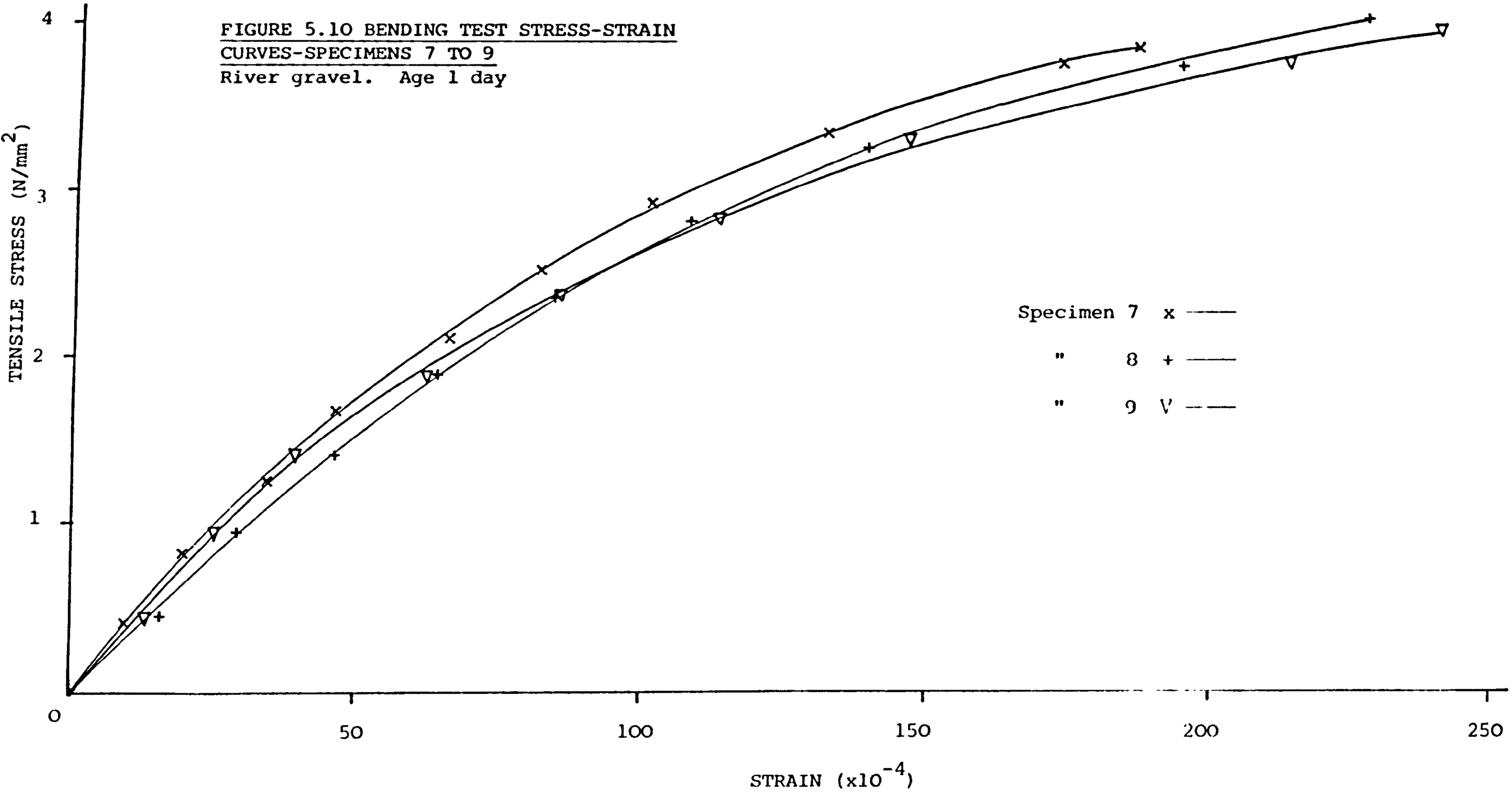

FIGURE 5.11 BENDING TEST STRESS-STRAIN CURVES-SPECIMENS 10 TO 12

River gravel. Age 3 days

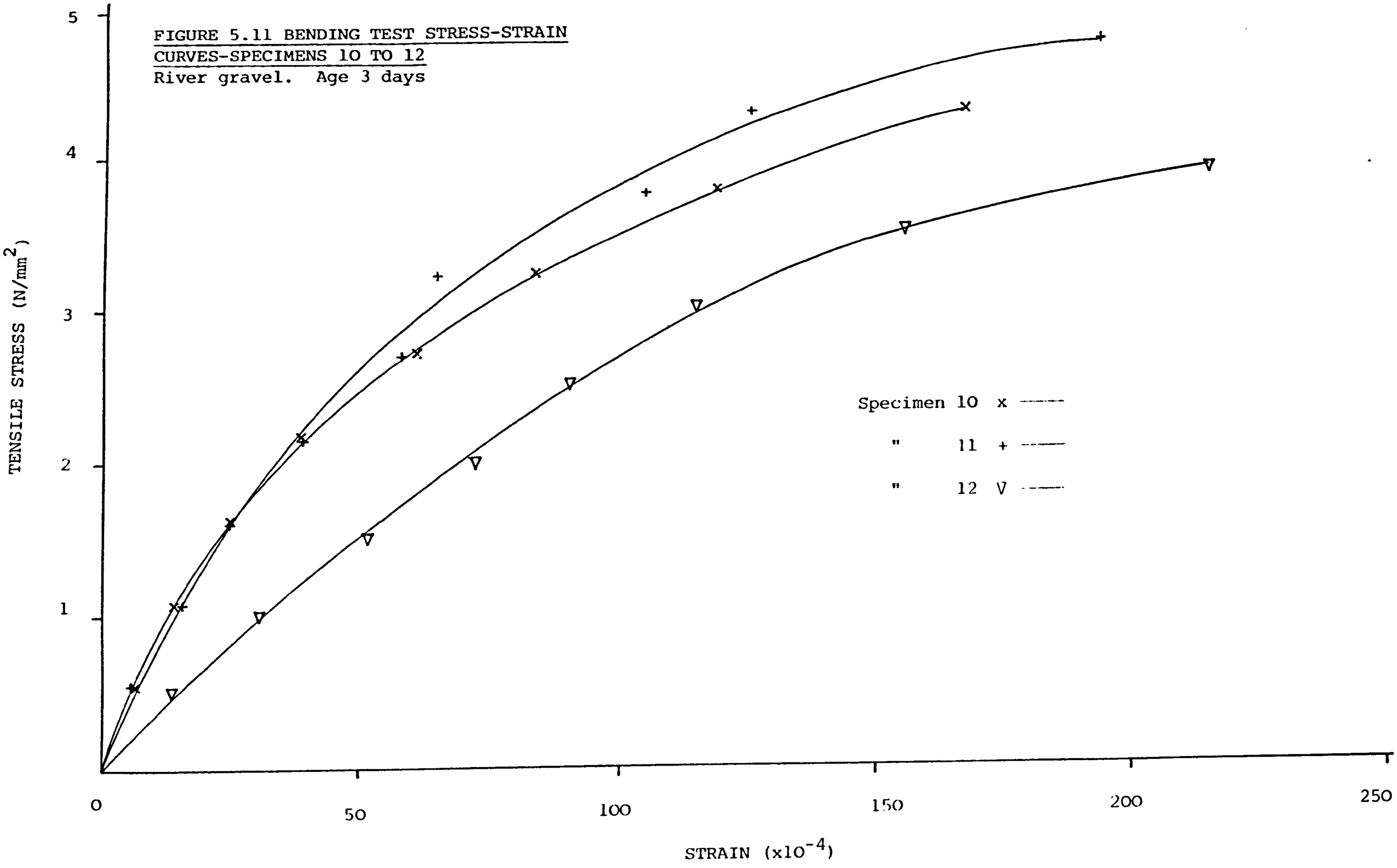

FIGURE 5.12 BENDING TEST STRESS-STRAIN CURVES-SPECIMENS 13 TO 15
River gravel. Age 9 days

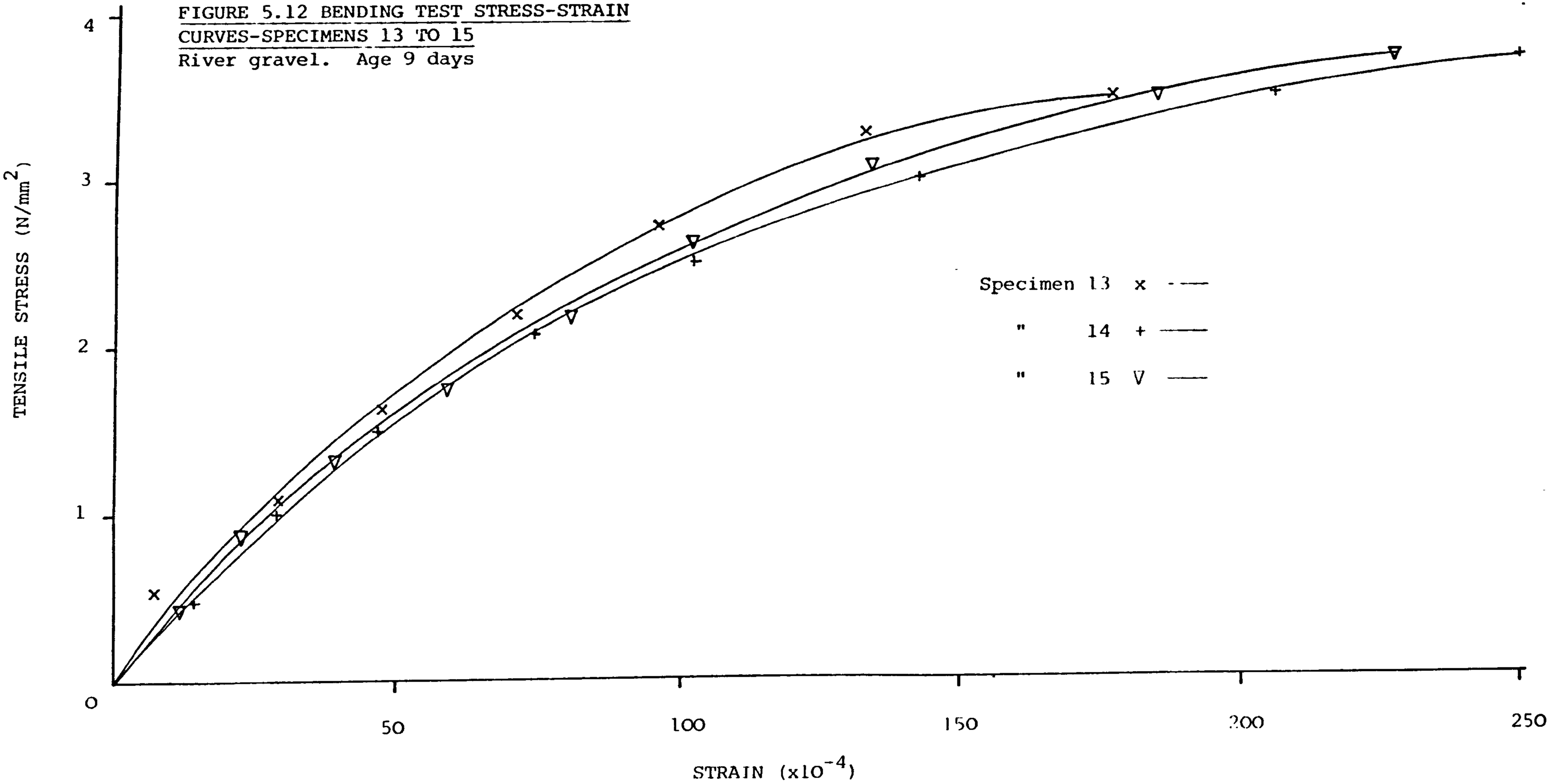

FIGURE 5.13 BENDING TEST STRESS-STRAIN CURVES-SPECIMENS 16 TO 18
Basalt. Age 1 day

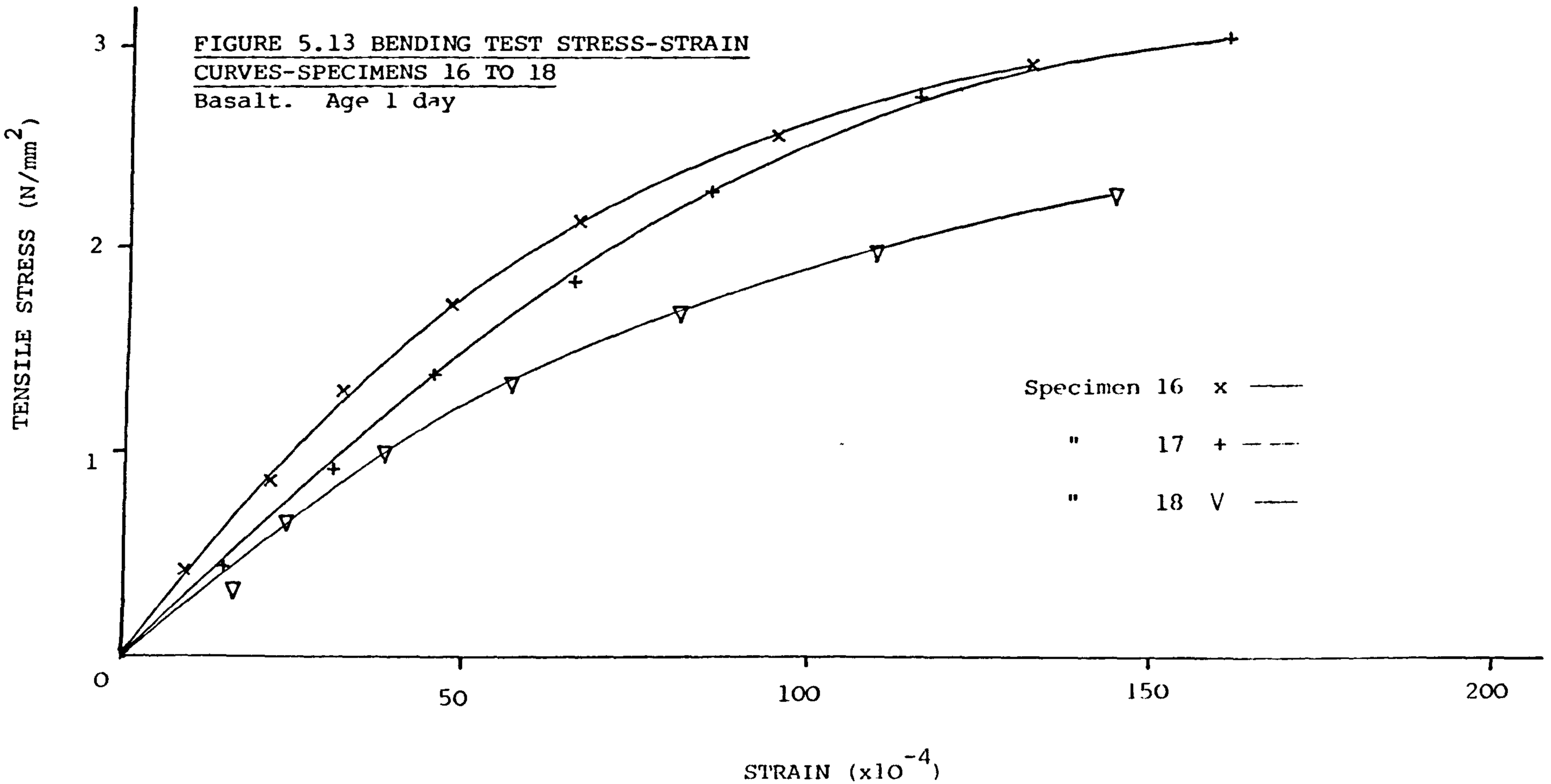

FIGURE 5.14 BENDING TEST STRESS-STRAIN CURVES-SPECIMENS 19 TO 21
Limestone. Age 1 day

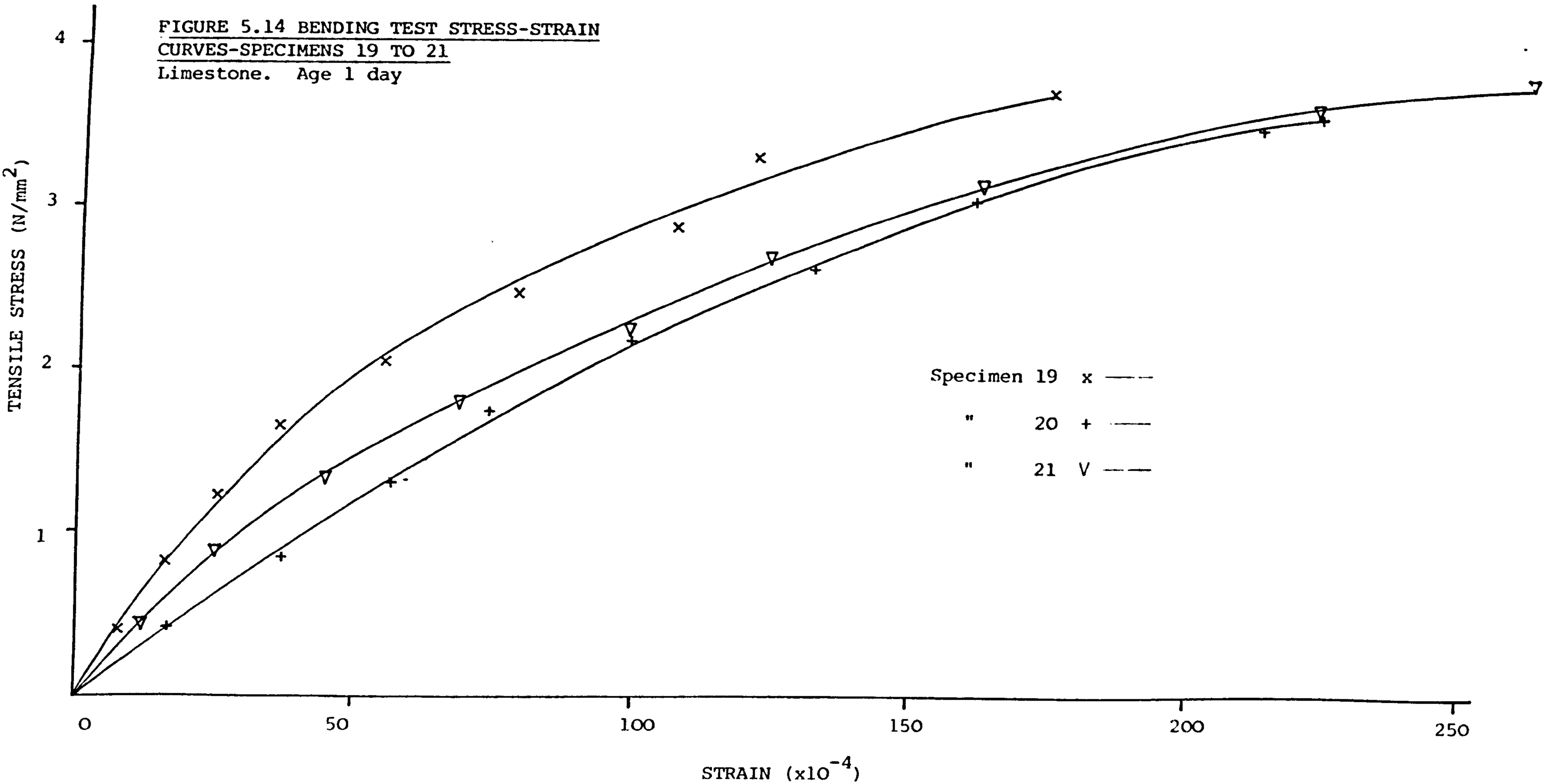

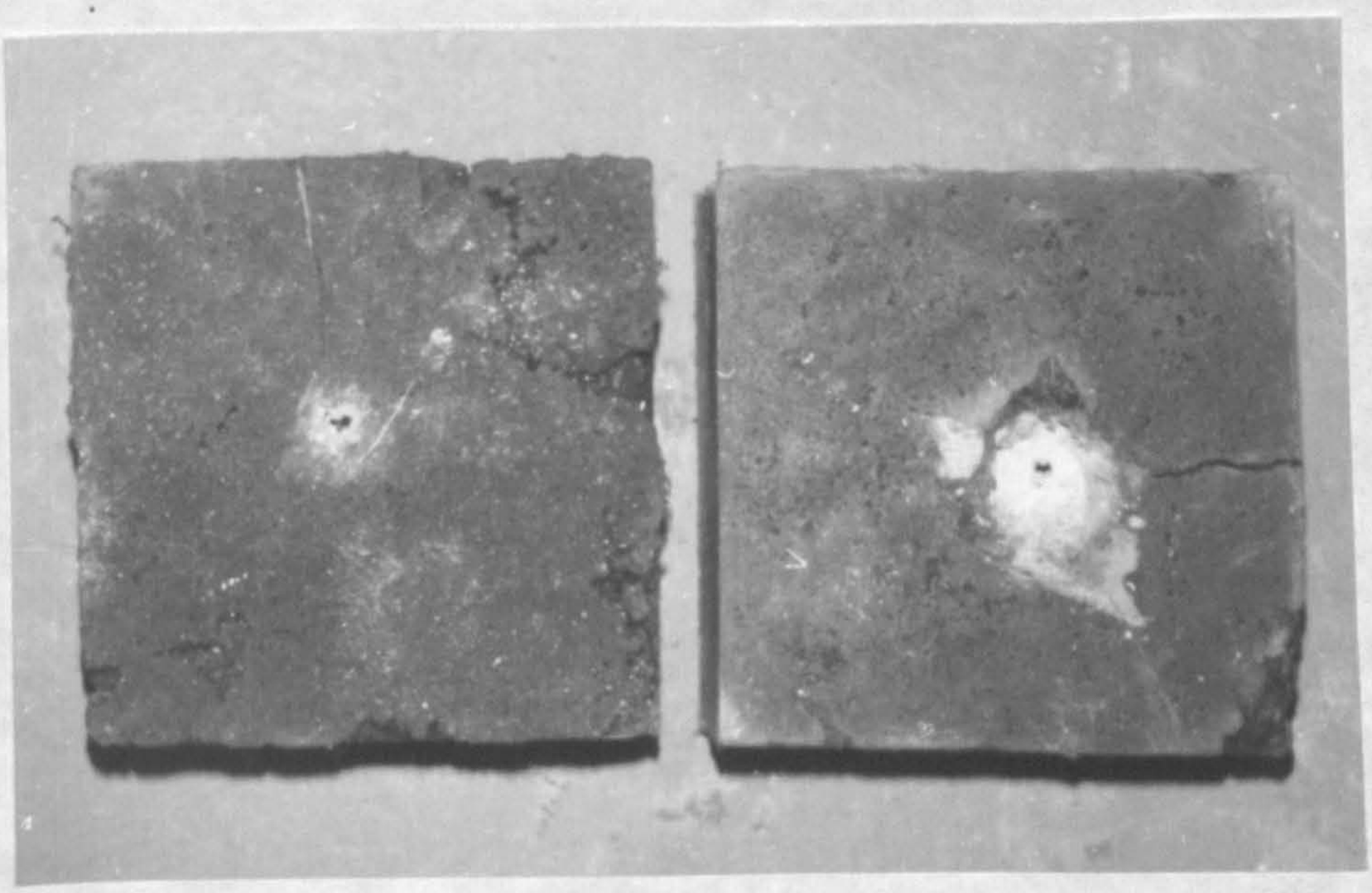

PLATE 5.1 TYPICAL IMPACT FACE DAMAGE, SERIES 11 (AP)

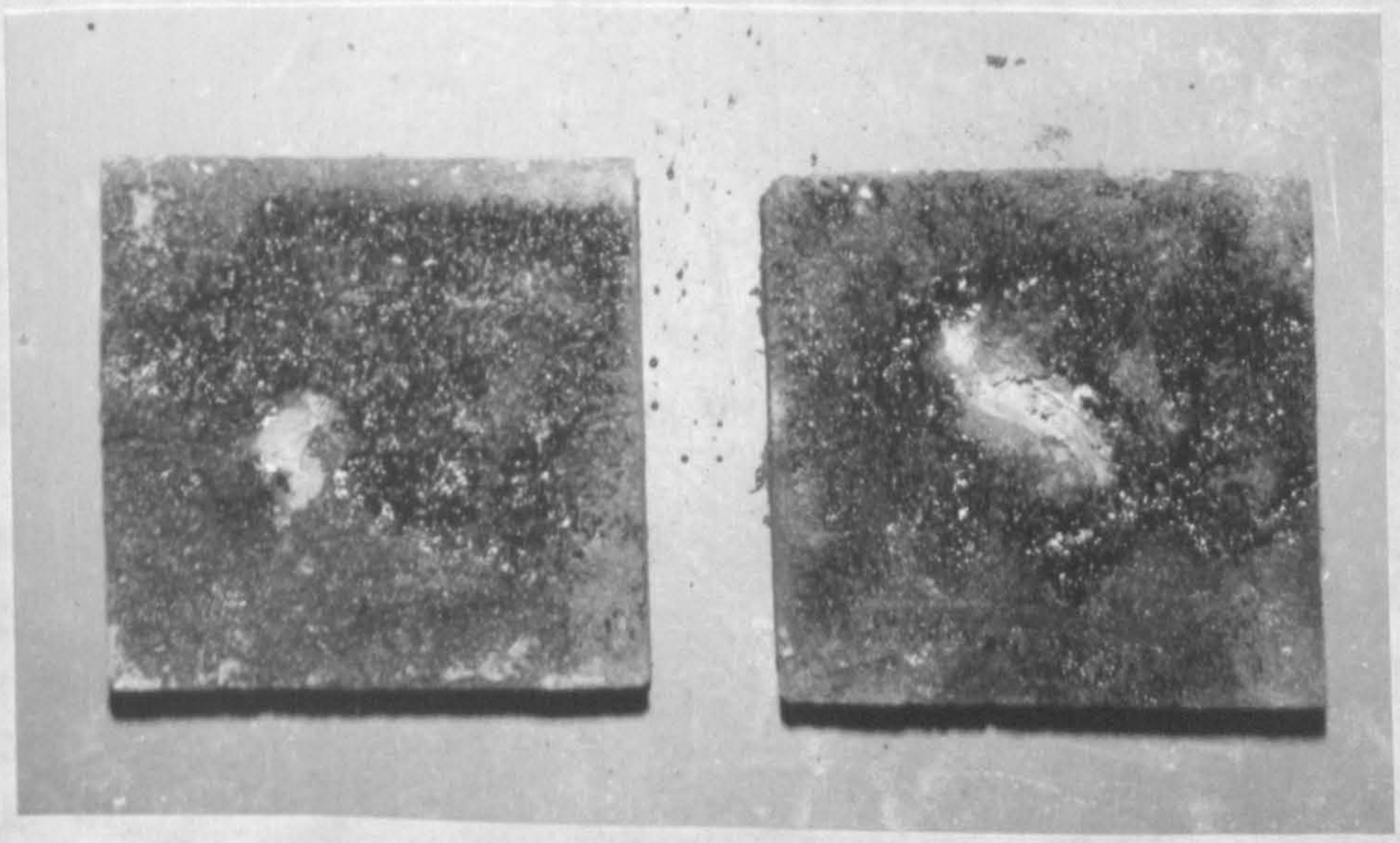

PLATE 5.2 REAR FACE SCABBING WHERE SERIES 11 SPECIMENS WERE PERFORATED (AP)

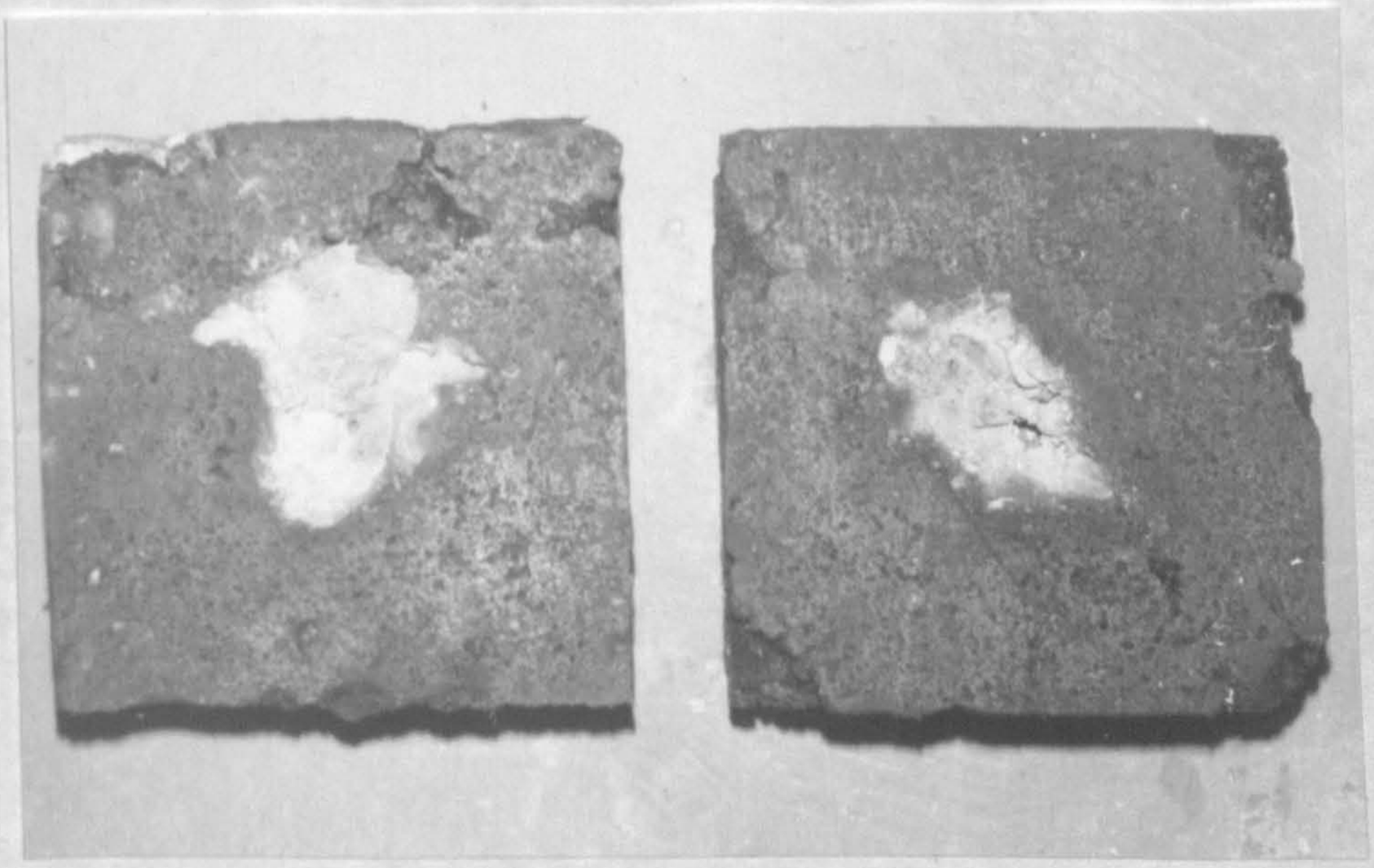

PLATE 5.3 TYPICAL IMPACT FACE DAMAGE, SERIES 12 (BALL)

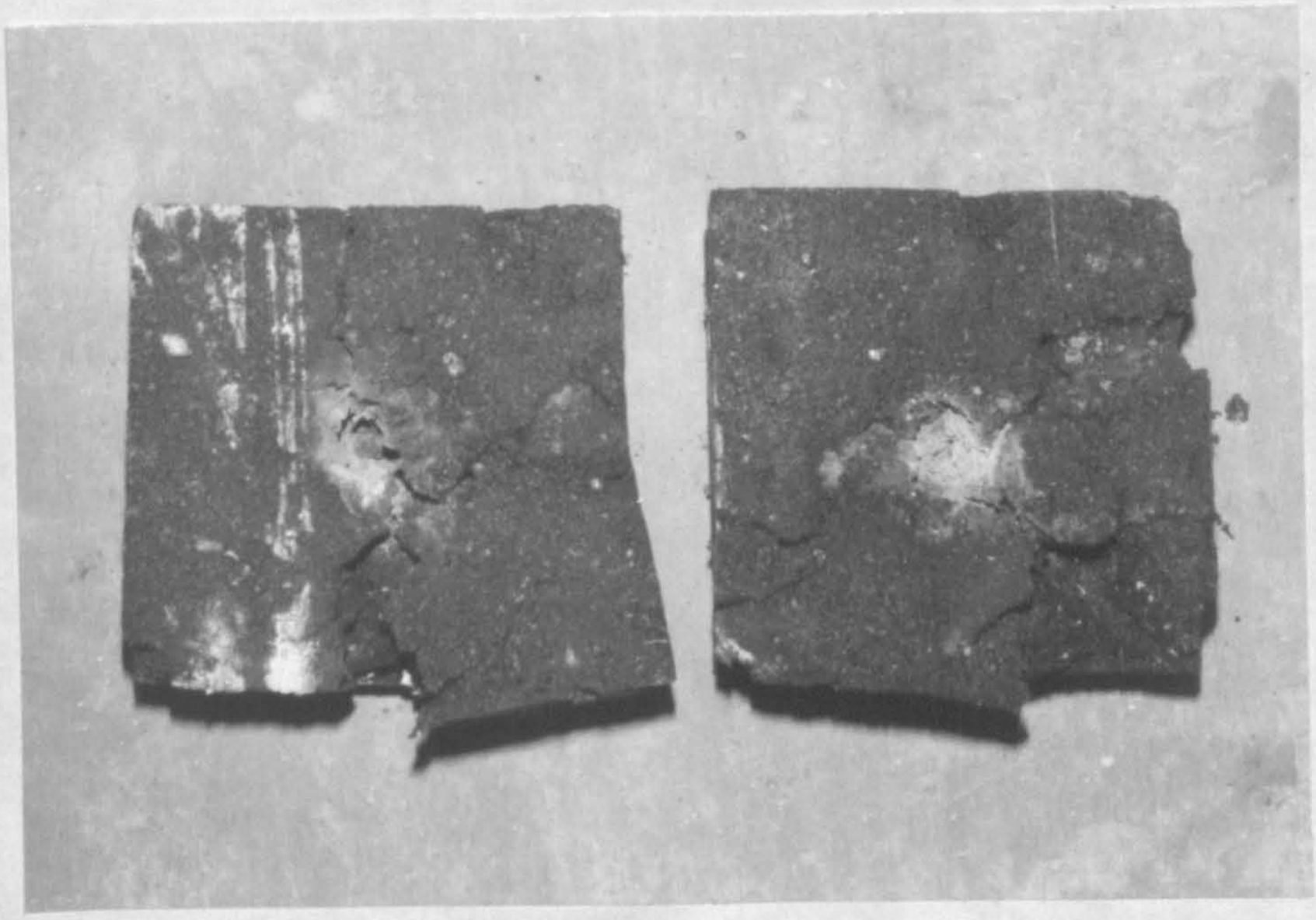

PLATE 5.4 TYPICAL IMPACT FACE DAMAGE, SERIES 15

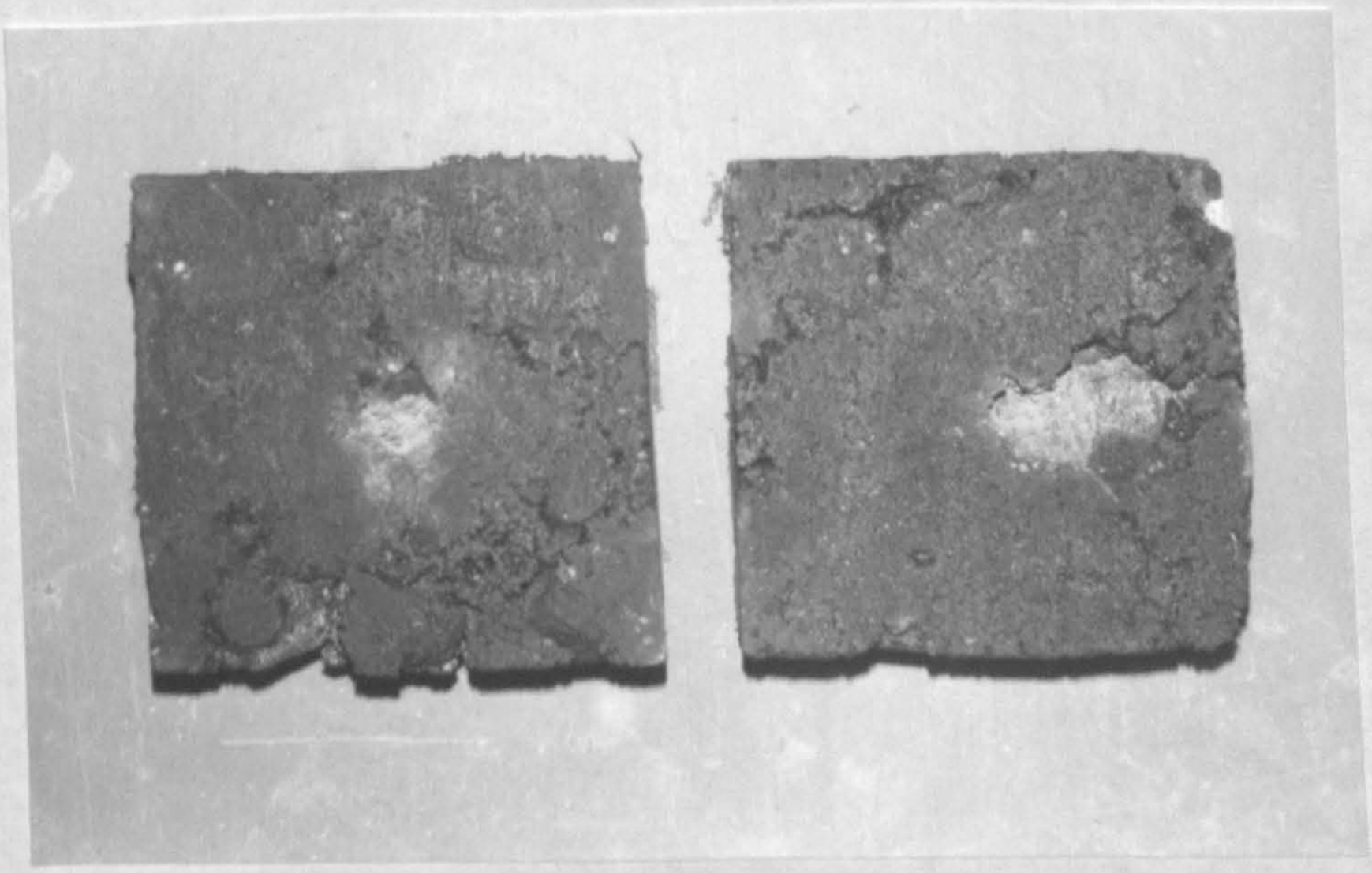

PLATE 5.5 TYPICAL IMPACT FACE DAMAGE, SERIES 16

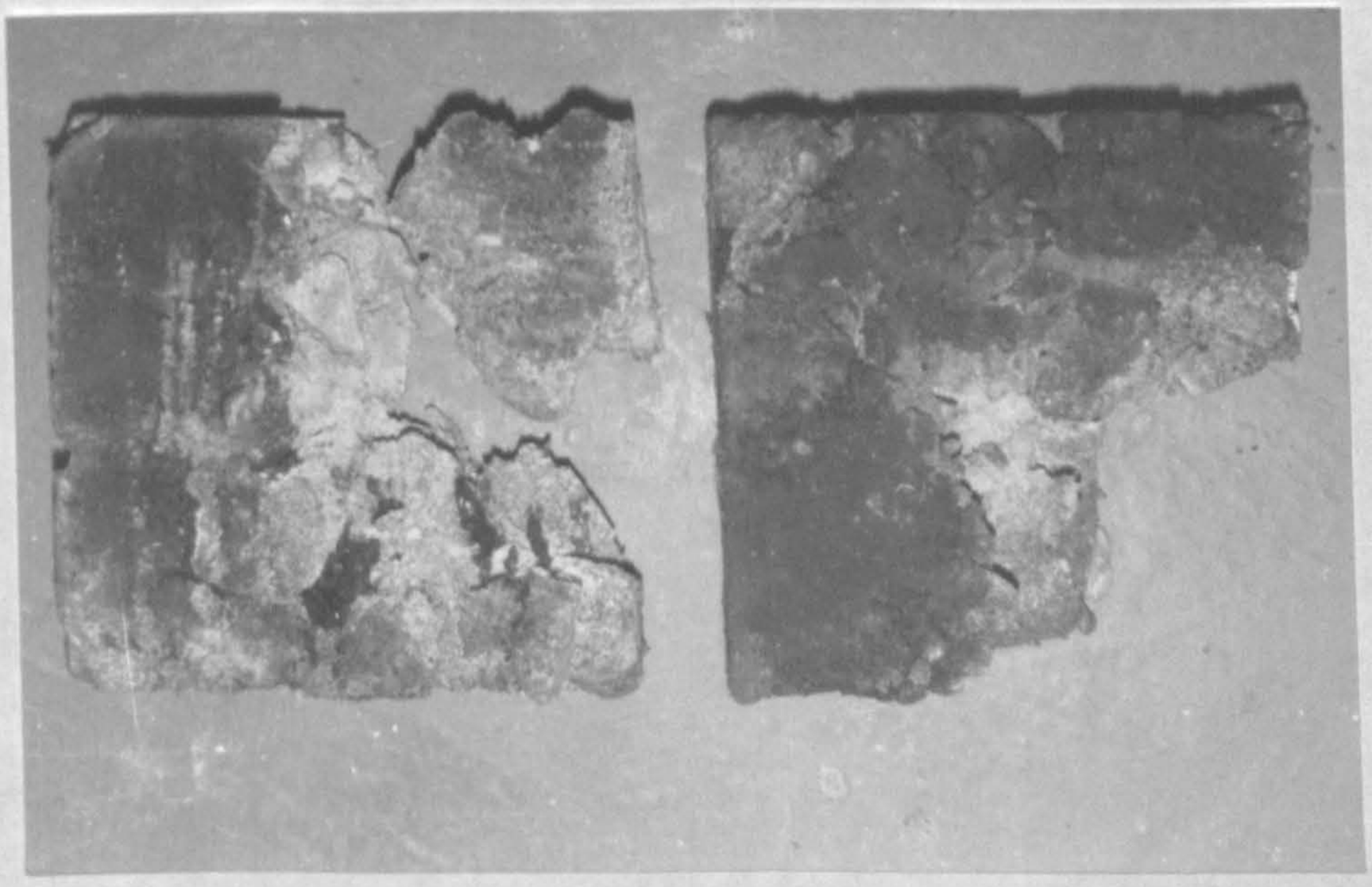

PLATE 5.6 TYPICAL IMPACT FACE DAMAGE, SERIES 17

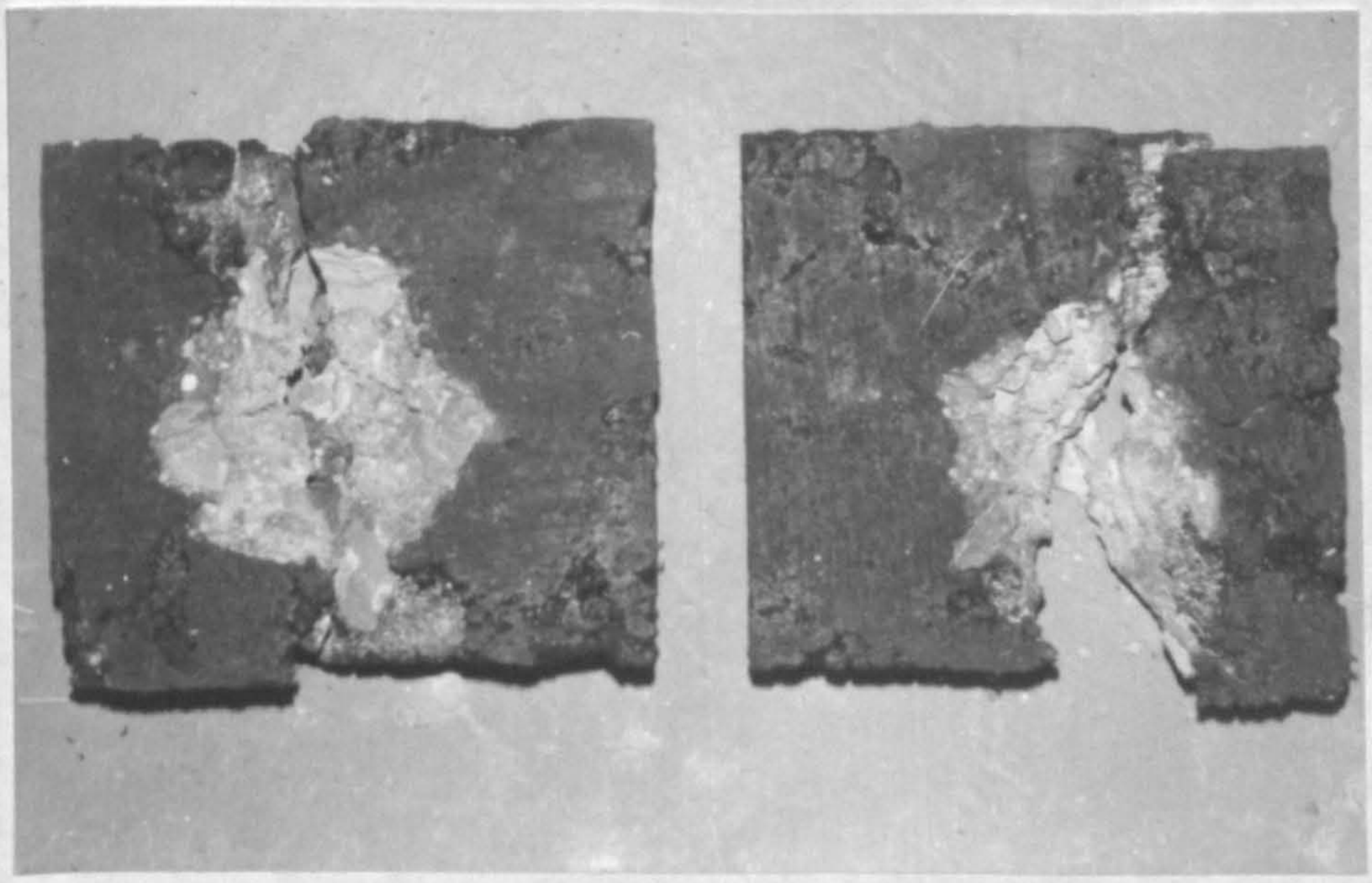

PLATE 5.7 TYPICAL IMPACT FACE DAMAGE, SERIES 18

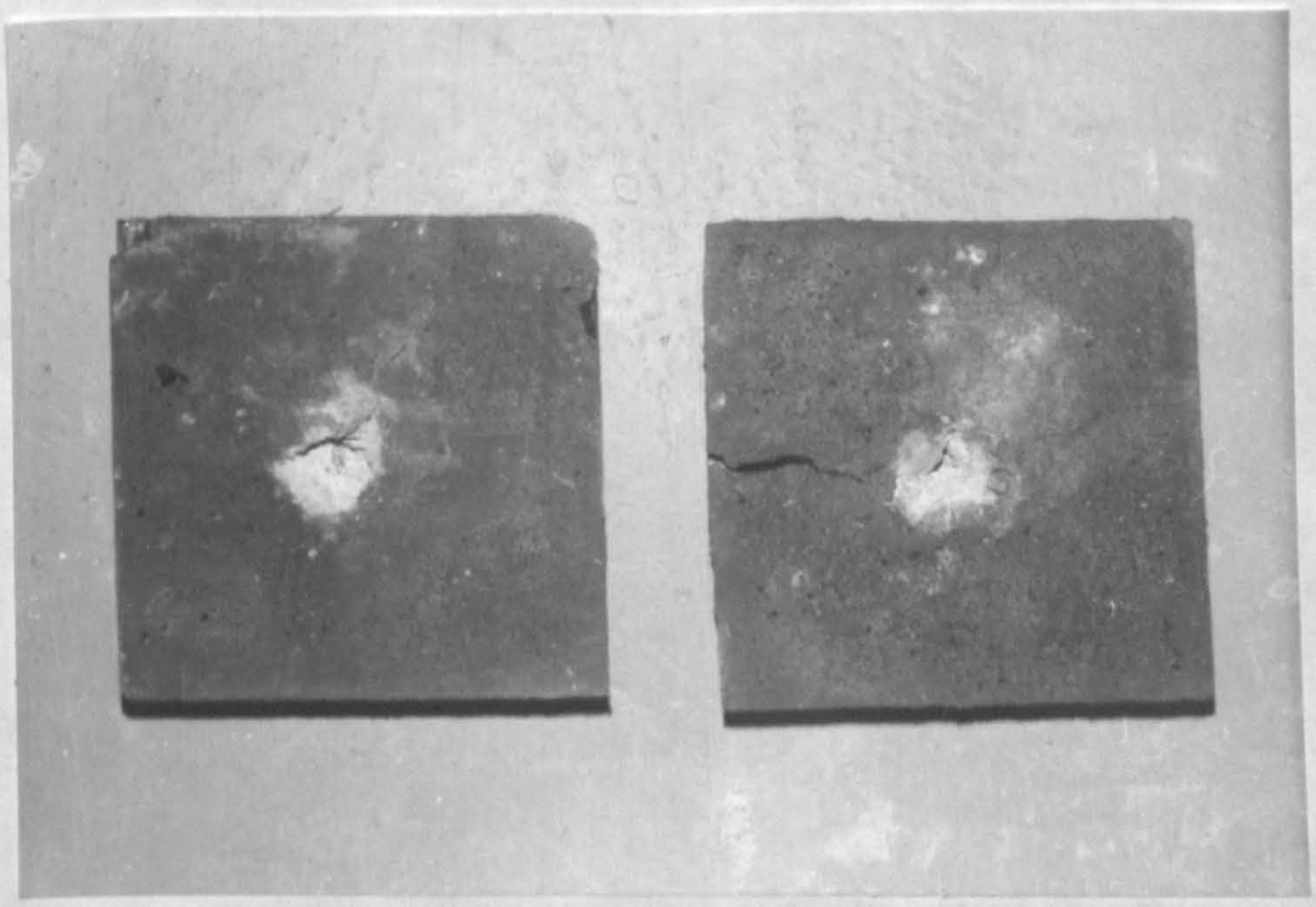

PLATE 5.8 TYPICAL IMPACT FACE DAMAGE, SERIES 19

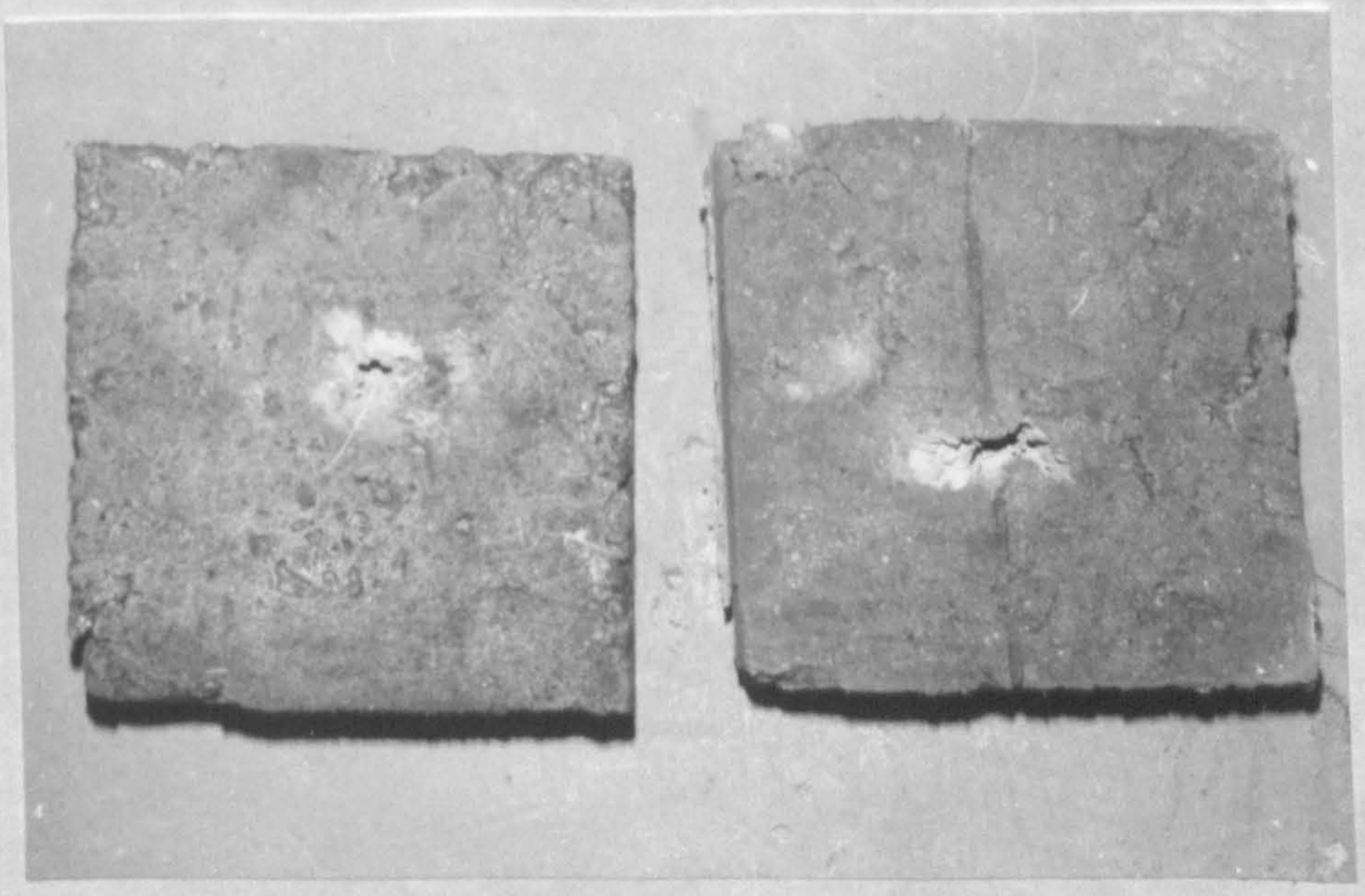

PLATE 5.9 TYPICAL IMPACT FACE DAMAGE, SERIES 20

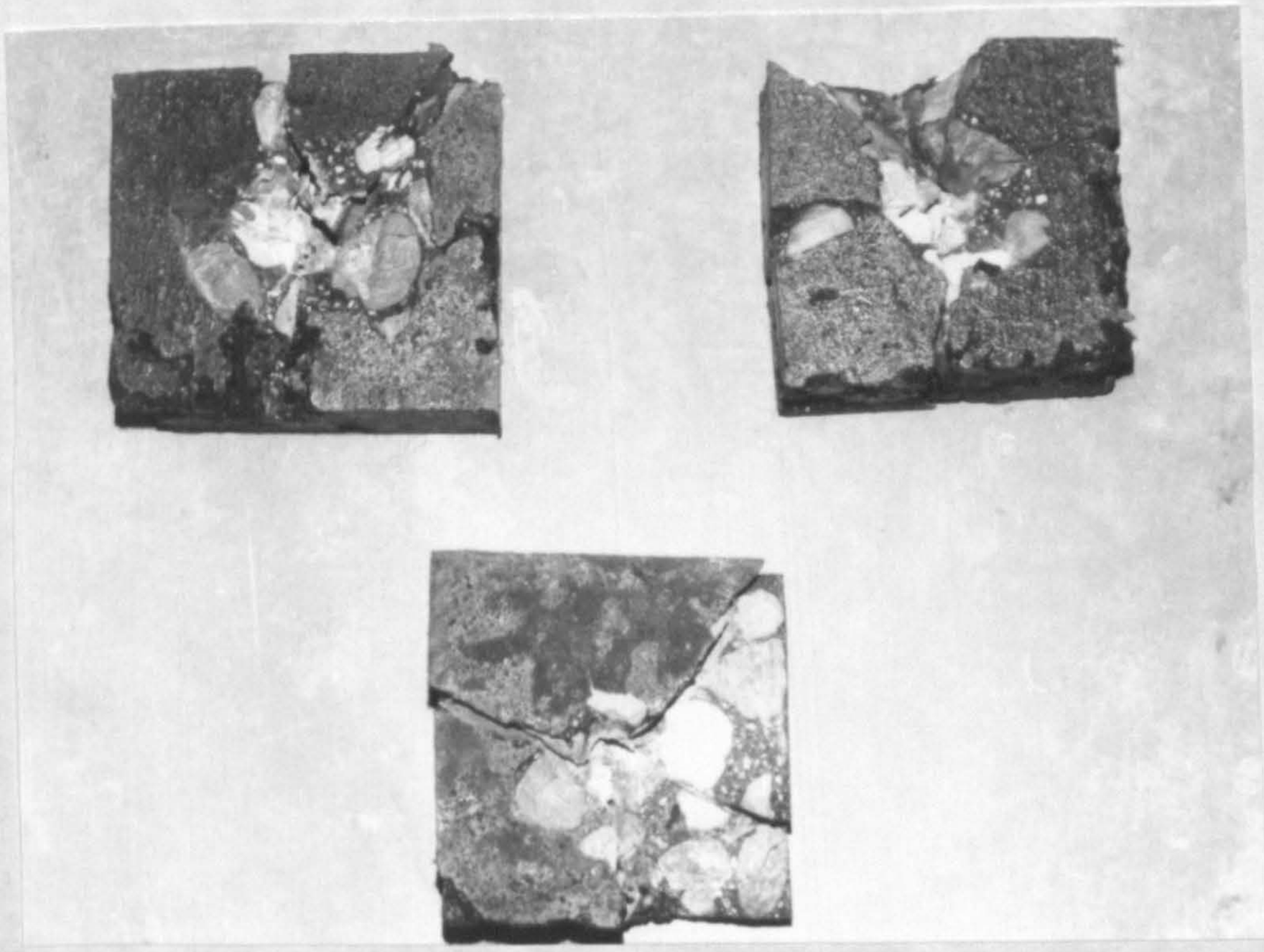

PLATE 5.10 TYPICAL IMPACT FACE DAMAGE FOR COLD SPECIMENS, SERIES 22

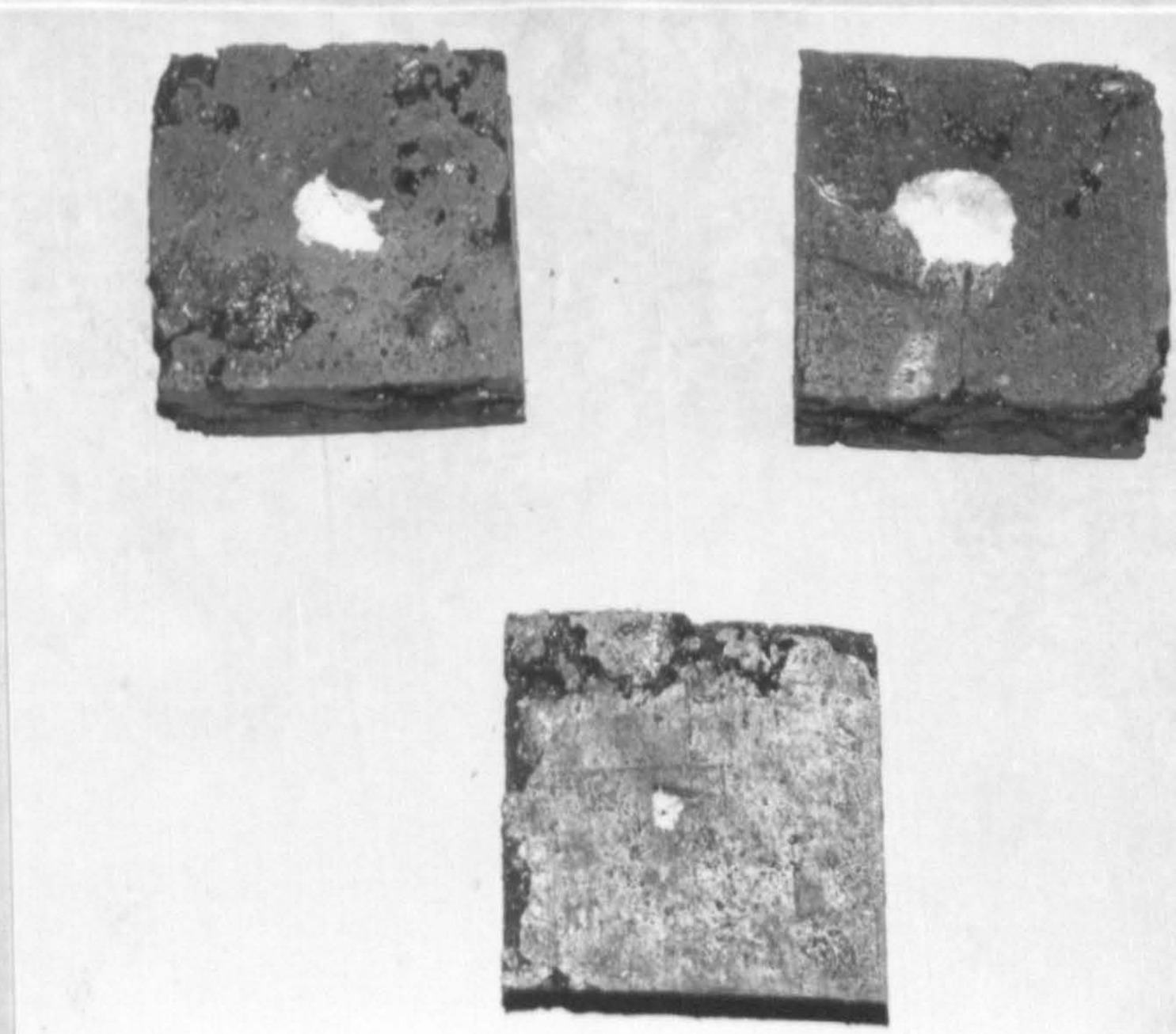

PLATE 5.11 TYPICAL IMPACT FACE DAMAGE FOR HOT SPECIMENS, SERIES 23

CHAPTER 6

DISCUSSION OF RESULTS

6.1 Projectile Velocity and Impact Accuracy Measurements

Figure 5.1 and Table 5.1 summarised the results of velocity measurements for both ball and A.P. ammunition. Comparison with manufacturers' data in Tables 3.8 and 3.9 is difficult because of the different ranges at which velocity was measured,but results show values of the same order with velocities reducing slightly with increasing range. The idea of measuring velocities was originally adopted so that any 'rogue' bullets would be detected and the results of these tests ignored. However, all measured velocities were within a fairly narrow band and standard deviations were small. The spread of results was greatest with ball ammunition, the mean velocity being 794 m/s with a standard deviation of 7.6 m/s. Two sets of data were available for A.P. ammunition. Early tests were carried out during winter in an unheated range and the mean velocity was 785 m/s with a standard deviation of 5.6 m/s. Later tests were carried out at a higher ambient temperature of about 15°C and the mean velocity was 810 m/s with a standard deviation of 6.6 m/s.

The possible reason for bullet velocity differences merit discussion

(i) As described above, the temperature of the bullet is of importance, primarily because of the ignition characteristics of the explosive propellant : a lower temperature means a slower burn. It is also possible that because of differing projectile and cartridge case thermal expansion characteristics, the force necessary for separation changes, also influencing the initial stages of acceleration.

(ii) Bullet mass variation is known only for armour piercing ammunition : 9.6 to 9.9 g, i.e. an assumed average of 9.75 g. However, the ball ammunition, with an average mass of 9.3 g is likely to show a similar variation. The bullet mass will

affect the acceleration in the gun barrel; by Newton's. Second Law, acceleration is inversley proportional to mass. Following this logic, at a given time after the start of detonation, the bullet will be further along the barrel if its mass is smaller. The amount of propellant gas generated is constant, and so the pressure, and hence the force, on the bullet is lower at a given time for a lower mass bullet. However, this effect is considered to be secondary, and for simplicity a constant force is assumed.

Newton's second law is

$$P = ma \qquad 6.1$$

where P = force

m = mass of bullet

a = acceleration

Also $$v^2 = 2a\ell \qquad 6.2$$

where ℓ = length (of barrel)

hence $$\frac{mv^2}{2\ell} = P$$

$$\therefore \quad mv^2 = 2P\ell = \text{constant} \qquad 6.3$$

Ignoring the reduction in velocity between muzzle and target, using mean AP velocity and mass

$$\underline{\text{Constant} = 9.75 \times 807.2^2 = 6.35 \times 10^6}$$

Moving to an extreme mass value

$$v = \sqrt{\frac{6.35 \times 10^6}{9.9}} = \underline{801.1} \text{ m/s}$$

thus $\underline{\delta v = 6.1 \text{ m/s}}$

Thus the effect (approximate) of the mass variation is less than the standard deviation measured.

(iii) Possible variation in the propellant mass (no data available).

The accuracy of the firings, some measurements of which were given in Table 5.1,was such that a nominal 150 mm square target face was acceptable for shots aimed centrally at it.

6.2 Accuracy of Penetration Measurements

Using the sectioning method, it was estimated that the normal penetration depth measurements were accurate to ±1 mm for shallow penetrations and ±2 mm for deeper penetrations. Where extensive damage had occurred to the target e.g. those in Series 22 tested at -7°C, errors may have been greater.

Additional errors arose when the penetration path length was determined, but the total error was less than 5%. This is unlikely to be very significant when compared to the large scatter of penetration path lengths obtained from similar samples.

6.3 Linear Response Surfaces

Although this method was applied only to Series 2 (Diorez/limestone/A.P.) and Series 3 (Diorez/river gravel/A.P.) tests, the results indicated that

(i) there was a large experimental scatter

(ii) the effect of the percentage resin was either small, or, if it was significant, it was equally distributed about the centroid

(iii) penetration tended to reduce with higher percentage aggregate

(iv) large aggregate size appeared most favourable

(v) higher polymer hardness appeared most favourable

These points influenced the designs for the quadratic response surface tests.

6.4 Quadratic Response Surfaces

In all these series of tests (Series 4-10) there was a considerable scatter of the experimental results. Some idea of the amount of scatter may be gained by examining the values of penetration path lengths in each series for the centroid mix targets. Results are summarised in Table 6.1.

Although not statistically significant, the variations shown in Table 6.1 illustrate the difficulty in trying to identify complex trends with a number

of variables, where the effect of factor level variation may be of the same order of magnitude as the experimental scatter. The lack of fit tests which were applied in Chapter 5 were the most appropriate, but were such that the surface would have to have been a very bad fit to fail these tests.

It was hoped that using the quadratic response surfaces a minimum penetration position could be found on the surfaces. However, this did not happen so a departure from the standard experimental design method was necessary, namely corner testing. Lowest penetrations were finally obtained at the extremes of one or more of the x variable ranges.

In the case of rounded river gravel with 2851 resins and A.P. ammunition (Series 7), an acceptable solution was obtained from the response surface after first stage corners tests, with no ambiguity in the results.

None of the other series of tests yielded conclusive results at the end of first stage corner tests and therefore these series had to be further extended by second stage corner tests. Even at this stage,certain assumptions had to be made for conclusions to be drawn. For example, after a small number of confirmatory tests using targets of small size limestone aggregate with 2851 resins (cf Table 5.11), the general assumption was made that even if the response surface indicated better resistance in a corner of small aggregate size, this would be ignored and further corner testing concentrated on large aggregate corners.

After this second stage corner filling the solutions which were obtained from series 8 (basalt/2851 resins) and 9 (limestone/2851 resins) were found to be unacceptable when tests were carried out to check required block thicknesses. Both solutions gave targets which, because of low resin contents, suffered considerable damage (Tables 5.19 and 5.20 respectively), and the resin content had to be increased.

Comparing the trends represented by the quadratic response surfaces for each series is difficult, because of the complexity of the equations. Each of the four x variables appears as a linear term, square term and a product

term with each of the other x variables. Tables 5.15 and 5.16 gave the coefficients after the main stage tests and corner fitting tests respectively. The former is best for comparison purposes because the values are not influenced by the different asymmetries introduced by corner filling. Examination of this table shows little consistency between any two series. Variation of the response surface from series to series may be due to a number of factors such as

(i) random experimental scatter,

(ii) variation in the rock material properties,

(iii) variation in the % voids from series to series as the angular crushed rock aggregates did not pack as densely as rounded river gravel aggregate,

(iv) a slightly inferior polymer/rock bond with the crushed rock aggregates due to dust on the surface of the aggregate particles.

6.5 Thickness Tests

Results of tests to check on the required thickness of the various composites were given in Tables 5.18 - 5.21 and the mixes and thicknesses finally adapted were in Table 5.22. During these tests further confirmation of two of the basic assumptions was achieved. Firstly comparison between A.P. and ball ammunition (Series 11 and 12 respectively, Table 5.18) showed that larger penetrations were recorded when A.P. ammunition was used. Secondly, comparison between optimum mixes of the two resin types with river gravel (Table 5.21) showed that the 2851 resins give superior performance to Diorez.

For river gravel/2851 resins, Series 11 and 14 (Table 5.18), the thickness required for 80-90% confidence is 75 mm and for 97.5-99% confidence is 100 mm.

When thickness tests were carried out on both limestone/2851 resin and basalt/2851 resin composites prepared to the best cost effective x variable combinations, considerable damage occurred to the targets (Series 15 and 17 respectively). This was possibly due to weakening of the composite structure

by the presence of excessive voids which were created when trying to mix the composite at low resin contents. To improve mixing characteristics and hence reduce the damage to an acceptable level, the resin content was increased until satisfactory results were obtained (Series 16 and 19).

Because of the inferior performance of these two aggregate composites to the river gravel composite, and hence there being less likelihood of their actual use, suggested thicknesses of composite for both levels of confidence are based on the results obtained from the series of tests carried out on targets prepared for the lower (80-90%) confidence level. Because of the reduced rear boundary effect the proposed thickness for the 97.5 to 99% confidence level will be slightly conservative. Suggested thicknesses for the basalt/2851 composite are 110 mm (80-90% confidence) and 140 mm (97.5-99% confidence). For the limestone/2851 composite values are 100 mm (80-90% confidence) and 130 mm (97.5-99% confidence).

Large standard deviations were evident in all thickness test series (Tables 5.18 - 5.21). Variations in penetration path length are more likely with the larger aggregate particles because the projectile will interact with a smaller number of particles than it would with smaller aggregate particles. Penetration path length will be greatly influenced by how near to the front surface the projectile has its first impact with an aggregate particle. Detailed examination was carried out on targets from test series 11 to try to determine the depth at which the bullet first hit aggregate. Ignoring the three perforated targets which will be discussed later, first impact on an aggregate particle ranged from the front surface of the target to a depth of 21 mm. Normal penetration from the impact surface in these targets varied from 26 mm to 65 mm, a range of 39 mm and had a standard deviation of 11.0 mm. Normal penetrations measured from the point of first impact with an aggregate particle ranged from 19 mm to 47 mm, a range of 26 mm, and had a standard deviation of 8.2 mm. This reduced range and reduced standard deviation indicate that the variability in similar targets is not so great as at first indicated.

A method of ensuring early impact with an aggregate particle would improve consistancy and performance.

The three targets in Series 11 which were perforated were examined in detail. In test 5 and test 19 the bullet entry hole was very clean and distances to first impact with an aggregate particle were 27 mm and 18 mm respectively. In both tests aggregate particles, 27 mm and 24 mm thick respectively, were knocked out of the back of the targets on perforation. This knocking out of rear face particles was noted on most targets which were perforated in other series. In all these tests there was no back face support, only edge support. Therefore if the composite was used as cladding, the incidence of perforation would probably be considerably less, as the bullet would have to fracture the back face rock particle rather than simply displace it.

When the specimen in test 18 was examined by sectioning, it was found that an aggregate particle had been hit at a depth of 8 mm from the front surface. The unique thing about this test was that, having penetrated through the 21 mm thick rock particle, the bullet path through the remaining 51 mm of composite was entirely through matrix material.

The mean penetration path lengths obtained in the thickness test series were probably disturbed slightly by the nominal value of thickness plus 10 mm used when perforation occurred. However, comparison of results of series 14 (river gravel/2851 resin, 100 mm thick), series 16 (basalt/2851 resin, 110 mm thick) and series 19 (limestone/2851 resin, 120 mm thick) in which very few perforations occurred, shows that limestone and basalt composites gave penetrations of the same order, but river gravel composites offered better penetration resistance. Aggregate impact and crushing values from Table 3.1 would have suggested a better performance from the basalt than the limestone and comparison of the aggregate impact values of the basalt and river gravel would have suggested similar performance from them. However,

the aggregate hardness may only have a significant effect if it is sufficiently hard to cause fragmentation of the core of the A.P. bullet and hence destroy the efficient shape of the projectile. It was interesting to note that in series 16 using basalt composite 80% more intact A.P. bullet cores were recovered during sectioning than were recovered from the river gravel composite specimens.

By comparing the results of sectioned specimens given in Table 5.28 with the dry voids measurements of Table 3.1 it can be seen that the packing of the aggregate in the specimens is similar to that obtained for uncompacted levels in the cube moulds.

This is to be expected as the viscosity of the polymer, and the friction of the sand, will encourage a degree of 'locking' of the rock aggregate during compaction of the composite. However, the smaller value of standard deviation for limestone is puzzling, as in shape it is similar to basalt. The most likely explanation is that the higher resin content in series 19 allowed the composite to 'flow' into a more even pattern that with the other two mixes.

Comparison between mean to standard deviation ratios for voids and penetration (Table 6.2) shows a larger value for the former; insufficient for it to be an overriding cause of penetration variation.

The method of approach used in this thesis enabled a balance to be obtained between a comprehensive and a detailed investigation. However, it does not give information concerning the physical relities of the penetration event. It would be possible, using high-speed photography, to film the interaction between a single rock particle (large enough to give a low frequency of misses at low range) and a projectile. With a modern rotating mirror camera this may be difficult because of syncronisation problems: the camera system itself initiates the filmed event when circumstances are correct. With a projectile the delay is large, including firing solenoid and trigger operation, propellant ignition, projectile acceleration and

flight. However, with an electronic high speed camera, the flight of the projectile can be used to trigger the camera. If mirrors were used to give a split view of the event (from side and, say, above) then estimates of mass, velocity and trajectory for each rock and projectile fragment could be made.

If this process was repeated for a low-speed collision, with little or no fragmentation, then the extent of energy absorption by momentum and fragmentation could be compared. Inherent inaccuracy of aiming would provide a spectrum of collision angles.

If it was possible to obtain failure stress and modulus information for differing rock types tested in this way, then rock properties correlating with maximum kinetic energy absorption/transference could be sought.

6.6 Supplementary Penetration Tests

6.6.1 Testing of Hornfels Composite

The limited testing of composite containing smaller size hornfels aggregate showed inferior performance to river gravel composite, but superior performance to both basalt and limestone composites. Again, the aggregate impact values from Table 3.1 would suggest that the hornfels, being much harder than the river gravel, would lead to lower penetrations. Percentage voids for the hornfels aggregate when tested in the 152 mm cube moulds was very similar to those of basalt and limestone, although composites based on the latter two offered less resistance to penetration. All the evidence points to penetration resistance of any aggregate type being dependent on the % voids value, the aggregate size and some measure of the aggregate hardness e.g. aggregate impact value. The larger the aggregate particles and the smaller the percentage voids, the better the penetration resistance. Above a certain hardness, necessary to cause bullet fragmentation, an increase in hardness will improve penetration resistance.

The fact that impact resistance is dependent on a number of aggregate

parameters makes extrapolation of the results of this study to other aggregate types difficult. However two mix design methods are suggested in Appendix A.4.One is a rigorous method involving penetration testing of a series of samples, whereas the other is an approximate method.

6.6.2 Target Temperature Effects

The tests carried out in series 22 (-7°C) and series 23 (+34°C), Table 5.24 showed that higher than ambient temperature had little effect on the penetration resistance, but a low temperature increased the penetration resistance. However, this improved penetration resistance at -7°C was accompanied by increased brittleness of the targets with much greater damage around the impact zone.

Polymers, in general, exhibit a glass transition temperature which for a given material increases with strain rate. Below this transition temperature, glassy (brittle) behaviour is exhibited, and above it, normal elastic behaviour is exhibited. Comparison of Plates 5.1 and 5.10 shows that a transition has occurred from elastomeric to brittle behaviour, with a high degree of fragmentation occurring in many of the low temperature specimens. If the composite is being used in panels, say 1 m to 2 m square, the effects of cracking due to brittleness at low temperatures is likely to be less marked than with the small targets used in the tests. Also, it should be noted that the penetration resistance is not impaired by this brittle behaviour, but the servicibility of the composite after impact may be in doubt. A burst of fire is likely to cause much more damage to the composite at low temperature when cracking due to an initial impact will lower the resistance to penetration in the surrounding area.

6.7 Static Tests

6.7.1 Uniaxial Compressive Tests

With the exception of one series of tests, the stress-strain plots from the tests showed a reasonable degree of reproduceability. Possible reasons for inconsistencies are the sensitivity of the polymer to mixing

inaccuracies, the difficulty in obtaining even compaction (especially in the cylinder moulds used), the sensitivity of the polymer ingredients to moisture, and the fact that the ingredients slowly degrade during storage.

The Poisson's ratio-strain plots, averaged for each set of three specimens, were inconsistant at low stress levels, but at high stress levels there was a consistent trend of increase to Poisson's ratios greater than 0.5. The inconsistency at low strain was probably due to measurement errors caused by surface irregularities on the specimens and the failure of the transducers to slide smoothly over the specimen surfaces. The high values of Poisson's ratio at large strains was due to internal splitting of the composite as failure progressed, evidence of which could be seen on the outside of the specimen.

The strength and deformation characteristics of the material mean that it is adequate for use as cladding panels, or infill 'blockwork' walls.

6.7.2 Creep Tests

The results from the creep tests were very inconsistent, with large variations in both initial strain and the creep rate. This is possibly due to the fact that the creep loading machine was working much below its normal load, and it is possible that friction within the machine caused the load to decrease slightly when the specimen crept, rather than remain constant. In addition, the DEMEC gauge was not very accurate for measuring the magnitude of the strains being produced.

However, by assuming that the creep rate does not increase,and extrapolating the highest creep rate obtained,a creep strain of 5×10^{-4} would take approximately 3 years. This was calculated on the basis of a 10 m high wall of composite, and is so small that it would cause no practical problems.

6.7.3 Bending Tests

Results and calculations given in Chapter 5 showed the maximum panel size for worst case loading during handling is of the order of 2½ m square for river gravel/2851 resin. It is not anticipated that panels this large would be used, and so no problems should arise. For the mixes using the other rock types, the maximum would be different, because of different failure stresses.

The variation in the repeated tests were similar to those in the uniaxial compressive tests, and are attributed to the same causes. In addition voids, especially in the tensile area of the beam, would have a more serious effect than in the compression tests, as aggregate 'locking' is not relevant in tension.

The variation of properties and behaviour with time can be seen in Table 5.28 for river gravel and 2851 resin. The most noticeable points are the high early strengths (almost full strength at 8 hours) and the apparent reduction in strength between 3 and 9 days. The reason for this is probably that the 3 day tests used a fresh batch of polymer, whereas the other tests did not. The tests do show that the use of the composite after 24 hours is acceptable, and this could be reduced to 8 hours if confirmatory penetration tests (Appendix A4) are carried out at this time using the mixes from the 24 hour tests presented in this report.

6.8 Field Use

6.8.1 Construction Methods

To construct a low rise building of a semi-permanent nature which had to offer resistance against small arms fire, infill panels of the composite could be used in a frame structure. With no backing material to stop backface scabbing thicker panels would have been designed on the basis of a very high degree of confidence on stopping a bullet. As demonstrated in Section 6.7.2 panels could be built up to a height of 10 m without any significant straining due to self weight occurring. Care would have to be taken to ensure that the panels were joinedtogether in such a way that the resistance to projectile penetration at the joints was high.

A more probable use of the composite is as a cladding on existing buildings. The cladding could be attached by either hangers or by adhesive. In the former case care would have to be taken that the local stress concentrations were sufficiently low to prevent damage to the composite, and in the latter case the panels would probably require degreasing before application of the adhesive.

A third possibility is to use small panels, say up to 1.5 m high linked together on angled timber frames as small sentry posts.

6.8.2 Large Scale Manufacture

In considering large scale production of panels of the composite certain problems will have to be overcome. The major problem is that the sand and rock aggregate have to be perfectly dry, otherwise the properties are inferior.

Another problem is that of keeping the mixer clean. If continuous casting is being carried out, this is not a major problem as each subsequent mixing operation will incorporate the residue of the previous mix. Other ways of overcoming this problem are to use either disposable mixing containers or liners,or incorporate a scraper into the mixing equipment to keep the container surface clean.

Moulds for casting should be clean and oiled. The use of polythene liners in the moulds may facilitate demoulding. Compaction should be by mechanised tamping.

Since only one hardness of resin is being used, the resin could be supplied in batches with the 2851/219 and 2851/304 types preblended in the ratio 5 parts 2851/219 resin to 4 parts 2851/304 resin (cf Table 3.7). The ratio of blended resin to 2875/003 isocyanate for Shore 80 A^{O} hardness is such that 3 kg of blended resin should be mixed with 700 g of isocyanate. Both components could be prepacked in sealed containers, the larger one being sufficiently large to act as a container for mixing in the isocyanate. Using this as a basis,Table 6.3 gives mix quantities for various sizes of panel prepared to optimum mix proportions with rounded river gravel. A small allowance has been made for wastage. A suggested manufacturing procedure is as follows

(i) Dry sand and rock aggregate.

(ii) Weigh sand and aggregate to nearest 2.5 kg and mix in main mixer.

(iii) Using a small mixer thoroughly mix 2851 resin blend and isocyanate, preferably in a disposable container. Thirty seconds should be sufficient, depending on equipment.

(iv) Pour resin onto rock and sand and mix for at least two minutes. Check that composite appears to be *thoroughly* mixed.

(v) Pour mix into oiled moulds and compact using an electrical or pneumatic tamper.

(vi) Put next batch of sand and rock into main mixer to clean it.

(vii) Demould after 1½ hours.

Series Number	Number of Tests	Penetration Path Length, D'mm				$\frac{D'max}{D'min}$
		Minimum D'min	Maximum D'max	Mean $\bar{D}$	Standard Deviation	
4	10	53.0	117.1	75.2	20.8	2.21
5	7	64.4	112.5	91.7	15.5	1.75
6	7	72.1	176.9	122.5	36.8	2.45
7	7	37.7	66.8	49.6	9.8	1.77
8	7	73.2	122.5	103.2	19.8	1.67
9	7	61.5	117.9	100.0	24.3	1.91
10	7	37.6	53.6	44.6	4.4	1.43

Table 6.1

Variation in measured penetration path lengths for similar samples in each test series

	Voids (%)			Penetration $\overline{D}$ (mm)		
	Mean	Standard Deviation	Mean / S.D.	Mean	Standard Deviation	Mean / S.D.
Series 11 River gravel	46.8	5.5	8.5	50.0	19.7	2.54
Series 16 Basalt	50.2	5.9	8.5	81.3	23.6	3.44
Series 19 Limestone	48.3	2.7	17.9	75.0	23.4	3.21

Table 6.2

Comparison of mean and standard deviation

for voids and penetration

Note: Voids data from Table 5.28.

Penetration data from Tables 5.18, 5.19, 5.20.

Ingredient	Panel size								
	1m x 1m			1½m x 1½m			2m x 2m		
	Thickness mm			Thickness mm			Thickness mm		
	80	100	120	80	100	120	80	100	120
Batched 2851 resins (kg)	15	18	21	33	39	48	57	72	84
2875/003 isocyanate (kg)	3.5	4.2	4.9	7.7	9.1	11.2	13.3	16.8	19.6
dried sand (kg)	60	70	82.5	130	155	190	225	282.5	330
dried rock (kg)	110	135	155	245	290	355	425	535	625
Total (kg)	178.5	227.2	263.4	415.7	493.1	604.2	720.3	906.3	1058.6

Notes 1. The weights of resin and isocyanate must be measured very accurately
2. The figures take into account a small amount of wastage.

Table 6.3

Mix weights to produce different size panels

of optimum mix 2851 resins/rounded river gravel composite

CHAPTER 7

CONCLUSIONS AND RECOMMENDATIONS FOR FURTHER WORK

7.1 Conclusions

1. The physical realities of the penetration event are extremely complex, involving loss of projectile kinetic energy by tensile and compressive failure, plastic flow, momentum transfer, and friction.
2. Although the nature of the composite meant that there was considerable scatter in penetration measurements from tests on similar specimens, response surface theory allowed the interaction of a number of variables to be examined to obtain optimum cost effective mixes.
3. Higher penetrations were found with A.P. ammunition than with ball ammunition.
4. Polyurethanes were found to be the most suitable polymers, with 2851 resin composites performing better than Diorez 570 resin composites.
5. The lower the resin content, the more economical the composite.
6. A certain minimum percentage resin (9%-11%) was necessary to ensure adequate mixing and prevent excessive damage on impact.
7. For 2851 resins, harder resin mixes, in terms of Shore A^{O} hardness, resulted in lower penetrations, but more brittle behaviour.
8. Best performance was achieved when using large size rock aggregate particles (26.5 mm - 37.5 mm). For realistic thicknesses of composite this is the maximum size of aggregate which should be used.
9. Aggregate and sand for composite manufacture must be perfectly dry.
10. The effect of rock type on the measured penetration depends on both rock hardness (described by aggregate impact value) and rock particle packing density (described by % voids). Generally, the harder the rock and the denser the packing, the greater will be the composite resistance. In addition, the penetration achieved before the projectile encounters the first rock particle is important.

11. Of the three main rock types tested, best performance was achieved using rounded river gravel (26.5 mm to 37.5 mm).

12. Best performance was found from a composite with 9.8% (by weight) 2851 resin (hardness 80 Shore A^{O}), 59% 26.5 mm to 37.5 mm rounded river gravel and 31.2% zone 1 or zone 2 sand.

13. Recommended mixes for the other two main rock types and 2851 resins are

    (a) 9% (by weight) resin (hardness 80 Shore A^{O}), 58% 26.5 mm - 37.5 mm crushed basalt and 33% zone 1 or zone 2 sand.

    (b) 11% (by weight) resin (Hardness 80 Shore A^{O}), 59% 26.5 mm - 37.5 mm crushed limestone and 30% zone 1 or zone 2 sand.

14. A suggested general mix for other untested rock types is 10% (by weight) 2851 resins (hardness 80 Shore A^{O}), 59% 26.5 mm to 37.5 mm rock aggregate and 31% zone 1 or zone 2 sand.

15. Recommended thickness of 2851 resin composites for an 80%-90% confidence level are 75 mm for rounded river gravel, 110 mm for crushed basalt and 100 mm for crushed limestone (For other untested rock aggregates see recommendations in Appendix A4).

16. Recommended thickness of 2851 resin composites for a 97.5%-99% confidence level are 100 mm for rounded river gravel, 140 mm for crushed basalt and 130 mm for crushed limestone (For other untested rock aggregates see recommendations in Appendix A4).

17. Cratering of the impact surface of the finally adopted mixes was minimal.

18. Where perforation of finally adopted mix composites did occur, scabbing of the target rear surface was minimal.

19. Changes from ambient temperature of finally adopted mix targets did not lead to any increase in penetration.

20. Brittle behaviour was evident in targets tested at -7°C.

21. Static tests on the optimum mix rounded river gravel/2851 resin composite show that the material is adequate for non load bearing applications.

22. The composite using 2851 resins may be demoulded after about an hour and a half, and almost full strength can be achieved 8 hours after casting.

7.2 Recommendations for Further Work

1. Further studies using 26.5 mm to 37.5 mm aggregate of different rock types using the standard mix to attempt to get a relationship between aggregate impact value, % voids and penetration.

2. Studies of full scale manufacture.

3. Studies of layered construction with a composite containing smaller size aggregate at the impact face to ensure the projectile hits rock particles before it penetrates any significant distance into the composite.

4. Studies of the effect of repeated fire on the composite.

5. Studies of low temperature effects using larger area targets in which brittle behaviour is likely to be less significant.

6. Studies of rock particle/projectile interaction using high speed photography, allied with static rock property tests.

7. Further work on the behaviour of the composite during non-normal impact (i.e. ricochet) and when subjected to contact explosive charges.

REFERENCES

ALLEN, W.A., MAYFIELD, E.B. and MORRISON, H.L. (1957a) Dynamics of a projectile penetrating sand. J. Appl. Phys, Vol. 28, No. 3, pp. 370-376.

ALLEN, W.A., MAYFIELD, E.B. and MORRISON, H.L. (1957b) Dynamics of a projectile penetrating sand. J. Appl. Phys, Vol. 28, No. 3, pp. 1331-1335.

ANDERSON, W.F., WATSON, A.J. and JOHNSON, M.R. (1980) The properties of an elastomeric and rock composite. Final report AT/2031/082 MV, Department of Civil and Structural Engineering, University of Sheffield.

BACKMAN, M.E. and GOLDSMITH, W. (1978) The mechanics of penetration of projectiles into targets. Int. J. Engng Sci., Vol. 16, No. 1, pp. 1-99.

BERNARD, R.S. (1975) Development of a projectile penetration theory; Report 2- Deep penetration theory for homogeneous and layered targets. Army Engineer Waterways Experiment Station, Vicksburg, Missouri, AEWES-TR-S-75-9-2.

BERNARD, R.S. and HANAGUD, S.V. (1975) Development of projectile penetration theory; Report 1 - Penetration to shallow and moderate depths. Army Engineer Waterways Experiment Station, Vicksburg, Missouri, AEWES-TR-S-75-9-1.

BRITISH STANDARDS INSTITUTION (1970) B.S. 1881: Methods of testing concrete, Part 3 : Methods of making and curing test specimens.

BRITISH STANDARDS INSTITUTION (1973) B.S. 822: Specifications for aggregates from natural sources for concrete, Part 2.

BRITISH STANDARDS INSTITUTION (1975) B.S. 812: Methods of sampling and testing mineral aggregates, Part 2 : Physical properties, Part 3 : Mechanical properties.

BUTLER, D.K. (1975) An analytical study of projectile penetration into rock. Army Engineer Waterways Experiment Station, Vicksburg, Missouri, AEWES-TR-S-75-7.

COCHRAN, W.G. and COX, G.M. (1957) Experimental Designs. Wiley Publications, New York.

DANIEL, I.M. and ROWLANDS, R.E. (1975) On waves and fracture progagation in rock. Experimental Mechanics, Vol. 15, No. 12, pp. 449-457.

DAVIES, O.L. (1954) The Design and Analysis of Industrial Experiments. Oliver and Boyd, London.

DAVEY, A.B. and PAYNE, A.R. (1964) Rubber in Engineering Practice. MacLaren and Sons Ltd., London.

DEPARTMENT OF SCIENTIFIC AND INDUSTRIAL RESEARCH (1959) Roadstone test data presented in tabular form. Road Research Road Note No. 24.

DUNLAP, W.A. (1972) Influence of soil properties on penetration resistance. Proc. Conf. Rapid Penetration of Terrestrial Materials, Texas A & M University, pp. 515-526.

GIBBS, F.W. and PRESCOTT, P.F. (1974) A preliminary investigation into gravel armour. Tech. Memo. 74850, M.o.D. M.V.E.E. (Christchurch).

GOLDSMITH, W. (1960) Impact. Edward Arnold, London.

GOODIER, J.N. (1964) On the mechanics of indentation and cratering in solid targets of strain-hardening metal by impact of hard and soft spheres. TR 002-64, Poulter Laboratories, Stanford Research Institute, Menlo Pk., California.

HADALA, P.F. (1975) Evaluation of empirical and analytical procedures used for predicting the rigid body motion of an earth penetrator. AEWES-TR-S-75-7, Army Engineer Waterways Experiment Station, Vicksburg, Missouri.

HANAGUD, S. and ROSS, B. (1971) Large deformation, deep penetration for a compressible strain-hardening target material. J. Am. Inst. Aeronautics and Astronautics, Vol. 9, No. 5, pp. 905-911.

JONAS, G.H. and ZUKAS, J.A. (1978) Mechanics of penetration; analysis and experiment. Int. J. Engng Sci., Vol. 16, No. 11, pp. 879-903.

KAR, A.K. (1978) Projectile penetration into buried structures. Proc. Am. Soc. Civil Engrs, J.Struct.Div., Vol. 104, No. ST1, pp. 125-139.

KOLSKY, H. (1949) An investigation of the mechanical properties of materials at very high rates of loading. Proc. Physical Soc., Vol. 62, Sect. B, pp. 676-700.

KOLSKY, H. (1950) The propagation of stress pulses in viscoelastic solids. Philosophical Mag., Vol. 1, Pt. 2, pp. 693-710.

LOVEL, E., AL-HASSANIS, T.S. and JOHNSON, W. (1974) Fracture in solid spheres and circular discs due to a 'point' explosive impulse on the surface. Int. J. Mech. Sci., Vol. 16, pp. 193-9.

LUNDBURG, B. (1976) A split Hopkinson bar study of energy absorption in dynamic rock fragmentation. Int. J. Rock Mechanics, Min. Sci. and Geomech. Abstr., Vol. 13, No. 6, pp. 187-197.

MAURER, W.C. and RINEHART, J.S. (1960) Impact crater formation in rock. J. Appl. Phys Vol. 31, No. 7, pp. 1247-1252.

MORRISON, H.L. and ALLEN, W.A. (1955) New surface area formed by a projectile striking limestone particles. Meteorites, Vol. 1, pp. 328-336.

MURFF, J.D. and COYLE, H.M. (1973) Prediction method for projectile penetration. Proc. Am. Soc. Civil Engrs, J. Soil Mech. and Fdn Div., Vol. 99, No. SM11, pp. 1033-1037.

RICKETTS, T.E. and GOLDSMITH, W. (1970) Dynamic properties of rocks and composite structural materials. Int. J. Rock Mechs. Min. Sci., Vol. 7, No. 3, pp. 315-335.

RIPARBELLI, C. and BROWN, C.T. (1972) On the mechanism of formation of a crater following impact by a high speed penetrator and a method to predict the crater profile. Proc. Conf. Rapid Penetration of Terrestrial Materials, Texas A & M University, pp. 281-307.

ROHANI, B. (1972) High velocity fragment penetration of soil targets. Proc. Conf. Rapid Penetration of Terrestrial Materials, Texas A & M University, pp. 251-279.

ROHANI, B. (1975) Analysis of projectile penetration into concrete and rock targets . Army Engineer Waterways Experiment Station, Vicksburg, Missouri, AEWES-MISC-PAPER-S-75-25.

ROSS, B. and HANAGUD, S. (1969) Penetration studies of ice with application to arctic and subarctic warfare. Stanford Research Institute, Menlo Pk., California, NWRC 7000-452-4.

ROSS, B. and HANAGUD, S. (1971) Penetration studies of ice with application to arctic and subarctic warfare. Stanford Research Institute, Menlo Pk., California, NWRC 7000-452-5.

SELIG, E.T. (1964) Characteristics of stress wave propagation in soils. Proc. Symp. on Soil Structure Interaction, Univ. Arizona, pp. 27-61.

SHIOYA, T., KAWATA, K. and HASHIMOTO, S. (1976) A preliminary investigation on the penetration of high speed rigid projectiles into epoxy resins. Trans. Japan Soc. Aero. Space Sci., Vol 19, No. 43, pp. 15-22.

SILVERSTEIN, C.C. (1969) Permanent compression of a contained granular bed following impact with a rigid body. J. Appl. Mechs, Vol. 36, pp. 545-550.

THIGPEN, L. (1974) Projectile penetration of elastic-plastic earth media. Proc. Am. Soc. Civil Engrs, J. Geot. Engng Div., Vol. 100, No. GT3, pp. 279-294.

THOMPSON, L.J. (1966) Dynamic penetration of selected projectiles into particulate media. Sandia Corporation, Albuquerque, N.Mex.,SC-RR-66-376.

VANZANT, S.W. (1963) Dynamic rock penetration at atmospheric pressure. Proc. 5th Symp. on Rock Mech., Univ. of Minnisota, pp. 61-91 (ed. C. Fairhurst).

YEW, C.H. and STIRIBIS, P.P. (1978) Penetration of projectile into terrestrial targets. Proc. Am. Soc. Civil Engrs, J. Engng. Mech. Div., Vol. 104, No. EM2, pp. 273-286.

YOUNG, C.W. (1969) Depth prediction for earth penetrating projectiles. Proc. Am. Soc. Civil Engrs., J. Soil Mech. and Fdn. Div., Vol. 95, No. SM3, pp. 803-817.

APPENDIX A1 - MANUFACTURERS AND SUPPLIERS OF MATERIALS AND EQUIPMENT

A1.1 Resins

The resins used in the main study were:

Diorez 570	Briggs & Townsend Ltd., Ashfield House, Ashfield Road, Cheadle, Cheshire.
2851/219 2851/304	Donald McPherson & Co. Ltd., Warth Mills, Radcliffe Road, Bury, Lancashire.

The resins examined but not included in the main test program were:

Polysulphide rubber	Thiokol Chemicals Ltd., Station Tower, Station Square, Coventry.
Unsaturated polyester resin; widely available, normally brittle: a slightly flexible form was obtained	B.P. Chemicals Ltd., Devonshire House, Mayfair Place, Piccadilly, London.
Epoxy resins	Widely available.
Neoprene latex	Du Pont Ltd., Du Pont House, 18 Breams Buildings, Fetter Lane, London.
Polythixon	Keilawarra Ltd., 28-29 Southampton Street, London. WC2E 7JA
Silicone rubber	Plastics Division, Ciba-Geigy (UK) Ltd., Duxford, Cambridge

Hydroxyl terminated polybutadiene	Corneluis Chemical Co. Ltd., Ibex House, Minories, London. EC3
Butadiene	Revertex Ltd., Temple Fields, Harlow, Essex.
Polyurethane (polyester)	Baxenden Chemical Co. Ltd., Paragon Works, Baxenden, Nr. Accrington, Lancashire.

A1.2 Rock aggregate and sand

River gravel	Blue Circle Aggregates Ltd., Hemmington Quarry, Nr. Derby.
Basalt	Waterswallow's Quarry, Buxton, Derbyshire.
Limestone	Topley Pike Quarry, Buxton, Derbyshire.
Sand (Zone 2)	Blue Circle Aggregates, Rugelay Road, Hednesford, Cannock, Staffs.

A1.3 Equipment

7.62 mm ball & A.P. ammunition	Conjay Arms Co. Ltd., 118 Craven Park Road, London. NW1D 8QD
Firing solenoid	Phillips Control (Sales) Ltd., Church Path, Lynchford Road, Farnborough, Hants.
Light bulb velocity measuring rig	RLP Miniature Bulb Co., Carey Avenue, Barnsley, Yorkshire

Photodiode, velocity measuring rig	R.S. Compondents Ltd., P.O. Box 427, 13-17 Epworth Street, London. EC2P 2HA
No. 3 Pressure housing and 7.62 mm proof barrel	Woolwich Arsenal, via. M.V.E.E., Barrack Road, Christchurch.
Saw and blades	Clipper Manufacturing Company, Thurmaston Boulevard, Barkby Road, Leicester.

APPENDIX A2 - RESPONSE SURFACE THEORY

(after Cochran and Cox, 1957, Chapter 8A)

A2.1 Introduction

Response surface theory developed out of factorial experiments, where the yield of (say) a process is examined for different combinations of levels (values) of various factors (variables). If all of these factors are quantitative variables then it is possible to think of the yield, or response, y, as a function of the levels of these variables, i.e.

$$y_u = \phi\ (x_{iu}, x_{2u} \ldots\ldots, x_{ku}) + e_u \qquad \ldots\ A2.1$$

$u = 1, 2, \ldots.$ n represents the n observations in the factorial experiment,

x_{iu} represents the level of the i^{th} factor in the u^{th} observation polynomial,

$\bar{\phi}$ is the polynomial function called the response surface,

e_u ,the residual, measures the experimental error of the u^{th} observation.

The degree of the polynomial ϕ has no theoretical limit. However, practical application normally limits the degree to 1 or 2. The experimental designs based on these degrees are called first order designs and second order designs respectively. Polynomials are relatively easy to fit to experimental data, but become very unreliable when extrapolated beyond the field of investigation.

A2.2 First Order Designs

For a polynomial of the first degree, the multiple linear regression of y_n on the k x variables is

$$y_u = b_o + b_1 x_{1u} + b_2 x_{2u} \ldots\ldots\ldots + b_k x_{ku} + e_u \qquad \ldots\ A2.2$$

where b_o to b_k are coefficients.

At this stage it is necessary to introduce the concept of coding of factor levels. This is carried out to simplify data manipulation. Suppose the factor x_1 is being examined at numerical values of (say) 63, 67, 71(in combination with various levels for x_2 to x_k), three levels only being necessary for first order designs. These values would then be coded about a central value of zero, with the interval between them being reduced to unity. Hence the coded levels of factor x_1 become -1, 0, +1, the coding equation being $x_1(\text{coded}) = \frac{x_1 - 67}{4}$. The levels of variables do not have to be in a linear progression. For instance, the factor x_2 is a discrete variable which can take only values in a series such as 10, 20, 40, 80, 160 etc, then any part of the series may be coded in the normal way. For example, levels of x_2 at 20, 40, 80 may be coded as -1, 0, 1, with non-linear coding equation. However, this sort of non-linear coding is likely to cause lack of fit in a first degree polynomial.

It is usually necessary to repeat the combination with all factor levels at zero to obtain an estimate of e_u, and hence the lack of fit (see A2.4).

The use of the first order design in this project provides an adequate simple example (cf Section 4.3.2.).

First degree polynomials are not very useful in themselves, but do provide a pointer to factor level combinations of interest. The method of steepest ascent is a procedure which may be used to determine in which direction and in what proportions factor levels should be altered in order to optimize the yield, y. This method was not used in this project, for reasons detailed in Section 4.3.2.

A2.3 Second Order Designs

The general form of a quadratic (second degree) polynomial is illustrated by the equation for 2 x-variables

$$y_u = b_o + b_1 x_{1u} + b_2 x_{2u} + b_{11} x_{1u}^2 + b_{22} x_{2u}^2 + b_{12} x_{1u} x_{2u} + e_u \quad .. \text{ A2.3}$$

A minimum of four factor levels are necessary for quadratic designs, three for curve fitting, and one for estimation of errors.

The experimental planning of the penetration tests in the project was based on a central composite rotatable design with $4x$ variables. A pictorial plan of such a design in 2 x variables was given in Figure 4.3.

Such a design may be subdivided into 3 parts

(i) The four points (-1,-1),(1,-1),(-1,1) and (1,1) constitute a 2^2 factorial (i.e. 2 factors each at 2 levels),

(ii) The four points (-2,O),(2,O),(O,-2),(O,2) are the extra points included to form a central composite design. The figure formed by these points is called a <u>star</u>,

(iii) Five points are added at the centre to give roughly equal precision to y_p within the design area, where y_p is the <u>predicted</u> value of y from the fitted polynomial. y_p differs from y_u because of the 'lack of fit' of the quadratic response surface.

A2.4 <u>Errors, and Lack of Fit</u>

The term e_u in equations A2.2 and A2.3 is composed of 2 components

(i) measurement errors, etc,

(ii) experimental scatter due to variations beyond experimental control i.e. experimental error.

In addition, there is lack of fit between the response surface fitted by regression and the true response surface. Thus the difference between an experimentally obtained value of y and a predicted value of y (the residual) is e_u plus lack of fit.

The purpose of repeating tests at the central coded value is to estimate e_u, and hence, as the residuals are known, lack of fit may be calculated and

tested for acceptability.

For first order designs, an F test is applied to check whether the variances of the (error + lack of fit) distribution is significantly greater than the error distribution. Referring to a linear design of the type outlined in Section 4.2.3 but using the general notation of this Appendix this means that

$$\frac{\sum_{i}^{11}(y_p - y_u)^2 - \sum_{9}^{11}(y_u - \bar{y}_u)^2}{\sum_{9}^{11}(y_u - \bar{y}_u)^2} \times \frac{n_2}{n_1} < F_{n_1,n_2} \qquad \ldots \text{A2.4}$$

where y_p is the predicted response

$\bar{y}_u$ is the mean response over the range given

n_1 and n_2 are the degrees of freedom for lack of fit and pure error

F_{n_1,n_2} is the relevant value of the F distribution at the chosen significance level

For the quadratic response surface at each stage of analysis the test is similar

$$\frac{\overset{\text{TOTAL}}{\Sigma(y_p - y_u)^2} - \overset{\text{DESIGN CENTRE}}{\Sigma(y_u - \bar{y}_u)^2}}{\underset{\text{CENTRE}}{\overset{\text{DESIGN}}{\Sigma(y_u - \bar{y}_u)^2}}} \times \frac{n_2}{n_1} < F_{n_1,n_2} \qquad \ldots \text{A2.5}$$

APPENDIX A3 - COMPUTING

A3.1 Multiple Polynomial Regression - PENET, with Datafile DATA

This program made use of the Statistical Package for Social Sciences, SPSS. The listing is

```
SPSS*CF DATA,    ROUTE STG
RUN NAME         MULT REGN
VARIABLE LIST    Y, X1 TO X4
 /  OF CASES     (number of test points used)
INPUT MEDIUM     OTHER
INPUT FORMAT     FREEFIELD
COMPUTE          C1=X1*X2
COMPUTE          C2=X1*X3
COMPUTE          C3=X1*X4
COMPUTE          C4=X2*X3
COMPUTE          C5=X2*X4
COMPUTE          C6=X3*X4
COMPUTE          S1=X1*X1
COMPUTE          S2=X2*X2
COMPUTE          S3=X3*X3
COMPUTE          S4=X4*X4
REGRESSION       VARIABLES = Y,X1 TO X4,C1 TO C6,S1 TO S4
                 REGRESSION Y WITH X1 TO X4,C1 TO C6,S1 TO
                 S4(2) RESID=Ø/
STATISTICS       4,6
READ INPUT DATA
```

The only changing value in this program is on line 4 shown as (number of test points used).

The datafile DATA contains the coded factor levels for each test, along with the measured penetration path length, in a freefield format e.g.

```
 78.Ø    -1    -1    -1    -1
103.Ø    +1    -1    -1    -1
 82.9    -1    +1    -1    -1
```

The datafile was updated as required for each PENET analysis. The useful part of the output gives the response surface equation and a table showing, for each combination of factor levels, the measured penetration path length, and the

value of the response surface at that point, i.e. the predicted penetration path length. The differences between these two values, the residuals, are also listed, and from these the lack of fit calculations are carried out (section A2.4).

A3.2 Matrix Inversion Program - MATINV

This program was available in the Department of Civil and Structural Engineering, and was run on cards

```
Ø       JOB(jobname),(username)
1       RUN FORTRAN
2       MASTER CPT2
3       DIMENSION A(12,12),X(12),B(12)
4       DO1I=1,N
5     1 READ(1,1Ø1)(A(I,J),J=1,N)
6       WRITE(2,2Ø1)N,N
7       DO3I=1,N
8     3 WRITE(2,2ØØ)(A(I,J),J=1,N)
9       READ(1,1Ø1)(B(I),I=1,N)
1Ø      WRITE(2,2Ø2)N
11      WRITE(2,2ØØ)(B(J),J=1,N)
12      CALL MATINV(A,12,N)
13      DO2I=1,N
14      X(I)=Ø.Ø
15      DO2J=1,N
16    2 X(I)=X(I)+A(I,J)*B(J)
17      WRITE(2,2Ø3)N,N
18      DO4I=1,N
19    4 WRITE(2,2ØØ)(A(I,J),J=1,N)
2Ø      WRITE(2,2Ø4)
21      WRITE(2,2Ø5)(I,X(I),I=1,N)
22  1ØØ FORMAT(IØ)
23  1Ø1 FORMAT(12,FØ.Ø)
24  2ØØ FORMAT(1X,12F1Ø.3)
25  2Ø1 FORMAT('ØMATRIX A('I2,'X',I2,')
26  2Ø2 FORMAT('ØVECTOR B',I2,')')
27  2Ø3 FORMAT('ØINVERSE OF MATRIX A(',I2,'X',I2,')')
28  2Ø4 FORMAT('ØSOLUTION')
29  2Ø5 FORMAT('X(',I2,')=',F1Ø.3)
3Ø      STOP
31      END
32      SUBROUTINE MATINV(D,ID,M)
33      DIMENSION D(ID,ID)
34      DO3I=1,M
35      RM=D(I,I)
36      D(I,I)=1.Ø
37      DO1K=1,M
38      D(I,K)=D(I,K)/RM
39      DO3J=1,M
```

```
4Ø        IF(J.EQ.I)GOTO3
41        RM=D(J,I)
42        D(J,I)=Ø.Ø
43        DO2K=1,M
44     2  D(J,K)=D(J,K)-RM*D(I,K)
45     3  CONTINUE
46        RETURN
47        END
48        FINISH
49        4
5Ø     ⌈        ⌉
51     |        |
52     |  DATA  |
53     |        |
54     |        |
55        ****
```

The first fourdata lines take the form of the x coefficients of each of the four equations formed by differentiating the response surface with respect to each variable in turn. The final line is the righthand side of the equation

For example, if the set of equations were

$$\begin{bmatrix} +1.0 & +2.1 & +3.7 & +4.3 \\ +5.9 & +6.5 & -7.6 & -8.1 \\ -9.9 & -10.3 & -11.7 & -12.8 \\ +13.6 & -14.9 & +15.1 & -16.2 \end{bmatrix} \begin{bmatrix} x_1 \\ x_2 \\ x_3 \\ x_4 \end{bmatrix} = \begin{bmatrix} -17.1 \\ +18.5 \\ -19.6 \\ +20.3 \end{bmatrix} \quad \ldots\ldots \text{A3.1}$$

The data input would be

(line no.)

5Ø	+1.0	+2.1	+3.7	+4.3
51	+5.9	+6.5	-7.6	-8.1
52	-9.9	-10.3	-11.7	-12.8
53	+13.6	-14.9	+15.1	-16.2
54	-17.1	+18.5	-19.6	+20.3

A3.3 Determination of the Eigenvalues of a Determinant - EIGEN

The coefficients of the four equations used in section A3.2 were manipulated as described by Davies (1954) to give a 4 x 4 determinant which was then solved

to give its eigenvalues using EIGEN. These eigenvalues were the coefficients of the canonical transformation of the response surface.

The program listed below made use of a standard eigenvalue NAG routine, available on the University of Sheffield computer

```
Ø       JOB(jobname),(username)
1       RUN FORTRAN, JD(URE),DEFPD 2, ROUTE STG
2       LIBRARY (SUBGROUPNAGF)
3       LIBRARY (SUBGROUPNAGG)
4       PROGRAM(programname1)
5       INPUT 5=CRØ
6       OUTPUT 6=LPØ
7       TRACE 1
8       END
9       MASTER(programname2)
1Ø      REAL A(4,4),R(4),E(4)
11      READ (5,9Ø)((A(I,J,),J=1,4),I=1,4)
12      IFAIL=1
13      CALL FØ2AAF(A,4,4,R,E,IFAIL)
14      WRITE (6,95)R
15  95  FORMAT(1X,4FL1Ø.4)
16  9Ø  FORMAT(4FØ.Ø)
17      STOP
18      END
19      FINISH
2Ø      [       ]
21      [ data  ]
22      [       ]
23      [       ]
24      ****
```

The data is in the form of a determinant, e.g.

```
2Ø      -5.1    -6.5    -7.2    +8.9
21      -9.8    +10.7   +11.3   +12.4
22      +13.7   +14.6   +15.7   +16.1
23      +17.3   +18.5   +19.1   -20.6
```

A3.4 The Calculation of Predicted Penetration Path Length - CODEFIT

PENET, described in section A3.1, yielded the equation of the response surface, and the actual and predicted penetration path lengths at the combinations of coded variable levels used in the experiments.

CODEFIT amplifies on this by calculating predicted penetration path length over all combinations of x variables between levels -2 and +2, at any

increment. With an increment of 1, 5^4 values will appear on the output, with the corresponding variable level information. The program contained the equation of the response surface, and hence had to be modified at each run from the results of PENET. The example below contains equation 5.5

```
 Ø        PROGRAM(programme)
 1        OUTPUT 2=LPØ
 2        TRACE 1
 3        END
 4        MASTER FIT
 5        DO1 I1=1,5
 6        DO1 I2=1,5
 7        DO1 I3=1,5
 8        DO1 I4=1,5
 9        X1=1.*I1-3
1Ø        X2=1.*I2-3
11        X3=1.*I3-3
12        X4=1.*I4-3
13        DP=75.18+4.2*X1-Ø.Ø8*X2-18.79*X3-9.82*X4+4.35*X1*X2
14       *-5.36*X1*X3-2.28*X1*X4-1.98*X2*X3+8.64*X2*X4
15       *+5.83*X3*X4-6.29*X1*X1-Ø.59*X2*X2+Ø.3*X3*X3+1.4*X4*X4
16    1   WRITE(2,3Ø)DP,X1,X2,X3,X4
17   3Ø   FORMAT(5(3X,F7.2))
18        STOP
19        END
20        FINISH
21        ****
```

The output took the following form, listing D_p', x_1, x_2, x_3, x_4

```
14Ø.24     -2.00     -2.00     -2.00     -2.00
1Ø1.84     -2.00     -2.00     -2.00     -1.00
 66.24     -2.00     -2.00     -2.00      0.00

          etc., to

 42.28      2.00      2.00      2.00      2.00
```

APPENDIX A4 - SUGGESTED METHODS FOR DETERMINING THE THICKNESS OF COMPOSITE FOR ANY ROCK TYPE

Two simple methods for determining composite thickness with any rock type are suggested, one of which involves some trial testing and hence gives a more accurate solution. Both methods assume that the composite is composed of 10% (by weight) 2851 resin (Hardness 80 Shore A^{o}), 59% rock aggregate (largest available to a maximum of 40 mm) and 31% zone 1 or zone 2 sand.

A4.1 Accurate Method

Twenty blocks, 150 mm x 150 mm x 100 mm thick, are cast and tested with A.P. ammunition at a range of 20 metres. The specimens would then be sectioned to find vertical penetration depths. However, if more than five perforations occur in the series of twenty tests, another series should be carried out on blocks 120 mm thick.

Assuming that perforations are equivalent to a penetration of the block thickness + 10 mm, the mean vertical penetration, $\bar{D}$, and the standard deviation, σ, of the twenty tests are calculated.

For any degree of confidence using probability points on a statistical t - distribution, the thickness of composite, t_m, required can be calculated

For 80% confidence	:	$t_m = \bar{D} + 0.86\sigma$
For 90% confidence	:	$t_m = \bar{D} + 1.32\sigma$
For 95% confidence	:	$t_m = \bar{D} + 1.72\sigma$
For 97.5% confidence	:	$t_m = \bar{D} + 2.09\sigma$
For 99% confidence	:	$t_m = \bar{D} + 2.53\sigma$

A4.2 Approximate Method

If firing tests cannot be carried out on composites prepared with an untested aggregate, then the nominal thicknesses given in Table A4.1 may be used. These values only apply to aggregate where the uncompacted % voids

determined to BS 812 are less than 50%. Also any rock aggregate with an aggregate impact value, as specified by the supplier, of greater than 25 is unsuitable.

Confidence level	Aggregate impact value between 25 and 15	Aggregate impact value less than 15
80%	110 mm	95 mm
90%	120 mm	105 mm
95%	130 mm	115 mm
97.5%	140 mm	120 mm
99%	150 mm	130 mm

Table A4.1

Suggested thickness of

composite containing untested rock aggregate